Reactivation of pre-existing crustal discontinuities: the southern Upper Rhine Graben and the northern Jura Mountains – a natural laboratory

Inauguraldissertation

zur

Erlangung der Würde eines Doktors der Philosophie

vorgelegt der

Philosophisch-Naturwissenschaftlichen Fakultät der Universität Basel

von

Kamil Marek Ustaszewski

aus

Innsbruck, Österreich

Basel, 2004

Genehmigt von der Philosophisch-Naturwissenschaftlichen Fakultät

auf Antrag von

_____

Prof. Stefan Schmid

_____

Prof. Peter Ziegler

_____

Prof. Jan Behrmann

Basel, den 8. Juni 2004

_____

Prof. Dr. Marcel Tanner
(Dekan)

to the loving memory of my grandparents
Ludmiła and Tadeusz Wódkiewicz

„Wissen Sie, eine Doktorarbeit besteht zum großen Teil aus anderen Doktorarbeiten (...). Eine neue Doktorarbeit ist immer auch eine Art Orgie von alten Doktorarbeiten, die sich untereinander, äh, befruchten, damit etwas Neues, etwas noch nie Dagewesenes aus ihnen hervorgeht.''

Dr. Oztafan Kolibril

Aus:
W. Moers, „Rumo und die Wunder im Dunkeln''

Abstract

This thesis is devoted to the analysis of faults that were repeatedly reactivated under changing stress fields. The investigations were carried out at the junction between the Upper Rhine Graben and the Jura Mountains. This area represents the intersection between part of the western European Cenozoic rift system and the northern Alpine foreland. It has been shaped by an interplay between extensional and compressional tectonic forces and involved the repeated reactivation of crustal-scale faults since the Late Palaeozoic. At present, it is characterised by increased seismicity, giving proof of ongoing tectonic activity. Therefore, studying the tectonic evolution of this area can improve the understanding of various tectonic processes that shape the earth's crust.

Extension in the Upper Rhine Graben intitated in the Late Eocene under W-E- to WNW-ESE-oriented extension. Its southern end connects into the Rhine-Bresse transfer zone. This transfer zone linked the simultaneous extension in both the Upper Rhine Graben and the Bresse Graben, another branch of the European Cenozoic rift system. The transition from mainly rift-perpendicular extension in the Upper Rhine Graben to sinistral transtensive movements in the Rhine-Bresse transfer zone was predetermined by ENE-trending basement faults delimiting a Late Palaeozoic trough system in the subsurface. Rifting involved the reactivation of these ENE-trending basement faults as sinistral transtensive strike-slip faults, simultaneously with normal faulting along NNE-oriented faults. In the sedimentary cover, this was manifested in simultaneous extensional flexuring above ENE-trending faults and growth faulting above NNE-oriented faults. The interaction of these differently oriented faults led to cumulative throw and localised depocenters in the Late Eocene to Early Oligocene.

The formation of the thin-skinned Jura Mountains in the Late Miocene to Early Pliocene initiated under NW-SE- to N-S-oriented compression and was related to Alpine orogeny. In the study area, the detached sediments encountered a fault pattern inherited from Palaeogene rifting. While ENE- to E-trending faults led to the nucleation of frontal thrusts and anticlines, NNE-trending faults paralleling the Rhine Graben served as transfer zones. Along these transfer zones, sinistral oblique ramps developed and allowed the detached sediments to be transferred sinistrally to the north. As a result, the northern Jura Mountains reveal a geometry that largely mimics the structural pattern inherited from Palaeogene extensional tectonics.

Thin-skinned Jura folding was followed by post-Late Pliocene thick-skinned fault reactivation, as evidenced in the spatial coincidence between subsurface faults and surface anticlines. This youngest tectonic phase, characterised by horizontal shortening rates below 0.1 mm/a, is most presumably ongoing at present, as evidenced by faulted Late Pliocene gravels and deflected rivers.

Dynamically scaled sand-silicone models showed that within wrench systems, the reactivation of faults in a sand cover, separated from a basal discontinuity by a viscous décollement layer, is strongly controlled by the mechanical coupling between "basement" and "cover" across a décollement layer. The coupling in turn depends on the displacement rates applied to the basal plate. The experimental setup was inspired from the Rhine-Bresse transfer zone (RBTZ) that connected the Upper Rhine Graben with the Bresse Graben. This transfer zone bears evidence for the reactivation of basement-rooted structures in Neogene times. The experimental results suggest not only that fault reactivation in the RBTZ has occurred under low displacement rates, but they also provide an explanation for partial stress decoupling between cover and basement.

Organisation of this thesis

The present thesis is organised in a "cumulative" manner and consists of 7 chapters, four of which were prepared for submission to scientific journals. The topics of the individual chapters and the contributions of the various authors are outlined below.

Chapter 1: Introduction

This chapter outlines the scope of this thesis and provides an introduction to the geology of the study area.

Chapter 2:
Simultaneous normal faulting and extensional flexuring during rifting: an example from the southernmost Upper Rhine Graben

by

Kamil Ustaszewski, Markus E. Schumacher, Stefan M. Schmid

published in: *International Journal of Earth Sciences 94: 680-696*

This chapter addresses the kinematics of Palaeogene rifting at the southern end of the Upper Rhine Graben. The study combines field evidence with reflection seismic data and illustrates the palaeostresses that prevailed in the sedimentary cover during the simultaneous formation of half-grabens and extensional flexures. A newly presented kinematic model emphasises the role of pre-existing faults during the early rift evolution.

The first author has performed all the fieldwork and sampling of fault-slip data for the kinematic analysis. He also interpreted the seismic and subsurface data and compiled the subsurface maps. Eventually, he also wrote a first draft of the manuscript. The second author helped to shape ideas on fault kinematics both in the field and in the office. He furthermore assisted in the interpretation of the reflection seismic data. The third author has contributed to the study during fieldwork and particularly in correcting early text versions.

Chapter 3:
Control of pre-existing faults on geometry and kinematics in the northernmost part of the Jura fold and thrust belt

by

Kamil Ustaszewski and Stefan M. Schmid

submitted to: *Tectonics*

This chapter investigates the kinematics that prevailed during the formation of the frontalmost part of the Late Miocene to Early Pliocene thin-skinned Jura Mountains. Based on a detailed geometric and kinematic analysis that integrates outcrop and subsurface data, the fundamental role of pre-existing faults on shaping the frontal, highly asymmetric Jura anticlines is again highlighted. The study also provides evidence for a transition from thin- to thick-skinned

tectonics at the Jura Mountains – Upper Rhine Graben junction after the Late Pliocene. The first author has performed the fieldwork, the palaeostress analysis and the subsurface data interpretation. He also constructed the cross sections and developed the kinematic models. The second author provided the background knowledge on structural aspects, gave critical input on the regional setting and helped finalising the manuscript.

Chapter 4:

Plio-Pleistocene transpressional reactivation of Paleozoic and Paleogene structures in the Rhine-Bresse transform zone (northern Switzerland and eastern France)

by

M. Giamboni, K. Ustaszewski, S. M. Schmid, M. E. Schumacher and A. Wetzel

published in: *International Journal of Earth Sciences 93:207-223*

This chapter addresses the geomorphological evolution in the southernmost Upper Rhine Graben and adjacent Jura from Late Pliocene to recent times. The centrepiece of this study is the documentation of systematically aligned gentle syn- and anticlines in the southernmost Upper Rhine Graben, perceptible in a contour map of the base of Late Pliocene fluvial gravels. The analysis of the drainage pattern, based on high-resolution digital elevation models, suggests that the deformation has continued into Pleistocene to recent times.

The study represents collaboration with another PhD student in Basel (the first author). The first author has constructed the contour map, the drainage pattern analysis and prepared a first draft of the manuscript and figures 1 to 5 and 8 to 10. The second author has collected additional structural data (Fig. 2) that helped refining the contour map. He also compiled and interpreted the subsurface and reflection seismic data and has constructed the geological cross-section (Figures 6 and 7). He has furthermore made kinematic interpretations of the folds in the Base Pliocene (bottom insert in Fig. 5) and wrote the corresponding parts of the manuscript. Both first and second author have made the interpretations of the geoelectrical profiles together. The third author was the first to point out the tectonic origin of certain structures in the field and encouraged the first two authors in writing this manuscript. The fourth and fifth authors contributed by reviewing early versions of the manuscript.

Chapter 5:

Fault reactivation in brittle-viscous wrench systems – dynamically scaled analogue models and application to the Rhine-Bresse Transfer Zone

by

Kamil Ustaszewski, Markus E. Schumacher, Stefan M. Schmid and Dick Nieuwland

published in: *Quaternary Science Reviews 24, 365-382*

This chapter represents an experimental approach on the effects of fault reactivation in transpressional wrench settings, based on dynamically scaled sand-silicone models. The

experimental results are confronted with the structural grain of the Rhine-Bresse transfer zone, which bears evidence for transpressional fault reactivation since the Neogene. The study gives insight on fault reactivation in brittle-viscous systems. It shows that the "basement-triggered" fault reactivation in a brittle cover separated from the basement by a viscous décollement layer is strongly dependent on the coupling between cover and base across the décollement.

The first author has designed the experimental setup and performed all the experiments himself. The second author has contributed by giving practical hints on the experimental design and on kinematic aspects. He has furthermore helped interpreting the experimental results. The third author has contributed to the regional geological context and has corrected early versions of the manuscript. The fourth author has assisted in the experimental part of the study.

Chapter 6:
Post-Late Pliocene to recent thick-skinned tectonics at the southern end of the Upper Rhine Graben

This chapter represents a yet unperfected manuscript that is also intended for publication. It provides additional evidence for Post-Late Pliocene thick-skinned tectonics in the southernmost Upper Rhine Graben by combining results from outcrop fault-slip data, geomorphology, subsurface and geophysical data. A newly compiled map of the Base-Tertiary surface, covering much of the southernmost graben, reveals the compressive and/or transpressive reactivation of basement faults. Furthermore, estimates on the displacement rates since the Late Pliocene are made based on a restoration of the base of folded Late Pliocene gravels. Relying on the contour map of the Late Pliocene gravels presented in chapter 4, this thesis' author has performed all the additional interpretation of surface and subsurface data himself.

Chapter 7: summary

This chapter summarises the results described in the previous chapters and raises a few points for future research.

Appendix 1

Selected original and interpreted reflection seismic sections and logs of exploration wells used for seismic reflector correlations and for the construction of subsurface maps.

Appendix 2

This section presents the results of joint measurements performed in the Late Pliocene Sundgau gravels.

Contents

Chapter 1 - Introduction

1.1. Objectives of this thesis

The assessment of earthquake hazard for a given region usually starts with the identification of the tectonic framework (geometry, kinematics and spatial pattern of faults as sources of seismic energy release). In this process, the recognition of neotectonic activity is of predominant importance. However, since geological structures have a polyphase history in most cases, their kinematics may change repeatedly through time in response to changing stress fields. As a result, current fault kinematics are often difficult to unravel.

It is furthermore of paramount importance in seismic hazard assessment whether neotectonic deformation is primarily thin-skinned or thick-skinned, i.e. whether deformation is restricted only to a relatively thin sedimentary succession above a certain detachment layer or whether it includes the crystalline basement. Solving these questions is particularly difficult in intraplate settings that are characterised by relatively low strain rates and low to moderate seismicity.

It is the scope of the present thesis to document the role of various crustal-scale faults under changing kinematic scenarios. This study was performed at the junction between the Upper Rhine Graben and the Jura Mountains, an area where the European Cenozoic rift system interferes with the northern Alpine foreland. The area was chosen because of its ongoing tectonic activity, manifested not only by instrumentally recorded seismicity but also by several harmful earthquakes that affected e.g. the city of Basel in historical times.

The envisaged problems were tackled by integrating various geological and geomorphologic observations with available subsurface data and information on the recent stress field.

The present study was carried out in the framework of both the EUCOR-URGENT and ENTEC research initiatives. EUCOR-URGENT (Upper Rhine Graben: Evolution and Neotectonics) is a collaborative network of 25 Universities and governmental agencies from Germany, France, the Netherlands and Switzerland, whose focus was on the seismic hazard and neotectonics in the Upper Rhine Graben and surrounding areas, as well as on the sustainable management of the water resources in its Tertiary to Quaternary graben fill. EUCOR-URGENT was launched in 1999 for a period of four years. Similarly, the multinational interdisciplinary ENTEC (ENvironmental TECtonics) research and training network, funded by the European Community and – for the participants from Swiss research institutions – the Swiss Ministry for Education and Science (BBW), addressed relationships between deeper lithospheric processes, neotectonics and surface processes in the Northern Alpine foreland. ENTEC was initiated in spring 2001 by a consortium of the Netherlands Research Center for Integrated Solid Earth Science, Basel University, Freiburg University, Karlsruhe University, Strasbourg University, ETH Zürich, BRGM, TNO-NITG and Vienna

University. Its objectives were to quantify the effects of the ongoing Alpine collision on intraplate deformation of the northwestern European foreland and their impact on surface geomorphology and natural hazards. Three natural laboratories were selected: 1) the Lower Rhine Graben, 2) the Upper Rhine Graben and 3) the Vienna Basin. These three areas record the manifestation of neotectonics within the Alpine orogen (the Vienna Basin), at its front (the Upper Rhine Graben) and in a far field area (the Lower Rhine Graben). All three are the sites of some of the highest concentrations of industrial activity and urban development in Europe.

1.2. Geological frame

The Upper Rhine Graben (URG) forms part of the western European Cenozoic rift system (Fig. 1.1). This rift system extends from the North Sea into the Mediterranean Sea and comprises (from north to south) the Lower Rhine Embayment, the URG, the Bresse Graben, as well as the Limagne graben system in the Massif Central. Morphologically, the URG forms a very conspicuous part of this rift system. This is particularly true for its southern part, where the URG forms a distinct plain surrounded by the Vosges and Black Forest massifs in the west and east, respectively, and the Jura Mountains in the south.
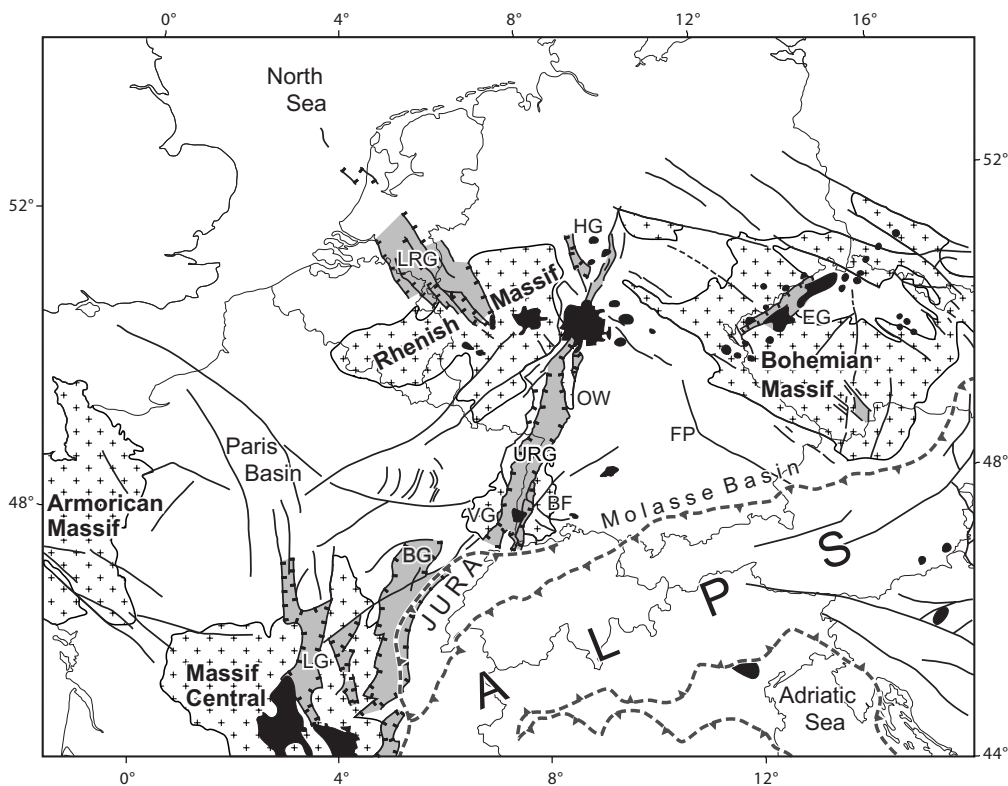
Fig. 1.1: the European Cenozoic rift system (grey shading). Crosshatch pattern: Variscan massifs. Black: Late Cretaceous to Cenozoic volcanics. BF = Black Forest, BG = Bresse Graben, FP = Franconian platform, EG = Eger Graben, HG = Hessen Graben, LG = Limagne Graben, LRG = Lower Rhine Graben, OW = Odenwald, URG = Upper Rhine Graben, VG = Vosges. After Ziegler et al. (2004).

At present, the southern URG is an area of increased seismicity (Fig. 1.2). The city of Basel, for instance, has been repeatedly harmed by earthquakes in historical times. The most severe earthquake occurred in 1356 AD and resulted in the almost complete destruction of the city. Nowadays, the region is highly urbanised and hosts numerous industrial facilities. It is therefore considered highly vulnerable to earthquakes. Despite dedicated research (Meyer et al., 1994; Nivière and Winter, 2000; Meghraoui et al., 2001; Lambert et al., 2005), the seismic source of the 1356 AD earthquake (strike slip, thrust or normal faulting? reactivation of Oligocene or Permo-Carboniferous faults?) has not yet been unambiguously identified.
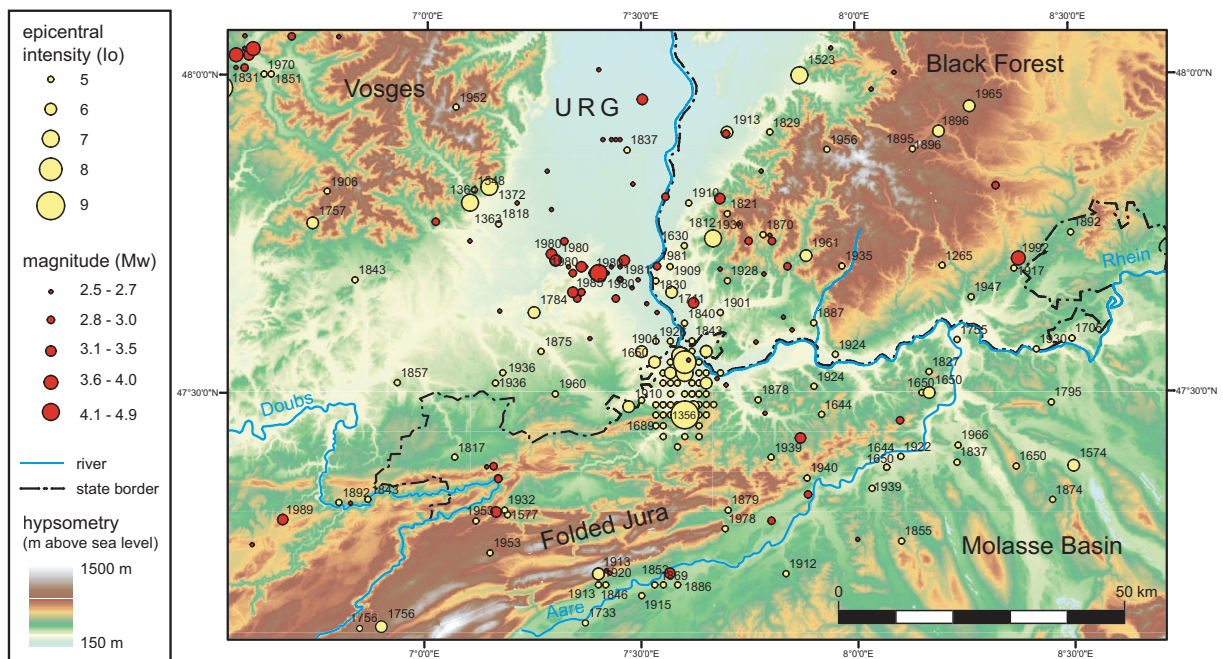
Fig. 1.2: distribution of seismicity in the southernmost URG and adjacent areas, superposed onto a digital elevation model. Yellow dots: historically recorded seismicity since 1300 AD, red dots: instrumentally recorded seismicity (with moment magnitudes equal or greater than 2.5) between 1980-2002. The sizes of the dots of epicentral intensities and moment magnitudes are scaled such that the energy release is comparable. The historically recorded seismicity is clearly concentrated in the SE corner of the URG, the strongest recorded event being the 1356 AD Basel earthquake. Data source: Swiss Seismological Service (2003).

1.2.1. Structure of the southern URG

The geological-tectonic framework of the southern URG and its surroundings are illustrated in Fig. 1.3. The structure of the southernmost URG can be depicted in a WNW-ESE-trending crustal-scale cross section, compiled from various sources (Fig. 1.4). The faults and the depth of the base-Tertiary surface in the westernmost part of the section were taken from a structural model developed at the CRNS in Nancy (Bourgeois et al., 2004). The geometry of the Illfurth fault was modified after Vonderschmitt (1942). The structure of the entire Ferrette Graben and the western part of the Allschwil Graben are based on own interpretations of reflection seismic and exploration well data. From the Allschwil Fault to the eastern end of the cross section, other existing cross section have been adapted (Gürler et al., 1987).
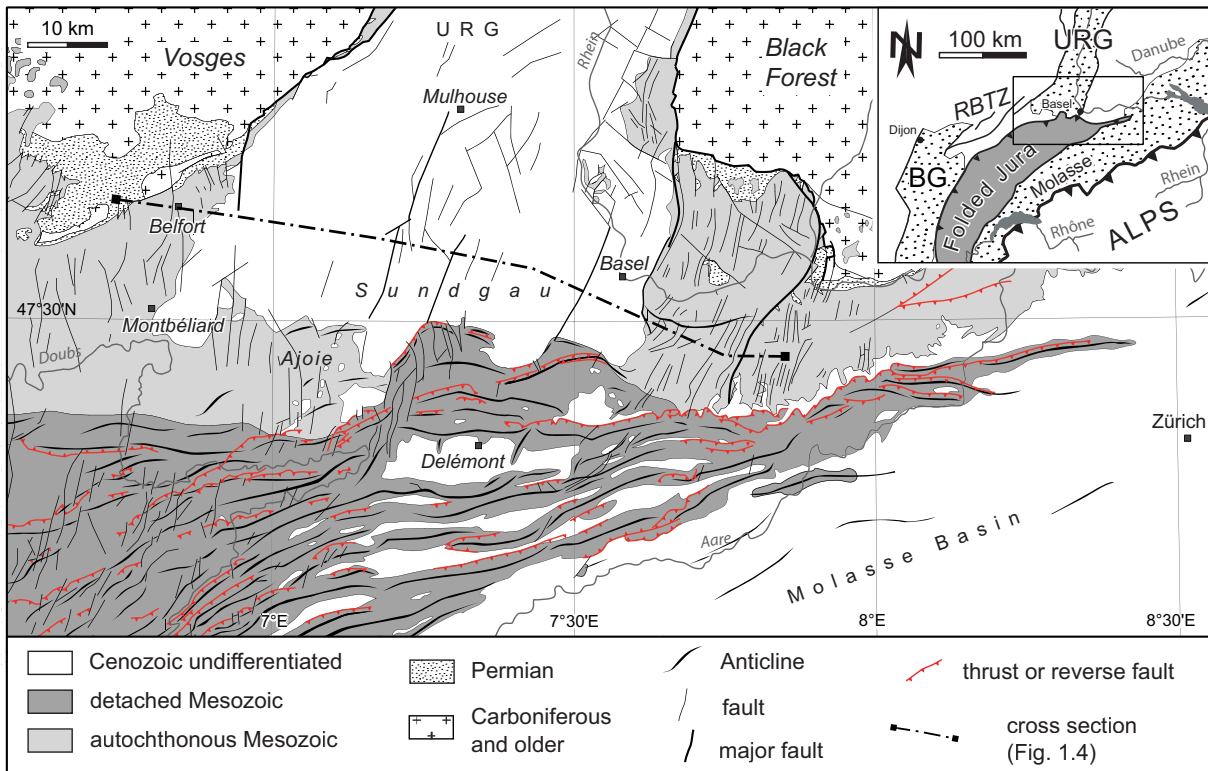
Fig. 1.3: tectonic map of the southern end of the URG and adjacent areas. Geographical names are set in italics.

Twelve exploration wells are aligned along or projected into the cross section, respectively, and constrain the thickness of the Tertiary syn-rift and Mesozoic pre-rift sediments. The thickness of the Permian sediments has been implemented from Boigk and Schöneich (1970) and Häring (2003). The position of the upper crust – lower crust boundary, believed to coincide with the brittle-ductile transition by many (but not all) authors, is constrained for the easternmost part of the section only (Bonjer, 1997; Laubscher and Noack, 1997; Mayer et al., 1997) and was extrapolated onto the rest of the section. The depth of the MOHO is taken from Dèzes et al. (2004).

The southernmost URG essentially consists of four E-dipping half-grabens, each of them bounded by a W-dipping normal fault. The presence of these half-grabens implies a slightly listric geometry of the half-graben bounding normal faults. Presumably the detachment horizon for these listric faults is found near the brittle-ductile transition. The syn-rift sediments in the hanging-wall of the half-grabens show a wedge-shaped geometry, tapering out towards W.

Rift-related subsidence started in the Late Priabonian and more or less simultaneously in all four half-grabens. The area of strongest rift-related subsidence is found in the Dannemarie Basin in the W, where more than 1000 m of syn-rift sediments, including evaporites and basinal marls have been deposited. E of the Illfurth fault, only up to a few hundreds of metres of syn-rift sediments are preserved. There, the sedimentary facies indicates that the Late Priabonian to Early Rupelian sediments were deposited under shallow water to even terrestrial conditions. This suggests that this area was already in a "horst"-like
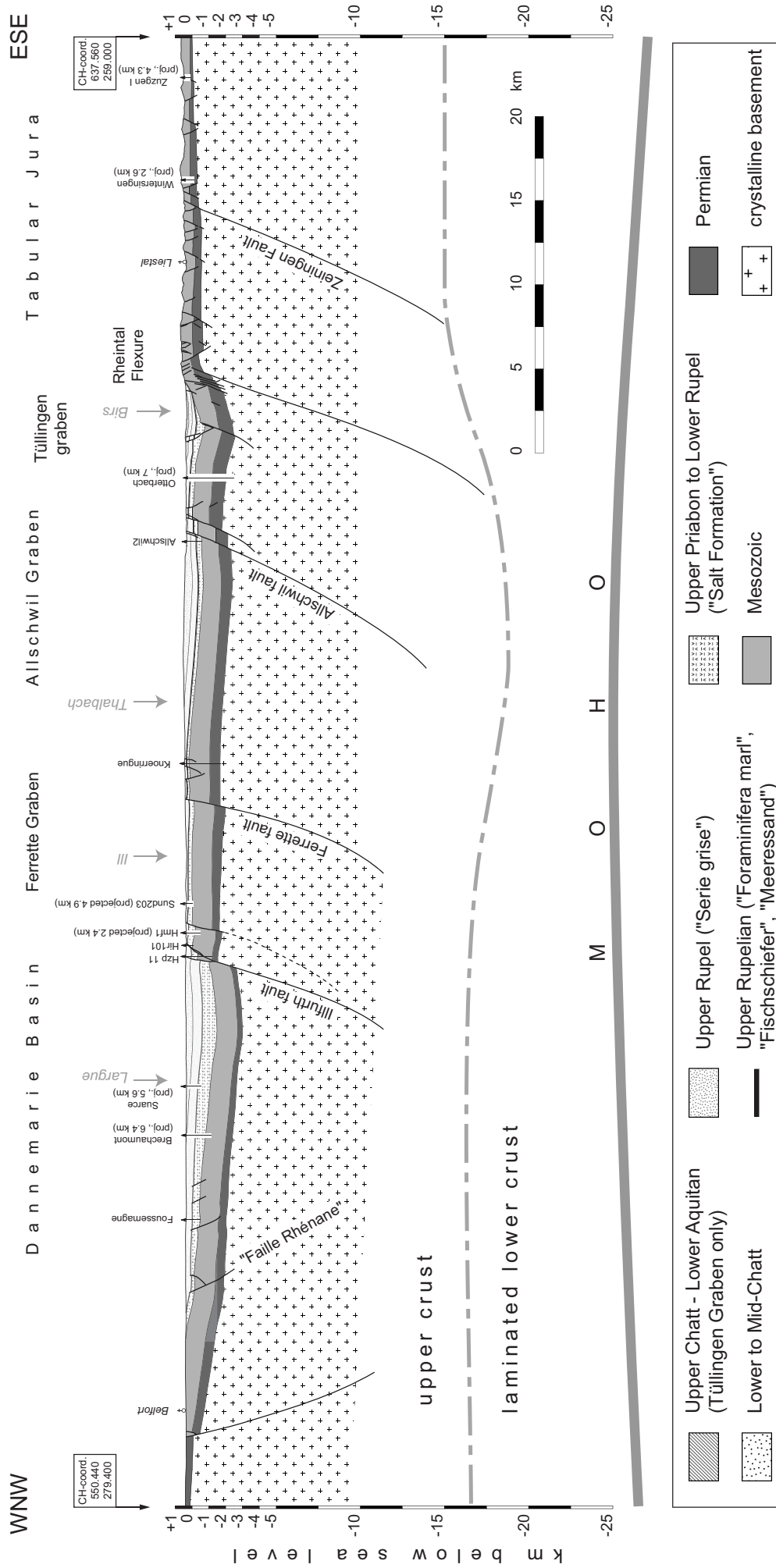
Fig.1. 4: crustal-scale cross-section across the southernmost URG. Geographic names are in italics. See Fig. 1.3 for location of the section. Refer to the text for details.

position at the time of rifting. However, a uniform "Mulhouse horst" extending between the Illfurth fault and to the east of borehole "Knoerringue", presented by earlier authors (Sittler, 1969; Doebl, 1970), does not exist. Rather, this area consists of another E-ward tilted half-graben, delimited by the Ferrette fault, which apparently was not recognised by previous workers.

The Allschwil graben further to the east essentially displays the same geometry as the Dannemarie Basin, but with decreased thickness of the syn-rift sediments. East of the Allschwil fault, another half-graben is found: the Tüllingen graben. Here, the youngest syn-rift sediments of the southernmost URG of Late Chattian to possibly Early Aquitanian age are preserved in the so-called Tüllingen syncline. The Tertiary sediments taper out along the Rheintal Flexure, which is underlain by a major W-dipping basement fault. Most presumably this basement fault represents the graben-bounding master fault at the southern end of the URG and concentrates a great amount of current seismicity.

E of the Rheintal flexure, numerous narrow grabens are present, which are mostly restricted to the sedimentary cover. These grabens contain mostly Mesozoic sediments only, whereas Tertiary sediments have been largely eroded and are only occasionally preserved. The observation that the faults bounding these narrow grabens often converge in a Mid-Triassic décollement suggests that the narrow grabens have formed during Palaeogene extension due to the stretching of the Mesozoic sedimentary cover between the graben-bounding Rheintal Flexure and a major breakaway further E, the basement-rooted Zeiningen fault (Laubscher, 1982).

The extension stored in the cross section (Fig. 1.4) is estimated quickest by comparing the deformed and restored lengths of reference horizons between two "pin points". Here, the top of the Mesozoic succession was chosen as such a reference horizon, because its position is well constrained from subsurface data across the largest part of the cross section. By assuming a constant thickness of the Mesozoic succession, the top Mesozoic horizon was then extrapolated onto those parts of the cross section, where it has already been eroded. This needed to be applied only to the western and eastern ends of the cross section, respectively. Fig. 1.5 shows the deformed and restored lengths of the top Mesozoic horizon, measured between a western pin point, which coincides with the western end of the cross section, and an eastern pin point, situated 3 km E of the Zeiningen Fault. The positive length change equals the extension amount and is on the order of 4 km. Dividing the length change by the restored length gives an extension e of +5.3%. Taking a time interval of 7 Ma for the main subsidence pulse in the southern URG, the corresponding strain-rate can be estimated to be on the order of 10^{-16} s^{-1}. These calculations show that the southern URG is both a low strain and low strain-rate rift.

top Mesozoic

surface topography

+1 0 -1 -2 -3 -4 -5 km

0 5 10 15 20 km

l_1 = 80.33 km

l_0 = 76.31 km

Δl = +4.02 km

$$e = \frac{\Delta l}{l_0} = + 5.3\ \%$$

$$\dot{e} = \frac{e}{t} = 2.5 * 10^{-16}\ s^{-1} \quad (t = 7\ Ma)$$

l_1 ... deformed length Δl ... length change $\dot{e}$ ... strain-rate
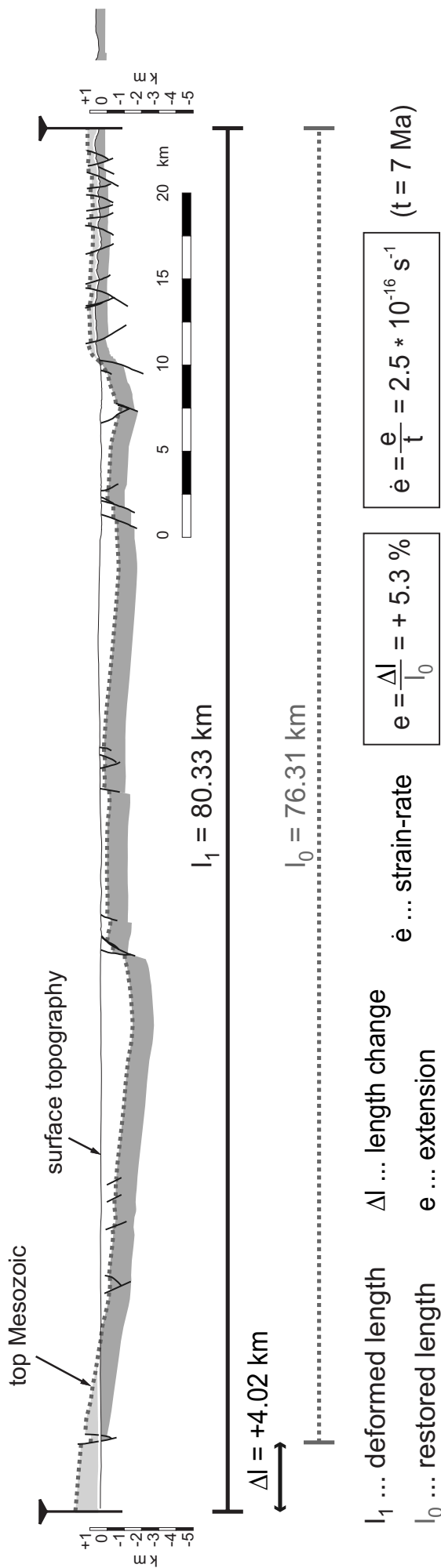
l_0 ... restored length   e ... extension

Fig. 1.5: line-length-restored version of the cross-section in Fig. 1.4. The restored line is the Top of the Mesozoic.

References

Boigk, H. and Schöneich, H., 1970. Die Tiefenlage der Permbasis im nördlichen Teil des Oberrheingrabens. In: J.H. Illies and S. Mueller (Editors), Graben Problems. Proceedings of an International Rift Symposium held in Karlsruhe 1968, International Upper Mantle Project. E. Schweitzerbart'sche, Stuttgart, pp. 45-55.

Bonjer, K., 1997. Seismicity pattern and style of seismic faulting at the eastern borderfault of the southern Rhine Graben. Tectonophysics, 275: 41-69.

Bourgeois, O., Le Carlier de Veslud, C., Ford, M. and Diraison, M., 2004. 3D modelling of the Dannemarie Basin, Nancy, http://www.crpg.cnrs-nancy.fr/MODEL3D/rhine.html.

Dèzes, P., Schmid, S.M. and Ziegler, P.A., 2004. Evolution of the European Cenozoic Rift System: interaction of the Aalpine and Pyrenean orogens with their foreland lithosphere. Tectonophysics, 389: 1-33.

Doebl, F., 1970. Die tertiären und quartären Sedimente des südlichen Rheingrabens. In: J.H. Illies and S. Mueller (Editors), Graben Poblems. Proceedings of an International Rift Symposium held in Karlsruhe October, 10-12, 1968. E. Schweitzerbart'sche, Stuttgart, pp. 56-66.

Gürler, B., Hauber, L. and Schwander, M., 1987. Die Geologie der Umgebung von Basel mit Hinweisen über die Nutzungsmöglichkeiten der Erdwärme, Schweizerische Geologische Kommission, Bern.

Häring, M., 2003. Das Neueste zum Projekt Deep Heat Mining in Basel, http://www.geothermal.ch/Einstieg_ d.html.

Lambert, J., Winter, T., Dewez, T. and Sabourault, P., 2005. New hypotheses on the maximum damage area of the 1356 Basel earthquake (Switzerland). Quaternary Science Reviews, 24: 381-399.

Laubscher, H., 1982. Die Südostecke des Rheingrabens - ein kinematisches und dynamisches Problem. Eclogae Geologicae Helvetiae, 75(1): 101-116.

Laubscher, H. and Noack, T., 1997. The deep structure of the Basel Jura. In: O.A. Pfiffner, P. Lehner, P. Heitzmann, S. Mueller and A. Steck (Editors), Deep structure of the Swiss Alps. Results of NRP 20. Birkhäuser, pp. 54-58.

Mayer, G., Mai, P., Plenefisch, T., Echtler, H., Lueschen, E., Wehrle, V., Mueller, B., Bonjer, K., Prodehl, C. and Fuchs, K., 1997. The deep crust of the Southern Rhine Graben: reflectivity and seismicity as images of dynamic processes. Tectonophysics, 275: 15-40.

Meghraoui, M., Delouis, B., Ferry, M., Giardini, D., Huggenberger, P. and Spottke, I., 2001. Active normal faulting in the Upper Rhine Graben and paleoseismic identification of the 1356 Basel earthquake. Science, 293: 2070-2073.

Meyer, B., Lacassin, R., Brulhet, J. and Mouroux, B., 1994. The Basel 1356 earthquake: which fault produced it? Terra Nova, 6: 54-63.

Nivière, B. and Winter, T., 2000. Pleistocene northwards fold propagation of the Jura within the southern Upper Rhine Graben: seismotectonic implications. Global and Planetary Change, 27: 263–288.

Sittler, C., 1969. Le Fossé Rhénan en Alsace. Aspect structural et histoire géologique. Revue de Géographie physique et de Géologie dynamique (2), 11(5): 465-494.

Swiss Seismological Service, E.T.H.Z., 2003. ECOS - Earthquake Catalog of Switzerland, Swiss Seismological Service, http://seismo.ethz.ch/.

Vonderschmitt, L., 1942. Die geologischen Ergebnisse der Bohrungen von Hirtzbach bei Altkirch (Ober-Elsass). Eclogae Geologicae Helvetiae, 35(1): 67-99.

Ziegler, P.A., Schumacher, M.E., Dèzes, P., van Wees, J.-D. and Cloetingh, S., 2004. Post-Variscan evolution of the lithosphere in the Rhine Graben area: constraints from subsidence modelling. In: M. Wilson (Editor), Permo-Carboniferous magmatism and rifting in Europe. Geological Society of London Special Publications. Geological Society, pp. 289-317.

Chapter 2 -

Simultaneous normal faulting and extensional flexuring during rifting - an example from the southernmost Upper Rhine Graben

Kamil Ustaszewski , Markus E. Schumacher, Stefan M. Schmid

Abstract

The southern end of the Upper Rhine Graben is formed by a major continental transfer zone, which was localised by the reactivation of ENE-oriented basement faults of Late Palaeozoic origin. A combination of subcrop data (derived from exploration wells and reflection seismic lines) and palaeostress analysis provided new constraints on the timing and kinematics of interacting basement faults. Rifting in the southern Upper Rhine Graben began in the Upper Priabonian under regional WNW-ESE-directed extension, oriented roughly perpendicular to the graben axis. In the study area this led to the formation of NNE-trending half-grabens. Simultaneously, ENE- trending basement faults, situated in the area of the future Rhine-Bresse Transfer Zone, were reactivated in a sinistrally transtensive mode. In the sedimentary cover the strike-slip component was accommodated by the development of en-échelon aligned extensional flexures. Flexuring and interference between the differently oriented basement faults imposed additional, but locally confined extension in the sedimentary cover, which deviated by as much as 90° from the regional WNW-ESE extension. The interference of regional and local stresses led to a regime of radial extension at the intersection between the Upper Rhine Graben and Rhine-Bresse Transfer zone.

Keywords: *extension, fault reactivation, Upper Rhine Graben, Rhine-Bresse Transfer zone, palaeostress analysis*

2.1 Introduction

2.1.1 Objectives and previous work

The N- to NE-trending Bresse- and Upper Rhine Graben (URG) structures (top right inset in Fig.1) form the central segments of the European Cenozoic rift system. Their simultaneous opening was kinematically linked by activity along the Rhine-Bresse Transfer Zone (RBTZ), which formed along pre-existing, ENE- to NE-oriented crustal discontinuities, inherited from the Variscan orogeny and subsequent (Late Carboniferous to Permian)

post-orogenic transtension (Laubscher 1986; Ziegler 1992; Schumacher 2002). Transfer of rifting from the Bresse Graben to the URG implies sinistral motions along the RBTZ (Laubscher 1972; Laubscher 1973; Illies 1981; Ziegler 1992). The analysis of striated faults in the Mesozoic to Cenozoic cover revealed that Eo-/Oligocene extension across the Bresse and Upper Rhine Graben, as well as in the RBTZ, occurred under a WNW-ESE oriented minimum principal stress $\sigma3$, perpendicular to the graben axis (Bergerat 1987; Larroque and Laurent 1988; Lacombe et al. 1993). Due to the inaccessibility of the basement in the RBTZ, the kinematics of basement faults in this zone were inferred indirectly, for instance from comparison with analogue models of oblique rift systems. Extension applied obliquely to the external boundaries of models built above two diverging basal sheets, produces steeply dipping en-échelon faults (Elmohandes 1981; Tron and Brun 1991; McClay et al. 2002). Such models imply transtensional reactivation of the basal discontinuity and yield fault patterns comparable to those encountered in the RBTZ. Consequently, it was argued that the fault pattern in the RBTZ formed in response to regional-scale sinistral transtensional reactivation of ENE- to NE-oriented basement faults trending obliquely to the extension direction (Lacombe et al. 1993).

The aim of this study is to provide further constraints on the kinematics, the stress field and the interaction of differently oriented faults in response to Palaeogene rifting. Subsurface information, derived from industry type reflection seismic lines and well logs, was compiled into new subcrop maps and combined with kinematic analyses from faults collected in the sedimentary cover. This led to the development of a new kinematic model for the Palaeogene rifting episode. Our model emphasises the importance of pre-existing faults and illustrates the simultaneous interaction between differently oriented basement faults at the transition from the URG to the RBTZ.

2.1.2 Geological setting

The area investigated in this study is located at the junction between the southernmost URG and the RBTZ (top right inset in Fig. 1). The southern part of the Tertiary fill of the URG is juxtaposed against autochthonous and detached Mesozoic sediments (Fig. 1). These sediments overlie a Palaeozoic basement (comprising clastic and volcanoclastic lithologies of Devonian to Upper Permian age), outcropping in the Vosges and Black Forest massifs. The Mesozoic cover ranges in age from Lower Triassic to Upper Jurassic. In northern Switzerland, the autochthonous Mesozoic cover is usually referred to as Tabular Jura due to the sub-horizontal orientation of the sediments of predominantly Jurassic age. The Mesozoic of the Folded Jura has been detached along Mid- and Upper Triassic evaporites during Upper Miocene to Lower Pliocene thin-skinned folding and thrusting. Cenozoic sediments (Eocene to Quaternary) not only constitute the fill of the URG, but are also preserved in basins and grabens within the Tabular Jura, as well as in intra-montane synclines within the Folded Jura. The largest of these synclines is the lozenge-shaped Delémont Basin (Fig. 1). The eastern

and western borders of the URG are characterised by discrete faults. The Dannemarie Basin ("DM" in Fig. 1) is the area of largest rift-related subsidence in the southernmost URG and is bounded in the east by the Illfurth fault ("IF"). Additional important faults located within the graben further to the east are the Ferrette ("Fe") and the Allschwil ("Al") faults.

The overall E-W-trending southern graben border, on the other hand, is formed by extensional flexures (monoclines) and/or compressional anticlines. The flexures formed during Eo-/Oligocene rifting. They were partly reactivated in post-Oligocene times under compression in conjunction with Jura folding (Ferrette and Landskron anticlines). Of particular interest to this study is the en-échelon alignment of two gentle anticlines further to the west: the so-called Florimont and Réchésy (labelled "F" and "R" in Fig. 1, respectively), which formed by reactivation of formerly extensional flexures (Giamboni et al. 2004). The E-W-trending southern border of the URG is interrupted by three conspicuous embayments, containing Tertiary sediments, which encroach southward on the Jura domain (Fig. 1). Numerous N- to NNE-, ENE- and subordinately NW-striking normal faults dissect the Mesozoic series of the Tabular Jura and the Tertiary fill of the URG.
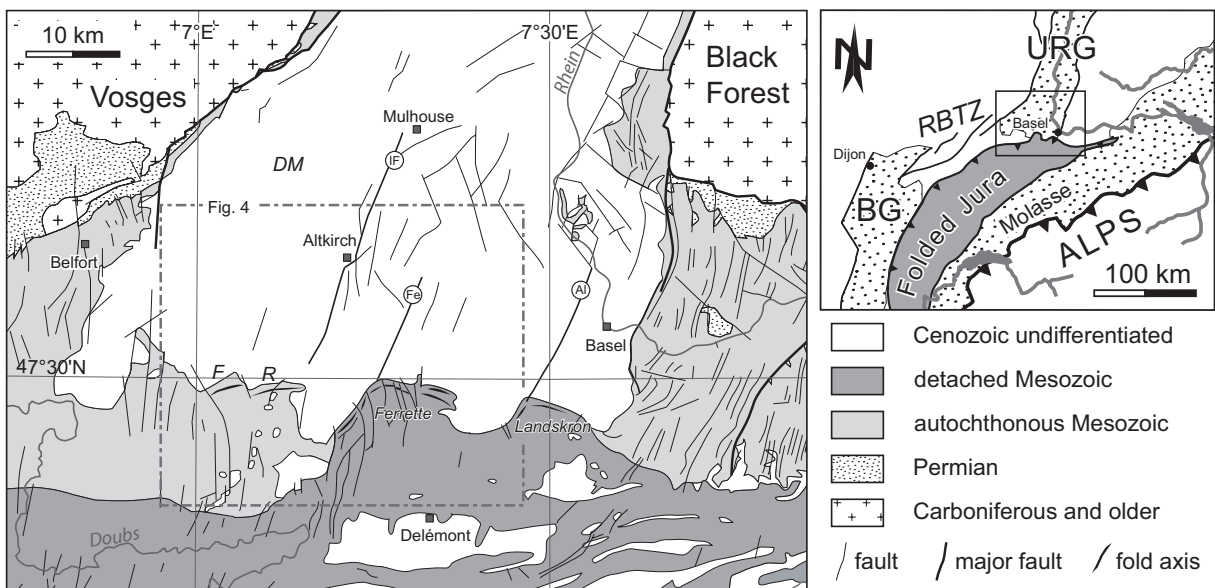
Fig. 1: Geologic-tectonic map of the southernmost Upper Rhine Graben and adjacent areas. Al = Allschwil Fault, DM = Dannemarie Basin, F = Florimont flexure, Fe = Ferrette fault, IF = Illfurth Fault, R = Réchésy flexure. Fold axes are only shown along the Jura front. Neogene thrusts are not shown. Top right: BG = Bresse Graben, RBTZ = Rhine-Bresse Transfer Zone, URG = Upper Rhine Graben.

2.1.3 Palaeogene rifting

Rift-related subsidence of the southern URG began in Late Eocene times and persisted until the Late Oligocene to Early Miocene (Pflug 1982). During an initial phase of rifting, half-grabens and gentle flexures formed in conjunction with W-dipping NNE-SSW-striking normal faults. Flexures formed also along the southern border of the URG (Liniger 1970a; Laubscher 1982; Fig. 1). While partly bituminous marls and evaporites accumulated in the Mulhouse and Dannemarie basins (Salt Formation; Doebl 1970; Sissingh 1998), fresh-

to brackish-water and even terrestrial sedimentation prevailed on horsts in the southernmost graben part ("Melania limestone" Member of the Lower Salt Formation, "Haustein" Member of the Upper Salt Formation; Sissingh 1998). Coarse conglomerates formed along the graben margins in response to increasing uplift and erosion of the rift flanks (Duringer 1988). This style of sedimentation persisted until the Lower Rupelian (Duringer 1988; Picot 2002).

Full marine conditions were not established before the Upper Rupelian transgression of the "Foraminifera Marl", "Fischschiefer", and "Meletta beds" (Fischer 1965a; Fischer 1969; Duringer 1988). These sediments grade southward into thin-bedded, compact calcarenites, the so-called "Meeressand", indicating coastal facies (Fischer 1965a). The spatial distribution of the Upper Rupelian sediments includes domains within the Tabular and Folded Jura as far south as the Delémont Basin (Fig. 1). During the Chattian, sedimentation once again became brackish ("Cyrena Marls") and eventually fluvio-lacustrine ("Alsacian Molasse"; Fischer 1965a; Fischer 1969). Upper Chattian to lowermost Aquitanian freshwater limestones formed in a period when connections to the marine realm were interrupted (Sissingh 1998).

During the Burdigalian, rift-related subsidence of the southern URG stopped and its sedimentary fill was subjected to erosion (Laubscher 1992; Dèzes et al. submitted). This erosion was related to the uplift of the Vosges-Black Forest arch, which developed either in response to the arrival of the northward migrating Alpine forebulge (Laubscher 1987; Laubscher 1992) or in response to lithospheric folding (Ziegler et al. in press). The uplift was associated with a change in the regional stress pattern from vertical $\sigma 1$ and WNW-ESE trending $\sigma 3$ to horizontal and NNW-SSE-trending $\sigma 1$ (Larroque and Laurent 1988). Marine Burdigalian sediments, unconformably overlying Chattian to lowermost Aquitanian freshwater limestones in the Delémont Basin, mark the transgression of the Upper Marine Molasse (OMM; Koch 1923). Hence, this transgression is by no means related to renewed extension in the Upper Rhine Graben, but rather to subsidence of the Molasse Basin in front of the advancing Alpine orogen (Sissingh 1998). This is clearly evidenced in the Tabular Jura east of Basel, where Eo-/Oligocene normal faults are unconformably overlain and sealed by the transgression of the OMM (Buxtorf 1901; Bitterli-Brunner 1988).

2.2 Control of Late Palaeozoic structures on Palaeogene rifting

The distribution of partly fault-controlled Permo-Carboniferous troughs in northern Switzerland and adjacent France and Germany is given in Fig. 2. The thickness of Carboniferous to Permian sediments (Boigk and Schöneich 1970; Boigk and Schöneich 1974) is constrained by outcrops (Lutz 1964) and by 22 exploration wells, some of which bottomed in the basement (Schmassmann and Bayramgil 1945; Diebold 1989; Häring 2003). The subsurface faults shown in Fig. 2 were adopted from French subcrop maps (Debrand-Passard and Courbouleix 1984), reports of the Swiss National Cooperative for Storage of
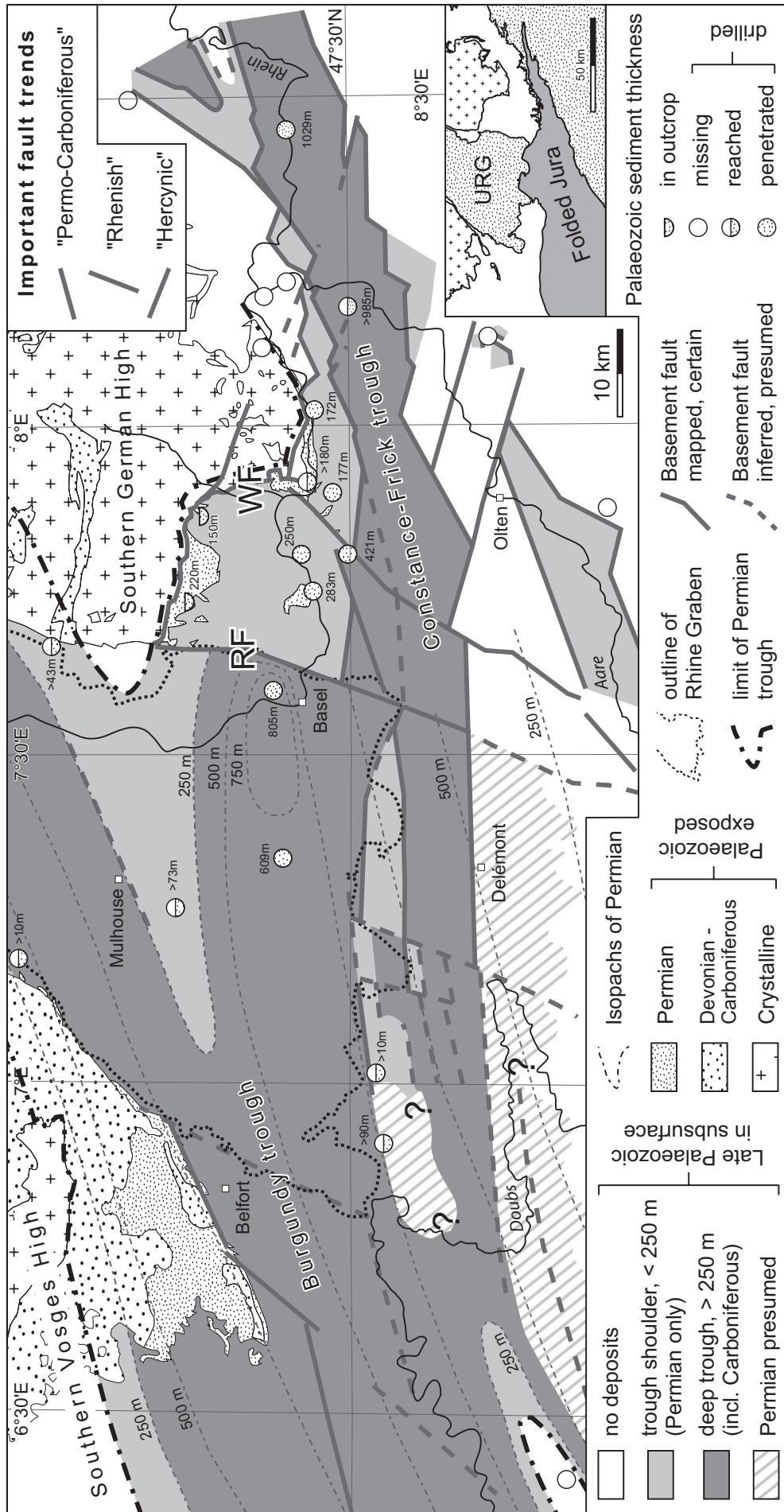
Fig. 2: Late Palaeozoic troughs and highs in the southernmost Upper Rhine Graben and adjacent areas. "RF" = Rhenish Fault, "WF" = Wehratal Fault. For orientation, the outline of the URG is shown by a black dashed line. Bottom right inset: overview map of present-day situation.

Nuclear Waste (Laubscher 1986; Sprecher and Müller 1986; Diebold 1989; Diebold and Naef 1990) and results of the Swiss National Research Program NRP20 (Diebold and Noack 1997; Laubscher and Noack 1997; Pfiffner et al. 1997). Isopachs and fault traces were locally modified according to our own observations.

The salient feature of Fig. 2 is the occurrence of a system of generally ENE-trending, narrow and elongated, predominantly fault-bounded troughs beneath the northern Folded Jura Mountains and their foreland. This 10-15 km wide trough system extends from Lake Constance in the east into the central part of Fig. 2 ("Constance-Frick trough") and is filled with up to 1000 m of Permo-Carboniferous clastic sediments. It follows the structural grain of the Variscan belt and developed in response to post-Variscan transtension (Ziegler 1990). Differential subsidence in these intramontane troughs ended in Mid-Permian times, giving way to regional thermal subsidence of the area (Ziegler et al. in press).

The western continuation of the Constance-Frick trough into the study area coincides with the southern termination of the URG and the location of the RBTZ. Due to the scarcity of well data in this area, the structure of this part of the trough is mainly constrained by reflection seismic data. In the southern Vosges further to the west, the thickness of Permo-Carboniferous sediments is constrained by outcrops. A distinction was made between "deep troughs" (thickness of Permian sediments >250 m) and "trough shoulders" (<250 m Permian). Despite limited well and seismic control it is obvious that the Constance-Frick trough links up with the southern branch of the Burgundy trough. Nevertheless, a narrow horst apparently separates the Burgundy and Constance-Frick trough in the area of the southernmost URG (Fig. 2). A large part of this Late Palaeozoic trough system terminates to the east at the NE- to N-trending Wehratal Fault ("WF" in Fig. 2). While Permian clastics are present below the Triassic Buntsandstein west of the WF, they are missing east of this fault, where Buntsandstein rests directly on the granitic basement of the Black Forest. This suggests Late Palaeozoic differential vertical motions across this fault.

The "Rhenish fault" ("RF" in Fig. 2) further to the west, was also active during the Late Palaeozoic and has a trend similar to the WF. Its location coincides with the eastern border fault of the southernmost URG. It also separates areas of contrasting thickness of Permo-Carboniferous sediments (i.e. >800 and <300 m west and east of the RF, respectively, see Fig. 2). The spatial coincidence of the Rhenish fault with the south-eastern border fault of the future URG illustrates that parts of it were localised along pre-existing Late Palaeozoic faults. Geomagnetic studies revealed other such NNE-trending Late Palaeozoic faults in the subsurface of the URG and in the Vosges and Black Forest (Edel and Fluck 1989). In the southern Black Forest Upper Carboniferous to Permian lamprophyres and aplitic dikes are subparallel to the URG (Werner and Franzke 2001 and references therein). Evidence for Mesozoic reactivation of Late Palaeozoic faults has recently been provided by stratigraphic investigations in the northern Swiss Jura Mountains where facies-boundaries between basins and highs tend to be aligned with the Rhenish fault and other features of the Permo-

Carboniferous trough (Allenbach 2000; Allenbach 2002; Wetzel et al. 2003).

In summary, the location of the southern end of the URG and its connection with the Bresse Graben via the RBTZ appears to be controlled by two pre-existing fault sets. A first set consists of ENE-trending faults, referred to as the "Permo-Carboniferous set", which, for example, delimits the small Palaeozoic high located between the western part of the Constance-Frick trough and the easternmost main part of the Burgundy trough. The second, "Rhenish" set refers to the NNE-trending faults. In the following we apply these terms also to fault sets that were active during Tertiary rifting, since localisation of the URG and the RBTZ was controlled by these Late Palaeozoic fault systems.

2.3 Subsurface data

2.3.1 Structure of the base of the Mesozoic surface

In order to define the structural configuration of the base of the Mesozoic surface (or base-Mesozoic surface for short), a contour map of this surface, including the fault trends dissecting it, was compiled. A network of industry-type reflection-seismic lines was analysed, covering an approximately 30 by 20 km wide area straddling the southernmost URG and the southward adjacent Tabular and Folded Jura (bottom centre inset in Fig. 3). Moreover, six exploration wells (Schmidt et al. 1924; BRGM unpublished) allowed the correlation of seismic reflectors with drilled lithologies (Fig. 3). Four of these wells penetrated the Tertiary fill and bottomed in Mesozoic sediments, whereas the other two reached Palaeozoic siliciclastics and/or the crystalline basement. The correlated logs of the penetrated Tertiary and Mesozoic sedimentary succession together with the observed seismic interval velocities of three of the wells are shown in Fig. 3. The base of the Mesozoic succession is often marked by an angular unconformity between Permian clastic series and the overlying basal Triassic Buntsandstein. The Mesozoic series exhibit a remarkably constant thickness, as evident from well logs and strictly parallel seismic reflections. Once the base of the Mesozoic had been identified (by finding the angular unconformity), it was extrapolated throughout the remaining part of a seismic section and subsequently onto intersecting lines. The top Mesozoic-unconformity is often marked by onlapping Tertiary reflections. Furthermore, this unconformity gives rise to a discrete reflector due to the high acoustic impedance contrasts between the uppermost Mesozoic and lowermost Tertiary layers.

After identification of the base of the Mesozoic on the seismic lines, its depth (in seconds two-way-travel time, s TWT) was plotted on a map and contoured manually. The resulting map (seismic reference datum at 500 m above sea level, Fig. 4) shows that the depth of the base-Mesozoic surface ranges from 0.55 to 1.3 s TWT in the mapped area. This corresponds to a depth range of between about 650 m and 1350 m below sea level, as calculated from seismic velocities obtained from the exploration wells Buix1 (base-Mesozoic
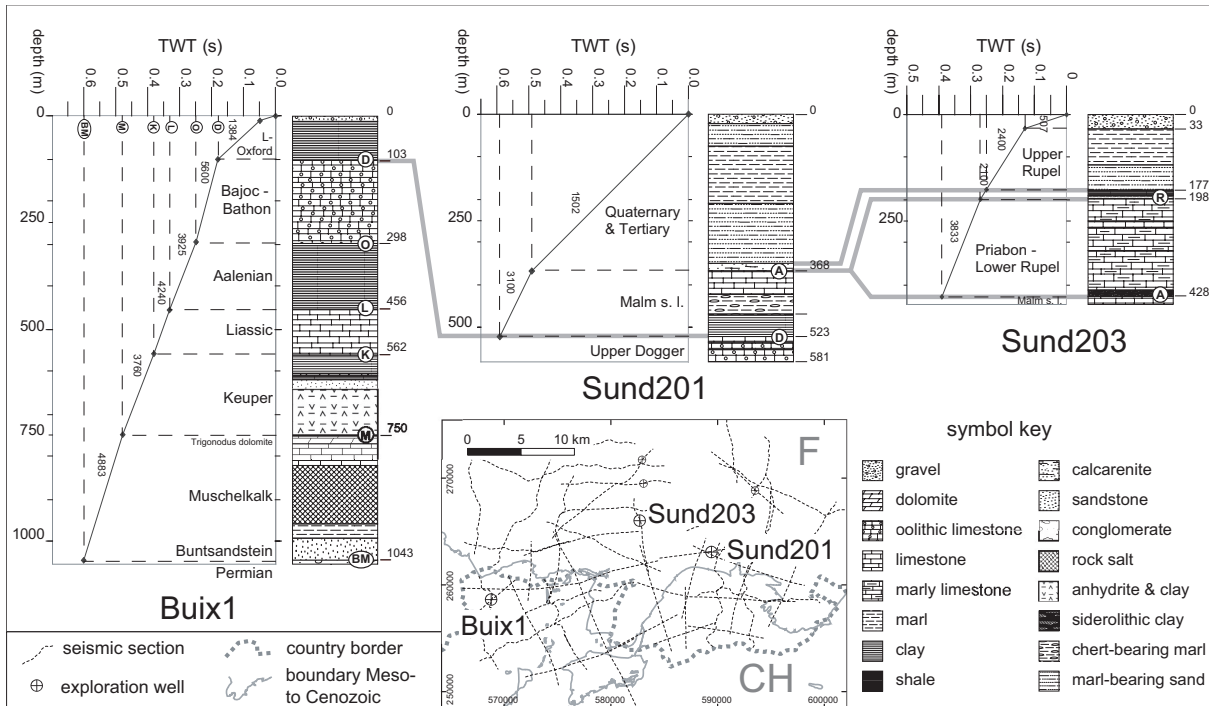
Fig. 3: Logs of three exploration wells in the study area, showing the Mesozoic to Palaeogene stratigraphy, plotted versus two-way travel times in seconds (s TWT). The resulting interval velocities are in metres per second. BM = base Mesozoic, M = top Muschelkalk, K = top Keuper, L = top Lias, O = top Aalenian, D = top Dogger, A = top Malm. The approximately 20 m thick Upper Rupelian interval (wells Sund201 and Sund203) corresponds to the most important reflector ("R") in the syn-rift sediments. Bottom centre inset: location of the investigated seismic lines and six explorations wells used. Numbers on map margin refer to Swiss National coordinates.
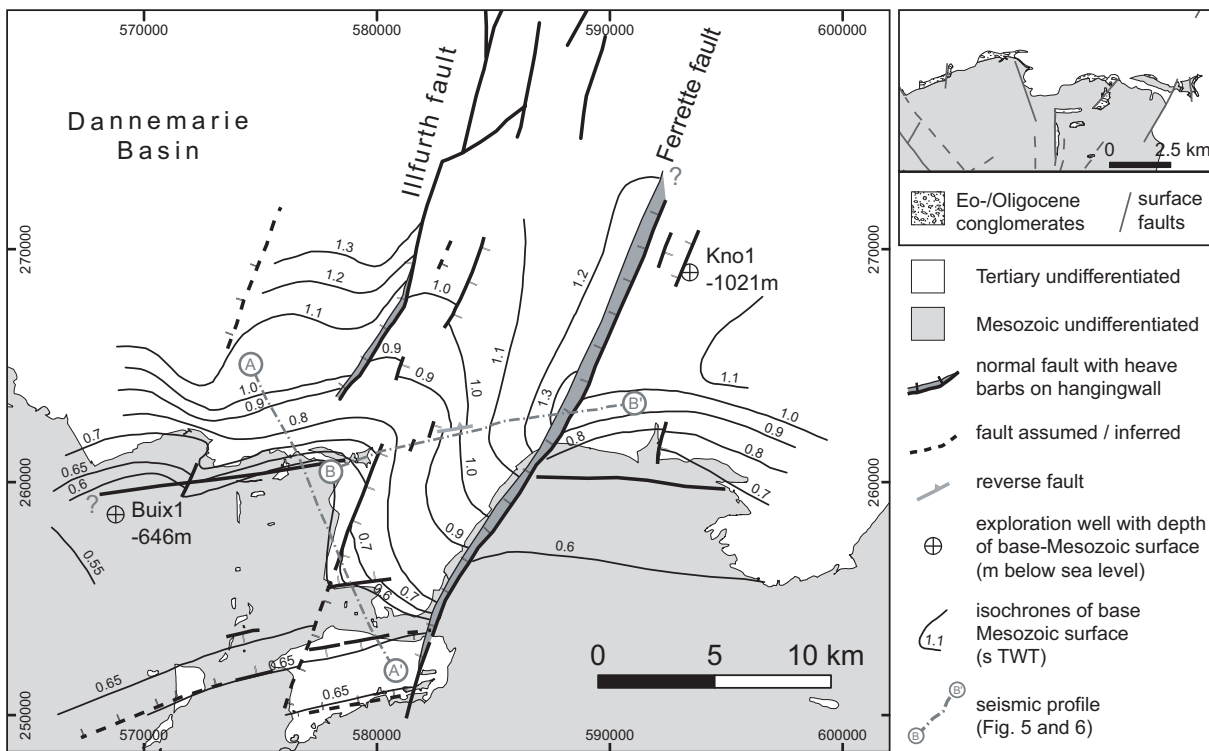
Fig. 4: Structural map of the base-Mesozoic surface in s TWT and dissecting faults. The reference datum is at 500 m above sea level. Numbers on map margin refer to Swiss National coordinates. Top right inset: distribution of Eo-/Oligocene conglomerates along the en-échelon flexures.

at 646 m below sea level) and Kno1 (base-Mesozoic at 1021 m below sea level), both of which had penetrated the base of the Mesozoic succession. The shallowest elevations of the base-Mesozoic surface are found beneath the exposed Mesozoic in the south, where this surface reveals only moderate relief. Substantial relief is observed in the area of the URG, where the base of the Mesozoic reaches its greatest depth in the Dannemarie Basin (Fig. 4).

Two sets of differently oriented normal faults dissect the base-Mesozoic surface: the Rhenish set, which trends NNE (N20°-30°), parallel to the URG, and the Permo-Carboniferous set, which trends ENE (N70°-80°), parallel to the Late Palaeozoic trough system (compare with Fig. 2). Fault heave is only significant along two of the mapped faults. The largest fault identified (Ferrette Fault, Fig. 4) can be traced for 25 km in a NNE-direction. It probably extends further south into the Folded Jura Mountains, as deduced from the parallelism between the fault trend and the strike of the western part of the conspicuously northward-protruding Neogene Ferrette anticline as well as from numerous minor faults in the detached Mesozoic (Fig. 1). The Ferrette Fault reveals a top-to-the-W normal fault geometry and forms the eastern boundary of an Eo-/Oligocene half-graben. The throw of this fault varies along strike, ranging from approximately 0.1 s TWT in the south to approximately 0.3 s TWT along its central parts, corresponding to values in the order of 170 to 500 m. Further to the north its throw diminishes again, suggesting a northward termination of the Ferrette Fault outside of the area mapped. Interestingly, the greatest throw is measured in the area of the along-strike prolongation of the ENE-oriented Florimont and Réchésy flexures (eastern part of profile BB' indicated in Fig. 4).

West and east of the Ferrette fault, additional NNE-trending normal faults were mapped, the most important of which is the "Illfurth Fault", delimiting the Dannemarie Basin to the east (Fig. 1). Interestingly, the throw of this fault progressively diminishes southwards, until it becomes insignificant along an ENE-oriented zone paralleling the en-échelon aligned flexures (Fig. 4).

The most important of the ENE-trending faults (Permo-Carboniferous set) is located beneath the Florimont and Réchésy flexures (Figs. 1, 4 and 5). Apart from the evidence provided by Fig. 5, its existence can be inferred from the en-échelon arrangement of the flexures, which indicates that an underlying basement fault accommodated sinistral wrench motions parallel to the RBTZ (Ustaszewski et al. in press). Other faults paralleling this trend, were identified further south within the autochthonous Mesozoic and along the northern and southern border of the lozenge-shaped Tertiary basin located at the southern end of profile AA' (Fig. 5). The amount of throw along the latter faults is in the order of 0.05 s TWT, corresponding to some 80-90 m.
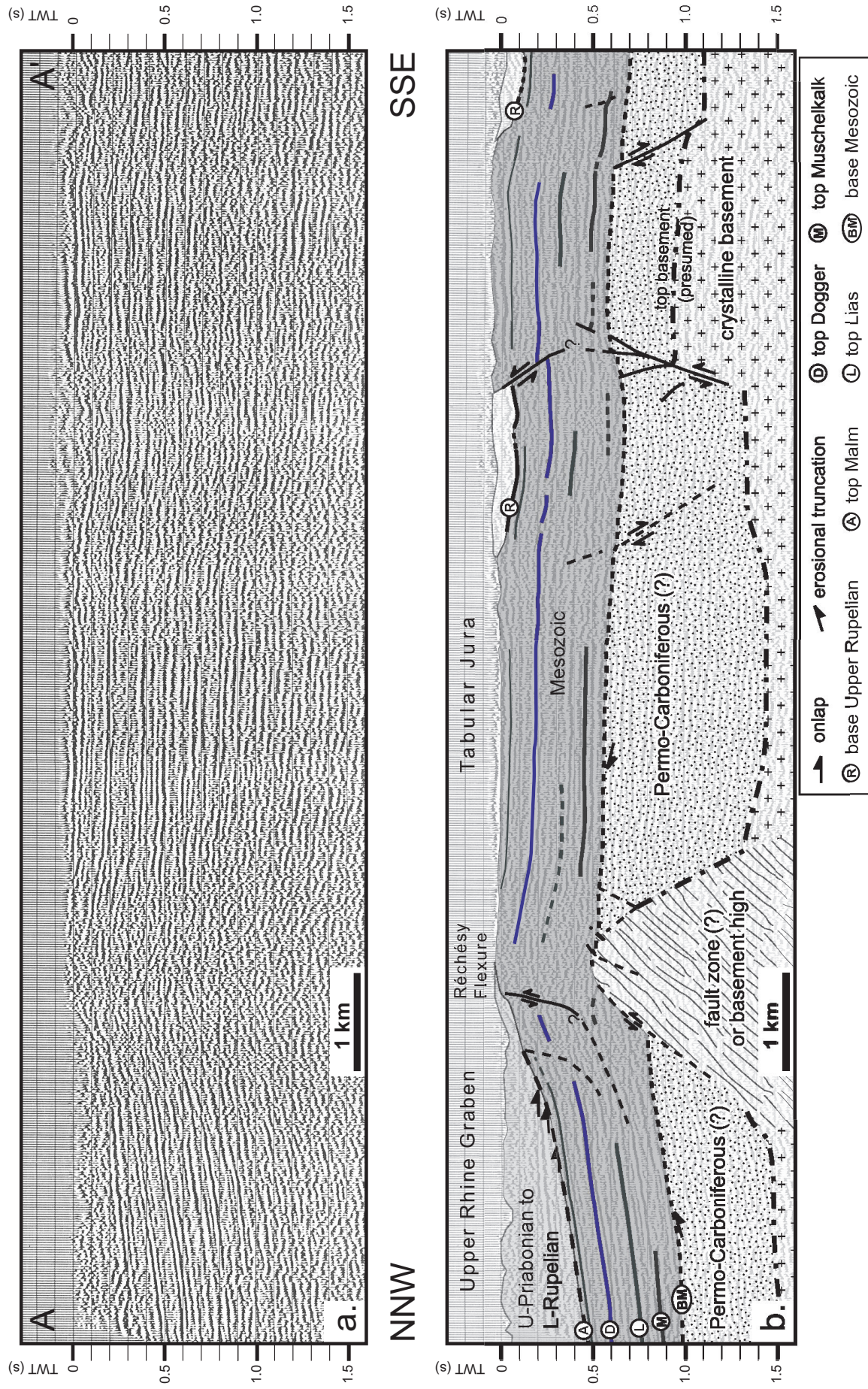
2.3.2 Seismic sections

Fig. 5 depicts a NNW-SSE-trending, 13.5 km long reflection-seismic profile that crosses the Réchésy flexure (see Fig. 1), located at the southern margin of the URG (for location see Fig. 4). North of the crest of the flexure, Mesozoic strata (characterised by strictly parallel reflections) dip uniformly to the north. Upper Priabonian to Lower Rupelian syn-rift sediments onlap the top-Mesozoic unconformity and wedge out along the northern flank of the flexure. Across the flexure's crest, Mesozoic seismic reflectors are intensely disturbed. The base of the Mesozoic is vertically offset across a relatively wide basement fault zone with a top to the north normal fault component that trends approximately ENE (Fig. 4). This fault zone presumably represents a reactivated Late Palaeozoic high angle basement fault, delimiting Permo-Carboniferous troughs and highs (see Fig. 2).

South of the hinge of the flexure, Mesozoic reflectors dip gently to the south. This is due to post-Late Pliocene reactivation and shortening that modified the formerly extensional flexure into a gentle anticline (Giamboni et al. 2004). Further south, in the Tabular Jura, characterised by sub-horizontal Mesozoic reflections, the seismic line runs across the southwestern end of a small Tertiary embayment. South of a gentle anticline (Vendlincourt anticline; Meyer et al. 1994), which inverts an approximately 2.5 km wide Mesozoic horst, Mesozoic reflectors again dip southward beneath the fill of a small intramontane Tertiary basin. The former Mesozoic horst north of this basin is bounded by ENE-trending basement faults. Again, these faults presumably formed during Permo-Carboniferous transtension, and were reactivated in extension during the Palaeogene. At the base of the Mesozoic level, their throw is in the order of c. 0.05 s TWT, corresponding to some 80-90 m.

Along the northern rim of the Florimont and Réchésy flexures, outcropping conglomerates consist exclusively of Upper Jurassic material (top right inset in Fig. 4). Sedimentological criteria indicate transport in wadi-like settings (Duringer 1988), whereas intercalations of calcarenites suggest deposition in a coastal environment. Biostratigraphic markers within lithologically identical conglomerates further south in the Tabular Jura testify to their Upper Priabonian to Lower Rupelian age (Picot 2002; Picot et al. in press). This indicates that the Florimont and Réchésy flexures started to form during the Upper Priabonian.

Fig. 6 shows a WSW-ENE oriented reflection-seismic profile across an approximately 9 km wide half-graben (for location see Figure 4) that is bounded in the east by the west-dipping, basement-rooted Ferrette growth fault. Upper Priabonian to Lower Rupelian syn-rift sediments form an asymmetric wedge, which onlaps the base-Tertiary unconformity towards the west. In the immediate vicinity of the fault, an almost transparent seismic facies possibly indicates the presence of poorly sorted, Priabonian-Rupelian conglomerates (beneath the "R" reflector). This is compatible with the occurrence of similar conglomerates adjacent to faults and flexures in the study area (top right inset in Fig. 4). Westward, the syn-rift sediments taper out towards an east-dipping basement fault, forming the western boundary of the half-graben

Fig. 5: NNW-SSE-trending reflection-seismic line crossing the E-W-trending extensional Réchésy flexure at the URG - Jura boundary (data courtesy of Shell International EP). For location see Fig. 4. (a): un-migrated, stacked time section, (b): interpreted section.
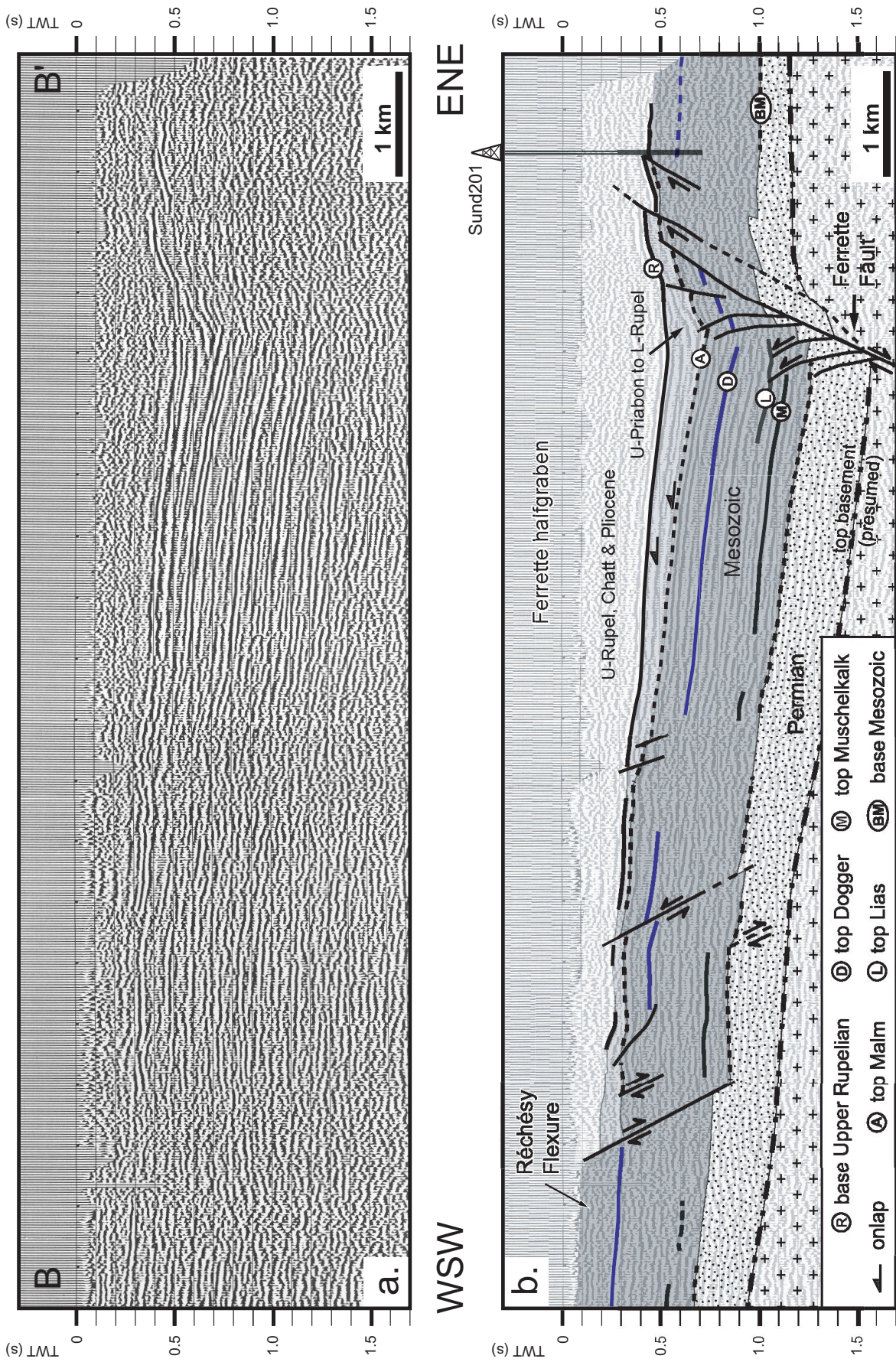
Fig. 6: WSW-ENE-trending reflection-seismic line across the NNE-trending Ferrette half-graben bounded by URG-parallel normal faults (data courtesy of Shell International EP). For location see Fig. 4. (a): un-migrated, stacked time section, (b): interpreted section.

and corresponding to the eastern, fault-bounded termination of the Réchésy flexure.

The syn-rift-sediments contained in this half-graben consist of marly and platy "Haustein" limestones. These sediments, which were penetrated by borehole "Sund203", located some 3 km north of the seismic line (see Fig. 3), are of Upper Priabonian to Lower Rupelian age, as inferred from biostratigraphic data gathered in outcrops along the front of the Jura Mountains (Fischer 1965a; Fischer 1965b; Liniger 1970b; Duringer 1988; Picot 2002; Picot et al. in press). A pronounced reflector, corresponding to the Upper Rupelian "Meeressand" ("R" in Fig. 6, see also Fig. 3), oversteps the footwall of the Ferrette fault where Upper Priabonian to Lower Rupelian sediments are missing. This is evidenced by borehole "Sund201" (Fig. 3 and 7), which penetrated Upper Rupelian marine strata resting on Oxfordian limestones. Hence, the Upper Rupelian "Meeressand" transgression invaded areas previously unaffected by rift-related subsidence. The "Meeressand" calcarenites, which grade upwards into marine marls ("Meletta beds"), covered the domain of the autochthonous and detached Mesozoic as far south as the Delémont Basin in the Folded Jura (Fig. 1). The seismically less reflective layers above the "R" reflector are attributed to Uppermost Rupelian to Chattian marine to fluvio-lacustrine sands and marls, which represent the youngest syn-rift sediments preserved in the area. These are covered by weakly reflective Late Pliocene fluvial gravels and subordinate Quaternary Loess.

The throw along the westward dipping Ferrette growth fault approaches 0.3 s TWT, corresponding to almost 500 m. The presence of an half-graben normally implies a listric geometry of the controlling fault. However, evidence for listricity of the Ferrette fault can hardly be detected on the seismic section (Fig. 6). This suggests a detachment at deeper levels, i.e. within the crystalline basement, conceivably at its brittle-ductile transition (compare Laubscher and Noack 1997). Similar half-graben structures, bounded to the east by westward dipping normal faults, have been described in the southeastern corner of the URG (see cross sections 8 and 9 in Gürler et al. 1987) and were studied in outcrops of the Folded Jura south of Basel (Laubscher 1998).

The west-dipping Ferrette fault was reactivated under compression (or transpression), as evidenced by two top-to-the-E reverse offsets of the "R" reflector to the west of borehole Sund201. The vertical offset across the more prominent western reverse fault amounts to some 0.05 s, i.e. <100 m. This fault reactivation presumably occurred during the Aquitanian (Laubscher 1992).

2.3.3 Well log interpretation

Fig. 7 gives simplified stratigraphic columns for three exploration wells located within the Ferrette half-graben, on the Ferrette horst and on the eastern flank of the half-graben, respectively (see also Fig. 3). For all three wells the base of Upper Rupelian strata was chosen as a reference horizon. In the basinal wells Sund203 and Kno1 the Tertiary syn-rift sedimentation starts with Upper Priabonian to Lower Rupelian marly "Haustein"

limestones, whereas the Ferrette block (well Sund201) was only overstepped during the Upper Rupelian transgression. The thickness of this Upper Rupelian transgressive interval is in the order of 20 m in all three wells. Whereas subsidence of the Ferrette half-graben (around well Sund203 in Fig. 7) was clearly controlled by activity along the Ferrette fault (Figs. 4, 6), which breaks through the Mesozoic series, the simultaneous subsidence of the depocenter to the NE of it (around well Kno1 in Fig. 7) was controlled by extensional flexuring along ENE-striking basement faults that parallel the Permo-Carboniferous faults. The sedimentary record of these three exploration wells thus shows that Upper Eocene to Lower Oligocene growth faulting along the Rhenish fault set and flexuring along the Permo-Carboniferous fault set occurred simultaneously. In order to elucidate the stress field responsible for this fault interaction, a kinematic analysis of surface faults was performed.
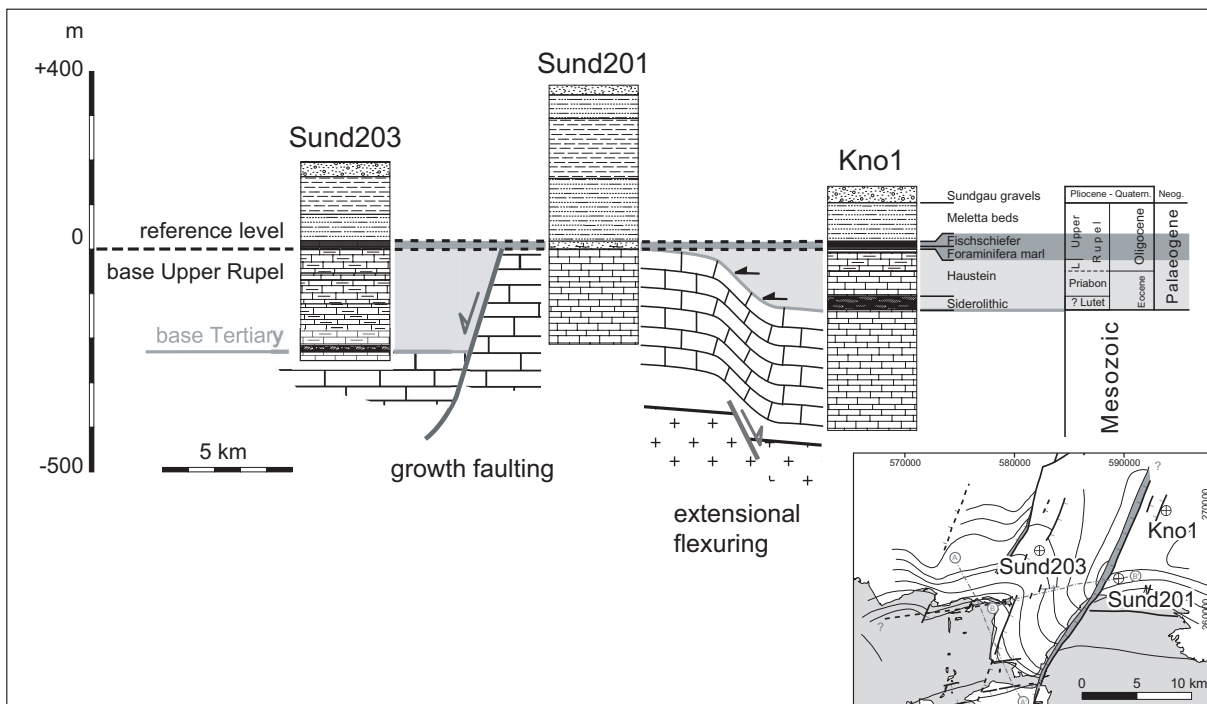
Fig. 7: Correlation of three exploration wells with the base of Upper Rupelian sediments (shaded dark grey) as a common reference horizon. See text for discussion. Bottom right inset: base-Mesozoic structure with well locations.

2.4 Kinematics of rifting inferred from fault-slip data

2.4.1 Fault-slip data collection

The orientations of faults and their slickensides were measured at numerous sites in the study area in order to derive the palaeostress axes orientations. A great part of the data was measured in Jurassic limestones (such as those depicted in Fig. 8) and to a lesser extent in Palaeogene syn-rift sediments (e.g. Fig. 9). Fault-slip senses were inferred from various shear sense indicators on the fault planes (Hancock 1985; Petit 1987). The most abundant indicators were slickolites, best developed in micritic Upper Jurassic limestones. Less frequently, we found slickenfibres, mainly in oolithic limestones of both Mid- and Upper
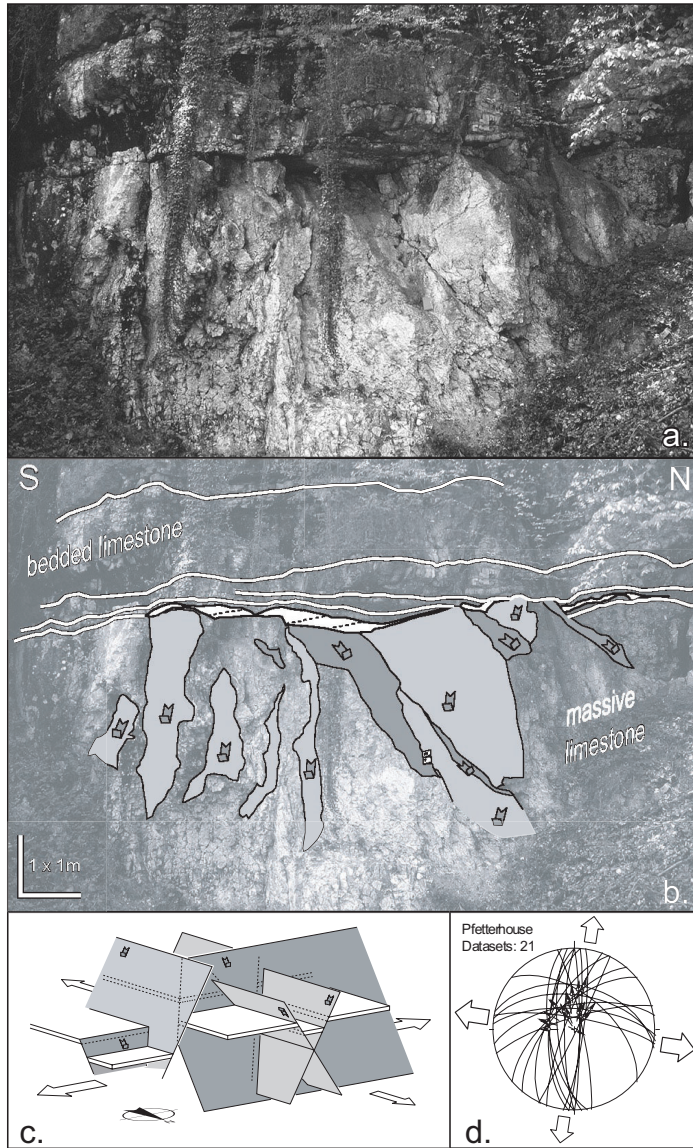
Fig. 8: (a): Intersecting normal faults in an outcrop of Oxfordian limestones at the eastern termination of the Réchésy flexure. (b): Interpreted line drawing of (a). E-W-striking fault planes (darker shading) intersect with N-S-trending faults (lighter shading). Both sets of normal faults are offset along a sub-horizontal bedding plane (white) with striations developed during Late Neogene shortening of the flexure. (c): Illustration of two intersecting, mutually orthogonal fault sets resulting in extension into two perpendicular directions. A marker bed is shown in white. (d): Fault planes from (a) shown in the stereographic projection (equal area, lower hemisphere). Small arrows indicate movement of the hanging-wall block. Large arrows indicate inferred extension directions.
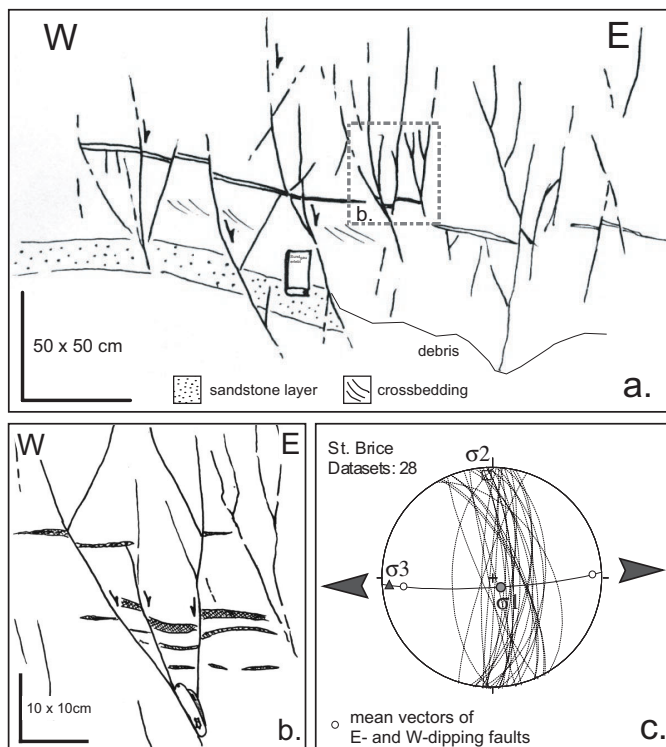
Fig. 9: (a): Small-scale conjugate normal faults in Chattian sands. (b): Detail from (a) with displaced markers. (c): great-circle representation of fault planes and derived principal stress axes. The orientation of σ1 and σ3 are found by bisecting the obtuse and acute angles between the poles to the mean of W- and E-dipping fault planes, respectively ("bisector method").

Florimont
Datasets: 11

fault plane with hangingwall slip sense

bedding plane

○ σ1   □ σ2   ▲ σ3

rotation axis = strike of bedding
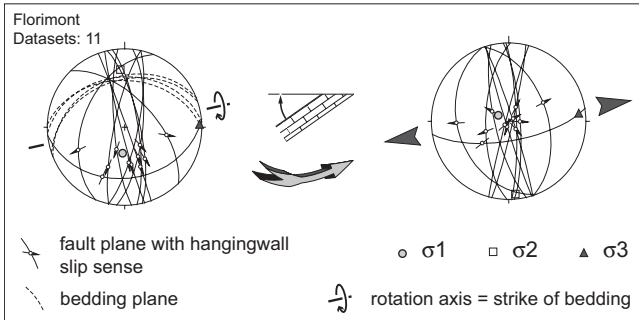
Fig. 10: Principle of back-rotating fault-slip data in order to account for tilting after fault formation. Back-rotation brings the bedding planes back into their originally horizontal position.

Jurassic age. Crescentic (or lunate) fractures, tensile cracks and/or Riedel shear planes were restricted to massive, coralliferous Oxfordian limestones and/ or to cataclasites near to or directly within fault zones. In the case of unstriated fault planes (especially in Palaeogene syn-rift sediments), the shear sense was inferred from conjugate fault geometry or from displaced markers. The quality of slip sense indicators was classified as excellent, good or poor in order to allow for weighting during subsequent palaeostress axes calculations. Additionally, the "importance" of faults was estimated in a qualitative manner based on (1) the dimensions of the exposed part of the fault plane, (2) the amount of displacement (if detectable) and (3) the presence or absence of cataclasite or fault gouge.

Overprinting relationships (superimposed slickensides, cross-cutting faults, Fig. 8) allowed the establishment of a relative chronology of faulting. This, in turn, permitted a separation of heterogeneous fault populations into homogeneous subsets that reflect one particular deformation phase only. Where field evidence and regional geologic context indicated that tilting had occurred due to post-Palaeogene folding, the fault-slip sets were rotated into a position where bedding was horizontal, before performing stress axes calculations (Fig. 10). In this study, we focus on the fault kinematics of rift-related extension of the URG only. Correspondingly, the fault sets described in the following section represent already separated, homogeneous subsets.

2.4.2 Analysis of fault-slip data

28 locations in the study area yielded a sufficient number of faults per site (6 or more) to derive palaeostress axes orientations. 92% of the measured fault striations reveal pitch angles (i.e. the angle between the lineation and the horizontal, measured in the inclined fault plane) of 60° or more (Fig. 11). Hence, the majority of the faults are classified as nearly ideal dip-slip normal faults, whereas strike-slip faults are absent. The orientations of the maximum, intermediate and minimum principal stress axes (σ1, σ2 and σ3) have been determined by a variety of methods. In the case of faults lacking striations, but exhibiting a conjugate geometry and displaced markers, the principal stress axes orientations were derived as follows. The conjugate fault planes were plotted as poles. Fault planes dipping in opposite directions were separated into two subsets and the mean vectors were determined for each subset. A great circle through the mean vectors was constructed. The obtuse and acute bisectors on the great circle between the two mean vectors defined the orientations of σ1 and σ3, respectively (e.g. Fig. 9).
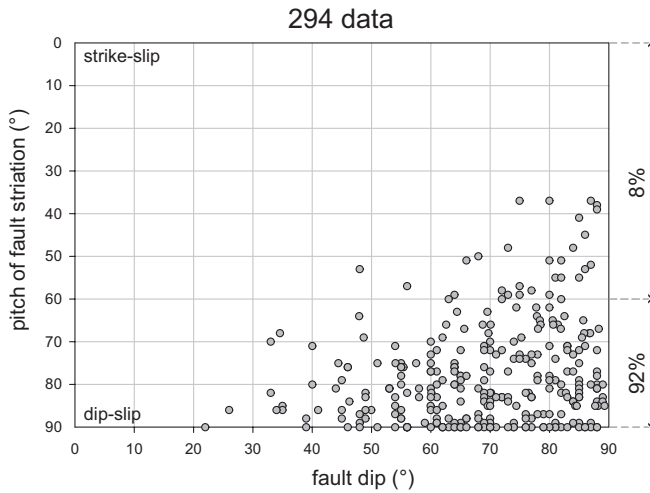
Fig. 11: Plot of fault striation pitch versus fault dip for the collected fault-slip sets. For discussion see text.

For datasets with less than 10 fault-slip pairs, the P-T-axes method was applied (Marrett and Allmendinger 1990; Peresson 1992). "TectonicsFP", the software package used for calculation and graphical output (Reiter and Acs 1996-2000), allowed for arbitrarily choosing the angle between fault plane and the incremental shortening axis (P). Following our observations of conjugate normal faults, which enclose an angle of c. 60° (Fig. 9), we chose an angle of 30° throughout. Assuming coaxial deformation, the principal stresses σ1, σ2 and σ3 of a given dataset coincide with the mean orientations of the P-, B- and T-axes, respectively.

Given a minimum of 10 fault-slip pairs per dataset, palaeostress tensors were calculated, yielding the principal stress axes orientations and the ratio $R=(\sigma2 - \sigma3)/(\sigma1 - \sigma3)$, with $\sigma1 \geq \sigma2 \geq \sigma3$ and $0 \leq R \leq 1$. The tensors were obtained using (1) the numerical dynamic analysis or NDA (Spang 1972; Sperner and Ratschbacher 1994) and (2) the direct inversion technique (Angelier and Goguel 1979; Angelier 1984; Angelier 1989). For each tensor we also calculated the average misfit angle α, which is the deviation between the calculated slip lineation and the measured lineation for each fault-slip pair. The angle α allows one to estimate the quality of the computed stress tensors. Tensors with average misfit angles greater than 15° were considered unreliable and were thus rejected. In addition, the tensor quality rank (TQR) was calculated (Delvaux et al. 1997) and allowed a classification of stress tensors into good (TQR ≥ 1.5) and medium quality (0.5 ≤ TQR < 1.5).

The orientations of the principal stress axes, the distribution of P- and T-axes, as well as the R-values were considered for inferring the tectonic regime. We distinguished between (1) plane strain extension (or extension for short; σ1 vertical, σ3 horizontal; well defined clusters of both P- and T-axes; σ1 > σ2 > σ3; 0.25<R<0.75; no deformation in σ2-direction) and (2) radial extension (σ1 vertical, σ3 horizontal but poorly defined; well defined cluster of P-axes, great-circle distribution of T-axes; σ1 > σ2 ≈ σ3; 0<R<0.25). Given the generally observed gentle plunge of σ3, the extension direction was solely defined as the azimuth of σ3.

The results of the principal stress axes determinations are summarised in Fig. 12 and Table 1. All plots in Fig. 12 are lower hemisphere, equal area projections. Faults are represented by great circles; the slip directions are shown as arrows indicating the movement directions of the hanging-wall blocks. Dashed lines represent conjugate faults without slip lineations. The corresponding principal stress axes are represented by filled circles (σ1), open

25
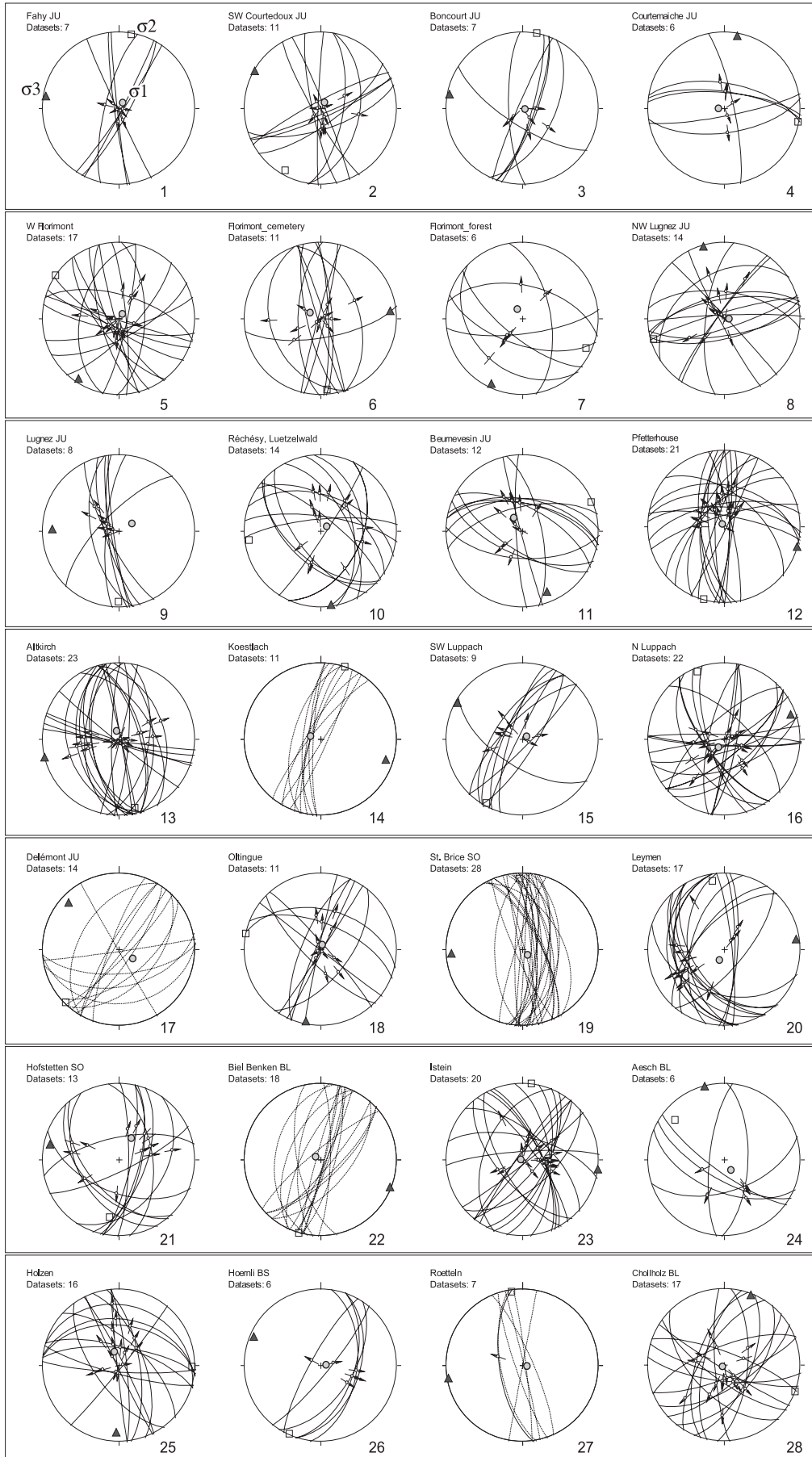
Fig. 12: Stereographic representation of fault sets and palaeostress orientations obtained at 28 sites (equal area, lower hemisphere projections). Numbers at the lower right of each plot correspond to the numbering of the datasets in Table 1.

No.	Location	X-coord	Y-coord	Lithology	Age	σ1 azimuth	σ1 plunge	σ3 azimuth	σ3 plunge	method	R	N	n	α	TQR	qual	regime
1	Fahy JU	565900	253100	micritic limestone	Oxford	037	83	280	04	PT-axes		7	7				extension
2	Courtedoux JU	567800	249175	micritic limestone	Kimmeridge	035	83	300	01	NDA	0.11	11	11	13	0.8	medium	radial ext
3	Boncourt JU	568400	260500	micritic limestone	Oxford	107	84	281	03	PT-axes		7	6				extension
4	Courtemaiche JU	569750	256640	oolithic to micritic limestone	Oxford	267	84	010	04	PT-axes		6	6				extension
5	W Florimont	571000	261950	micritic limestone	Oxford	041	84	214	06	Direct Inversion	0.09	17	16	6	2.5	good	radial ext
6	Florimont	572100	262175	micritic limestone	Oxford	300	82	084	07	NDA	0.48	11	10	7	1.3	medium	extension
7	Florimont	572425	261900	micritic limestone	Oxford	333	79	206	07	PT-axes		6	5				extension
8	NW Lugnez JU	573400	259775	coralliferous limestone	Oxford	092	85	344	02	NDA	0.41	14	13	13	0.9	medium	extension
9	Lugnez JU	574560	258975	micritic limestone	Kimmeridge	061	74	272	14	PT-axes		8	7				extension
10	Réchésy	577075	261450	laminated limestone	Oxford	055	82	172	04	Direct Inversion	0.26	14	13	11	1.1	medium	extension
11	Beurnevésin JU	577275	260300	micritic limestone	Kimmeridge	327	74	158	16	Direct Inversion	0.07	12	12	3	4	good	radial ext
12	S Pfetterhouse	579475	260875	coralliferous & bedded limestone	Oxford	325	87	105	02	NDA	0.31	21	21	8	2.6	good	radial ext
13	Altkirch	585500	275800	marl and oolithic limestone	Lower Rupel	347	81	257	00	NDA	0.38	23	16	13	0.9	medium	extension
14	Koestlach	588100	261600	oolithic limestone	Dogger	288	78	108	12	bisector		11					extension
15	SW Luppach	591500	261075	micritic limestone	Oxford	059	85	299	03	PT-axes		9	9				extension
16	N Luppach	592050	262200	micritic limestone	Oxford	213	79	069	09	Direct Inversion	0.07	22	20	6	3	good	radial ext
17	Delémont JU	593150	244320	sand	Chatt	127	72	313	12	bisector		14					extension
18	Oltingue	594879	260800	oolithic to micritic limestone	Oxford	023	83	192	04	Direct Inversion	0.13	11	11	8	1.4	medium	radial ext
19	St. Brice SO	599300	260125	marly sand	Chatt	065	76	265	14	bisector		28					extension
20	Leymen	603300	259850	coralliferous limestone	Oxford	202	78	082	06	Direct Inversion	0.27	17	17	15	1.1	medium	extension
21	Hofstetten SO	605000	257675	coralliferous limestone	Oxford	031	63	283	09	Direct Inversion	0.16	13	10	6	1.3	medium	radial ext
22	Biel-Benken BL	606475	262525	sand	Chatt	306	87	112	03	bisector		18					extension
23	Istein	606750	281000	coralliferous limestone	Oxford	265	89	097	01	NDA	0.26	20	20	11	1.8	good	extension
24	Aesch BL	612425	256900	coralliferous limestone	Oxford	146	77	345	00	PT-axes		6					extension
25	Holzen	614536	282990	coralliferous limestone	Oxford	343	75	183	14	Direct Inversion	0.05	16	16	4	4	good	radial ext
26	Hoernli BS	615875	267600	marly limestone	Muschelkalk	087	84	293	05	PT-axes		6					extension
27	Roetteln	617222	276256	oolithic limestone	Dogger	090	88	260	02	bisector		7					extension
28	Chollholz BL	617825	262375	oolithic limestone	Dogger	214	87	021	03	Direct Inversion	0.10	17	14	12	1	medium	radial ext

Table 1: Palaeostress reconstruction sites (Swiss National coordinates) with prevalent lithology and stratigraphic age. R = (σ2-σ3)/(σ1-σ3), N = number of data per site, n = number of data with known slip sense. α = average misfit angle, TQR = tensor quality rank (Delvaux et al. 1997), TQR = n(n/N)/ α. radial ext = radial extension.

squares (σ2) and filled triangles (σ3), respectively. The so derived σ3 or extension directions were plotted at the corresponding sites in the form of diverging arrows in Fig. 13. Datasets from eight locations of Larroque and Laurent (1988) were also included. The frequency distribution of the extension directions reveals an ESE-WNW oriented maximum (Fig. 13, top left inset).

The principal stress axes distributions are shown in the right inset in Fig. 13. The σ1-axes are tightly clustered in a sub-vertical orientation. Hence, a regime of pure extension is observed at all sites. The contoured σ3-axes reveal a maximum at 280/11, which is oriented approximately perpendicular to the trend of the URG. However, the maximum of σ3-axes is less well defined and the σ3-axes scatter much more. Several datasets exhibit extension directions deviating up to 90° from the WNW-ESE-oriented maximum. Deviating datasets are concentrated around the flexures that form the boundary between the URG and the adjacent Jura to the south. At outcrop scale, the datasets yielding these deviating extension directions comprise conjugate normal faults, which strike parallel to the trend of the flexures at map scale (e.g. datasets 8 and 11 in Fig. 12). Datasets from areas where Permo-Carboniferous and Rhenish fault sets overlap, reveal normal faults with highly variable strike offsetting each other (Fig. 8 and datasets 2, 12, 16 and 18 in Fig. 12). This suggests simultaneous Tertiary-age activity along both Permo-Carboniferous and Rhenish fault sets.

Reduced stress tensors were calculated for 15 datasets (Table 1). The R-values obtained range between 0.48 and 0.05, i.e. between plane strain extension and radial extension. All datasets revealing radial extension are located either directly on flexures, at intersections between Rhenish and Permo-Carboniferous faults or at intersections between Rhenish and Hercynic faults (datasets 25 and 28 in Fig. 12). At these localities, σ3 continuously switched directions, permitting normal faulting parallel to two directions at high angles to each other.

Two structural domains, outlined in the vicinity of the roughly E-W-trending flexures delimiting the URG to the south (dashed boxes in Fig. 13), are of particular interest. Domain A encompasses the two en-échelon aligned Florimont and Réchésy flexures (Fig. 1) that remained largely unaffected by compression, apart from slight N-S shortening in post-Late Pliocene times (Giamboni et al. 2004). Domain B covers the eastern part of the frontal Ferrette fold, which formed during Upper Miocene to Lower Pliocene thin-skinned Jura folding and where Neogene shortening is moderate (Fischer 1965a; Fischer 1965b). The P- and T-axes from the 9 and 3 fault-slip sets collected in domains A and B, respectively, are shown in Fig. 14. P-axes cluster in a vertical orientation, whereas T-axes are subhorizontal and radially distributed. This is typical of radial extension.

In summary, the analysis of fault sets indicates that away from the flexures forming the boundary between the exposed Mesozoic sediments and the URG, extension was predominantly perpendicular to the graben. Along the southern border of the URG, however, there is good evidence for radial extension, with a preference for extension along the pre-existing, sub-perpendicular Rhenish and Permo-Carboniferous fault sets (Fig. 2).

This suggests that towards the southern margin of the URG the stress field changed due to interference between these two fault sets. This confirms previously reached conclusions based on subsurface data.
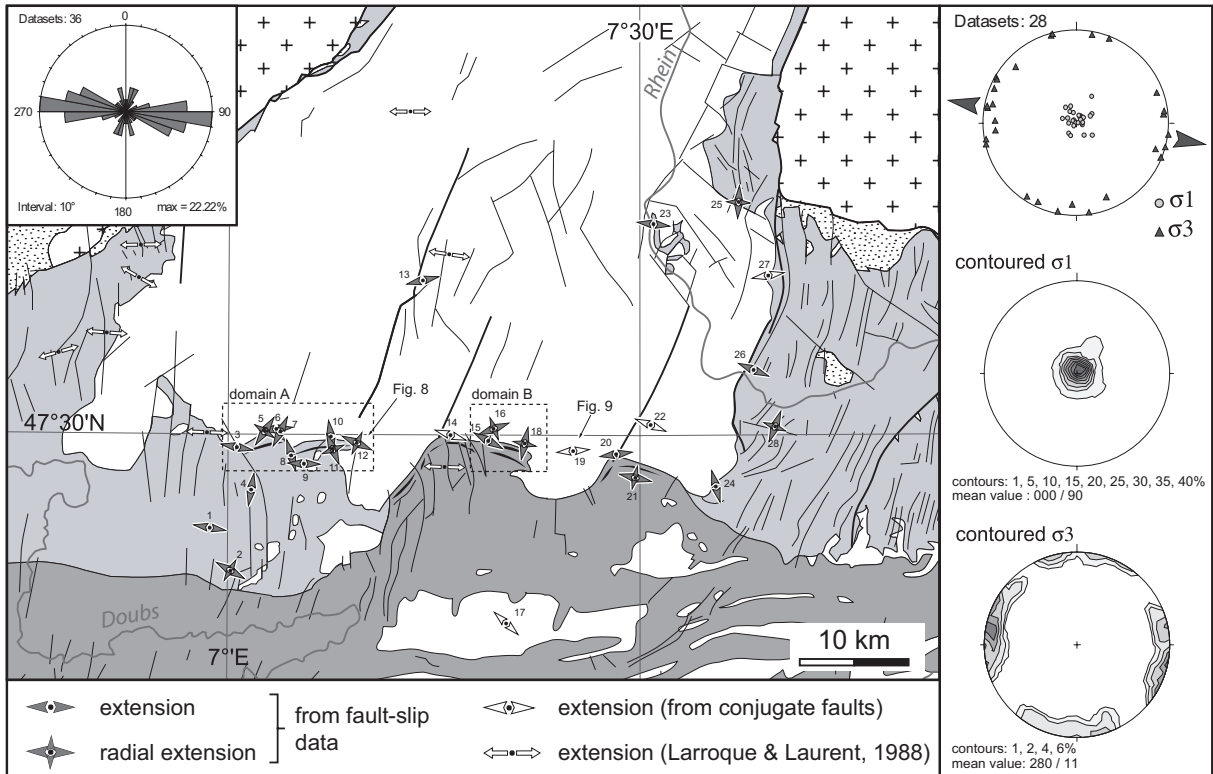
Fig. 13: Extension directions (diverging arrows) during Eo-/Oligocene rifting in the southernmost URG and adjacent Jura Mountains. Range of the figure and patterns are identical to Fig. 1. Numbers next to each arrow symbol correspond to the numbering of the datasets in Table 1. Upper left inset: frequency distribution of extension directions obtained at 36 locations (28 locations from this study and 8 locations from Larroque and Laurent 1988). Interval width is 10°. Inset on right: distribution of $\sigma1$- and $\sigma3$-axes for the 28 sites collected in this study (top), contoured $\sigma1$- (middle) and $\sigma3$-axes (bottom).
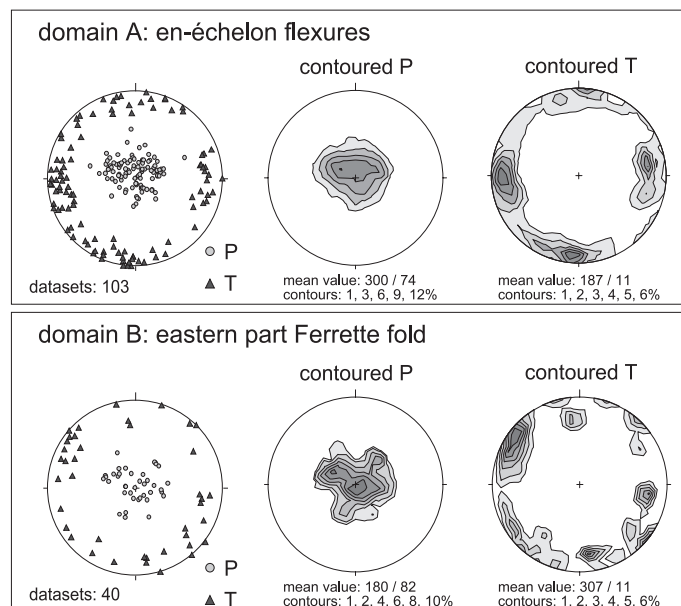
F**ig. 14**: Contoured P- and T-axes for faults from domains A and B (see Fig. 13 for location).

2.5 Discussion and Interpretation

The reflection-seismic and well data presented above, compiled into a base-Mesozoic structure map, show the interference of Rhenish and Permo-Carboniferous fault sets at the southern end of the URG. Half-graben structures and growth faults developed above Rhenish faults, whereas the extensional flexures were associated with Permo-Carboniferous faults. The throw on both Rhenish and Permo-Carboniferous faults was cumulative and reached values of close to 500 m exactly at the intersection of the two fault trends. An investigation of the stratigraphic record of wells, combined with biostratigraphic data from conglomerates associated with the faults and flexures, shows that growth faulting along Rhenish normal faults and extensional flexuring above Permo-Carboniferous basement faults were simultaneous, starting in the Upper Priabonian and lasting until the Lower Rupelian. An Upper Rupelian transgression overstepped the borders of both the extensional flexures and the half-grabens.

The kinematic analysis of outcrop-scale faults in Mesozoic pre-rift and Palaeogene syn-rift sediments, discussed in the previous chapter, reveals a predominance of WNW-ESE-oriented extension, approximately perpendicular to the trend of the southern URG. Extension affected sediments as young as Chattian and is consequently attributed to Eo-/Oligocene URG rifting. This WNW-ESE-oriented extension is compatible with results obtained from other parts of the URG, the Tabular Jura (Larroque and Laurent 1988), the RBTZ (Bergerat 1987; Villemin and Bergerat 1987; Lacombe et al. 1993), as well as - on a larger scale - from the European Platform (Bergerat 1987). Consequently, the derived WNW-ESE-directed extension is considered a regional trend. However, we observe that this WNW-ESE-oriented, regional extension is superimposed with simultaneous N-S-oriented extension along the southern end of the URG, which leads to radial extension. This radial extension is found predominantly in the vicinity of the extensional flexures delimiting the URG to the south and in areas where Rhenish and Permo-Carboniferous, or subordinately Rhenish and Hercynic fault sets overlap. In these cases the determination of a unique extension direction becomes meaningless, as simultaneous extension occurred in strongly varying directions. The radial extension is illustrated by the distribution of P- and T-axes and the R-values of the reduced stress tensors.

In the vicinity of the flexures at the southern end of the URG, extension directions deviating from the regional WNW-orientation are at high angles or even perpendicular to the strike of the flexures. These deviating extension directions are most probably due to stretching of the limestone-dominated sediments in the outer arc of the flexured Mesozoic cover. Such arcing or flexuring of the sediments above the steeply dipping top-to-the-N basement fault was facilitated by decoupling along mechanically weak layers, such as the up to 100 m thick halite and anhydrite intercalations in the Mid- and Upper Triassic, penetrated by well Buix1 (Fig. 3). Additionally, the local stress field was influenced by the interaction of Rhenish and Permo-Carboniferous faults (and subordinately also by interference between

Rhenish and Hercynic fault sets), resulting in radial extension. In summary, we propose that the orientation of pre-existing structures and the interaction between the different fault sets caused the observed stress field changes along the southern border of the URG.

The Permo-Carboniferous faults trend at angles between 20-25¡ to the inferred extension direction (WNW-ESE) derived at localities away from the flexures. Combined with the observed en-échelon alignment of the Florimont and Réchésy flexures, this suggests that the reactivated underlying ENE-oriented Permo-Carboniferous basement fault also accommodated a sinistral wrench component in addition to the top-to-the-N normal component. The simultaneous activity along growth faults and extensional flexures might thus reflect the transition from rift-perpendicular extension prevailing further north in the URG to sinistral transtensive movements in the RBTZ (Laubscher 1970; Bergerat and Chorowicz 1981; Illies 1981; Lacombe et al. 1993).

However, it remains uncertain, where exactly and how the sinistral wrench movements inferred for Permo-Carboniferous faults, accounting for some 5-7 km of extension across the URG (Lacombe et al. 1993), was transmitted to the brittle sedimentary cover of the RBTZ. Strike-slip faults (or faults with a pronounced oblique-slip component) are conspicuously absent in the sedimentary cover of the investigated area (Fig. 10) and apparently also elsewhere in the region (Larroque and Laurent 1988; Lacombe et al. 1993). One explanation for the absence of strike-slip faults in the cover is that the strike-slip component along the ENE-trending basement faults was partitioned between basement and sedimentary cover along a Mid- and/or Upper Triassic detachment (such as inferred for the Florimont and Réchésy flexures) and led to en-échelon extension in the cover. In addition, the total amount of sinistral strike-slip motion might have been dissipated by flexuring of the detached Mesozoic cover across several pre-existing Permo-Carboniferous faults.

The geometric relationship between extensional growth faulting, flexuring and syn-rift sedimentation at the end of the Lower Rupelian is summarised in a block diagram, given in Fig. 15. This block diagram covers part of the area for which the base Mesozoic structure map of Fig. 4 was constructed. The NNE-trending Ferrette fault bounds the east-dipping Ferrette half-graben. A smaller normal fault, antithetic with respect to the Ferrette fault, bounds the half-graben in the west. The half-graben geometry implies a listric configuration of the Ferrette fault with a detachment level presumably rooted at the crustal brittle-ductile transition. En-échelon aligned flexures are developed above an ENE-oriented high-angle basement fault, which reveals sinistral strike-slip kinematics with a pronounced oblique-slip component. Decoupling across Middle Triassic evaporites allowed extensional flexuring of the overlying Mesozoic strata. Extensional growth faulting and flexuring occurred under regional WNW-ESE-extension. However, extensional flexuring above reactivated Permo-Carboniferous basement faults induced local N-S-oriented extension. This led to a local superposition of both extensional directions. Simultaneous faulting and flexuring created accommodation space and relief that allowed the accumulation of onlapping syn-rift

lacustrine to brackish marls and the development of debris fans in the immediate vicinity of normal faults and flexures.
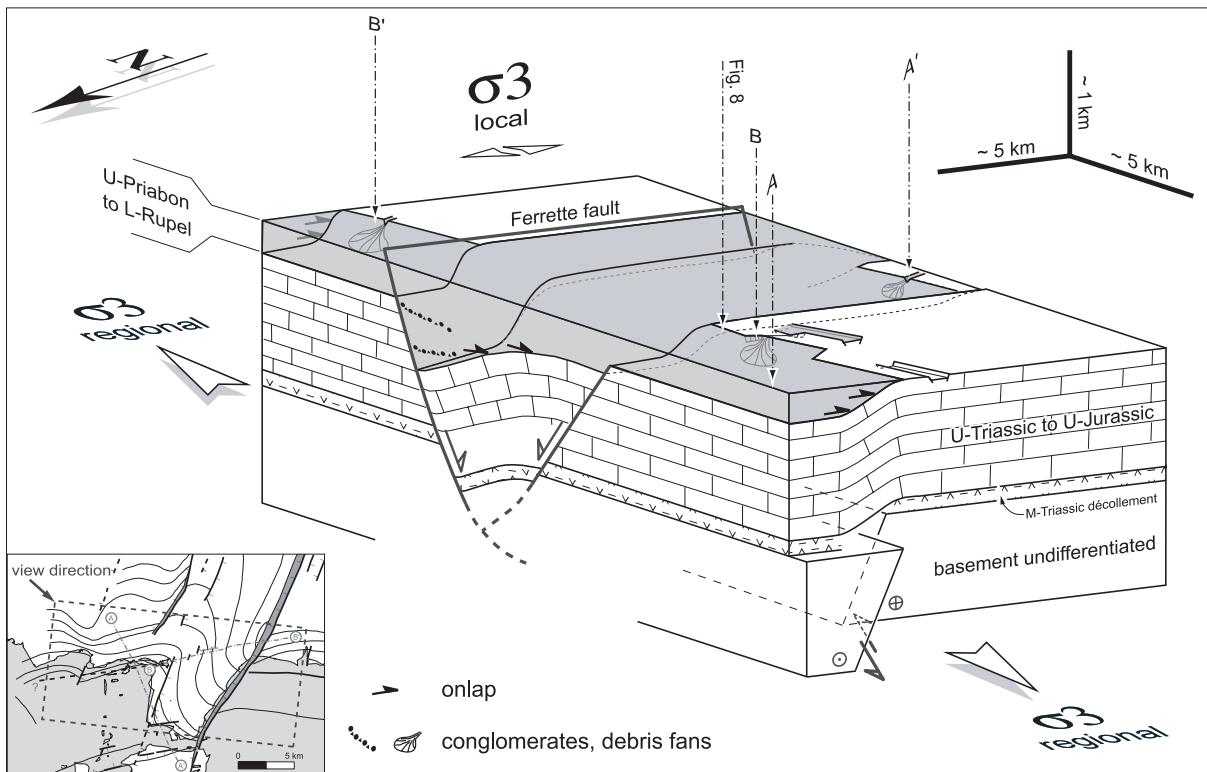
Fig. 15: Block diagram illustrating the simultaneous development of half-grabens and extensional flexures under regional WNW-oriented extension during the Upper Priabonian to Lower Rupelian. Approximately 3-times vertical exaggeration. For discussion see text. The Illfurth fault has been omitted. Positions of seismic cross sections (Figs. 5 and 6) and of Fig. 8 are indicated. Bottom inset shows extent of block model on map in Figure 4 (dashed rectangle).

2.6 Conclusions

At the southern end of the URG the NNE-trending extensional fault system interferes with the ENE-trending system of the RBTZ. Rifting initiated in Upper Priabonian times under regional WNW-ESE-extension, roughly perpendicular to the graben axis. Within the URG, NNE-striking half-grabens with hanging-wall growth faults formed. Simultaneously, ENE-trending extensional flexures evolved above reactivated Permo-Carboniferous basement faults that controlled the transition from the URG to the RBTZ. The en-échelon alignment of these flexures suggests that the underlying ENE-oriented basement faults accommodated sinistral wrench movements in addition to the throw.

The interference of extensional flexuring and growth faulting resulted in cumulated throws along NNE-trending, half-graben-bounding normal faults during the Upper Priabonian to Lower Rupelian. An Upper Rupelian transgression overstepped areas previously unaffected by rifting, including the northernmost Jura as far south as the Delémont Basin.

To the north of the RBTZ, regional WNW-ESE-extension is well defined along the fault system of the URG. However, along the RBTZ there is evidence for roughly N-S-directed extension. This deviating stress field is mostly restricted to areas located near extensional flexures, where NNE- and ENE-trending faults interfere. As this deviating N-S-extension trends perpendicularly to the extensional flexures, it is thought to reflect stretching of the sedimentary cover above top-to-the-N brittle basement faults. Outcropping fault-slip sets reveal simultaneous activity along NNE-trending extensional growth faults and ENE-trending extensional flexures and thus document the coexistence of E-W and N-S directed extensional stresses, defining a locally confined regime of radial extension.

References

Allenbach R (2000) Synsedimentary tectonics during the Oxfordian of northern Switzerland. unpublished PhD thesis, Geologisch-Paläontologisches Institut, University of Basel, Basel: p 91

Allenbach R (2002) Synsedimentary tectonics in an epicontinental sea: A new interpretation of the Oxfordian basins of northern Switzerland. Eclog. Geol. Helv. 94(3):265-287

Angelier J (1984) Tectonic analyses of fault slip data sets. Journal of Geophysical Research 89(B7):5835-5848

Angelier J (1989) From orientation to magnitudes in paleostress determinations using fault slip data. J. Struct. Geol. 11(1-2):37-50

Angelier J, Goguel J (1979) Sur une méthode simple de détermination des axes principaux des contraintes pour une population de failles. C. R. Acad. Sc. Paris 288:307-310

Bergerat F (1987) Stress Fields in the European Platform at the time of Africa-Eurasia Collision. Tectonics 6(2):99-132

Bergerat F, Chorowicz J (1981) Etude des images Landsat de la zone tranformante Rhin-Saône (France). Geologische Rundschau 70(1):354-367

Bitterli-Brunner P (1988) Geologischer Führer der Region Basel, Birkhäuser, Basel, p 232

Boigk H, Schöneich H (1970) Die Tiefenlage der Permbasis im nördlichen Teil des Oberrheingrabens. In: Illies JH, Mueller S (eds) Graben Problems. Proceedings of an International Rift Symposium held in Karlsruhe 1968, International Upper Mantle Project. E. Schweitzerbart'sche, Stuttgart, pp 45-55

Boigk H, Schöneich H (1974) Perm, Trias und älterer Jura im Bereich der südlichen Mittelmeer-Mjösen-Zonen und des Rheingrabens. In: Illies JH, Fuchs K (eds) Approaches to Taphrogenesis. Proceedings of an International Rift Symposium held in Karlsruhe, April, 13-15, 1972. E. Schweizerbart'sche, Stuttgart, pp 60-71

BRGM (unpublished) Banque du sous-sol. Subsurface database available at the BRGM Alsace, Strasbourg.

Buxtorf A (1901) Geologie der Umgebung von Gelterkinden im Basler Tafeljura. In: Beiträge zur Geologischen Karte der Schweiz, vol 11. Geologische Kommission der Schweizerischen Naturforschenden Gesellschaft, Bern, p 106

Debrand-Passard S, Courbouleix S (1984) Synthèse Géologique du Sud-Est de la France, volume 2: Atlas comprenant 64 planches en couleurs. In: Mémoire du Bureau de recherches géologiques et minières, vol 126. BRGM, p 614

Delvaux D, Moeys R, Stapel G, Petit C, Levi K, Miroshnichenko A, Ruzhich V, San'kov V (1997) Paleostress reconstruction and geodynamics of the Baykal region. Tectonophysics 282(1-4):1-38

Dèzes P, Schmid SM, Ziegler PA (submitted) Evolution of the European Cenozoic Rift System: interaction of the Alpine and Pyrenean orogens with their foreland lithosphere. Tectonophysics, 389: 1-33.

Diebold P (1989) Der Nordschweizer Permokarbon-Trog und die Steinkohlenfrage der Nordschweiz. Vierteljahrsschrift der Naturforschenden Gesellschaft in Zürich 133(1):143-174

Diebold P, Naef H (1990) Der Nordschweizer Permokarbontrog. Nagra informiert 2:29-36

Diebold P, Noack T (1997) Late Palaeozoic troughs and Tertiary structures in the eastern Folded Jura. In: Pfiffner OA, Lehner P, Heitzmann P, Mueller S, Steck A (eds) Deep structure of the Swiss Alps. Results of NRP 20. Birkhäuser, pp 59-63

Doebl F (1970) Die tertiären und quartären Sedimente des südlichen Rheingrabens. In: Illies JH, Mueller S (eds) Graben Poblems. Proceedings of an International Rift Symposium held in Karlsruhe October, 10-12, 1968, International Upper Mantle Project. E. Schweizerbart'sche, Stuttgart, pp 56-66

Duringer P (1988) Les conglomérats des bordures du rift cénozoïque rhénan. Dynamique sédimentaire et contrôle climatique. unpublished PhD thesis, Institut de Geologie, Université Louis Pasteur, Strasbourg: p 278

Edel JB, Fluck P (1989) The upper Rhenish shield basement (Vosges, Upper Rhinegraben and Schwarzwald): Main structural features deduced from magnetic, gravimetric and geological data. Tectonophysics 169:303-316

Elmohandes S-E (1981) The Central European Graben System: Rifting imitated by Clay Modelling. Tectonophysics 73:69-78

Fischer H (1965a) Geologie des Gebietes zwischen Blauen und Pfirter Jura (SW Basel), Kümmerly & Frey, Geographischer Verlag, Bern, p 106

Fischer H (1965b) Geologischer Atlas der Schweiz 1:25 000, Atlasblatt 49, Rodersdorf, mit Erläuterungen, Schweizerische Geologische Kommission, Bern

Fischer H (1969) Einige Bemerkungen zur "Übersichtstabelle zur Geologie der weiteren Umgebung von Basel". Regio Basilensis 10(2):234-238

Giamboni M, Ustaszewski K, Schmid SM, Schumacher ME, Wetzel A (2004) Plio-Pleistocene Transpressional Reactivation of Paleozoic and Paleogene Structures in the Rhine-Bresse Transform Zone (Northern Switzerland and Eastern France). Geologische Rundschau 93: 207-223, doi: 10.1007/s00531-00003-00375-00532.

Gürler B, Hauber L, Schwander M (1987) Die Geologie der Umgebung von Basel mit Hinweisen über die Nutzungsmöglichkeiten der Erdwärme, Beiträge zur Geologischen Karte der Schweiz, Lieferung 160 (Neue Folge), Schweizerische Geologische Kommission, Bern, p 33

Hancock PL (1985) Brittle microtectonics: principles and practice. J. Struct. Geol. 7(3-4):437-457

Häring M (2003) Das Neueste zum Projekt Deep Heat Mining in Basel. http://www.geothermal.ch/Einstieg_d.html (accessed on 01-09-2003)

Illies JH (1981) Mechanism of Graben formation. Tectonophysics 73(1-3):249-266

Koch R (1923) Geologische Beschreibung des Beckens von Laufen im Berner Jura. In: Beiträge zur Geologischen Karte der Schweiz, Neue Folge, vol 48. Schweizerische Geologische Kommission, Bern, p 61

Lacombe O, Angelier J, Byrne D, Dupin J (1993) Eocene-Oligocene tectonics and kinematics of the Rhine-Saone continental transform zone (Eastern France). Tectonics 12(4):874-888

Larroque J, Laurent P (1988) Evolution of the stress field pattern in the south of the Rhine Graben from the Eocene to the present. Tectonophysics 148:41-58

Laubscher H (1970) Grundsätzliches zur Tektonik des Rheingrabens. In: Illies JH, Mueller S (eds) Graben Problems. Proceedings of an International Rift Symposium held in Karlsruhe 1968, International Upper Mantle Project. E. Schweitzerbart'sche, Stuttgart, pp 79-86

Laubscher H (1972) Some overall aspects of Jura dynamics. American Journal of Science 272:293-304

Laubscher H (1973) Faltenjura und Rheingraben: zwei Grossstrukturen stossen zusammen. Jber. u. Mitt. oberrh. geol. Ver. 55:145-158

Laubscher H (1982) Die Südostecke des Rheingrabens - ein kinematisches und dynamisches Problem. Eclog. Geol. Helv. 75(1):101-116

Laubscher H (1986) The eastern Jura: Relations between thin-skinned and basement tectonics, local and regional. Geologische Rundschau 75(3):535-553

Laubscher H (1987) Die tektonische Entwicklung der Nordschweiz. Eclog. Geol. Helv. 80:287-303

Laubscher H (1992) Jura kinematics and the Molasse Basin. Eclog. Geol. Helv. 85(3):653-675

Laubscher H (1998) Der Ostrand des Laufenbeckens und der Knoten von Grellingen: die verwickelte Begegnung von Rheingraben und Jura. Eclog. Geol. Helv. 91:275-291

Laubscher H, Noack T (1997) The deep structure of the Basel Jura. In: Pfiffner OA, Lehner P, Heitzmann P, Mueller S, Steck A (eds) Deep structure of the Swiss Alps. Results of NRP 20. Birkhäuser, pp 54-58

Liniger H (1970a) Bemerkungen zur Tektonik am Südende des Rheingrabens. In: Illies JH, Mueller S (eds) Graben Problems. Proceedings of an International Rift Symposium held in Karlsruhe 1968, International Upper Mantle Project, 27. E. Schweitzerbart'sche, Stuttgart, pp 103-106

Liniger H (1970b) Geologischer Atlas der Schweiz 1:25 000, Atlasblatt 55: Bonfol, mit Erläuterungen, Kümmerly & Frey, Bern

Lutz M (1964) Stratigraphische und tektonische Untersuchungen am südwestlichen Schwarzwaldrand zwischen Wiesental und Hochrhein. Oberrhein. geol. Abh. 13:75-122

Marrett R, Allmendinger RW (1990) Kinematic analysis of fault-slip data. J. Struct. Geol. 12(8):973-986

McClay K, Dooley T, Whitehouse P, Mills M (2002) 4-D evolution of rift systems: Insights from scaled physical models. AAPG Bulletin 86(6):935-959

Meyer B, Lacassin R, Brulhet J, Mouroux B (1994) The Basel 1356 earthquake: which fault produced it? Terra Nova 6:54-63

Peresson H (1992) Computer aided kinematic analysis of fault sets. Mitt. Ges. Geol. Bergbaustud. Österr. 38: 107-119

Petit JP (1987) Criteria for the sense of movement on fault surfaces in brittle rocks. J. Struct. Geol. 9(5-6): 597-608

Pfiffner OA, Erard P, Stäuble M (1997) Two cross sections through the Swiss Molasse Basin (lines E4-E6, W1, W7-W10). In: Pfiffner OA, Lehner P, Heitzmann P, Mueller S, Steck A (eds) Deep structure of the Swiss Alps. Results of NRP 20. Birkhäuser, pp 64-72

Pflug R (1982) Bau und Entwicklung des Oberrheingrabens, Wissenschaftliche Buchgesellschaft Darmstadt, Darmstadt, pp 1-145

Picot L (2002) Le Paléogène des synclinaux du Jura et de la bordure sud-rhénane: paléontologie (Ostracodes), paléoécologie, biostratigraphie et paléogéographie. PhD thesis, Institute of Geology and Paleontology, University of Fribourg (Switzerland), Geofocus 5: p 240

Picot L, Becker D, Lapaire F, Ustaszewski K, Hug WA, Berger JP (2005) Sédimentologie, paléontologie et reconstruction des paléo-environnements côtiers de la bordure sud-rhénane (Groupe des Gompholites et Conglomérats, Paléogène, Jura, Suisse). Eclog. Geol. Helv. 98, doi: 10.1007/s00015-1154-9.

Reiter F, Acs P (1996-2000) TectonicsFP. Computer Software for Structural Geology, version 2.0 PR. http://www.tectonicsfp.com/

Schmassmann H, Bayramgil O (1945) Stratigraphie, Petrographie und Paläogeographie der Perm-Formation im schweizerischen Tafeljura und die Steinkohlenfrage der Nordschweiz. Tätigkeitsberichte der Naturforschenden Gesellschaft Baselland 15:15-114

Schmidt C, Braun L, Paltzer G, Mühlberg M, Christ P, Jacob F (1924) Bohrungen von Buix bei Pruntrut und Allschwil bei Basel. Beiträge zur Geologie der Schweiz. Geotechnische Serie, X. Lieferung: p 74

Schumacher ME (2002) Upper Rhine Graben: Role of preexisting structures during rift evolution. Tectonics 21(1):1006, doi:1010.1029/2001TC900022

Sissingh W (1998) Comparative Tertiary stratigraphy of the Rhine Graben, Bresse Graben and Molasse Basin: correlation of Alpine foreland events. Tectonophysics 300:249-284

Spang J (1972) Numerical Method for Dynamic Analysis of Calcite Twin Lamellae. Geological Society of America Bulletin 83(2):467-472

Sperner B, Ratschbacher L (1994) A Turbo Pascal program package for graphical presentation and stress analysis of calcite deformation. Zeitschrift der deutschen geologischen Gesellschaft 145:414-423

Sprecher C, Müller W (1986) Geophysikalisches Untersuchungsprogramm Nordschweiz: Reflexionsseismik 82. In: Nagra Technischer Bericht NTB 84-15, NAGRA, Baden, p 168

Tron V, Brun J-P (1991) Experiments on oblique rifting in brittle-ductile systems. Tectonophysics 188:71-84

Ustaszewski K, Schumacher ME, Schmid SM, Nieuwland D (2005) Fault reactivation in brittle-viscous wrench systems - dynamically scaled analogue models and application to the Rhine-Bresse Transfer Zone. Quaternary Science Reviews 24: 365-382.

Villemin T, Bergerat F (1987) L'évolution structurale du fossé rhénan au cours du Cénozoïque: un bilan de la déformation et des effets thermiques de l'extension. Bull. Soc. géol. France 3(2):245-255

Werner W, Franzke HJ (2001) Postvariszische bis neogene Bruchtektonik und Mineralisation im südlichen Zentralschwarzwald. Zeitschrift deutsche geologische Gesellschaft 152(2-4):405-437

35

Wetzel A, Allenbach R, Allia V (2003) Reactivated basement structures affecting the sedimentary facies in a tectonically «quiescent» epicontinental basin: an example from NW Switzerland. Sedimentary Geology 157:153-172

Ziegler PA (1990) Collision related intra-plate compression deformations in Western and Central Europe. Journal of Geodynamics 11(4):357-388

Ziegler PA (1992) European Cenozoic rift system. Tectonophysics 208:91-111

Ziegler PA, Schumacher ME, Dèzes P, van Wees J-D, Cloetingh S (2004) Post-Variscan evolution of the lithosphere in the Rhine Graben area: constraints from subsidence modelling. In: Wilson M (ed) Permo-Carboniferous magmatism and rifting in Europe. Geological Society, 289-317.

Chapter 3 - Control of pre-existing faults on geometry and kinematics in the northernmost part of the Jura fold and thrust belt

Kamil Ustaszewski and Stefan M. Schmid

Abstract

This study investigates the formation of the northernmost anticlines of the Late Miocene to Early Pliocene thin-skinned Jura fold and thrust belt and provides evidence that a transition to thick-skinned tectonics did occur in this particular area during the Late Pliocene. The northernmost anticlines of the Jura fold and thrust belt are characterized by pronounced along-strike asymmetries that were predetermined by a fault pattern inherited from Paleogene Upper Rhine Graben rifting. This fault pattern had disrupted the Triassic basal décollement of the Jura Mountains and controlled the nucleation of thrusts and folds, as well as transfer zones during the generally (N)NW-directed transport of the detached sedimentary cover. Sinistral, transpressive oblique ramps nucleated along Paleogene, NNE-trending basement normal faults and led to a northward protrusion of the Jura front, encroaching onto the southernmost Upper Rhine Graben. Shortening amount across the frontal anticlines is greatest along the oblique ramps and decreases along-strike towards E, necessitating a gentle clockwise rotation of the detached sediments. Despite the fact that the stress field in the sedimentary cover remained unchanged, thin-skinned folding and thrusting came to a halt in the Late Pliocene, giving way to thick-skinned tectonics, very probably governing neotectonic activity in the area. This transition might represent a geodynamic reorganization of the north-western Alpine foreland.

Keywords: *fault reactivation, kinematics, paleostress analysis, Jura Mountains, Upper Rhine Graben, neotectonics*

3.1 Introduction

3.1.1 Research objectives

The present day architecture of the north-western Alpine foreland is largely the result of an interplay between extensional and compressional tectonics that took place since the early Cenozoic [*Dèzes et al.*, 2004]. Resulting interferences are particularly complex in the northern Jura fold and thrust belt ("detached Mesozoic" of Fig. 1), where the southern Upper Rhine Graben (URG), formed during Eo- to Oligocene extension, abuts the northernmost Folded Jura, formed in response to collision in the Alps during Late Miocene to Early Pliocene

times (Fig. 1). The geometry of the northern Jura fold and thrust belt was strongly controlled by differently oriented basement-rooted extensional faults inherited from Paleogene rifting. They not only dissected the décollement horizon to become active later during thin-skinned Jura tectonics [*Laubscher*, 1961, 1987], but also were often reactivated in compression and/or transtension before, during and after the Late Miocene décollement of the cover series [*Giamboni et al.*, 2004; *Ustaszewski et al.*, 2005b]. This study contributes to the understanding of the control of such pre-existing faults and their reactivation by presenting a detailed case study from the northernmost part of the Folded Jura Mountains. Emphasis is given to the kinematics of pre-existing faults in both basement and sedimentary cover by integrating the following datasets: (1) new field observations and paleostress analyses, (2) new compilations of subsurface maps based on existing industry seismic reflection lines, (3) published geological maps and (4) newly constructed cross sections. After an introduction to the geological setting, outcrop-scale evidence for fault reactivation during thin-skinned Jura folding and appropriate cross-cutting relationships are presented. Paleostress orientations, derived from the collected fault-slip data, including timing constraints for these deformations, are provided next. Based on geological cross-sections and geometric considerations, a kinematic model for the formation of the northern Jura folds is proposed, highlighting the influence of inherited faults. Eventually, possible reasons for the cessation of décollement tectonics during the Late Pliocene and the subsequent transition to thick-skinned tectonics, very probably governing neotectonic activity in the area [*Giamboni et al.*, 2004; *Ustaszewski et al.*, 2005b], are discussed.

3.1.2 Geological setting

The arc-shaped, northwest-verging fold-and-thrust belt of the Jura Mountains forms the most external part of the Central and Western Alpine orogen (inset in Fig. 1). Branching off from the Western Alps near Chambéry, it extends along-strike over a distance of some 300 km to the northwest of Zürich [*Philippe et al.*, 1996; *Affolter and Gratier*, 2004]. It is separated from the Central Alps by the Molasse Basin, a flexural foreland basin that developed in response to the load of the NW-ward advancing Alpine orogen during the Oligocene to Miocene. In the W and N, the Jura Mountains encroach onto the N- to NNE-trending Bresse Graben and Upper Rhine Graben (URG), which are parts of the European Cenozoic rift system [*Ziegler*, 1992] that essentially formed during the Late Eocene to Oligocene. Bresse Graben and URG are separated by the Rhine-Bresse transfer zone (RBTZ), which linked simultaneous openings by sinistral transtensive movements. The location of the RBTZ was largely controlled by pre-existing, NE- to ENE-trending faults inherited from Late Variscan times [*Laubscher*, 1986; *Ziegler*, 1992; *Schumacher*, 2002; *Ustaszewski et al.*, 2005a]. The development of the Bresse Graben and URG in the northern Alpine foreland was, in a broad sense, contemporaneous with the collision phases of the Alpine and Pyrenean orogenies [*Dèzes et al.*, 2004]. The URG in particular forms the most conspicuous part
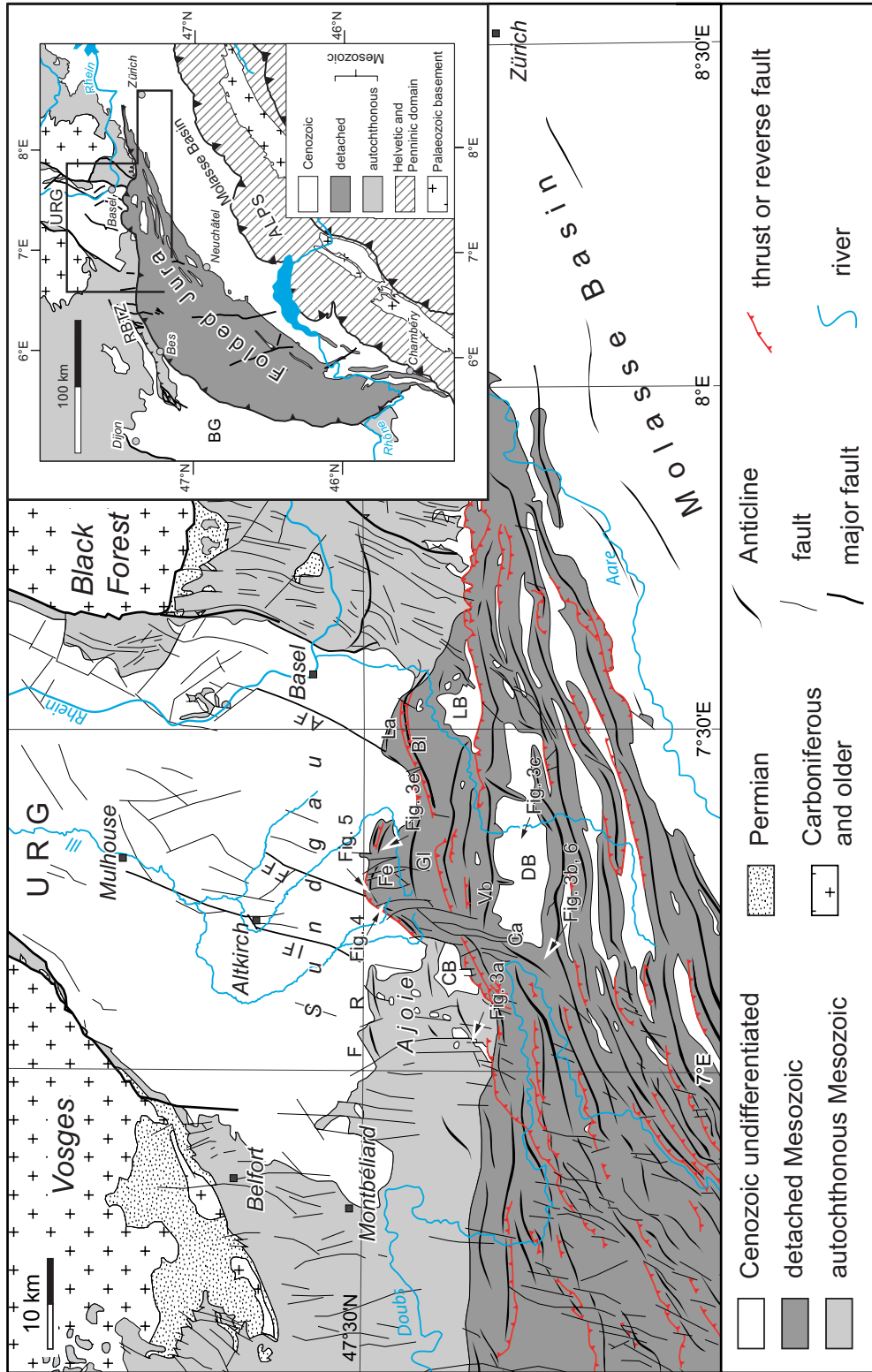
Fig. 1: tectonic map of the northern Jura fold-and-thrust belt, showing names mentioned in this study. Geographic names are in italics. Locations of Figures 3 to 6 are also indicated. Abbreviations: AF = Allschwil fault, Bl = Blauen anticline, Ca = Caquerelle anticline, CB = Charmoille basin, DB = Delémont basin, F = Florimont anticline, Fe = Ferrette anticline, FF = Ferrette fault, Gl = Glaserberg anticline, IF = Illfurth fault, La = Landskron anticline, LB = Laufen basin, Vb = Vorbourg anticline. In this study, the term "Ferrette Jura" refers to the entire frontal segment of the fold and thrust belt, whereas "Ferrette anticline" only refers to its frontal arc-shaped anticline. Note the conspicuous N-directed protrusion of the Folded Jura front along NNE-trending faults of the URG system. Inset at top right: tectonic position of the Jura belt between the Alps and the European Cenozoic rift system. Abbreviations: Bes = Besançon, BG = Bresse Graben, RBTZ = Rhein-Bresse transfer zone, URG = Upper Rhine Graben.

of the European Cenozoic rift system, extending over a length of some 300 km from the Rhenish Massif in the north to the Jura Mountains in the south and with an average width of 30 to 40 km. While subsidence in the northern part of the URG was continuous up to the Plio-Pleistocene, it has come to a halt in the southern part in the Early Aquitanian (Fig. 2). This cessation of subsidence was caused by widespread uplift of the Vosges-Black Forest arch. The development of this arch, which entailed uplift of the southern parts of the URG and a truncation of its sedimentary infill, was attributed either to the northward migration of the flexural forebulge of the Alps [*Laubscher*, 1992] or to large-scale lithospheric folding in response to the build-up of a NW-directed stress field that increased collisional coupling between the Alps and their northern foreland [*Ziegler et al.*, 2004]. From Early Miocene times onwards, the southern URG thus became part of the northwestern Alpine foreland and has since then remained under the influence of NW-SE-oriented compression. This led to erosion and/or non-deposition. Correspondingly, a major hiatus in the sedimentary record of the southern URG (Fig. 2) largely prevents analysis of its evolution after the Earliest Miocene.

A compressive reactivation of the URG border faults, such as the Rhine Graben flexure east of Basel, in the Burdigalian has been recently proposed [*Laubscher*, 2001, 2003]. However, exact age and causes of this flexuring remain unconstrained. Flexuring could equally well have been caused by the latest (Earliest Miocene) stages of extension. The kinematics of Early Miocene compressive events, which are linked to the widespread uplift of the Vosges-Black Forest arch, are yet only poorly constrained.

Ongoing shortening in the Alps during the Middle Miocene, leading to stacking of crustal slices in the external crystalline massifs of the Alps, and caused by ongoing subduction of European continental lithosphere [*Schmid et al.*, 1996], led to the decoupling of the Mesozoic sedimentary cover rocks along Mid- to Late Triassic evaporitic series [*Burkhard and Sommaruga*, 1998]. This enabled the propagation of shortening across the Molasse Basin towards the foreland, incorporating the detached sediments into a deforming wedge and creating the folds and thrusts of the Jura Mountains (Fig. 1). As a consequence, the Alpine thrust front propagated to the N and NW from the Serravallian (around 13 Ma) onwards. The northernmost parts of the Folded Jura, however, were probably not involved in deformation before Early Tortonian times (see stratigraphic constraints given in Fig. 2). The detached sediments were thrusted onto the autochthonous cover of the foreland. In northern Switzerland, this autochthonous cover is frequently referred to as "Tabular Jura" because of the horizontal layering of predominant Jurassic-age sediments. At the junction to the URG, the detached sediments encountered pre-existing structures inherited from Paleogene rifting, which had offset the Triassic décollement of the Jura Mountains. This inherited pattern influenced the shape of the northern parts of the developing thin-skinned fold and thrust belt [*Laubscher*, 1977, 1981; *Noack*, 1995]. The total shortening across the Folded Jura, as
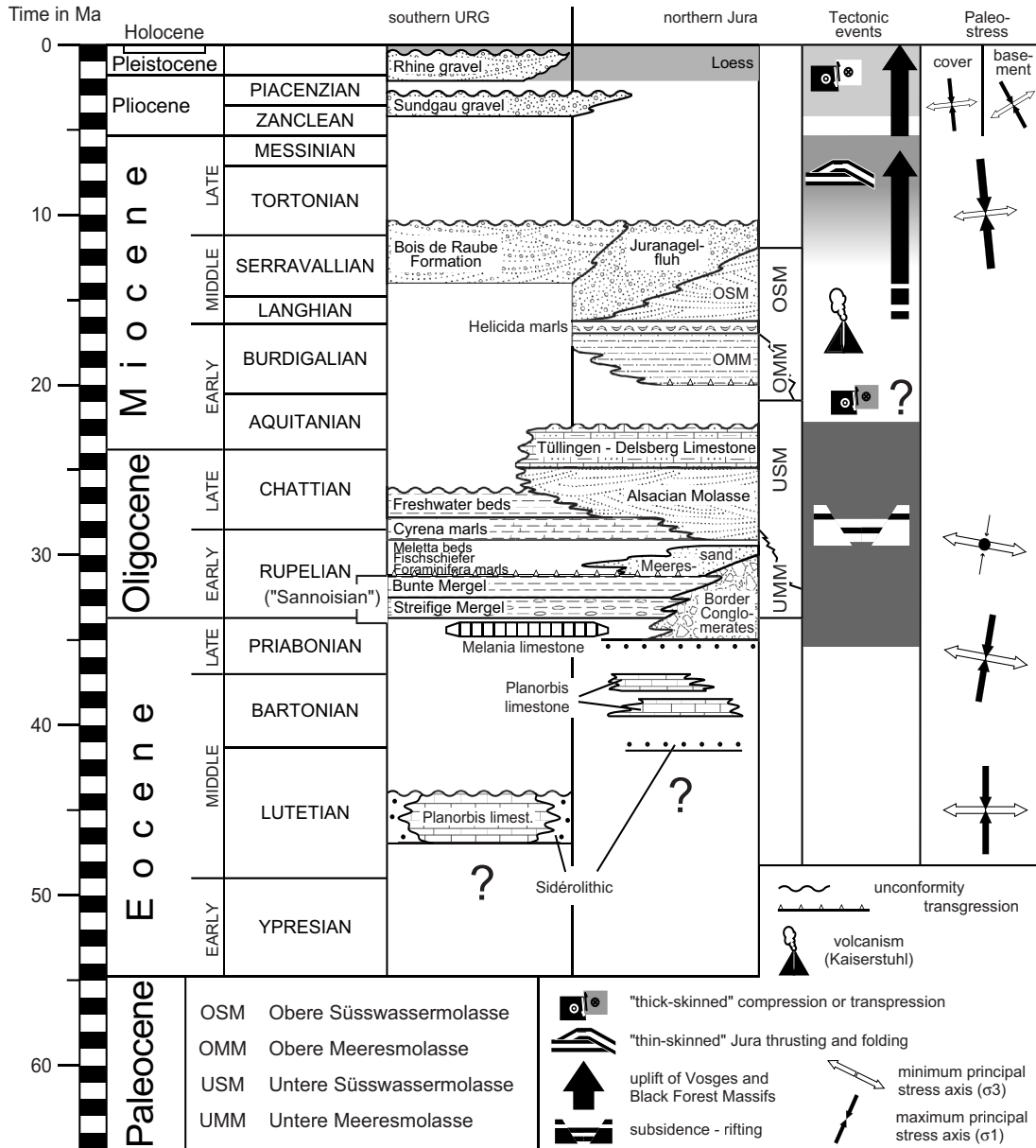
Fig. 2: Chronostratigraphic chart showing the Cenozoic evolution of the southern URG and the southerly adjacent Jura, modified after *Giamboni et al.* [2004].

measured between Molasse Basin and URG south-west of Basel, amounts to some 12 km [*Philippe et al.*, 1996].

Since the Late Pliocene (since about 3 Ma ago), NW-SE- to N-S directed shortening has propagated northward and encroached on the southernmost parts of the URG [*Meyer et al.*, 1994; *Nivière and Winter*, 2000; *Giamboni et al.*, 2004]. While the foregoing deformation was largely restricted to the sediments detached along the Mid- and Upper Triassic weak layers [*Philippe et al.*, 1996], this most recent shortening appears to be entirely rooted in the basement [*Meyer et al.*, 1994; *Giamboni et al.*, 2004]. In the present-day stress field the southeastern URG is subjected to sinistral transtensive strike-slip motion [*Larroque and Laurent*, 1988; *Schumacher*, 2002], as evidenced by the study of earthquake focal mechanisms [*Plenefisch and Bonjer*, 1997; *Deichmann et al.*, 2000; *Lopes Cardozo and Granet*, 2003;

Kastrup et al., 2004], whereas the area of the RBTZ is conceivably experiencing incipient dextrally transpressive inversion of Permo-Carboniferous troughs [*Meyer et al.*, 1994; *Ustaszewski et al.*, 2005b].

3.2 Analysis of fault-slip data and paleostress reconstruction

3.2.1 Fault-slip data collection

The orientations of faults and corresponding striations ("fault-slip sets") were measured at numerous sites in the study area in order to derive the orientations of what is commonly referred to as the orientation of "paleostress" axes, although these axes often may reflect types of incremental or even finite strain rather than principal axes of the paleostress tensor. The majority of the data were acquired in Mesozoic limestones and to a lesser extent in Tertiary sediments (e.g. Fig. 3a and c). Fault-slip senses were inferred from various shear sense indicators on the fault planes [*Hancock*, 1985; *Petit*, 1987]. The most abundant indicators were slickolites (oblique stylolites), best developed in micritic Upper Jurassic limestones. Less frequently, slickenfibres (oblique fibrous growth) were found, mainly in oolithic limestones of both Mid- and Upper Jurassic age (Fig. 3b). Crescentic (or lunate) fractures, tensile cracks and/or Riedel shear planes were restricted to massive, coralliferous Upper Jurassic limestones and/or to cataclasites near to or directly within fault zones. Occasionally, pressure solution pits and striated pebbles (Fig. 3a), horizontal stylolite peaks [*Plessmann*, 1972] or calcite-filled tension gashes (Fig. 3c), were also used to infer the shortening directions.

The quality of slip sense indicators was classified into "excellent", "good" and "poor" in order to allow for weighting during subsequent paleostress axes calculations. Additionally, the "importance" of faults was estimated in a qualitative manner based on (1) the dimensions of the exposed part of the fault plane, (2) the amount of displacement (if detectable) and (3) the presence or absence of cataclasite or fault gouge. Most of the analyzed faults, however, revealed slickolites associated with displacements in the order of a few mm only and, thus, record very small increments of strain.

Overprinting relationships (cross-cutting faults, superimposed slickensides, e.g. Figs. 3a to d) allowed establishing a relative chronology of faulting. This, in turn, permitted a separation of heterogeneous fault populations into homogeneous subsets that reflect one particular deformation phase only. The separation of polyphase fault populations was facilitated by the "incremental strain-axes" or P-T-axes method [*Marrett and Allmendinger*, 1990].

Fault-slip sets collected in tilted strata were rotated back into a position where bedding was horizontal before performing stress axes calculations. This procedure is justified by direct observations, which indicate that strata were mostly horizontal at the onset of reverse faulting/thrusting, yet before their involvement in folding (Fig. 3e and f). The stress
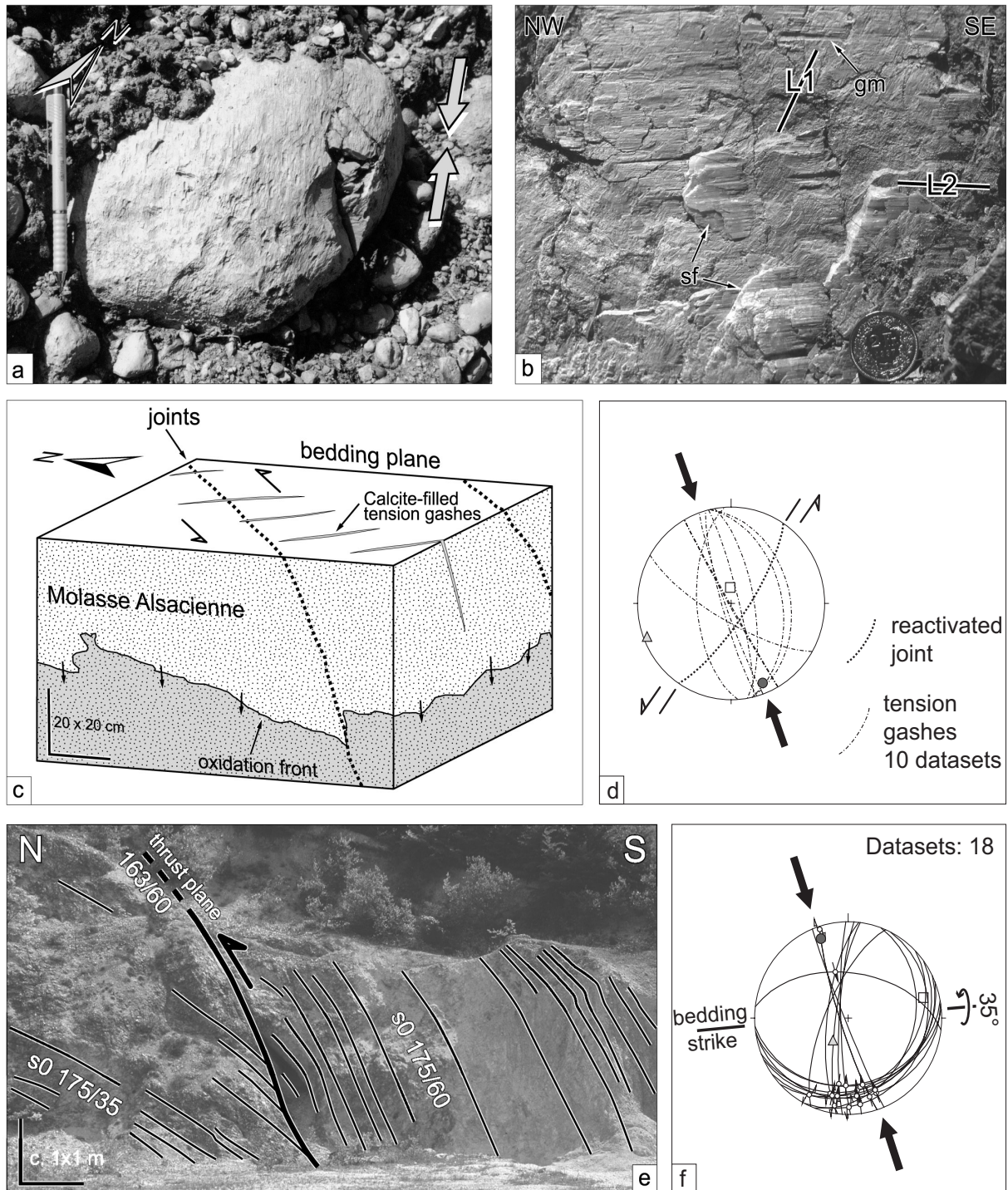
Fig. 3: Selected examples of cross-cutting relationships that constrain kinematics and relative age of deformation structures observed in the study area. (a) shortening directions inferred from horizontal pressure-solution pits and striations on limestone pebbles in Lower Oligocene, grain supported conglomerates at the Folded Jura front. Converging arrows indicate shortening direction. Pencil for scale. (b) Superimposed slickensides on a steeply inclined fault plane in Oxfordian limestones. The older slickenside generation (L1) is related to Palaeogene normal faulting. L2 forms both groove marks (gm) and fibrous steps (sf), which clearly overgrow L1. Coin for scale. (c) NNE-trending joints in Chattian sands in the Delémont Basin. The joints, delineated by an oxidation front, are crosscut by en-échelon aligned, calcite-filled tension gashes, suggesting that the joints accommodated minor sinistral strike-slip motion. (d) stereographic representation Jf data from (c). (e) southward tilted top-to-the-N thrust within Oxfordian limestones on the S-limb of the Ferrette anticline. (f) stereographic representation of fault-slip data at (e), back-rotated into a position where bedding is horizontal. All plots in this study are lower hemisphere, equal area projections. See Fig. 1 for locations of the outcrops.

45

axes derived from back-rotated fault-slip sets thus reflect the stresses at the onset of folding. Concerning the azimuths of the stress axes, the difference between "non-rotated" and "back-rotated" fault-slip sets was usually negligible, because few fault-slip data were measured in strata inclined by more than some 40°.

In this study, we focus on fault kinematics that post-date Paleogene rift-related extension of the URG recently described elsewhere [*Ustaszewski et al.*, 2005a]. Correspondingly, the fault kinematics described in the following represent already separated, homogeneous subsets of a more comprehensive analysis [*Ustaszewski*, 2004]. The structural data were visualized as lower hemisphere equal area projections using computer program "TectonicsFP", version 2.0 PR [*Reiter and Acs*, 1996-2000].

3.2.2 Cross-cutting relationships and timing constraints of fault kinematics

Before presenting the results of the paleostress analysis it is necessary to address problems of repeated reactivation of pre-existing faults, strain partitioning between strike slip faulting and folding, as well as relative and absolute timing constraints of the kinematics of faulting. In the following we present particularly clear examples that, amongst others, provide such valuable information.

A particularly clear example for the repeated formation of horizontal slickolites along strike-slip faults and their subsequent tilting due to ongoing folding was observed in a locality along the NNE-SSW-trending part of the Ferrette anticline ("Fe" in Fig. 1) and presented in Fig. 4. There, two generations of dextral slickolites on a subvertical fault plane, oriented perpendicularly to the strike of bedding, are observed. An older generation (L1) is overprinted by a younger generation (L2) that "incises" into L1. L1 is tilted by the same amount as the bedding planes, suggesting that it originally formed while bedding was still horizontal. After tilting of the beds due to folding during a second strain increment, pure dextral strike-slip faulting in a horizontal direction resumed, due to a third increment of deformation. This, and many other similar observations suggest that repeated permutation between folding and strike-slip faulting, such as postulated for the Jura arc in general [*Laubscher*, 1972], did also occur along the western rim of the Ferrette anticline.

Exemplary observations pointing towards multiple reactivation of pre-existing faults were also made near the northern tip of the Ferrette anticline, where the strike of this anticline abruptly sways around 60° from a NNE-SSW- into an E-W-trend. There (see data presented in Fig. 5), NNE-trending conjugate faults (inherited from Paleogene extension, Fig. 5c) were first reactivated as extension veins that accommodate E-W-extension during (N)NE-(S)SW-directed compression, presumably during the Early Miocene (Fig. 5d). The vein thickness reaches approximately 15 m in the outcrop. Later, i.e. during Jura folding in Late Miocene to Early Pliocene times the same veins became sinistrally offset (Fig. 5 a, b and e). Horizontal slickensides reveal various pitch angles, often on the same fault plane. The latter observation again shows that strike-slip faulting was concomitant with progressive folding
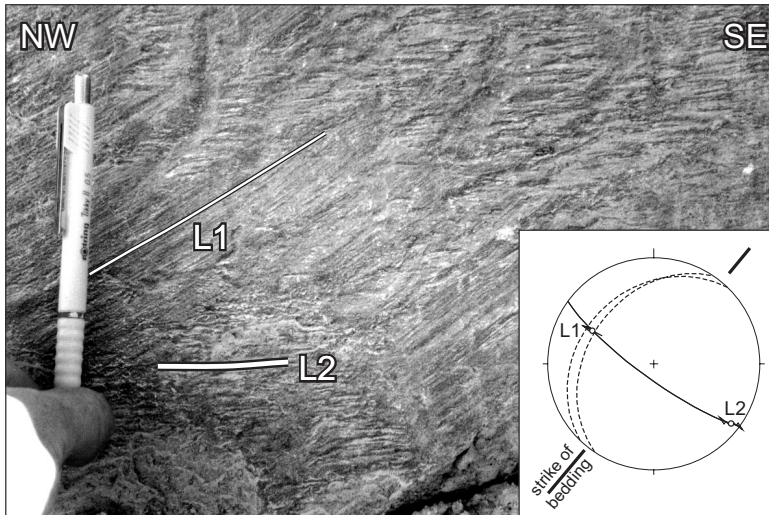
Fig. 4: Repeated formation of horizontal slickensides on a fault plane in Mid-Jurassic limestones along the Jura front, concomitant with progressive tilting. New slickolites (L2) "carve" into older slickolites (L1) that were already tilted during an earlier folding increment. Bottom right inset illustrates the situation in a stereoplot. See Fig. 1 for location.
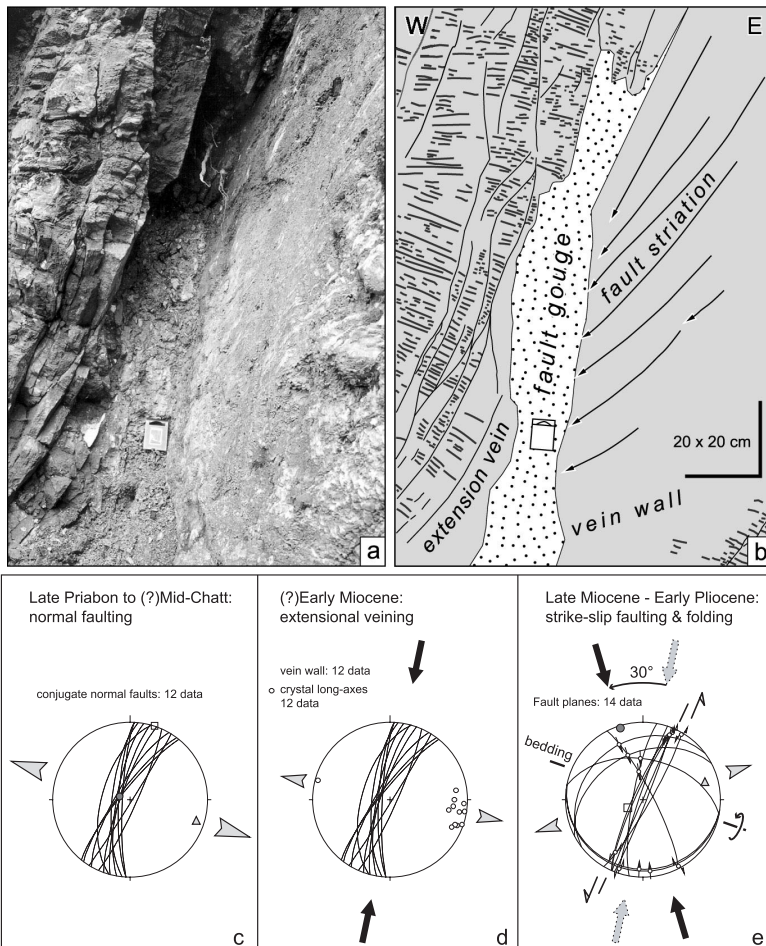
Fig. 5: Multiply reactivated faults in Mid-Jurassic limestones at the northernmost tip of the Ferrette Jura (Fault-slip set #31). Simultaneity of strike-slip faulting and folding accommodates extension perpendicular to the shortening directions. See Fig. 1 for location. (a) and (b) Sinistral offset of pre-existing extension veins, such as those plotted in Fig. 5d, during Jura folding in Late Miocene to Early Pliocene times in a typical outcrop exhibiting fault reactivation. (c) Orientations of NNE-trending conjugate faults inherited from Paleogene extension. (d) Orientations of extension veins accommodating E-W-extension during (N)NE-(S)SW-directed compression in the Early Miocene(?). (e) Orientations of strike slip faults offsetting extension veins and formed during Jura folding in Late Miocene to Early Pliocene times.

at the Jura front. Since this intermittent strike slip faulting is linked to ENE-WSW extension, it indicates minor extension perpendicular to the dominant direction of horizontal shortening that is accommodated by folding/thrusting. This minor extension is probably linked to the formation of the tightly curved deformation front of the Ferrette anticline.

At the southern end of the Caquerelle anticline ("Ca" in Fig. 1) dm-bedded, Upper Jurassic limestones are dissected by NNE-trending subvertical karst fissures, which most
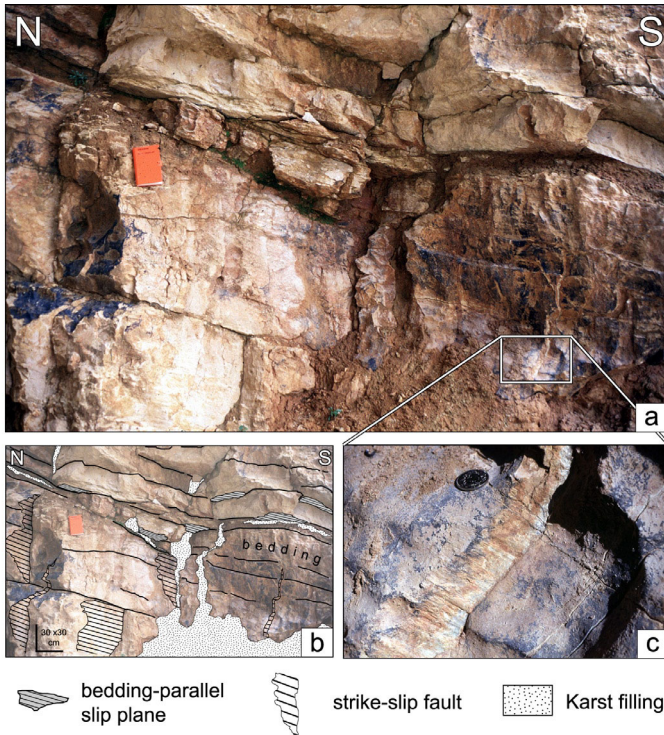
Fig. 6: (a) outcrop of Upper Jurassic limestones at the southern end of the Caquerelle anticline. The limestone is dissected by subvertical, NNE-trending karst fissures that contain OMM-OSM sediments [*Hug et al.*, 1997a, 1997b]. The walls of the karst fissures are affected by sinistral strike-slip faults, which are partly offset themselves along bedding-parallel slip planes (evidenced by the fissure infill smeared out along bedding planes). (b) interpreted line-drawing of (a), (c) detail of (a), coin for scale. See Fig. 1 for location.

likely formed along Paleogene joints. The sedimentary infill of these fissures contains marine (at the bottom) and continental faunas (on top) of Late Burdigalian to Serravalian age, which were correlated with deposits from the Molasse Basin south of the Jura Mountains [*Hug et al.*, 1997a, 1997b]. Small-scale sinistral strike-slip faults displace the karst fissures (Fig. 6). However, the same fissures are also offset by bedding-parallel slip related to folding of the Caquerelle anticline, as can be judged from the sedimentary infill smeared out along bedding planes. These outcrop-scale observations not only provide excellent timing constraints but also show that the formation of Jura folds (such as the Caquerelle anticline) is intrinsically connected with the reactivation of pre-existing, URG-parallel discontinuities. Such oblique folds form parallel to and above pre-existing Paleogene normal faults that did offset the future décollement horizon. Fig. 7 provides a schematic block diagram, further illustrating the sequence of deformation events recorded at the southern end of the Caquerelle anticline.

3.2.3 Paleostress determination

Based on superposition criteria such as those described above, more than 600 fault-slip data collected at 60 localities were attributed to deformation that post-dates Paleogene URG extension, linked to another set of fault slip data described elsewhere [*Ustaszewski et al.*, 2005a]. 53 fault-sampling localities yielded sufficient data for deriving the orientations of the principal kinematic axes and applying the inversion techniques described below. Each fault sampling location defined a dataset consisting of a minimum of 2 and up to 41 fault-slip sets.

The orientations of the principal shortening, intermediate and extension axes have been primarily determined by applying the Right Dihedra Method (RDM) [*Angelier and Mechler*, 1977; *Pfiffner and Burkhard*, 1987]. This method is a purely kinematic approach and applicable to any fault slip set. It only considers directions and senses of slip and makes
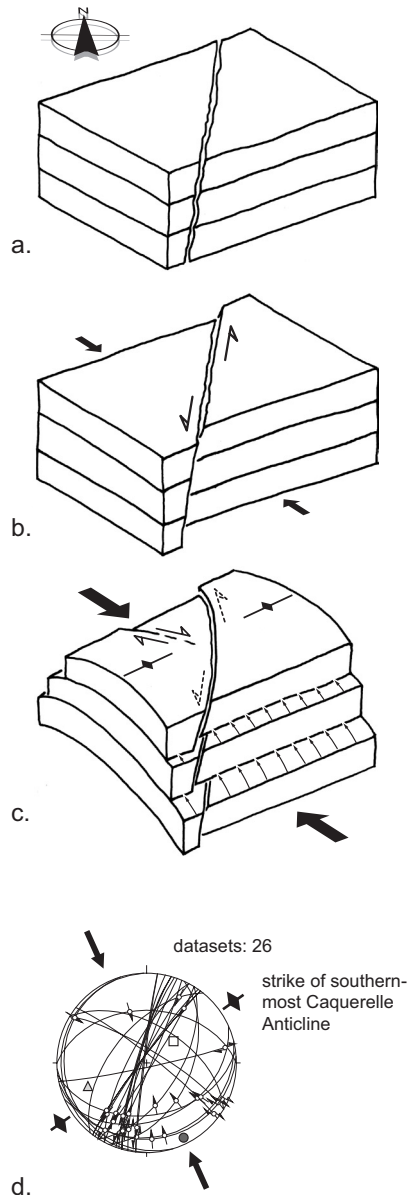
Fig. 7: schematic block diagram illustrating the deformation sequence as observed in Fig. 6. (a) bedded limestones dissected by NNE-oriented karst fissures, which originated as Paleogene joints. (b) sinistral reactivation of the karst fissures under compression. (c) flexural-slip folding partially offsets the fissures along bedding-parallel slip planes, but strike-slip faulting continues to a lesser extent. (d) stereographic representation of data collected at the outcrop of Fig. 6.
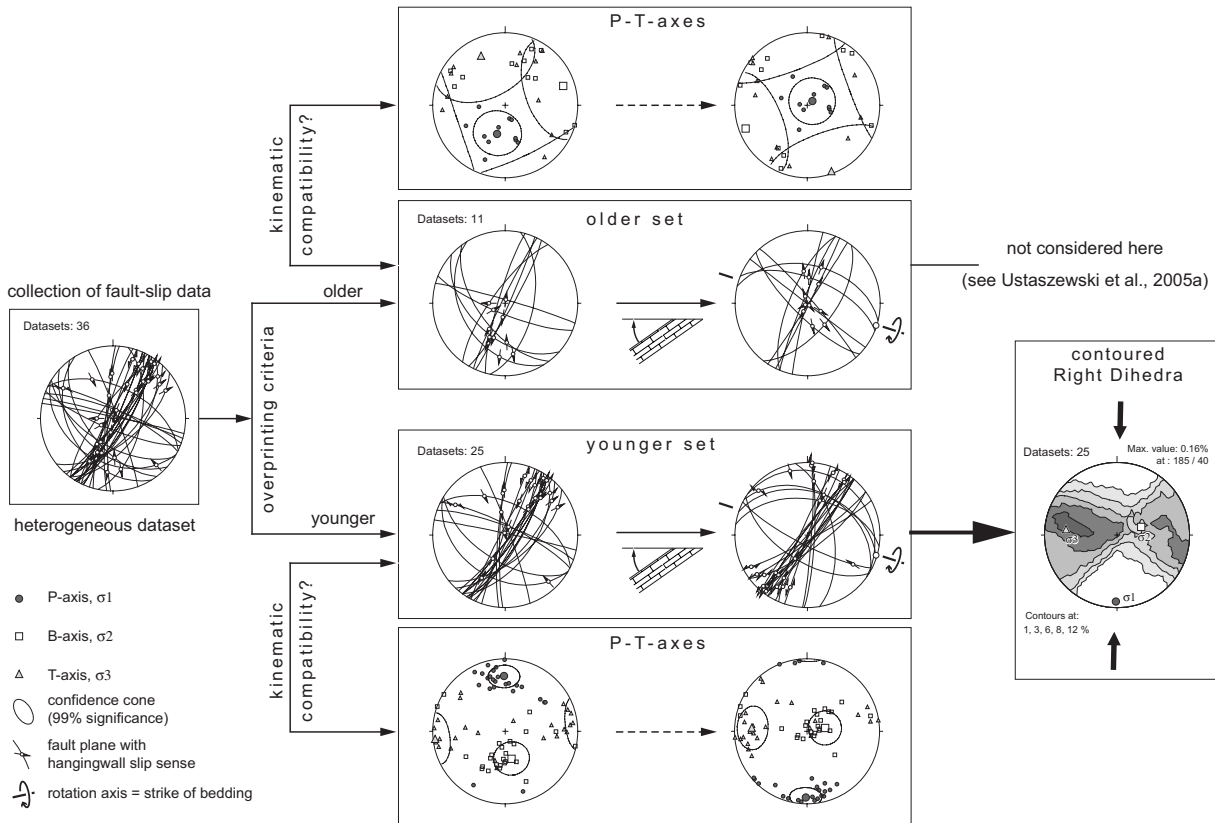
no assumptions regarding the angle of internal friction. Strictly speaking, the RDM yields the finite strain axes of a population of fault-slip sets [*Pfiffner and Burkhard*, 1987]. In order to conform to previous work, we refer to the axes derived with the RDM as "principal stress axes" (σ1, σ2 and σ3) or "paleostress" axes. The use of the RDM in the present study was justified because (1) the sampled fault-slip sets usually showed a homogeneous spatial coverage, (2) only fault-slip sets representing "pure shear" were considered for calculation (i.e. we rejected "simple-shear" fault-slip sets with one family of planes) and (3) the results were coherent with other "stress" markers observed, such as horizontal stylolite peaks. The results were considered reliable when the maxima and minima of the contours enclosed the positions of σ1 and σ3, respectively. This means that the obtained stress axes were kinematically consistent with the fault-slip senses recorded. Fault-slip data that were incompatible with the obtained stress axes were excluded from the dataset, first eliminating faults exhibiting low-quality slip-sense indicators. Furthermore, the results derived with the RDM needed to be coherent with results obtained with alternative methods applied to the same data set, namely the P-T-axes method [*Marrett and Allmendinger*, 1990]. A drawback of the RDM is that the derived stress axis orientations do not necessarily reflect an "Andersonian" stress state with two horizontal and one vertical stress axes [*Anderson*, 1951], particularly when a dataset consists of a blend of strike-slip and reverse faults. However, it was of predominant interest in this study to obtain the orientation of σ1, which proved to be subhorizontal for the majority of the data. The procedure of paleostress axes determination is exemplified for one fault-slip set in Fig. 8. In case of non-striated faults or tension gashes, the "Bisector Method" [*Ustaszewski et al.*, 2005a] was applied for deriving the paleostress axes.

The tectonic regime was inferred from the orientations of the principal stress axes and the distribution of P- and T-axes. Thereby we distinguished between (1) reverse faulting or

Fig. 8: Flow chart illustrating the process of separating heterogeneous fault-slip data into homogenous subsets by considering kinematic compatibility and overprinting criteria, as well as application of the Right Dihedra Method to derive the paleostress axes.

thrusting (σ1 horizontal, σ3 vertical; well defined clusters of both P- and T-axes), (2) strike-slip faulting (σ1 horizontal, σ3 horizontal; well defined clusters of both P- and T-axes), (3) transpression (σ1 horizontal and well defined cluster of P-axes, σ2 and σ3 poorly defined, great-circle distribution of B- and T-axes), (4) extension (σ1 vertical, σ3 horizontal). In case of small datasets (4 or less datasets), no classification of the tectonic regime was made. The azimuths of σ1 and σ3 define what we will refer to as "shortening" and "extension" directions when analyzing these directions in map view. The principal stress axes determined at each site are summarized in Fig. 9 and Table 1. The datasets are sorted from west to east. Shortening directions were plotted as converging arrows at the corresponding sites in Fig. 10. Fig. 10 also includes 11 datasets from the literature [*Philippe*, 1995; *Braillard*, in prep], as well as maximum horizontal stress directions inferred from in-situ stress measurements in the sedimentary cover in order to compare the paleostress data with the recent stress field [*Reinecker et al.*, 2003].

The orientations of the principal stress axes of the total of 53 datasets analyzed in this study are given in Fig. 11. The salient feature of this compilation of new data is that azimuths of σ1-axes range from NW to NNE, clustering around a N-S orientation with a mean vector of 176/02. The σ3-axes, on the other hand, are distributed along an E-W-oriented meridian, which reflects the tectonic regime characterized by the interchange between strike-slip and reverse faulting/thrusting. A nearly identical picture is obtained when only the datasets from
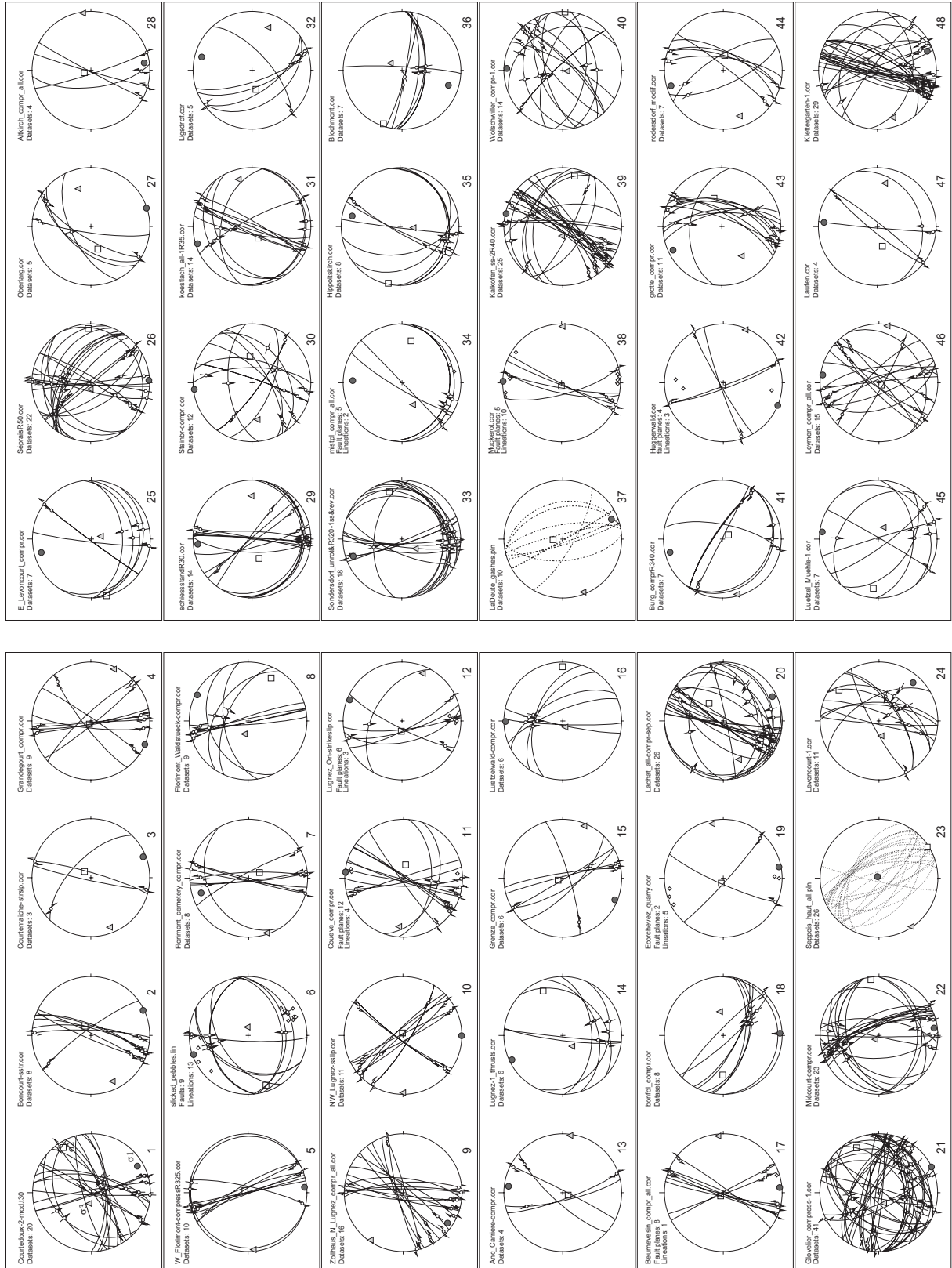
Fig. 9: Stereographic representation of fault sets and paleostress axes orientations obtained at 53 sites. Numbers at the lower right of each plot correspond to the numbering of the datasets in Table 1.

Fig. 9 (continued)

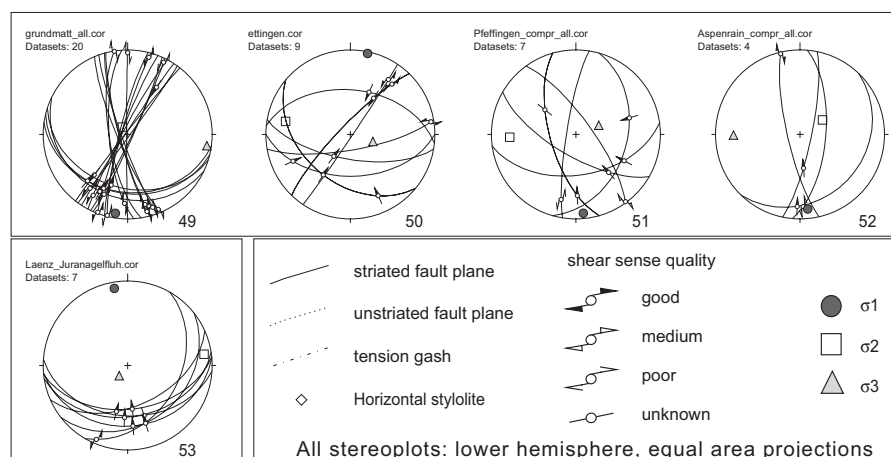| No.	Location	X	Y	Age	s1_azi	s1_pln	s2_azi	s2_pln	s3_azi	s3_pln	N	n	regime
1	SW Courtedoux (JU)	567800	249175	Kimmeridge	150	11	058	11	284	75	20	1	transpression
2	Boncourt JU	568400	260500	Oxford	154	02	058	75	245	15	8	0	strike-slip
3	W Courtemaiche JU	569750	256640	Oxford	158	05	044	78	249	11	3	0	strike-slip
4	Grandegourt JU	570650	257940	Oxford	204	01	294	85	114	05	9	0	strike-slip
5	W Florimont	571000	261950	Oxford	180	07	034	82	270	05	10	2	strike-slip
6	SE Courtedoux JU	571275	250350	U-Priabon to L-Rupel	342	03	252	15	074	75	9	0	reverse
7	Florimont village	572100	262175	Oxford	343	17	153	73	252	03	8	1	strike-slip
8	Florimont forest	572425	261900	Oxford	027	03	118	18	287	71	9	1	strike-slip
9	S Courcelles	573250	260000	Oxford	214	09	050	80	305	03	16	0	strike-slip
10	NW Lugnez JU	573400	259775	Oxford	180	01	079	86	270	04	11	0	strike-slip
11	Coueve JU	574075	256725	Oxford	006	01	098	71	276	19	12	0	strike-slip
12	Lugnez JU	574560	258975	Kimmeridge	022	05	273	76	113	13	6	0	strike-slip
13	SW Rechesy	574790	261050	Oxford	007	08	204	82	097	02	4	0	unknown
14	N Lugnez JU	574925	260150	Oxford	334	05	066	19	230	71	6	0	reverse
15	SE Rechesy	576325	261050	Oxford, U-Priabon to L-Rupel	202	05	338	83	112	05	6	0	strike-slip
16	E Rechesy	577075	261450	Oxford	359	03	090	09	250	81	6	0	reverse
17	Beurnevesin JU	577275	260300	L Kimmeridge	175	04	311	84	085	04	8	0	strike-slip
18	N Bonfol JU	577650	259250	L Kimmeridge	178	04	271	33	081	56	8	0	reverse
19	SE Vendlincourt JU	578775	255275	Oxford	169	04	291	83	078	06	2	0	strike-slip
20	W Glovelier JU	580300	242100	Upper Oxford	154	08	051	58	248	30	26	0	transpression
21	Glovelier JU	580660	241990	Kimmeridge	154	00	064	16	245	74	41	0	transpression
22	NW Miécourt JU	580700	253575	Kimmeridge	172	07	082	05	316	82	23	2	transpression
23	Seppois-le-Haut	581600	264400	U-Pliocene	037	87	146	01	236	03	26	0	extension
24	E Levoncourt	583075	255700	Oxford	132	14	038	15	262	69	11	0	transpression
25	E Levoncourt	583375	255850	Bajoc-Bathon	345	13	255	00	163	77	7	1	transpression
26	Séprais JU	584200	246700	Kimmeridge	178	01	087	09	275	81	22	3	transpression
27	N Oberlarg	584800	256950	Oxford	162	01	253	57	071	33	5	1	strike-slip
28	Altkirch	585500	275800	Lower Rupel	172	08	304	81	080	05	4	0	strike-slip
29	Durlinsdorf	585625	259550	Bajoc-Bathon	355	08	250	61	089	27	14	2	transpression
30	Durlinsdorf	585900	259450	Bajoc-Bathon	353	02	086	53	262	37	12	1	transpression
31	Koestlach	588100	261600	Bajoc-Bathon	343	03	242	72	074	18	13	0	transpression
32	W Ligsdorf	589225	257750	Oxford	015	13	258	63	110	23	5	0	strike-slip
33	W Sondersdorf	591400	259275	Oxford	341	14	075	18	216	67	18	3	reverse
34	SW Luppach	591500	261075	Oxford	003	17	102	28	244	56	5	0	reverse
35	Hippoltskirch	592775	258075	Oxford	012	18	282	02	186	72	8	0	reverse
36	SSW Blochmont	592875	255160	Oxford	198	19	289	04	031	71	7	1	reverse
37	S Delémont JU	593150	244320	Chattien	158	13	359	76	249	05	10	0	strike-slip
38	Muckerot	594812	259525	Oxford	001	01	278	86	091	04	5	0	strike-slip
39	S Fislis	594879	260800	Oxford	013	01	103	13	277	77	25	1	transpression
40	S Wolschwiller	597300	255950	Oxford	002	06	092	01	191	84	14	0	reverse
41	Burg im Leymental BL	600000	256200	Oxford	346	09	146	80	255	03	7	0	reverse
42	Huggerwald SO	600200	252750	Oxford	202	00	295	87	112	03	4	0	unknown
43	Biederthal	600500	257100	Oxford	334	09	074	49	237	40	11	0	unknown
44	Rodersdorf SO	601675	258600	Oxford	343	08	095	69	251	19	7	1	strike-slip
45	Muehle Luetzeltal	601700	252750	Oxford	007	05	276	17	112	72	7	0	unknown
46	Leymen	603300	259850	Oxford	008	04	222	85	098	03	15	0	strike-slip
47	Muehle Laufental	604000	251325	Oxford	005	10	255	62	100	26	4	0	unknown
48	E Flüh SO	605150	258750	Oxford	159	10	039	70	252	17	29	0	transpression
49	Grundmatt, S Ettingen BL	607225	258300	Oxford	189	06	324	81	098	06	20	0	transpression
50	S Ettingen BL	607525	258350	Oxford	012	02	281	23	107	67	9	0	reverse
51	Pfeffingen BL	610075	256800	Oxford	175	07	268	23	068	66	7	1	unknown
52	Chollholz BL	617825	262375	Bajoc-Bathon	172	16	055	56	271	27	4	0	unknown
53	S Diegten BL	627325	249800	Torton	350	08	082	09	219	77	7	1	reverse

Table 1: Paleostress reconstruction sites (Swiss National coordinates) with prevalent lithology and stratigraphic age. s1_azi, s2_azi, s3_azi = azimuth of sigma1, -2 and –3, respectively. s1_pln, s2_pln, s3_pln = plunge of sigma1, -2 and –3, respectively. N = number of fault-slip sets per site, n = number of faults with unknown slip sense.
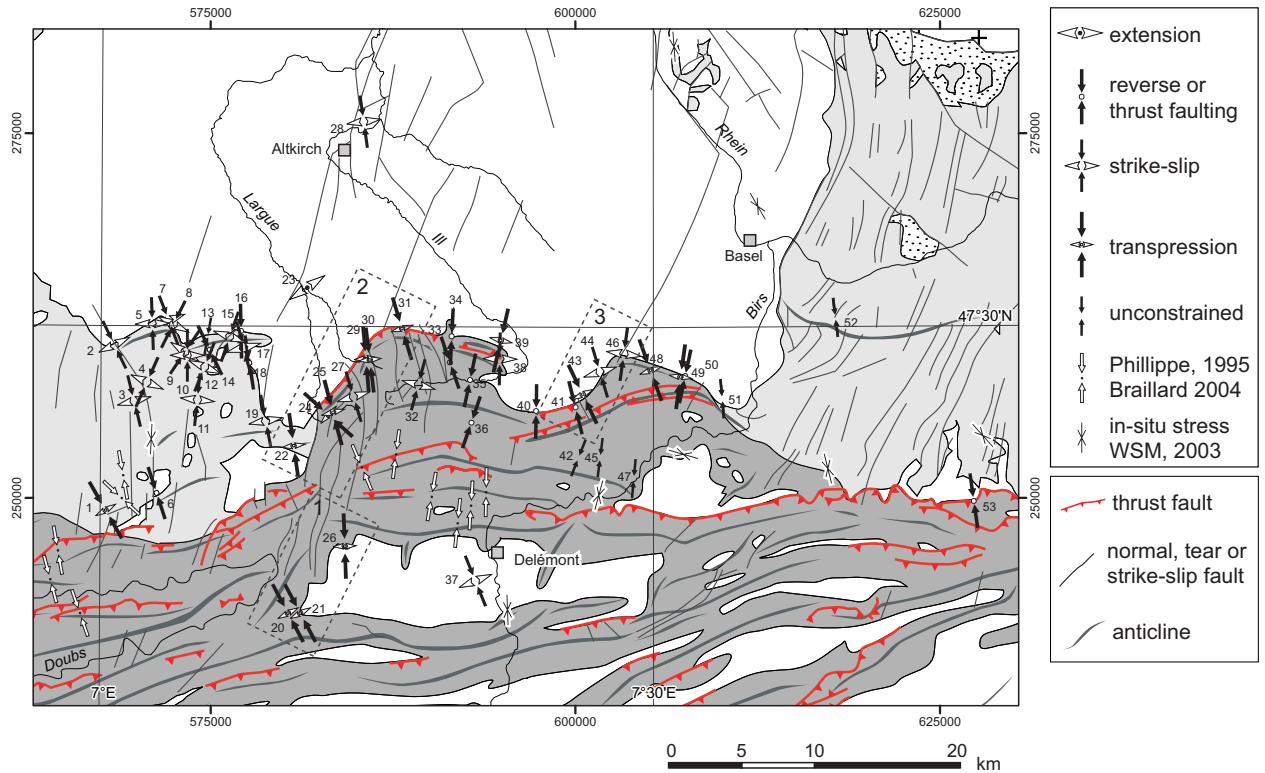
Fig. 10: Shortening (converging arrows) and extension directions (diverging arrows) derived for the northernmost Jura and adjacent URG [*Philippe*, 1995; *Braillard*, in prep]. In-situ stresses in the sedimentary cover, taken from the World Stress Map project [*Reinecker et al.*, 2003], are plotted for comparison. Numbers at map edges refer to the Swiss National grid. Patterns and map symbols are identical to those used in Fig. 1. Numbering of the datasets corresponds to Table 1 and Fig. 9. Dashed rectangles numbered 1 to 3 depict the domains considered in Fig. 12.
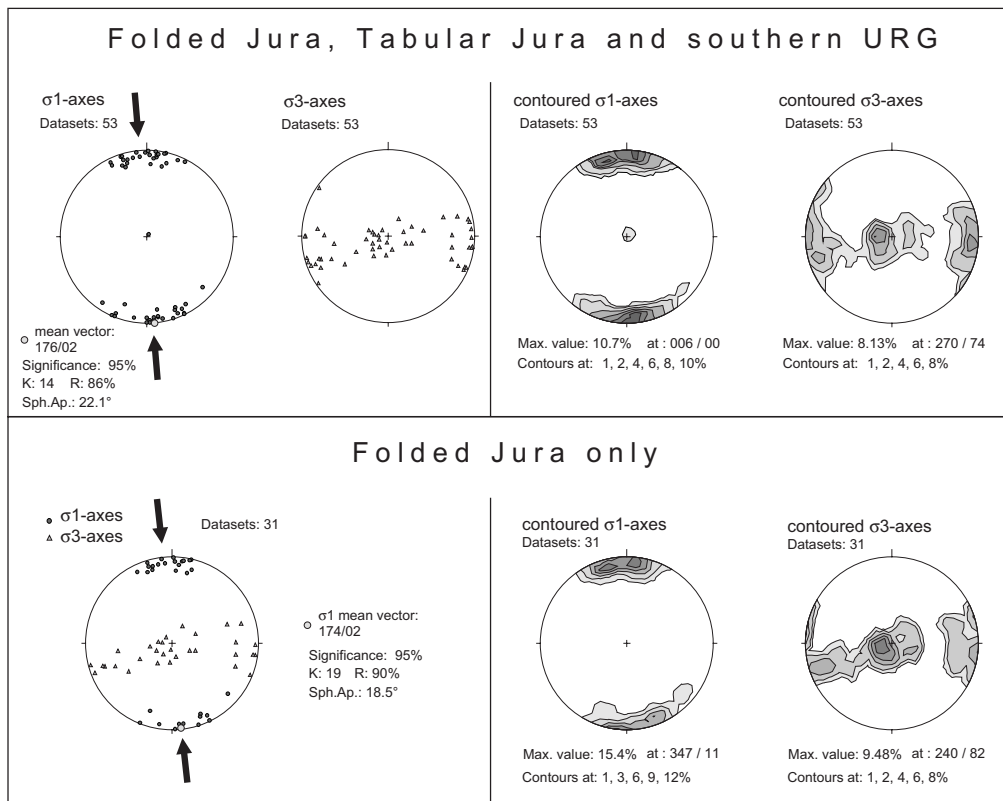
Fig. 11: Paleostress axes from 53 sites collected in this study. Upper row: data comprising the URG and the Folded and Tabular Jura. Lower row: datasets collected in the Folded Jura only.
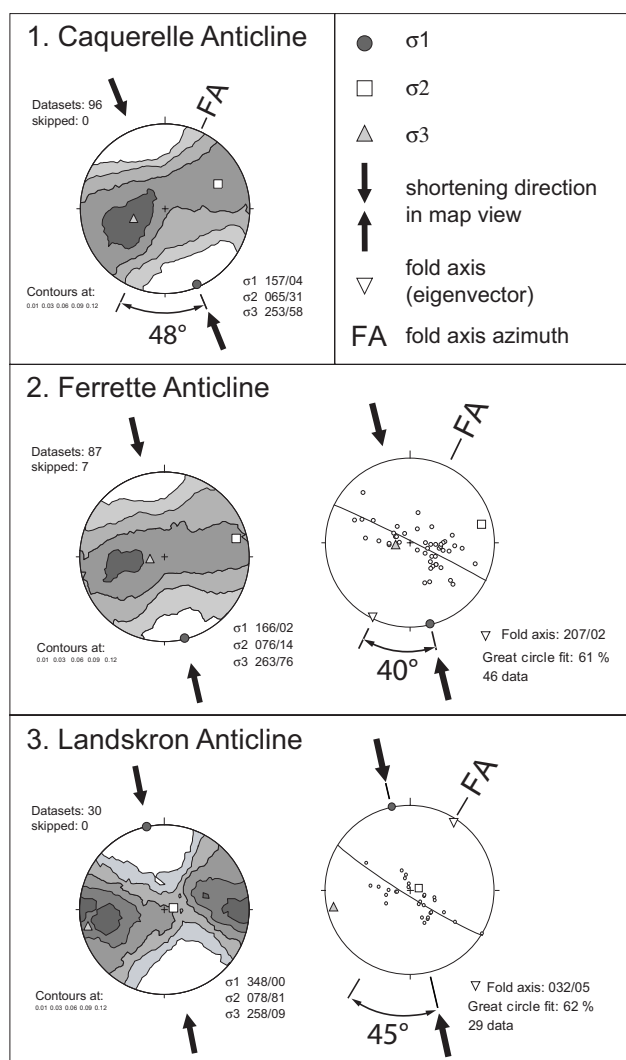
Fig. 12: contoured dihedra and paleostress axes derived in three domains in the Folded Jura (see Fig. 10 for location), demonstrating obliquity between shortening directions and fold trends. The trends of the fold axes (right column) are taken from tectonic maps (domain 1) or calculated from dip data (domains 2 and 3) by Eigenvector analysis.

the Folded Jura are considered (lower row in Fig. 11). In map view (Fig. 10), the shortening directions reveal a slightly northward-diverging fan-shape. This divergence is particularly pronounced at the immediate Jura front. In the W and along NNE-trending anticlines shortening directions are generally (N)NW-oriented. Towards E, they tend to sway into a N- to NNE-orientation.

Three domains that comprise areas where the anticlines strike NNE, i.e. parallel to pre-existing normal faults related to the opening of the URG, were defined (see domains 1, 2 and 3 in Fig. 10). Domain 1 encompasses the entire Caquerelle anticline. Domains 2 and 3 comprise the W segment of the Ferrette and Landskron anticlines, respectively. The large number of individual fault-slip sets collected in these domains was combined into the datasets for these domains as presented in Fig. 12. The left column in Fig. 12 shows bulk paleostress axes and contoured dihedra for these domains. In all three domains, the shortening directions are consistently NNW-oriented. In domains 1 and 2, the contours indicate that the orientations of σ1-axes are well defined, while σ3-directions define a girdle. This again indicates a transpressive regime in which strike-slip faulting and folding/thrusting interchanged. The contours for domain 3, however, reveal well-defined maxima for both σ1 and σ3, indicating a strike-slip regime for this domain. An important feature common to all three domains is the obliquity between fold trend and shortening directions (right column in Fig. 12). The shortening directions are at angles between 40° and 48° in respect to the NNE-trending anticlines. Note that several fault-slip sets measured within the three domains represent bedding-parallel slip planes that are directly related to folding. This, together with the observed obliquity between fold trend and shortening direction, suggests that the folds formed as ramp anticlines above sinistral oblique ramps.
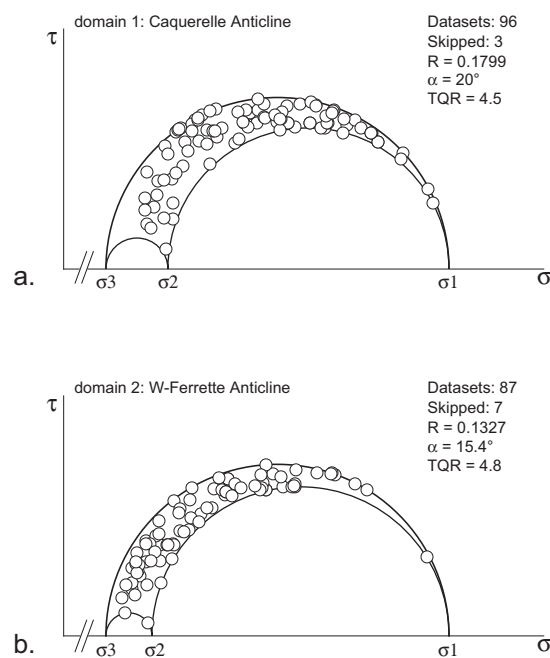
3.2.4 Calculation of "stress ratios" for two areas characterized by oblique ramps associated with Jura folding

It is very likely, and in many cases even proven, that fault-slip data, such as those that yielded the kinematically compatible paleostress orientations presented above, were generated by the reactivation of pre-existing faults or other pre-existing discontinuities that slipped by frictional sliding. Hence inferring "stress ratios" from 3-dimensional un-scaled Mohr-diagrams, such as those presented in Fig. 13 obtained from paleostress data collected within domains 1 and 2 outlined in Fig. 10, i.e. from domains encompassing sinistral oblique ramps, yields valuable information regarding the type of bulk strain achieved by the activation of a large number of fault slip sets.

The reduced un-scaled 3-dimensional "stress tensors" for the fault slip data presented in Fig. 13 were determined by the Numerical Dynamic Analysis [*Sperner and Ratschbacher*, 1994], after first determining the finite strain axes orientations for the bulk datasets with the RDM, i.e. after first finding the best kinematic solution. An angle of 45° was chosen between the incremental shortening axis P and the individual fault striation. In doing so, the "stress axes" determined by the NDA coincide with those determined by the purely kinematic approach of the RDM. For each tensor we also calculated the average misfit angle α, which is the deviation between the calculated slip lineation and the measured lineation for each fault-slip pair. The angle α allows evaluating the quality of the computed stress tensors. In addition, the tensor quality rank TQR (TQR = n(n/N)/α) is indicated [*Delvaux et al.*, 1997], which is another mean to assess the quality of the calculated "stress tensors". TQR values greater than 1.5, such as obtained in our case, are considered very reliable (Fig. 13 and Table 1).

As is seen from inspection of the data compiled in Fig. 13, the R-ratio is very small, implying that the "stress difference" $\sigma2$-$\sigma3$ is very much smaller compared to the stress differences $\sigma1$-$\sigma2$ or $\sigma1$-$\sigma3$. In terms of stress, these data would imply a frequent exchange between $\sigma2$ and $\sigma3$ during progressive deformation, hence a change between thrust and strike-slip mode while the sub-horizontal $\sigma1$ direction remains constantly N-S oriented, such as postulated for Jura folding on a large scale [*Laubscher*, 1972]. However, we prefer

domain 1: Caquerelle Anticline
Datasets: 96
Skipped: 3
R = 0.1799
α = 20°
TQR = 4.5

domain 2: W-Ferrette Anticline
Datasets: 87
Skipped: 7
R = 0.1327
α = 15.4°
TQR = 4.8

Fig. 13: Mohr-Circle diagrams for estimating "stress ratios" from fault-slip sets along oblique ramps in the domains of the Caquerelle (a) and Ferrette (b) anticlines (outlined in Fig. 10). Mohr circles were calculated for a reduced stress tensor that corresponds to the kinematic solution of the RDM. α = average misfit angle, TQR = tensor quality rank [*Delvaux et al.*, 1997], TQR = n(n/N)/ α, where N = number of data per site, n = number of data with known slip sense. See text for further discussion.

to look at these data in terms of the finite strain, which is produced by the partitioning between strains achieved by fault slip sets that accommodate thrusting and strike slip deformations, respectively. According to our interpretation in terms of finite strain, in combination with the information provided by Fig. 12, we infer from Fig. 13 that the amount of strain achieved by strike slip faulting nearly equals that achieved by thrusting. This results in an oblate strain ellipsoid and points to the nearly equally important role of strike slip faulting along pre-existing NNE-SSW-oriented faults, inherited from Paleogene rifting, as compared to thrusting and/or folding related to the formation of the transverse Ferrette and Caquerelle folds. Hence, in the case of these anticlines extreme caution has to be taken when inferring amounts of shortening and/or applying models regarding the formation of arcuate mountain belts [*Hindle and Burkhard*, 1999] from 2-dimensional cross-sections only, as has recently been discussed by *Affolter and Gratier* [2004].

3.2.5 Stratigraphic constraints regarding the timing of deformation related to the analyzed fault-slip data

Constraints on the timing of deformation have recently been improved and this section compares these new data with previously reported data. The maximum age of faulting associated with the formation of the northernmost part of the Jura fold and thrust belt is Late Serravallian to Tortonian, as given by the youngest sediments affected by deformation. This constraint is provided by the Serravalian to Tortonian "Bois de Raube" and "Juranagelfluh" gravels (Fig. 2), which were shed from the Vosges and Black Forest massifs, respectively [*Kälin*, 1997; *Kemna and Becker-Haumann*, 2003]. The "Bois de Raube" gravels crop out in the Ajoie and in the western Delémont Basins, and they are separated from the Vosges by the Vorbourg and Caquerelle anticlines (Fig. 1). The "Juranagelfluh" gravels are found in the eastern Delémont Basin, in the Laufen Basin and in the Tabular Jura SE of Basel (Fig. 1). Mammal remains in the Bois de Raube Fm. provided an age between 13.8-13.2 Ma for the southern occurrences (Delémont Basin) and a slightly younger age of 10.5 Ma for the northern occurrences (Charmoille Basin, "CB" in Fig. 1) of these deposits [*Kälin*, 1997]. These data provide a maximum age for folding of the Vorbourg ("Vb" in Fig. 1) and Caquerelle anticlines of around 13 Ma, while thrusting of the frontal Jura fold and thrust belt onto the autochthonous foreland did not occur before about 10.5 Ma ago [*Becker*, 2000].

The timing brackets regarding the minimum age of the Jura fold and thrust belt are less numerous and conclusive. In the southern Folded Jura near Neuchâtel the horizontally layered infill of karstic fissures found in an inclined limb of an anticline NW of Neuchâtel yielded a mammalian fauna with ages that range between 4.2 and 3.4 Ma [*Bolliger et al.*, 1993; *Steininger et al.*, 1996]. Hence, at this locality folding had ended before these fissures were filled in. However, this timing bracket does not necessarily constrain the minimum age

of the detachment of the Jura fold and thrust belt at its northern edge (i.e. within our study area), since deformation probably migrated in-sequence towards the foreland.

Clear evidence for later deformations is now available for the area of the autochthonous Mesozoic cover north of the Jura fold and thrust belt (northern part of our study area in the Ajoie, see Fig. 1). The Sundgau area (Fig. 1) is nestled by the fluvial "Sundgau gravels", which were deposited in an alluvial plain by an anostomosing braided river system and which were subsequently gently folded [*Giamboni et al.*, 2004], thus providing evidence for late Pliocene to recent deformations in this area. The stratigraphic age of the gravels, determined by mammal stratigraphy, ranges between 4.2 and 2.9 Ma [*Petit et al.*, 1996].

Although gently folded [*Giamboni et al.*, 2004] and locally faulted (such as at locality 23 listed in table 1, see also *Ustaszewski et al*. [2005b]), we interpret the deposition of the Sundgau gravels as post-dating the formation of the thin-skinned Jura fold and thrust belt, based on all data and observations available so far. The current extent of the Sundgau gravels is clearly limited to an area in the northern part of the Tabular Jura of the Ajoie area and the southern part of the URG, where they are found immediately adjacent to the front of the Ferrette anticline (Fig. 1). However, no such gravels are found above the Ferrette anticline [*Giamboni et al.*, 2004] or above the detached Mesozoic of the Jura fold and thrust belt in general. This suggests that the gravels were never deposited in the area of the detached Mesozoic in the first place, or alternatively, that they were eroded later on and concomitant with the formation of the Ferrette anticline. We give clear preference to the first hypothesis according to which a topographic swell, provided by the front of the detached Mesozoic, i.e. the pre-existing Ferrette anticline, would have prevented deposition of the Sundgau gravels in the area of the detached Mesozoic, indicating that the Ferrette anticline already existed as a topographic feature. Hence, the formation of the classical thin-skinned Jura fold and thrust belt in general probably pre-dates the onset of deposition of these gravels at 4.2 Ma ago. This would be in perfect agreement with the constraints available for the more internal parts of the Folded Jura discussed above. The alternative hypothesis is rejected because we would expect that Pleistocene deposits found along the northern slopes of the Ferrette anticline, constituting its erosional veneer, contain a large amount of Alpine-derived material typical for the Sundgau gravels [*Théobald et al.*, 1958; *Liniger*, 1970; *Ruhland et al.*, 1973] together with the locally derived material of Jurassic age. This is clearly not the case as the slope deposits along the Ferrette anticline contain exclusively locally derived Jurassic material and definitely no eroded and re-deposited Sundgau gravels [*Schneegans et al.*, 1934]. In summary, it is concluded that the biostratigraphic age of the Sundgau gravels [*Petit et al.*, 1996] provides a lower time bracket for thin-skinned Jura folding and thrusting that ended some 4.2 Ma ago.

The fault sets we collected within the detached Mesozoic include striated pebbles and small-scale reverse faults observed within the "Juranagelfluh" Formation, found beneath and in front of the frontal Jura thrust, where the Triassic décollement emerges to the surface (dataset 53 in Figs. 9, 10 and Table 1). Consequently, the fault-slip sets collected in the Folded Jura domain and presented in this work are considered to have probably formed between some 13 Ma (10.5 Ma in the north) and some 4.2 Ma ago.

In the autochthonous Mesozoic and the area of the URG (Fig. 1) it is not easy to decide as to when the measured fault sets formed, since this area is clearly also affected by post 4.2 Ma thick-skinned deformation [*Giamboni et al.*, 2004; *Ustaszewski et al.*, 2005b], suggesting further northward propagation of shortening. Only in one case could data have been obtained within the very poorly outcropping Sundgau gravels (locality 23 in Fig. 9). It is likely that the fault-slip data found in the immediate foreland of the frontal Jura thrust can be attributed to horizontal far-field stresses exerted by the nascent thin-skinned Jura belt onto its autochthonous foreland before some 4.2 Ma ago. On the other hand, the paleostress data obtained on fault sets formed during the formation of the two en-échelon-aligned anticlines at the Tabular Jura – URG boundary ("F" and "R" in Fig. 1), attributed to post-Late Pliocene shortening and coeval with the folding of the Sundgau gravels [*Giamboni et al.*, 2004]. These data do not show significant deviations from those obtained further to the south (Fig. 10 and 11). Note also that the maximum horizontal stress directions derived from in-situ stress measurements are largely identical with those derived from the paleostress analysis within both the Folded and Tabular Jura (Fig. 10). It is therefore concluded that no major change of the stress field did occur after some 4.2 Ma ago, i.e. after the onset of thick-skinned deformation of the autochthonous Mesozoic and the Tertiary deposits of the URG north of the thin-skinned Jura fold and thrust belt.

3.3 Inferences from map view and newly constructed cross sections

The Ferrette and Landskron anticlines, i.e. the northernmost anticlines of the Folded Jura depicted in Fig. 14, abruptly change strike by some 60-70°. The western, NNE-trending segments of the two anticlines are oriented parallel to a pair of prominent W-dipping Paleogene normal faults of the URG, both of them delimiting halfgrabens. The geometry of these halfgrabens can be inferred from the Base-Tertiary surface contours shown in Fig. 14, constructed from reflection seismic lines and well-data [*Ustaszewski*, 2004].

Two boreholes, whose location is indicated in Fig. 14, provide evidence that Mesozoic sediments of the northern limb of the Ferrette anticline overthrusted Paleogene syn-rift deposits of the URG, as depicted in Fig. 15a. The NNE-trending part of the Ferrette anticline exposes Lower to Mid-Jurassic sediments in its core. The entire western part of the Ferrette Jura is dissected by a dense array of tear faults that trend at angles of 15 – 20° to the strike of the anticline. Several anticlines appear sinistrally dragged along these NNE-oriented faults.
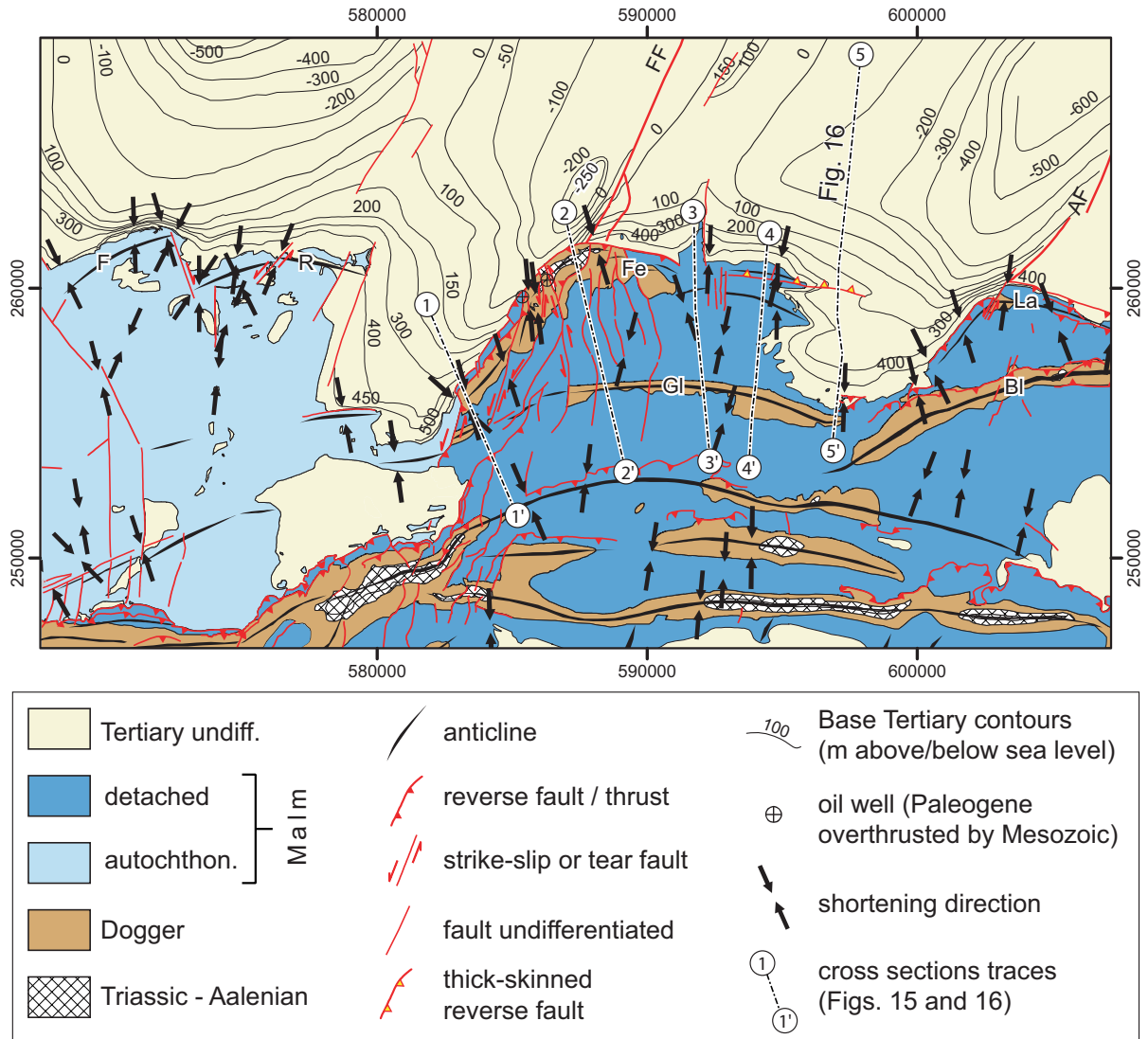
Fig. 14: geologic-tectonic map of the northernmost Folded Jura. The frontal Ferrette and Landskron anticlines change their trend by some 60-70° along-strike. Their western segments are parallel to (and partly overthrust) Paleogene halfgrabens. The shortening directions (converging arrows) tend to sway from a (N)NW- into a N- to NNE orientation along strike from W to E. Labeling of anticlines and faults corresponds to Fig. 1.

At the northernmost tip, where the anticline abruptly sways into an ESE-orientation, a minor top-to-the-S backthrust delimits a transpressive pop-up (see profile in Fig. 15b). Towards the ESE, the amplitude of the Ferrette anticline progressively diminishes until the gently folded Mesozoic strata plunge beneath Paleogene syn-rift sediments of the Tertiary fill of the Allschwil half-graben, located between the Ferrette and Landskron anticlines (Fig. 14). The associated axial plunge of the Ferrette anticline towards E is again a feature inherited from rifting, since the pre-rift Mesozoic sediments originally, i.e. before the formation of the Ferrette fold, gently dipped towards the E within the Allschwil half-graben.

The four cross-sections across the Ferrette Jura depicted in Fig. 15 roughly trend parallel to the shortening directions derived from the fault-slip data analysis. At the same time they are not everywhere perpendicular to the macro-structures they traverse. Particularly cross-sections 1-1' is oriented obliquely to the structural grain (Fig. 14). Cross-sections 1-1' and 2-2' (Fig. 15 a, b) were constructed using existing geological maps [*Schneegans et al.*,

59
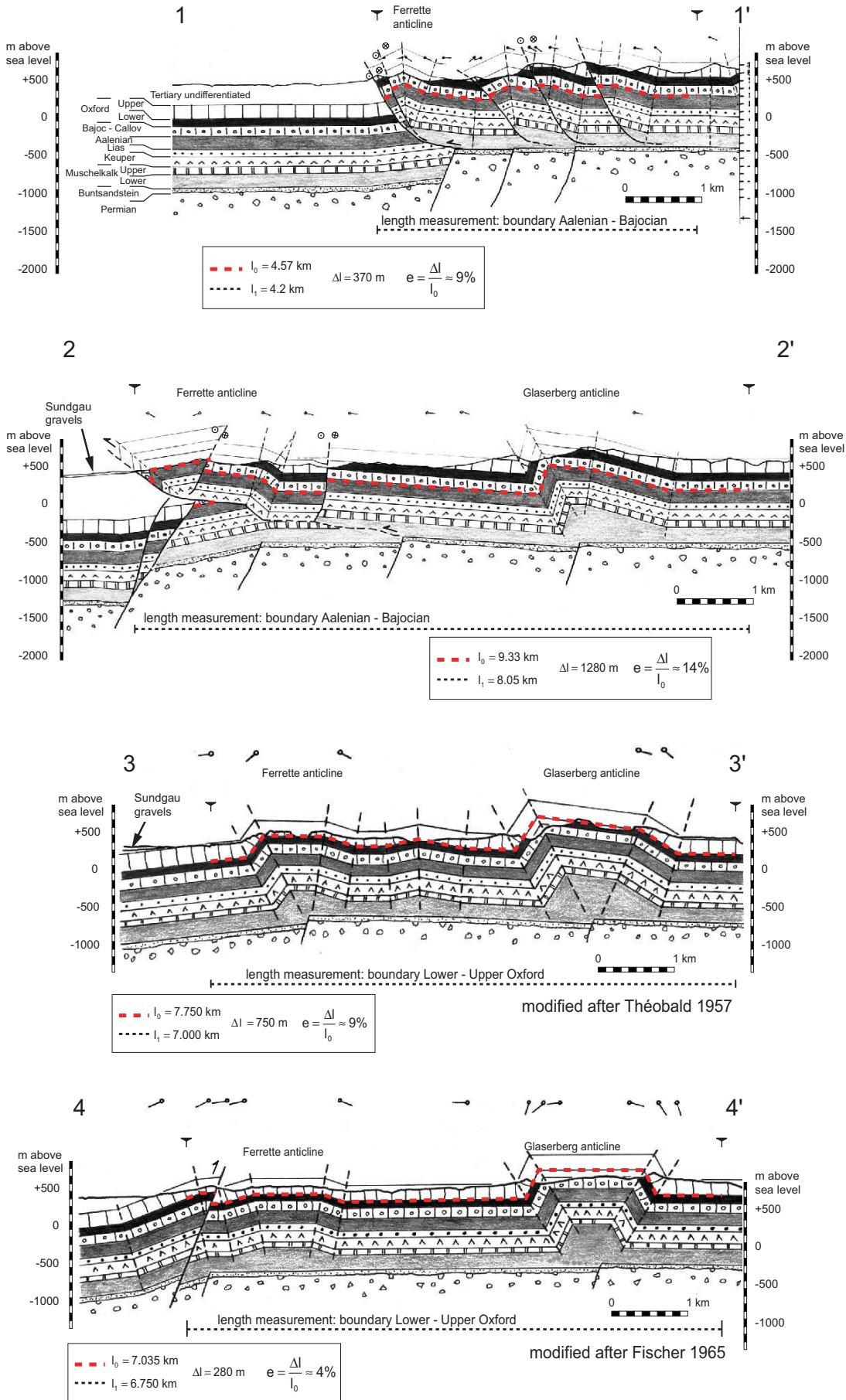
Fig. 15: cross-sections across the Ferrette Jura constructed roughly parallel to the shortening directions derived in this study (Figs. 9 and 10). See Fig. 14 for location of the sections.

1934; *Diebold et al.*, 1963; *Liniger*, 1970; *Ruhland et al.*, 1973; *Dannecker*, 1995], well logs [*Schneegans and Théobald*, 1948] and structural data collected by *Dannecker* [1995] and in the course of this study. Cross-sections 3-3' and 4-4' (Fig. 15 c, d) have been modified after *Ruhland et al.* [1973] and *Fischer* [1965], respectively. Cross-section 5-5' (Fig. 16) is part of a migrated reflection seismic profile shot by Enterprise Oil in 1987.

As is obvious from inspection of Fig. 14, the western, NNE-trending segment of the Ferrette anticline is located above an oblique ramp that nucleated above the steeply W-dipping, Paleogene Ferrette normal fault bounding the Ferrette half-graben. This graben-bounding normal fault was overthrusted by the advancing Jura front, as is evidenced by boreholes [*Schneegans and Théobald*, 1948]. Furthermore, several sinistral strike-slip faults, along which out-of-plane movements occurred, traverse those two cross-sections.

Cross-section 2-2' (Fig. 14, 15b) traverses the Ferrette anticline at the point where its strike changes from a NNE-trend into an ESE-orientation. This position marks the transition from the sinistral oblique ramp to a frontal ramp. This cross section also traverses the western end of an anticline located south of the Ferrette fold: the Glaserberg anticline ("G" in Fig. 14). Note that the N limb of this gentle anticline is considerably steeper than its S limb and that the flat-lying Mesozoic strata N of this anticline are found at a relatively lower elevation N of this anticline. This suggests that the Glaserberg anticline nucleated above a pre-existing E-W-striking basement step that was associated with extensional flexuring of the Mesozoic strata. Such E- to ENE-trending extensional flexures of Paleogene age are typical of the southern end of the URG [*Ustaszewski et al.*, 2005a]. They were studied in detail at the northern edge of the Tabular Jura in the Ajoie (the Florimont and Réchésy anticlines indicated in Figs. 1 & 14). Their en-échelon alignment has resulted from sinistral transtensive strike-slip faulting during the Paleogene along pre-existing Late Paleozoic ENE-trending basement faults underlying the flexures [*Ustaszewski et al.*, 2005a, 2005b]. Note that the Glaserberg and Blauen anticlines, as well as two minor flexures in the autochthonous Mesozoic immediately W of the Glaserberg anticline, are also aligned en-échelon (Figs. 1 and 14). These en-échelon flexures originally formed as Paleogene extensional flexures related to sinistral transtension above basement faults. In the case of the Glaserberg and Blauen anticlines these pre-existing flexures controlled the nucleation of anticlines during the décollement of the detached Mesozoic cover (Fig. 15) before some 4.2 Ma ago, while in the case of the very gentle Florimont and Réchésy folds the associated discrete basement steps were compressively reactivated in Late Pliocene to recent times [*Giamboni et al.*, 2004; *Ustaszewski et al.*, 2005b]. Transpressive deformation along the western, NNE-trending part of the Ferrette anticline, well documented by the fault slip data (Figs. 10 and 12), implies that movements must also have occurred in and out of the plane of cross-sections 1-1' and 2-2' (Fig. 15a,b). Hence, the shortening e ($e=dl/l_0$, $dl=l_0-l_1$), estimated for all five cross-sections by comparing deformed (l_1) and restored lengths (l_0) of marker horizons does not take into account horizontal shortening caused by out-of-plane dextral strike-slip displacements and

hence underestimates the amount of shortening in a direction parallel to these two sections. Bed lengths were measured between the northernmost occurrences of Mesozoic sediments and the horizontally layered sediments S of the Glaserberg anticline (see pin points given in Fig. 15). In cross-section 5-5' (seismic section of Fig. 16), the vertical scale roughly equals the horizontal scale within the Mesozoic sediments. It was thus admissible to compare the deformed and restored length of the well visible "D" reflector at a depth of c. 0.2 s TWT in the southern part of the section. Shortening in section 1-1' is in the order of 9%. Cross-section 2-2' reveals a shortening of 14%, before decreasing to 9% and 4% in sections 3-3' and 4-4', respectively. Hence, the greatest amount of within-plane shortening is achieved along section 2-2'. The component of shortening related to the formation of the Glaserberg anticline essentially remains constant in sections 2-2' to 4-4'. Hence, the differences in the amount of total in-plane shortening regarding sections 2-2' to 4-4' are entirely due to the changing geometry of the frontal Ferrette anticline. The westwards increasing amount of shortening also finds its expression in map view, in that the oldest outcropping sediments in the Ferrette anticline (Aalenian shales) crop out only in the west (Fig. 14). Note also that the gentle Ferrette anticline in the E laterally transforms into a frontal thrust some 2.5 km E of the northernmost tip of the Ferrette Jura (see Figs. 15 b-d).

At the northern edge of section 4-4', where shortening accommodated by the Ferrette anticline is very minor (Fig. 15d) and where the Mesozoic strata defining this gentle fold dip beneath the synrift sediments of the Paleogene Allschwil graben (Fig. 14), a steeply N-dipping, top-to-the-S reverse fault truncates the N-limb of the anticline. The reflection seismic line situated further east (cross-section 5-5' of Fig. 16) shows the continuation of this structure beneath the Paleogene synrift-fill of the URG. The seismic cross-section reveals an extensional flexure in the Mesozoic strata, on-lapped by synrift sediments of Paleogene age, as inferred from the S-ward tapering wedge (between the reflectors marked "A" and "R" in Fig. 16). The flexure sits above an E-W-trending, N-dipping high-angle basement fault of late Paleozoic origin and reactivated a first time during Paleogene rifting [*Ustaszewski et al.*, 2005a]. However, this same basement fault was reactivated a second time in compression, as is inferred from the steeply N-dipping, top-to-the-S reverse fault that truncated the synrift fill and that almost reaches to the surface. Since this fault clearly cuts through the décollement horizon, it most probably formed during the thick-skinned post-4.2 Ma stage. Similar features were observed elsewhere [*Giamboni et al.*, 2004; *Ustaszewski et al.*, 2005b]. It is important to note that the position of this top-to-the-S reverse fault coincides with an anticline detected by the folding of the base of the Sundgau gravels [*Giamboni et al.*, 2004; *Ustaszewski et al.*, 2005b], which proves its post-Late Pliocene age and its most probably thick-skinned origin. This observation confirms that pre-4.2 Ma Jura décollement tectonics were followed by thick-skinned tectonics.

When calculating the amount of within-plane shortening along profiles 4-4' and 5-5' depicted in Fig. 15 we subtracted the shortening due to this thick-skinned stage. This
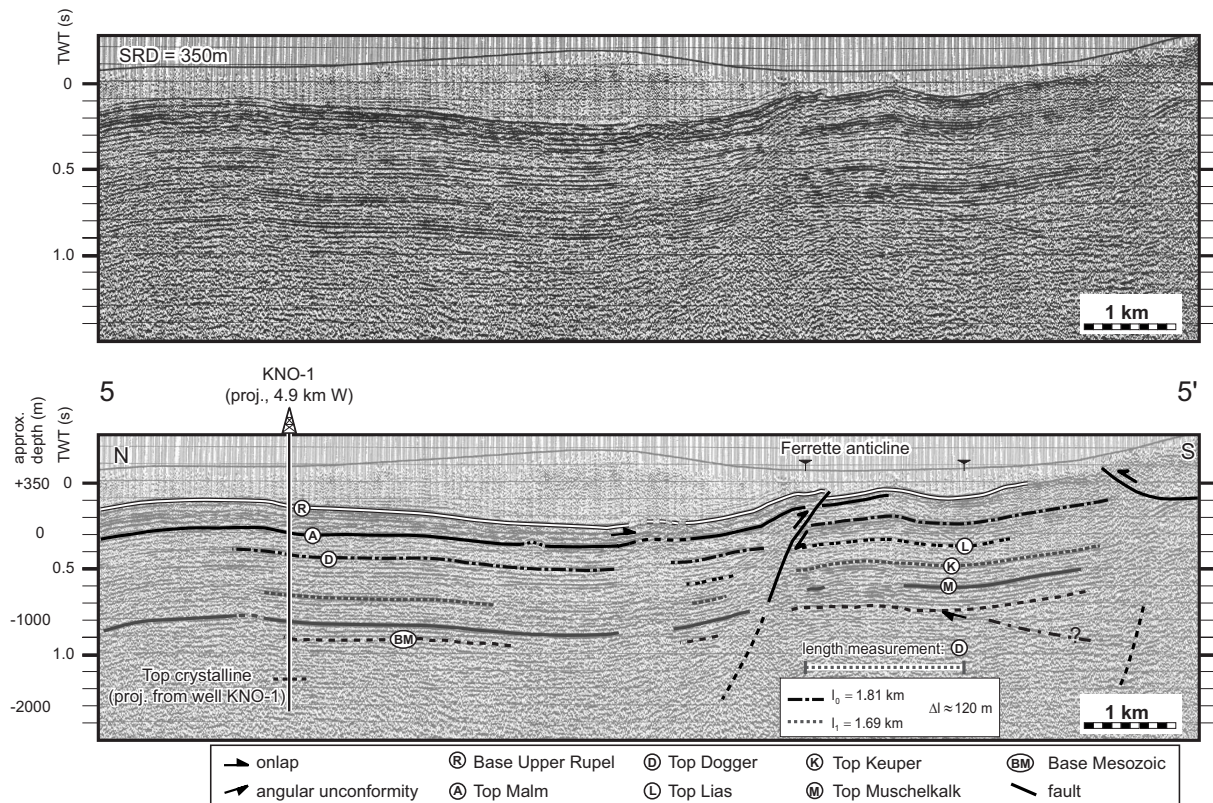
Fig. 16: N-S-trending industry-type reflection seismic line traversing a compressively reactivated Paleogene extensional flexure. For location see Fig. 14. Seismic data is the courtesy of Enterprise Oil.

allows discussing the diverging shortening directions observed in the area of the Ferrette and Landskron anticlines, and possibly associated rotations, during the thin-skinned stage of Jura folding, as is presented below.

3.4 Discussion

3.4.1 Why do shortening directions fan towards N at the Jura front?

The shortening directions in the study area, obtained from paleostress analysis of fault-slip data above, are consistently NNW- to NNE-oriented. In general, this confirms earlier studies on a larger scale [*Plessmann*, 1972; *Meier*, 1984; *Philippe*, 1995]. Our study, however, reveals a gentle fanning of the shortening directions towards N, particularly at the frontal Ferrette and Landskron anticlines. Moreover, several NNE-SSW-trending, transpressional anticline segments, such as the western parts of the Ferrette and Landskron, as well as the entire Caquerelle anticline (Fig. 10), show a pronounced obliquity between the structural grain and the shortening directions (Figs. 12 and 13). This clearly suggests their origin as ramp anticlines above sinistral oblique ramps. In addition, the shortening in the frontal Ferrette anticline increases along-strike from E to W (Figs. 15 and 16). However, transpressional deformation across the NNE-trending, oblique ramp segment of this anticline implies that within-plane shortening deduced from cross-sections of any orientation underestimates the total shortening. In the following, we further analyze the N-ward fanning
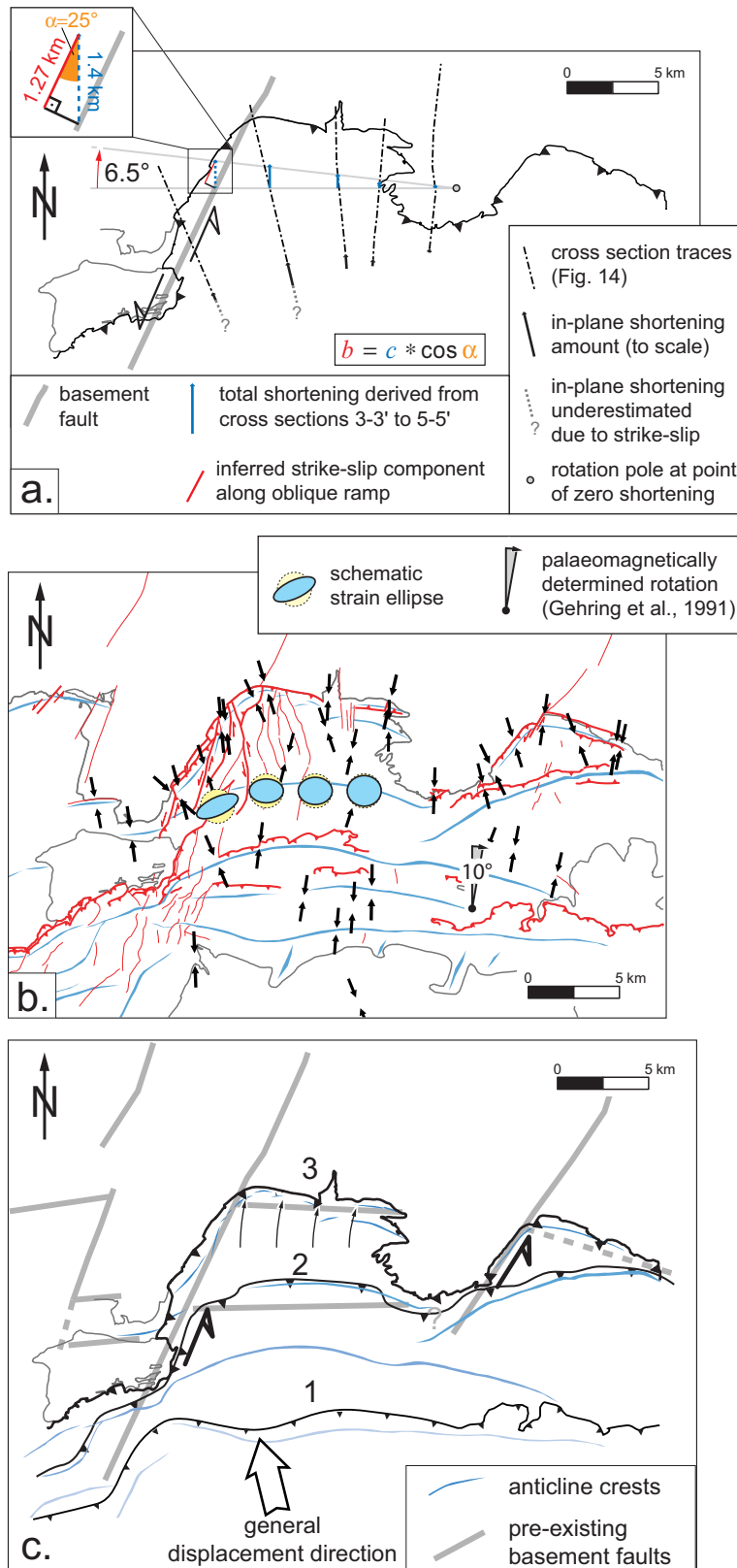
63

of shortening directions in conjunction with the observed W-ward increase of shortening across the frontal Ferrette anticline in order to discuss the role of possible block-rotations around vertical axes during décollement.

Firstly, we attempt to estimate the strike-slip component along the oblique ramp. To overcome the lack of suitable markers, we assume that the total shortening in the oblique ramp segment of the Ferrette anticline (in an N-S-direction) can be partitioned into a component perpendicular to the oblique ramp and a strike-slip component parallel to it. Fig 17a shows the shortening amounts derived from the cross-sections as black arrows plotted onto the trailing (=southern) ends of the cross-section traces. The arrows lengths are drawn to scale. An E-W-trending reference line was drawn south of the Ferrette anticline. Next, the shortening amounts in the sections with no out-of-sections movements (3-3' to 5-5') were plotted at the intersections of this reference line with the traces of the corresponding cross-sections (blue arrows in Fig. 17a). The leading edges of these arrows define a WNW-ESE-trending line. The intersection between this line and the E-W-trending reference line defines a point of zero N-S-shortening, situated E of cross-section 5-5' (open circle in Fig 17a). Assuming that the shortening increased linearly towards W, the two diverging lines were extrapolated W-ward until they intersected with the trace of the NNE-trending basement fault (the nucleus of the oblique ramp). This yields the total shortening of 1.4 km at the northern tip of the Ferrette anticline (=c, dashed blue arrow in Fig 17a). The strike-slip component along the oblique ramp (=b) can now be deduced from

$$b = c * \cos \alpha .$$

This yields b=1.27 km for $\alpha = 25°$ (red arrow in Fig. 17a). The W-ward increase of shortening across the Ferrette anticline necessitates a clockwise rotation of the detached sediments of c. 6.5° around a vertical axis, located at the pole of no shortening (open circle in Fig. 17a). Paleomagnetically determined clockwise rotations of c. 10° SE of the Ferrette Jura [*Gehring et al.*, 1991] confirm this assumption (rotation pole in Fig. 17b), further implying that the detached sediments have undergone rotations on a still larger scale between inherited NNE-trending oblique ramps. The N-ward fanning of shortening directions in map view therefore reflects the transition from pure N-S-convergence in the eastern, E-W-trending part of the Ferrette anticline to sinistral transpression along the NNE-oriented oblique ramp segment (schematic strain ellipses in Fig. 17b). The fan-shape of shortening directions was possibly emphasized by a passive clockwise rotation of the "less shortened" E-part of the anticline during detachment, at a time when shortening along the oblique ramp segment may still have been active. This scenario is supported by paleomagnetic evidence.

In summary, we propose the scenario for the formation of the frontal Jura anticlines sketched in Fig. 17c. As the deformation front advanced towards the foreland, the detached sediments encountered a NNE-trending, Paleogene basement fault that was obliquely oriented to the displacement direction (large white arrow in Fig. 17c) and which had offset the basal Triassic décollement. The deformation front E of the NNE-trending fault was

a.

$$b = c * \cos \alpha$$

basement fault — total shortening derived from cross sections 3-3' to 5-5'

inferred strike-slip component along oblique ramp

cross section traces (Fig. 14)

in-plane shortening amount (to scale)

in-plane shortening underestimated due to strike-slip

rotation pole at point of zero shortening

b.

schematic strain ellipse

palaeomagnetically determined rotation (Gehring et al., 1991)

c.

general displacement direction

anticline crests

pre-existing basement faults

Fig. 17: kinematic considerations on the N-ward fanning of shortening directions along the Ferrette Jura. (a) estimation of the strike-slip component along the oblique ramp segment of the Ferrette anticline. Extrapolation of the N-S-shortening obtained from cross-sections (Figs. 15 and 16) towards W gives the total shortening at the northern tip of the anticline. The strike-slip component is then deduced from disassembling the total shortening into a component parallel to the oblique ramp. (b) schematic strain ellipses across the Ferrette Jura, superimposed onto surface fault pattern, anticline crests and shortening directions from Fig. 14. The paleomagnetically determined clockwise rotation is in agreement with the rotation implied by the model in (a). (c) N-ward advance, sinistral transfer of the deformation front and rotation along NNE-trending normal faults shown at three stages:
1 = Vorbourg anticline,
2 = Glaserberg – Blauen anticlines,
3 = Ferrette – Landskron anticlines.

successively transferred to the N along a sinistral oblique ramp that formed above this discontinuity. This led to sinistrally dragged anticline crests (Figs. 14, 17b and c). Shortening concentrated at the transpressional oblique ramp and decreased towards E. This along-strike decrease of shortening induced a clockwise rotation of the detached sediments, which passively rotated the less shortened, E-part of the anticline, producing N-ward fanning shortening directions. These considerations on the kinematics of the Ferrette Jura front are summarized in a schematic block diagram (Fig. 18). They appear to be also applicable to the Landskron anticline, given the great similarities among these two frontal folds.
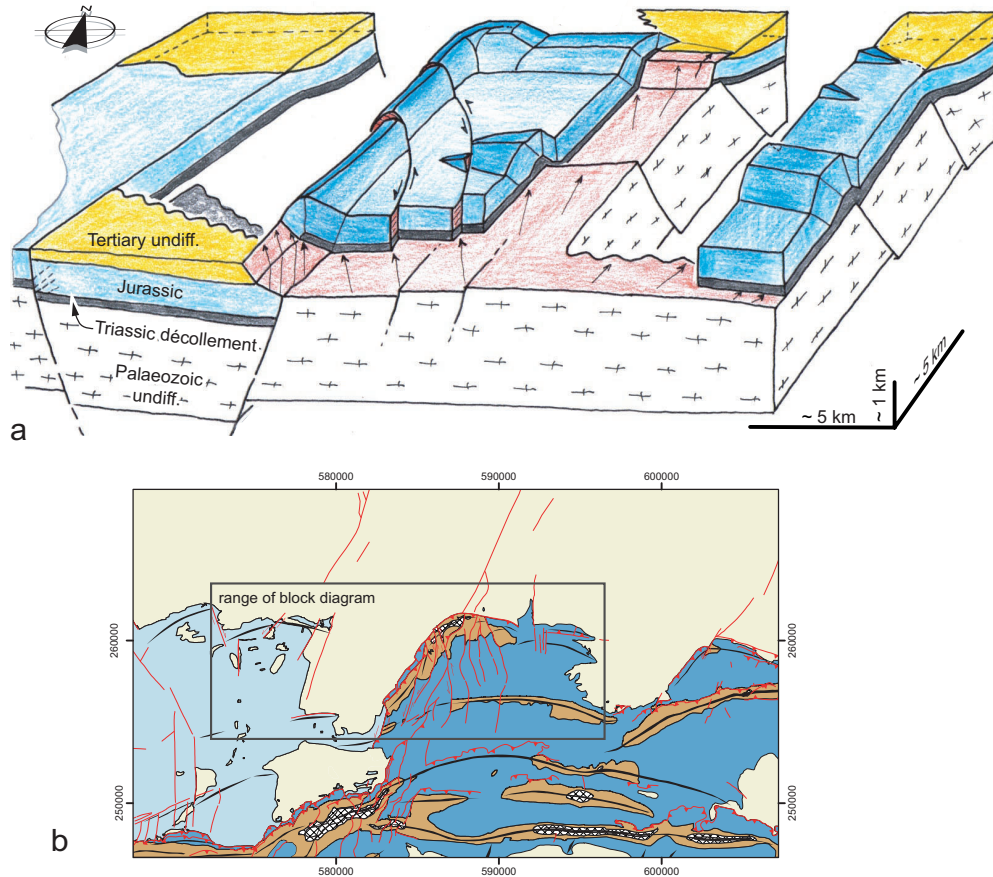
Fig. 18: (a) simplified block diagram illustrating the main tectonic features of the Ferrette Jura and the role of pre-existing basement faults, disregarding erosion. Faults active during the deformation are depicted in red, whereas inactive faults are in black. Displacement directions along the basal décollement are shown as thin black arrows. View direction is towards N. The pronounced along-strike asymmetries result from differently oriented basement faults, which control the along-strike change from a NNE-trending oblique ramp (above a Paleogene graben) to a frontal ramp (above an E-W-trending, formerly extensional flexure). (b) approximate range of the block diagram. For further discussion refer to text.

3.4.2 What induced the change from thin-skinned to thick-skinned deformation during the Late Pliocene?

We regard the evidence for basement-rooted fault reactivation to have followed Late Miocene to Early Pliocene thin-skinned folding and thrusting as conclusive (see also *Giamboni et al.*, 2004 and *Ustaszewski et al.*, 2005b). However, it appears surprising at first sight that this transition occurred without any (detectable) reorientation of the maximum horizontal stresses in the sedimentary cover. The thick-skinned reactivation is particularly well documented in an ENE-trending belt of basement faults that delineate the Permo-Carboniferous graben system in the subsurface, roughly paralleling the northern front of the eastern Jura Mountains (see Fig. 2 in *Ustaszewski et al.*, 2005a). Our data suggest that this transition is linked to the incipient inversion of these grabens, which implies that shortening within the pre-Mesozoic basement, taking place within the Alps during classical Jura folding ("Fernschub" or "distant push" theory in the sense of *Laubscher*, 1961) migrated northwards

into the Alpine foreland during the Late Pliocene. Based on evidence from reflection seismic profiles and cross section balancing considerations, inversion of Permo-Carboniferous grabens underneath the western Jura belt during a late stage or, alternatively, post-dating thin-skinned Jura folding and thrusting, was already invoked earlier [*Philippe*, 1994; *Philippe et al.*, 1996]. More recently, geomorphologic evidence from the southernmost URG revealed the spatial coincidence between gentle anticlines in the base of the Late Pliocene fluvial Sundgau gravels and transpressively/compressively reactivated basement faults [*Giamboni et al.*, 2004; *Ustaszewski et al.*, 2005b].

In the following, we speculate on the reasons that might have led to the transition from thin-skinned tectonics to basement-rooted deformation. Two possibilities are briefly outlined: (1) deactivation of intra-crystalline glide along the basal décollement, and (2) ongoing tectonic underplating in the foreland of the northwestern Alps [*Mosar*, 1999].

(1) The theory that décollement in the Jura fold- and thrust belt occurred by viscous flow by processes such as intracrystalline glide within the Mid- and Upper Triassic halite and anhydrite layers is rheologically viable and widely accepted nowadays [*Laubscher*, 1961; *Müller and Briegel*, 1980; *Jordan*, 1987]. Intracrystalline glide processes in evaporites can be activated at very low temperatures that are equivalent to an overburden column in the order of 1 km. Based on apatite fission track data, 1-3 km of uplift and erosion of the entire Swiss Molasse Basin after 5 Ma BP were recently documented [*Cederbom et al.*, 2004]. According to these authors, the uplift was triggered by accelerated erosion in the Swiss Alps in response to increased precipitation rates, leading to the isostatic rebound of the Alps together with the northerly adjacent foreland basin. It is believed that such an amount of erosion in the northern Molasse Basin may have caused the sedimentary overburden (and temperature) to fall beneath a critical threshold necessary to keep intracrystalline glide systems in the basal Jura décollement active. The age of the uplift is moreover in agreement with the minimum age of thin-skinned folding in the Northern Jura Mountains, as inferred from the onset of sedimentation of the Late Pliocene Sundgau gravels (see section 2.5).

(2) A crustal-scale transect across the north-western Alps, including the Molasse Basin and the Jura fold and thrust belt, exhibits a steep basal frontal thrust below the external massifs and a very narrow frontal portion [*Mosar*, 1999], an overall geometry that is believed to be unstable when analyzed in terms of the critical taper theory. By integrating geodetically determined uplift rates and the seismicity distribution, *Mosar* [1999] proposed that the Alpine orogenic wedge is currently in the process of accreting new basement nappes from the European crust at its base (below the Jura-Molasse transition) in an attempt to regain stability. If true, the propagation of such incipient thrust faults towards the foreland has conceivably already reached the area of the external Jura fold-and-thrust belt, as revealed by the reverse faulting mechanism of the Mw=4.5 earthquake in the RBTZ on February 23rd 2004, which was rooted in the basement with a focal depth of c. 10km [*Swiss Seismological Service*, 2004].

3.5. Conclusions

The Late Miocene to Early Pliocene formation of the thin-skinned Jura fold-and-thrust belt involved the migration of the deformation front far into the Alpine foreland. As the deformation front advanced into the area of the southern URG, it encountered a rift-related structural pattern that had disrupted the Middle and Upper Triassic basal décollement. Pre-existing basement faults served as nucleation points for thrust faults and oblique ramps in the detached sedimentary cover. Whereas E- to ENE-trending normal faults and extensional flexures that delimit an extensive Paleozoic trough system in the subsurface have localized frontal thrusts and anticlines, NNE-trending normal faults have localized sinistral oblique ramps. These NNE-trending oblique ramps, along which the deformation front of the Folded Jura was sinistrally transferred to the N, are characterized by (a) acute angles between the shortening directions and anticline strike, (b) transpressive deformation and (c) conspicuously dragged anticlines and faults across the NNE-trending faults, all indicative of a left-lateral sense of movement. The observed N-ward fanning of shortening directions obtained from fault-slip analysis can be explained by the along-strike decrease of shortening from W to E at the frontal anticline, which necessitated a gentle clockwise rotation of the detached sediments.

Despite the fact that no detectable stress field change occurred in the sedimentary cover, a geodynamic reorganization must have taken place after the Late Pliocene. This reorganization apparently led to the deactivation of the basal décollement in the Triassic and (subsequently or simultaneously) to the compressive inversion of formerly extensional basement faults in the Alpine foreland. It is speculated that one or a combination of the following factors might have induced this change: (1) post-5 Ma uplift of the Molasse Basin and concomitant erosion of 1-3 km of its Tertiary infill [*Cederbom et al.*, 2004]. This erosion lowered the overburden that is necessary to keep (thermally induced) intracrystalline glide in the basal décollement active below a critical threshold. (2) ongoing tectonic underplating of European crust in the foreland of the north-western Alps [*Mosar*, 1999].

References

Affolter, T., and J.P. Gratier, Map view retrodeformation of an arcuate fold-and-thrust belt: The Jura case, *J. Geophys. Res., 109*, doi:10.1029/2002JB002270, 2004.

Anderson, E.M., The dynamics of faulting and dyke formation with applications to Britain, 206 pp., Oliver and Boyd, Edinburgh, 1951.

Angelier, J., and P. Mechler, Sur une méthode graphique de recherche des contraintes principales également utilisable en tectonique et en seismologie: la méthode des dièdres droits, *Bull. Soc. géol. France, 19*, 1309-1318, 1977.

Becker, A., The Jura Mountains - an active foreland fold-and-thrust belt?, *Tectonophysics, 321*, 381-406, 2000.

Bolliger, T., B. Engesser, and M. Weidmann, Première découverte de mammifères pliocènes dans le Jura Neuchâtelois, *Eclogae Geologicae Helvetiae, 86*, 1031-1068, 1993.

Braillard, L., Fracturation du massif calcaire, morphogenèse et remplissages quaternaires en Ajoie (JU-Suisse). in *Geofocus*, Université de Fribourg, Fribourg, in prep.

Burkhard, M., and A. Sommaruga, Evolution of the western Swiss Molasse basin: structural relations with the Alps and the Jura belt, in *Cenozoic Foreland Basins of Western Europe*, vol. 134, edited by A. Mascle, C. Puidgefàbregas, H.P. Luterbacher and M. Fernàndez, pp. 279-298, Geological Society, London, 1998.

Cederbom, C.E., H.D. Sinclair, F. Schlunegger, and M. Rahn, Climate-induced rebound and exhumation of the European Alps, *Geology, 32*, 709-712, doi: 10.1130/G20491.1, 2004.

Dannecker, P., Tektonik des Pfirter Jura, Diploma thesis, 62 pp., Universität Karlsruhe, Karlsruhe, 1995.

Deichmann, N., D. Ballarin Dolfin, and U. Kastrup, *Seismizität der Nord- und Zentralschweiz*, 94 pp., NAGRA, Wettingen, 2000.

Delvaux, D., R. Moeys, G. Stapel, C. Petit, K. Levi, A. Miroshnichenko, V. Ruzhich, and V. San'kov, Paleostress reconstruction and geodynamics of the Baykal region, *Tectonophysics, 282*, 1-38, 1997.

Dèzes, P., S.M. Schmid, and P.A. Ziegler, Evolution of the European Cenozoic Rift System: interaction of the Alpine and Pyrenean orogens with their foreland lithosphere, *Tectonophysics, 389*, 1-33, 2004.

Diebold, P., H. Laubscher, A. Schneider, and R. Tschopp, Geologischer Atlas der Schweiz, Atlasblatt 40, St. Ursanne, mit Erläuterungen, Schweizerische Geologische Kommission, Bern, 1963.

Fischer, H., *Geologie des Gebietes zwischen Blauen und Pfirter Jura (SW Basel)*, 106 pp., Kümmerly & Frey, Geographischer Verlag, Bern, 1965.

Gehring, A.U., P. Keller, and F. Heller, Paleomagnetism and tectonics of the Jura arcuate mountain belt in France and Switzerland, in *Tectonophysics*, vol. 186, pp. 269-278, 1991.

Giamboni, M., K. Ustaszewski, S.M. Schmid, M.E. Schumacher, and A. Wetzel, Plio-Pleistocene Transpressional Reactivation of Paleozoic and Paleogene Structures in the Rhine-Bresse transform Zone (northern Switzerland and eastern France). *International Journal of Earth Sciences, 93*, 207–223, DOI: 10.1007/s00531-003-0375-2, 2004.

Hancock, P.L., Brittle microtectonics: principles and practice, *Journal of Structural Geology, 7*, 437-457, 1985.

Hindle, D., and M. Burkhard, Strain, displacement and rotation associated with the formation of curvature in fold belts; the example of the Jura arc, *Journal of Structural Geology, 21*, 1089-1101, 1999.

Hug, W.A., J.P. Berger, I. Clément, D. Kälin, and M. Weidmann, Miocene fossiliferous paleokarst (MN4) and OSM deposits (MN5-?) near Glovelier (Swiss Jura Mountains), in *Fifth Meeting of Swiss Sedimentologists (SwissSed) & Meeting of Molasse Group*, Fribourg (Switzerland), 1997a.

Hug, W.A., J.P. Berger, I. Clément, D. Kälin, and M. Weidmann, Sedimentological history of a Miocene fossiliferous paleokarst near Glovelier (Swiss Jura Mountains), in *18th IAS Regional European Meeting of Sedimentology*, Heidelberg (D), 1997b.

Jordan, P., Eine Methode zur Abschätzung tektonischer Scherraten aufgrund mikrostruktureller Beobachtungen, *Eclogae Geologicae Helvetiae, 80*, 491-508, 1987.

Kälin, D., Litho- und Biostratigraphie der mittel- bis obermiozänen Bois de Raube-Formation (Nordwestschweiz), *Eclogae Geologicae Helvetiae, 90*, 97-114, 1997.

Kastrup, U., M.L. Zoback, N. Deichmann, K.F. Evans, D. Giardini, and A.J. Michael, Stress field variations in the Swiss Alps and the northern Alpine foreland derived from inversion of fault plane solutions, *J. Geophys. Res., 109*, doi:10.1029/2003JB002550, 2004.

Kemna, H.A., and R. Becker-Haumann, Die Wanderblock-Bildungen im Schweizer Juragebirge südlich von Basel: Neue Daten zu einem alten Problem, *Eclogae Geologicae Helvetiae, 96*, 71-84, 2003.

Larroque, J., and P. Laurent, Evolution of the stress field pattern in the south of the Rhine Graben from the Eocene to the present, *Tectonophysics, 148*, 41-58, 1988.

Laubscher, H., Die Fernschubhypothese der Jurafaltung, *Eclogae Geologicae Helvetiae, 54*, 222-282, 1961.

Laubscher, H., Some overall aspects of Jura dynamics, *American Journal of Science, 272*, 293-304, 1972.

Laubscher, H., Fold development in the Jura, *Tectonophysics, 37*, 337-362, 1977.

Laubscher, H., The 3D propagation of décollement in the Jura, in *Thrust and Nappe Tectonics*, edited by McClay, pp. 311-318, Geological Society London, London, 1981.

Laubscher, H., The eastern Jura: Relations between thin-skinned and basement tectonics, local and regional, *Geologische Rundschau, 75*, 535-553, 1986.

Laubscher, H., Die tektonische Entwicklung der Nordschweiz, *Eclogae Geologicae Helvetiae, 80*, 287-303, 1987.

Laubscher, H., Jura kinematics and the Molasse Basin, *Eclogae Geologicae Helvetiae, 85*, 653-675, 1992.

Laubscher, H., Plate interactions at the southern end of the Rhine graben, *Tectonophysics, 343*, 1-19, 2001.

Laubscher, H., The Miocene Dislocations in the northern foreland of the Alps: Oblique subduction and its consequences (Basel area, Switzerland-Germany). *Jahresbericht und Mitteilungen des oberrheinischen geologischen Vereins, 85*, 423-439, 2003.

Liniger, H., Geologischer Atlas der Schweiz 1:25 000, Atlasblatt 55: Bonfol, mit Erläuterungen, Kümmerly & Frey, Bern, 1970.

Lopes Cardozo, G.G.O., and M. Granet, New insight in the tectonics of the southern Rhine Graben-Jura region using local earthquake seismology, *Tectonics, 22*, 1078, doi:10.1029/ 2002TC001442, 2003.

Marrett, R., and R.W. Allmendinger, Kinematic analysis of fault-slip data, *Journal of Structural Geology, 12*, 973-986, 1990.

Meier, D., Zur Tektonik des schweizerischen Tafel- und Faltenjura (regionale und lokale Strukturen, Kluftgenese, Bruch- und Faltentektonik, Drucklösung), *Clausthaler Geowissenschaftliche Dissertation, 14*, 1984.

Meyer, B., R. Lacassin, J. Brulhet, and B. Mouroux, The Basel 1356 earthquake: which fault produced it?, *Terra Nova, 6*, 54-63, 1994.

Mosar, J., Present-day and future tectonic underplating in the western Swiss Alps: reconciliation of basement/wrench-faulting and décollement folding of the Jura and Molasse basin in the Alpine foreland, *Earth and Planetary Science Letters, 173*, 143-155, 1999.

Müller, W.H., and U. Briegel, Mechanical aspects of the Jura overthrust, *Eclogae Geologicae Helvetiae, 73*, 239-250, 1980.

Nivière, B., and T. Winter, Pleistocene northwards fold propagation of the Jura within the southern Upper Rhine Graben: seismotectonic implications, *Global and Planetary Change, 27*, 263–288, 2000.

Noack, T., Thrust development in the eastern Jura Mountains related to pre-existing extensional structures, *Tectonophysics, 252*, 419-431, 1995.

Petit, C., M. Campy, J. Chaline, and J. Bonvalot, Major palaeohydrographic changes in Alpine foreland during the Pliocene-Pleistocene, *Boreas, 25*, 131-143, 1996.

Petit, J.P., Criteria for the sense of movement on fault surfaces in brittle rocks, *Journal of Structural Geology, 9*, 597-608, 1987.

Pfiffner, O.A., and M. Burkhard, Determination of paleo-stress axes orientations from fault, twin and earthquake data, *Annales Tectonicae, 1*, 48-57, 1987.

Philippe, Y., Transfer Zone in the Southern Jura Thrust Belt (Eastern France): Geometry, Development and Comparison with Analogue Modeling Experiments, in *Hydrocarbon and Petroleum Geology of France*, vol. 4, *Special Publication of the European Association of Petroleum Geologists*, edited by A. Mascle, pp. 327-346, A. Springer, 1994.

Philippe, Y., Rampes Laterales et Zones de Transfert dans les Chaines Plissées: Géometrie, Conditions de Formation et Pièges structuraux associés, PhD thesis, 272 pp., Université de Savoie & Institute Francais du Pétrole, Paris, 1995.

Philippe, Y., B. Colletta, E. Deville, and A. Mascle, The Jura fold-and-thrust belt: a kinematic model based on map-balancing, in *Peri-Tethys Memoir 2: Structure and prospects of Alpine Basins and Forelands.*, vol. 170, edited by P. Ziegler and F. Horvath, pp. 235-261, Mem. Mus. natn. Hist. nat., Paris, 1996.

Plenefisch, T., and K. Bonjer, The stress field in the Rhine Graben area inferred from earthquake focal mechanisms and estimation of frictional parameters, *Tectonophysics, 275*, 71-97, 1997.

Plessmann, W., Horizontal-Stylolithen im französisch-schweizerischen Tafel- und Faltenjura und ihre Einpassung in den regionalen Rahmen, *Geologische Rundschau, 61*, 332-347, 1972.

Reinecker, J., O. Heidbach, and B. Mueller, The 2003 release of the World Stress Map (available online at www.world-stress-map.org), 2003.

Reiter, F., and P. Acs, TectonicsFP, pp. Computer Software for Structural Geology, version 2.0 PR. http://www.tectonicsfp.com/, Innsbruck, 1996-2000.

Ruhland, M., J.G. Blanalt, and M. Bômont, Carte Géologique detaillée de la France à 1/50 000, Ferrette, feuille XXXVII-22, Ministère du développement industriel et scientifique, Bureau de recherches géologiques et minières, Service Géologique National, Orléans, 1973.

Schmid, S.M., O.A. Pfiffner, N. Froitzheim, G. Schönborn, and E. Kissling, Geophysical-geological transect and tectonic evolution of the Swiss-Italian Alps, in *Tectonics*, vol. 15, pp. 1036-1064, 1996.

Schneegans, D., and N. Théobald, Observations nouvelles sur le Chevauchement frontal du Jura Alsacien, *Bull. Soc. Geol France, 18*, 89-95, 1948.

Schneegans, D., N. Théobald, W.T. Keller, and A. Werenfels, Carte Géologique de la France à l'échelle du 1/50 000, feuille Ferrette XXXVII-21, in *Service de la Carte Géologique d'Alsace et de Lorraine*, Strasbourg, 1934.

Schumacher, M.E., Upper Rhine Graben: Role of preexisting structures during rift evolution, *Tectonics, 21*, 1006, doi:10.1029/2001TC900022, 2002.

Sperner, B., and L. Ratschbacher, A Turbo Pascal program package for graphical presentation and stress analysis of calcite deformation, *Zeitschrift der deutschen geologischen Gesellschaft, 145*, 414-423, 1994.

Steininger, F.F., W.A. Berggren, D.V. Kent, R.L. Bernor, S. Sen, and J. Agusti, Circum-Mediterranean Neogene (Miocene and Pliocene) marine-continental chronologic correlations of European Mammal Units, in *The Evolution of Western Eurasian Neogene Mammal Faunas*, edited by R.L. Bernor, V. Fahlbusch and H.-W. Mittmann, pp. 7-46, Columbia University Press, New York, 1996.

Swiss Seismological Service, ETH Zürich, Regional Moment Tensor Catalog, http://www.seismo.ethz.ch/ moment_tensor/2004/homepage.html, 2004.

Théobald, N., G. Dubois, and J. Goguel, Carte Géologique de la France à 1/50 000, feuille Altkirch-Huningue + notice explicative, XXXVII-21, in *Service de la Carte Géologique de la France*, Paris, 1958.

Ustaszewski, K., Reactivation of pre-existing crustal discontinuities: the southern Upper Rhine Graben and the northern Jura Mountains - a natural laboratory, PhD thesis, 135 pp., University of Basel, Basel, 2004.

Ustaszewski, K., M.E. Schumacher, and S.M. Schmid, Simultaneous normal faulting and extensional flexuring during rifting: an example from the southernmost Upper Rhine Graben, *International Journal of Earth Sciences, 94*, 680-696, DOI: 10.1007/s00531-004-0454-z, 2005a.

Ustaszewski, K., M.E. Schumacher, S.M. Schmid, and D. Nieuwland, Fault reactivation in brittle-viscous wrench systems - dynamically scaled analogue models and application to the Rhine-Bresse Transfer Zone, *Quaternary Science Reviews, 24*, 363-380, doi:10.1016/j.quascirev.2004.03.015, 2005b.

Ziegler, P.A., European Cenozoic rift system, *Tectonophysics, 208*, 91-111, 1992.

Ziegler, P.A., M.E. Schumacher, P. Dèzes, J.-D. van Wees, and S. Cloetingh, Post-Variscan evolution of the lithosphere in the Rhine Graben area: constraints from subsidence modelling, in *Permo-Carboniferous magmatism and rifting in Europe*, vol. 223, *Geological Society of London Special Publications*, edited by M. Wilson, pp. 289-317, Geological Society, 2004.

ORIGINAL PAPER

M. Giamboni · K. Ustaszewski · S. M. Schmid ·
M. E. Schumacher · A. Wetzel

Plio-Pleistocene transpressional reactivation of Paleozoic and Paleogene structures in the Rhine-Bresse transform zone (northern Switzerland and eastern France)

Abstract Pliocene to recent uplift and shortening in the southern Rhinegraben is documented by deformation of Pliocene fluvial gravels, deposited on a nearly planar surface, as well as by progressive deflection and capture of rivers. This deformation is suggested to result from thick-skinned tectonic movements as evidenced by observations on seismic records, which demonstrate a spatial coincidence between en-échelon anticlines at the surface and faults located in the crystalline basement. These findings contradict the often invoked thin-skinned tectonism in the recent tectonic history of the Rhinegraben. In particular the transfer zone between the Rhinegraben and the Bressegraben is very suitable for reactivation under the present day stress field. Thick-skinned reactivation of faults in the basement is also expressed by focal plane mechanisms of recent earthquakes showing strike-slip- rather than reverse faulting characteristics. This is of importance for the densely populated and industrialised southern Rhinegraben, previously affected by large earthquakes in historical times (e.g. Basel 1356).

Keywords Neotectonics · Fault reactivation · Southern Rhinegraben · Tectonic geomorphology · Geophysics

M. Giamboni (✉) · K. Ustaszewski · S. M. Schmid ·
M. E. Schumacher · A. Wetzel
Geologisch-Paläontologisches Institut,
Universität Basel,
Bernoullistrasse 32, 4056 Basel, Switzerland
e-mail: marzio.giamboni@buwal.admin.ch
Tel.: +41-31-3247103
Fax: +41-31-3230348

Present address:
M. Giamboni, Bundesamt für Umwelt,
Wald und Landschaft, GIS Fachstelle,
3003 Bern, Switzerland

Introduction

Hitherto, only limited efforts have been undertaken to relate the neotectonic activity of the Rhinegraben area to its structural configuration and the present stress field (e.g. Illies and Greiner 1979; Meyer et al. 1994; Schumacher 2002). The analysis of intraplate tectonics and pre-existing crustal discontinuities implies a high potential of fault reactivation (e.g. Laubscher 1992; Ziegler et al. 1995) that could induce earthquakes (e.g. Meyer et al. 1994; Deichmann et al. 2000). Therefore, it is desirable to relate the neotectonic deformation of the Rhinegraben area, which hosts major industrial and population centres, to its structural framework in order to determine which faults are most likely to move again within the short term.

The Basel area (Fig. 1), situated at the boundary between the Jura and the southern Rhinegraben, was shaken in historical times by several of the strongest earthquakes that occurred in NW Europe. Moreover, this area represents an ideal place for studying the reactivation of pre-existing crustal discontinuities as it is made up of several tectonic structures of different age, the older controlling the evolution of the younger (Fig. 1). The different tectonic stages, which shaped the area, are well documented, owing to the excellent database provided by many generations of geologists (Laubscher 2001, and references therein).

The "classic" interpretation of the Basel area distinguishes between three main phases of tectonism during the Cenozoic (e.g. Buxtorf and Koch 1920; Fischer 1965; Liniger 1967; Laubscher 1987). The first one was related to subsidence during Oligocene rifting and led to the formation of the Rhinegraben.

A second phase, Early Neogene in age, was accompanied by major stress field changes and caused the cessation of rifting in the southernmost Rhine Graben, as well as widespread uplift. During a third phase, Mio- to Pliocene in age, the area of the entire Jura Mountains became affected by Alpine orogeny: the classical thin-skinned Jura thrust-and-fold belt developed.

73

208

However, a fourth phase of tectonic activity during the Plio-Pleistocene is evident in an area north of the thin-skinned Jura belt. Previously, some authors (Erzinger 1943; Liniger 1967) recognised structures within the Tabular Jura and the adjacent Rhinegraben that formed after main Jura folding. They were often referred to as "Plio-Pleistocene subsidence". Despite this very important "pioneer work", the kinematics of this activity remained enigmatic.

A growing number of studies provides evidence for such a fourth phase of uplift and shortening in the southernmost Rhinegraben, in a zone linking the Bressegraben with the Rhinegraben (Fig. 1), which post-dated the formation of the thin-skinned Jura belt (Meyer et al. 1994; Nivière and Winter 2000; Fabbri et al. 2001; Ustaszewski et al. 2001; Laubscher 2001; Giamboni et al. 2003). However, there are contrasting ideas about the kinematic framework of this youngest episode, as shall be discussed in the following sections.

To elucidate the Cenozoic history of the southernmost Rhinegraben—the Ajoie area and around Montbéliard (Fig. 1)—we used field and borehole data, reflection seismic lines, geoelectric logs and data from geomorpho-logical mapping and DEM analysis. In addition to the three generally accepted tectonic episodes described above, we provide new evidence for the nature and kinematics of the recently identified fourth one. This youngest episode follows pre-existing normal faults and flexures of Eo-/Oligocene age and reflects thick-skinned inversion of basement faults. Deformation of Pliocene sediments, as well as changes in the drainage system due to uplift, suggest that this stage of tectonic activity persists from Pliocene to recent.

## Geological and tectonic framework

The study area is located in NW Switzerland west of Basel (Ajoie) and in northerly adjacent France. There, the southern part of the Rhinegraben is juxtaposed against the Tabular Jura and the northernmost Folded Jura (Fig. 1). The southern part of the Rhinegraben represents a hilly landscape with altitudes between 400 m in the south and 250 m in the north. At its south-western and western margin the Rhinegraben is surrounded by the Tabular Jura, which is topographically higher, but of humble
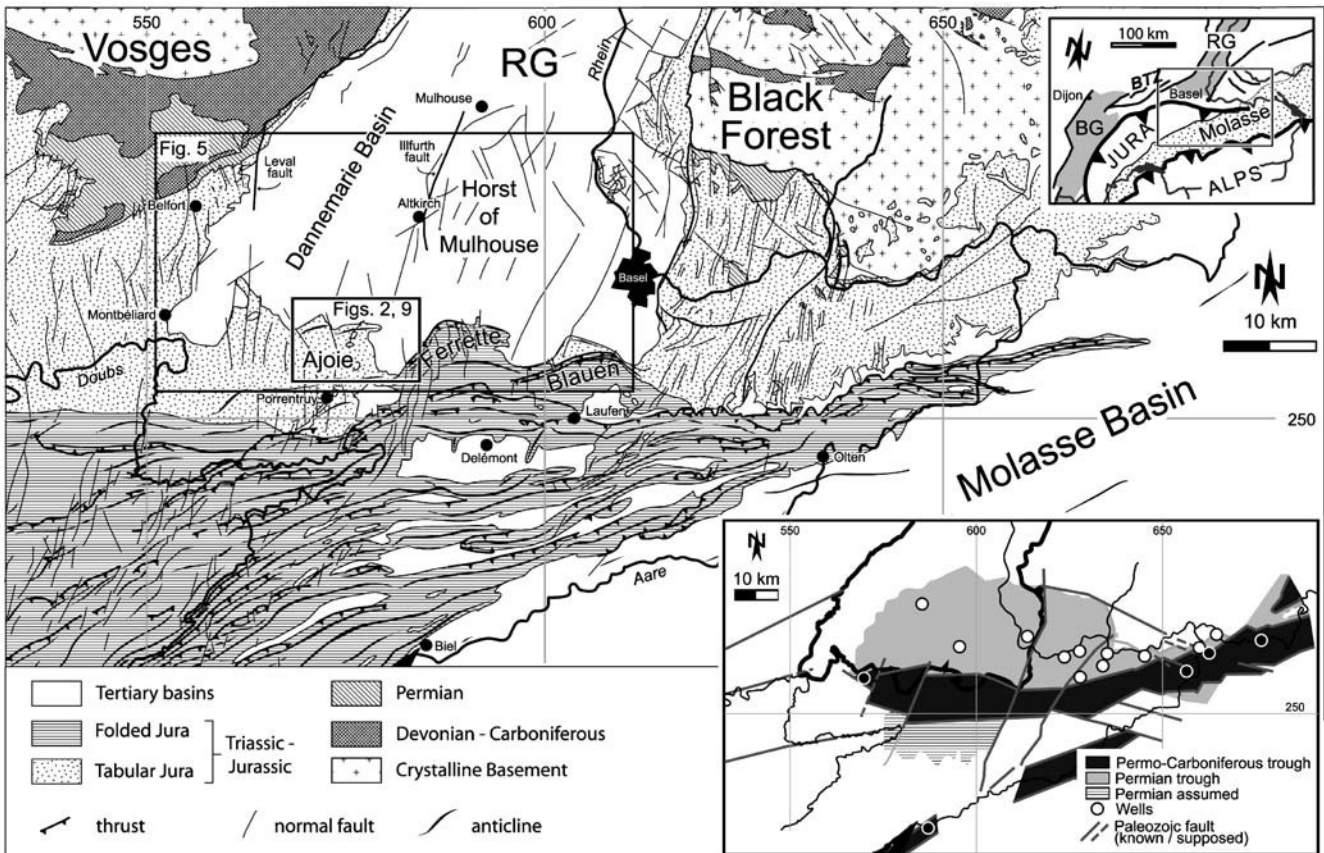
Fig. 1 Structural sketch map of the southern Rhinegraben and surrounding areas (redrawn after Fischer 1969). *Inset* in the upper right: Regional sketch map showing the tectonic setting of the southern Rhinegraben in the northern Alpine foreland. *Shaded*: Cenozoic rift basins; *dotted*: Alpine Molasse; *RG* Rhinegraben; *BG* Bressegraben; *BTZ* Rhine-Bresse Transform Zone. *Inset* in the lower right: Permo-Carboniferous troughs (redrawn and modified after Allenbach 2003). Eastwards the Northern Swiss Permo-Carboniferous trough connects with the Constance trough. Numbers on the map's edges are Swiss National coordinates
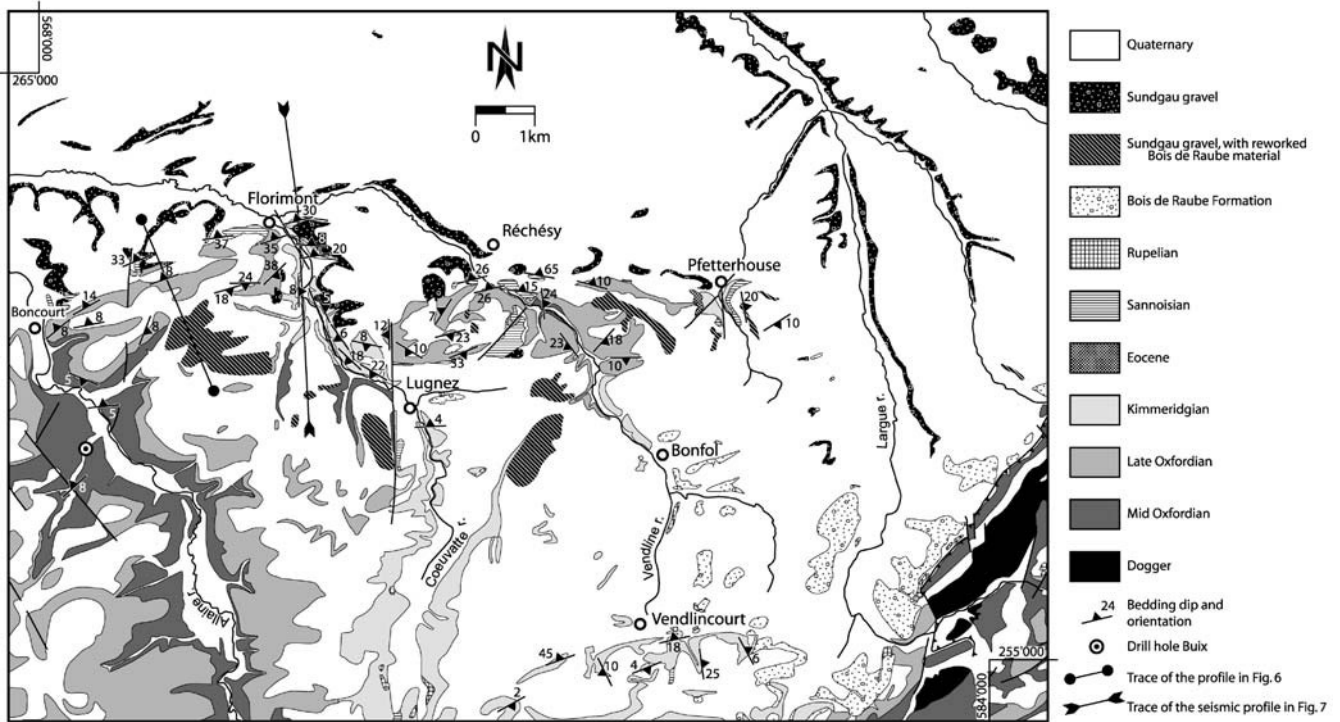
Fig. 2 Geological map of the northern Ajoie (modified after Liniger 1970). Traces of the cross section (Fig. 6) and the reflection seismic line (Fig. 7) are shown

relief. This rather flat relief is only disturbed by three small arcuate hills located at the junction between the Rhinegraben and the Tabular Jura. These hills correspond to the Vendlincourt, Réchésy and Florimont anticlines, which very gently fold this part of the Tabular Jura (Fig. 2). The highest elevations in the area are the southerly and easterly adjacent folds of the Folded Jura, i.e. the Ferrette and the Blauen anticlines (Fig. 1). Mesozoic and Tertiary sediments cover most of the area, and are in turn overlain by Pleistocene loess. Outcrops are rare.

Permo-Carboniferous troughs of northern Switzerland

A reflection seismic and drilling campaign by the NAGRA (Swiss National Cooperative for Storage of Nuclear Waste) led to the discovery of a conspicuous Late Paleozoic trough system in the subsurface of northern Switzerland, spanning from Lake Constance to Basel (e.g. Diebold 1990; Thury et al. 1994). This basin system extends further to the west into the area investigated in our study (bottom right insert in Fig. 1; Matter 1987; Diebold and Naef 1990; Philippe 1995; Krohe 1996; Diebold and Noack 1997; Laubscher and Noack 1997; Pfiffner et al. 1997).

This trough system developed in response to Post-Variscan transtensional tectonics and consists of a system of mostly WSW-ENE striking, narrow and elongated fault-bounded grabens, whose orientation follows the structural grain of the Variscan belt (Ziegler 1990b). Therein, up to several hundreds of meters of continental clastic sediments of Permian and Carboniferous age accumulated (Diebold et al. 1992). The history of these intramontane troughs ended in Late Permian times, as evidenced by the unconformably overlying, Early Triassic Buntsandstein formation.

Mesozoic subsidence

The Middle Anisian regional transgression (Muschelkalk) marks the first marine deposits in the area (Ziegler 1990a). During the Middle and Late Triassic, carbonates, intercalated with marls, and evaporites formed under shallow-marine to epicontinental conditions. The latter (Anhydritgruppe, Gipskeuper) provided the principal décollement horizons during Mio-/Pliocene Jura thin skinned thrusting (Laubscher 1961; Jordan and Nüesch 1989). During the Jurassic, marine conditions prevailed. Until recently, it was thought that this period was one of tectonic quiescence except for uniform thermal subsidence (Ziegler 1990a). However, recent sedimentological studies (Gonzales 1996; Allia 1996; Burkhalter 1996; Allenbach 2001, 2002, 2003; Wetzel et al. 2002) suggest reactivation of Late Paleozoic faults already during the Mesozoic, resulting in small-scale thickness and facies changes.

210

Fig. 3 Stratigraphic table for Cenozoic sediments in the southern Upper Rhinegraben and adjacent Tabular Jura and Jura Mountains (based on Sissingh 1998; Berger 2000). Tectonic events compiled from various sources, paleo-stress after Schumacher (2002). (See text for details)
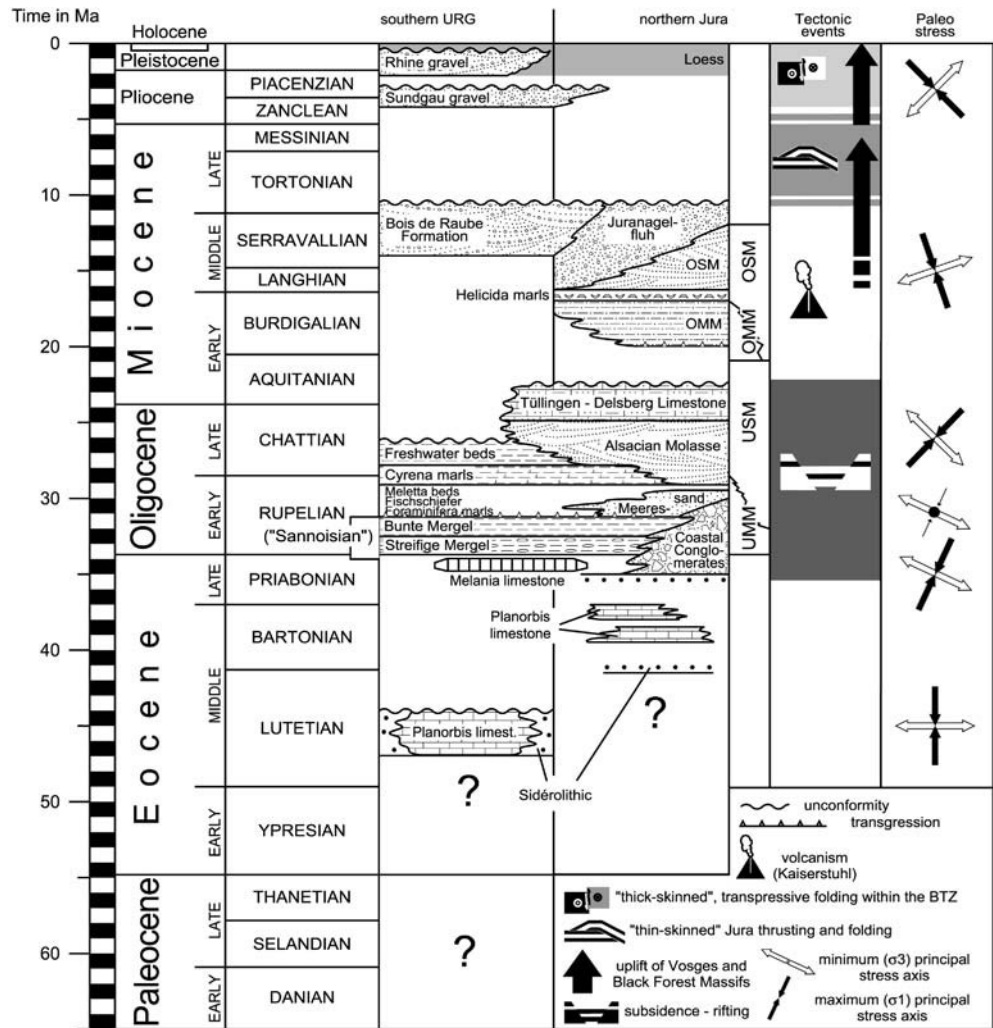
The oldest Mesozoic sediments outcropping in the study area are oolithic platform carbonates of Mid-Jurassic age (Dogger), exposed in the cores of the Ferrette and Blauen anticlines (Ruhland and Blanat 1973; Bitterli-Brunner et al. 1984). Shallow platform carbonates and neritic deposits of Oxfordian to Kimmeridgian age are the youngest Mesozoic sediments preserved. They are exposed along the Allaine, Coeuvatte and Vendline valleys in the Tabular Jura of the Ajoie (Fig. 2).

Cenozoic rifting

The N–NE-trending Bresse- and Rhinegraben form the central segments of the European Cenozoic rift system (Fig. 1). Rifting initiated in Late Eocene times and persisted until the Early Miocene (e.g. Pflug 1982; Bergerat et al. 1990). The sinistral Rhine-Bresse Transform Zone linked the two graben structures (Laubscher 1970; Rat 1978; Bergerat and Chorowicz 1981; Fig. 1) and nucleated along reactivated faults, related to the Permo-Carboniferous graben system (Laubscher 1986; Ziegler 1992; Schumacher 2002).

During the first phase of rifting shallow grabens and half grabens as well as slight flexures formed at the eastern and southern border of the southern Rhinegraben (Laubscher 1982). Particularly the Dannemarie basin, bounded by the Illfurth fault in the east, by the Leval fault in the west (Fig. 1) and by the flexures of Florimont and Réchésy in the south (Fig. 2), started to subside (Laubscher 1982). While lacustrine marls and anhydrite/halite accumulated in the Mulhouse and Dannemarie basins (Doebl 1970; Sissingh 1998), fresh- to brackish-water carbonates (Melania limestone; Fig. 3) were deposited on the horst of Mulhouse (Sittler 1972; Sissingh 1998). Coarse conglomerates formed along the graben margins in response to an increasing relief and erosion of the rift flanks. This style of sedimentation persisted until the Lower Rupelian (Duringer 1988). In the study area, the conglomerates are well exposed at the eastern side of the Ferrette anticline and along the northern border of the Tabular Jura in the Ajoie. During the Lower Rupelian a brackish-marine environment established (Blue Marls/Streifige and Bunte Mergel, Brianza et al. 1983; Sissingh 1998). Marine sedimentation dominated until the Late Rupelian (Doebl and Teichmüller 1979) and the "Meer-

essand", "Foraminifera Marl", "Fish Marl", and "Meletta Clay" formations accumulated (Fig. 3, Fischer 1965; Duringer 1988). During the Middle Chattian, sedimentation again became brackish ("Cyrenea Marls" formation) and finally fluvio-lacustrine ("Alsacian Molasse" formation, Fischer 1965). Middle Chattian Freshwater beds (including "Tüllinger Süsswasserkalke") formed in a system of lakes, during a period when connections to the marine realm were interrupted at both graben ends (Sissingh 1998).

During Aquitanian times, erosion and uplift in the area of the future Jura Mountains took place (Laubscher 1992, 2001). An angular unconformity formed between the Chattian to Lower Aquitanian Delsberg carbonates and the shallow marine Burdigalian sediments (transgression of the Upper Marine Molasse, OMM in Fig. 3; Buxtorf 1901; Koch 1923).

Renewed uplift started near the Burdigalian/Langhian boundary and led to tilting and erosion of the Burdigalian shallow marine beds (Laubscher and Noack 1997). In the course of this tectonic event, enhanced uplift of the Vosges and Black Forest massifs (Laubscher 1992, 2001) led to an evolving relief. Associated southward flowing rivers shed conglomerates deriving from the Vosges (Bois de Raube Formation; Kälin 1997) and the Black Forest (Juranagelfluh; Kälin 1993). Several tens of meters of predominantly coarse clastics were deposited in canyon-like channels (Kälin 1997; Laubscher 2001), extending far southward into the Tertiary basins of Laufen, Delémont and Porrentruy (Fig. 1).

Miocene Jura folding

During Serravallian times the Alpine thrust front started to propagate further northward and influenced—by long-range effects—the area of the present-day Jura Mountains: The Molasse basin, with its Mesozoic substrate, was detached along décollement horizons within Triassic evaporites. Initially only the southernmost parts of the Jura Mountains were incorporated into a deforming thin-skinned wedge of sediments situated in front of the effectively rigid Molasse basin. About 10.5 Ma ago (end of deposition of the Bois de Raube Formation, Kälin 1997) the southernmost part of the Rhinegraben area (i.e. the present-day Delémont and Laufen Tertiary basins, Fig. 1) also became involved in Jura folding, which lasted until 3.4 Ma before present (Bolliger et al. 1993; Kälin 1997). The time span of Jura folding itself is characterised by a lack of sedimentation.

While the location of the northern edge of the thin-skinned wedge is well constrained east of Basel (boundary between Folded and Tabular Jura) and again in the southern Ajoie (Mt. Terri thrust), it is only poorly constrained in the area of the Ferrette and Blauen chains southwest of Basel.

## Deposition of the Pliocene "Sundgau gravel"

A new episode of fluvial deposition, forming the so-called "Sundgau gravel" in the southern Rhinegraben and northern Tabular Jura (Ajoie), started in the Early Pliocene (around 4 Ma). These gravels consist of up to 70% of clasts eroded from the Alps and the Molasse basin (Liniger 1967). Bonvalot (1974) demonstrated that the "Sundgau gravel" represents the up-stream equivalent of the Pliocene "Cailloutis de Desnes" and "Sables de Neublans" formations in the northern Bressegraben. Rodent and mollusc assemblages provided a Late Zanclean to Piacenzian age (4.2–2.9 Ma) for these formations (see Petit et al. 1996; Fejfar et al. 1998). Thus, even if the deposition of the earliest portions of the "Sundgau gravel" temporally overlaps with a late stage of thin-skinned Jura folding, it still partly postdates it.

The paleo-drainage system in the Central Alps and their northern foreland changed significantly during the Zanclean: In the Early Pliocene Alpine drainage across the Swiss Molasse plain was first flowing eastward into the paleo-Danube river (Fig. 4a, Liniger 1966, 1967; Petit et al. 1996). The upper course of this paleo-Danube approximately corresponded to the catchment area of the present-day Aare and Rhône rivers. Hence, this system was referred to as "Aare-Danube" system by Liniger (1966). Enhanced subsidence in the Bressegraben during Early Pliocene times (Fig. 4 b, Rat 1978) caused an increment of headward erosion from the west, resulting in the capture of the paleo-Aare by the paleo-Doubs River during the Upper Zanclean (at 4.2 Ma, Petit et al. 1996; Fejfar et al. 1998). Furthermore, persisting uplift in the south-eastern Black Forest induced a decoupling of the paleo-Aare from the paleo-Danube. As a result, the paleo-Aare river flowed around the eastern tip of the Jura Mountains and passed through the southern part of the Rhinegraben into the Bressegraben. This river deposited the "Sundgau gravel" (Fig. 4 b).

During Piacenzian and Quaternary times, the Bressegraben underwent renewed uplift and was subjected to erosion (Sissingh 1998). Meanwhile, the southern and northern segments of the Rhinegraben underwent further subsidence (e.g. Doebl 1970; Schumacher 2002). Thereby, the paleo-Aare was captured once more and started to flow northward into the Rhinegraben (Fig. 4c) (Liniger 1966; Petit et al. 1996; Giamboni et al. 2003). Up to 200 m of Alpine gravel were deposited during the Pleistocene in the Rhine valley north of Basel.

Structural evidence for Middle Pliocene to recent tectonics

Most authors accept late Mio- to Pliocene Jura-folding as thin-skinned. It is not clear, however, if this episode of thin-skinned Jura folding persists until present. Recently, Nivière and Winter (2000) have proposed that the thin-skinned Jura Mountains have already propagated further north into the area of the southernmost Rhine Graben,

212
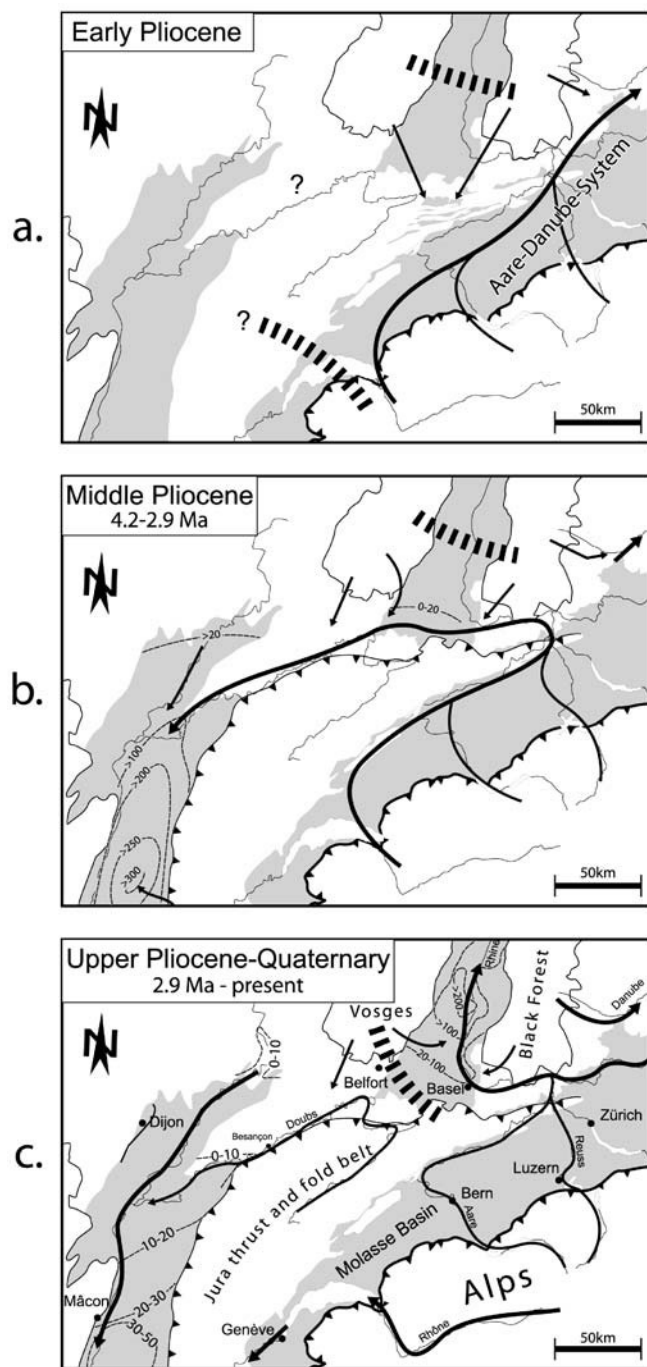
Fig. 4 Major changes in the paleohydrographic pattern in the north-western Alpine foreland since Miocene times (modified after Liniger 1966; Petit et al. 1996). Ages (rodent chronozones) given by Petit et al. (1996), updated after Fejfar et al. (1998). *Thin dashed lines* represent isopachs (in meters) of the Pliocene and Quaternary sediments for the Bressegraben (after Debrand-Passard and Courbouleix 1984) and for the Rhinegraben (after Doebl 1970). *Thick dashed lines* are major water divides

detached above Triassic evaporitic layers. On the other hand, there might have been a change towards a thick-skinned style of deformation (e.g. Meyer et al. 1994), or, alternatively, active shortening in the Alpine foreland

may have given way to a combined strike-slip and normal faulting mode of deformation, as suggested by seismo-tectonic evidence (Deichmann et al. 2000). The different proposed kinematic scenarios do not necessarily contradict each other, since the stress field in the region is known to be decoupled between sedimentary cover and its basement (Müller et al. 1987, 2001). The "Sundgau gravel" plays a crucial role to answer some of these questions.
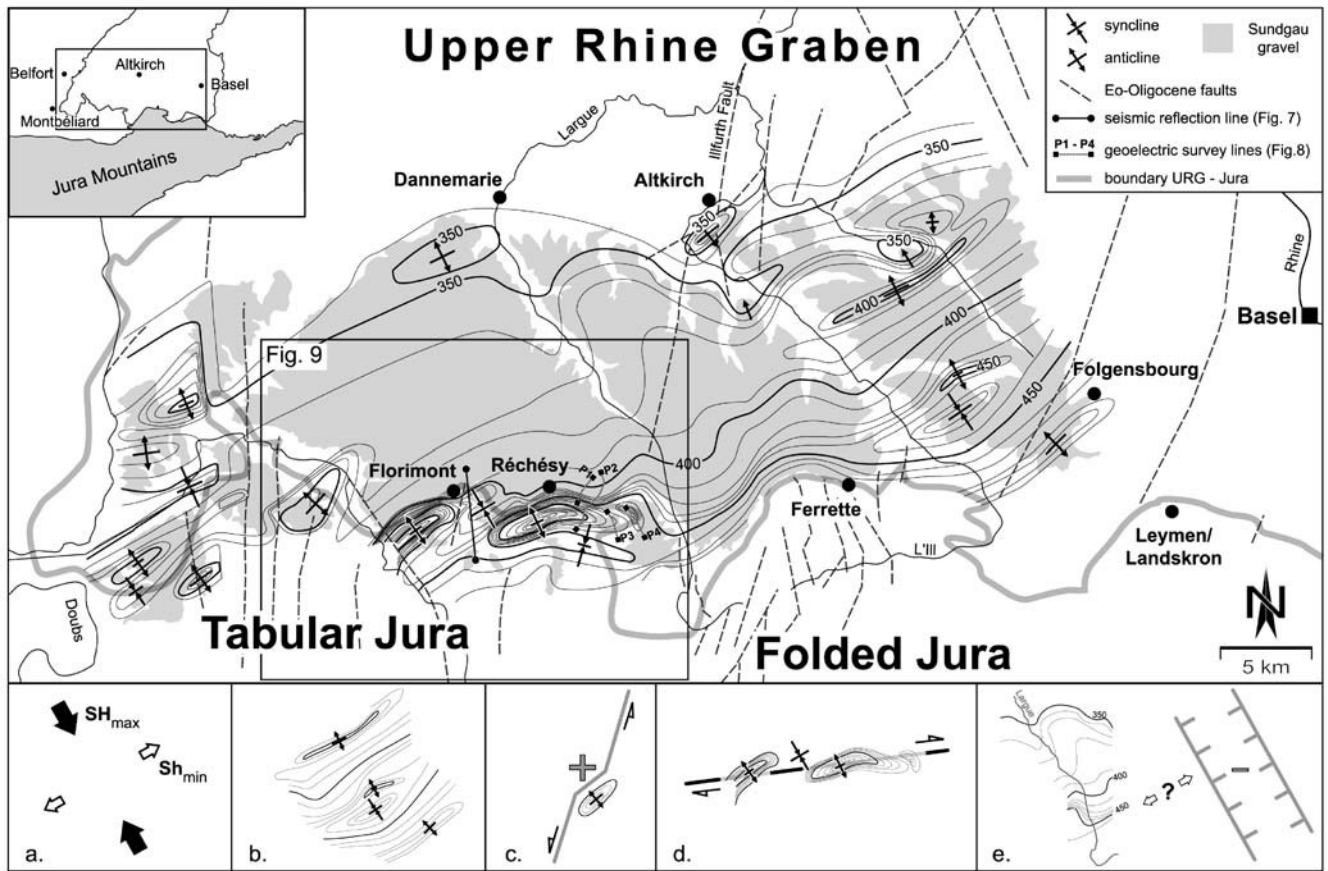
The "Sundgau gravel" base map

The Pliocene "Sundgau gravel" (2.9–4.2 Ma) was deposited by a shallow braided river, having a shifting network of unstable, low-sinuosity channels (Miall 1996). Depth of the channels was of the order of 1 m. The deposits are dominated by clast-supported, crudely bedded longitudinal bedforms and lag deposits, as well as transverse bedforms with planar cross-beds. Thin sandy, bar-top sheets are formed at bar margins by surface runoff. According to Schumm (1985), the slope of such low sinuosity braided rivers is in the order of 1.5 to 2.0‰.

These sedimentological characteristics strongly support the assumption that the base of the "Sundgau gravel" Formation formed on a nearly planar and horizontal surface. Therefore, this planar surface represents an ideal marker horizon to record post Middle Pliocene differential vertical displacements due to folding and/or faulting.

The "Sundgau gravel" is exposed within a 20-km-wide, E–W striking belt, delimited to the east by the Rhine river valley and to the west by the entrance into the narrow Doubs valley near Montbéliard (Fig. 5). The eastern parts of this gravel formation were eroded by the Rhine River during the Pleistocene and no remnants were found further upstream so far. Downstream and in the Doubs valley a few alluvial terraces of the Sundgau gravel system are preserved (Contini et al. 1973). Southeastward, the "Sundgau gravel" nestles the Ferrette anticline, and overlaps the northernmost part of Tabular Jura in the Ajoie (Fig. 5). North of the latitude of Dannemarie-Altkirch, a lateral transition from the "Sundgau gravel" to the Pliocene gravel and sands of the paleo-Aare tributaries from the Vosges Mountains, was observed (Théobald et al. 1976; Ménillet et al. 1989). The gravel thickness ranges from a few meters up to 30 m.

Théobald (1934) made a first attempt to reconstruct the "Sundgau gravel" base. In contrast to the present study, he did not take into account the southernmost outcrops in the northern Tabular Jura. Théobald's gravel base map shows increasing amounts of uplift from NW (near Dannemarie) to SE (i.e. towards the Ferrette anticline). He attributed the tilt of the gravel base to a wide-ranging uplift of the Tabular and Folded Jura after deposition of the "Sundgau gravel".

The "Sundgau gravel" base map presented in this study (Fig. 5) was constrained by borehole data, geological maps and field observations. In the eastern, southern and westernmost valleys of the area the base is in contact to

Fig. 5 Base map of the Pliocene "Sundgau gravel"; iso-lines are labelled in meters above sea level; traces of the reflection seismic line (Fig. 7) and the geo-electric survey lines (Fig. 8) are shown. Bottom inserts **a** to **e**: detail regions of the map put into viable kinematic scenarios within the recent stress field. "+" and "-" depict uplift and subsidence, respectively. Refer to text for details

the underlying Oligocene or Jurassic beds and is well constrained by field and well data. The central part south of Dannemarie, however, shows considerable lack of information, because rivers incise only into the "Sundgau gravel" beds. Furthermore, no subcrop data are available from this area.

Contouring revealed a system of more than ten narrow folds with predominantly SW–NE-trending and laterally plunging fold axes. The syn- and anticlines largely correspond to topographic depressions and highs, respectively, except at places where they are eroded by antecedent rivers. Even the different fold amplitudes exhibit a general conformability with the topographic structures. The area with the highest relief (up to 550 m), i.e. the northern Ajoie, exhibits the most accentuated anticlines with the largest amplitudes (90 and 120 m). In contrast, folds with small amplitudes (10–20 m), such as those west of Folgensbourg, south of Dannemarie or in the south-westernmost area near Montbéliard, correspond to a gentle, slightly undulating relief. A further significant feature visible on the map is the general rise of the "Sundgau gravel" base from north to south. This, and the accentuated rise at the northern rim of the Ferrette

anticline, conforms to the geometry of the Folded Jura front at this place.

Some of the minor undulations in the gravel's base (e.g. in the area W of Folgensbourg or S of Dannemarie) might correspond to the progressive filling of a not exactly planar surface. However, the alignment of folds observed in the gravel's base is highly systematic throughout the contoured area. This strongly suggests that their origin is indeed related to tectonic processes. In the following, we want to discuss some of these isohypse map features in the context of a viable kinematic framework (Fig. 5, bottom inserts a to e), which is in concordance with the recent regional stress field (Fig. 5a) as derived from earthquake focal mechanisms (Plenefisch and Bonjer 1997) and in-situ-stress measurements (Becker 2000; Häring 2001). The fold trends and the strike of the general southward rise of the gravel's base (exemplified in Fig. 5b) are exactly perpendicular to the recent maximum horizontal stress SHmax. Under such conditions, Rhine Graben faults (like the Illfurth fault, see Figs. 1 and 5) can be reactivated as sinistral wrench faults. Immediately S of Altkirch, a small anticline has formed precisely where the Illfurth fault is kinked. This feature is interpreted as a restraining bend (Fig. 5c). The two en-

214
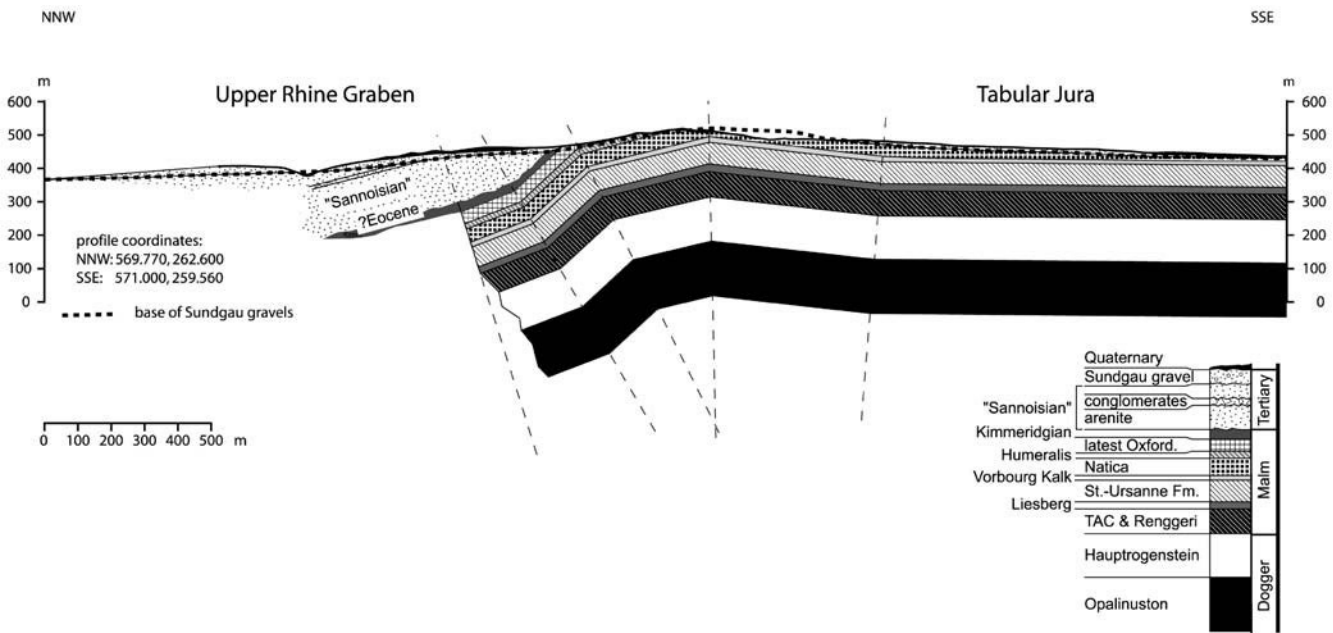
Fig. 6 Geological section across the Florimont anticline (based on data from Liniger 1970 and Figs. 2 and 5). Geology in the northern part of the section is poorly constrained due to the lack of outcrop and subcrop data. Note the close correlation between topographic crest, maximum elevation of folded Pliocene sediments and hinge line of the folded Mesozoic substratum. The "Sundgau gravel" unconformably overlies Paleogene and Mesozoic strata. For location see Fig. 2

échelon aligned anticlines with the greatest amplitude (90 and 120 m) formed at the place of compressively or transpressively reactivated extensional flexures, which are situated above ENE-oriented basement faults related to the Paleozoic trough system (Fig. 5d). Finally, the "south-stepping" isohypses in the valleys dissecting the "Sundgau gravel" base (particularly pronounced in the Largue valley), as well as the trend of the valleys themselves are oriented perpendicular to Shmin. This suggests that minor normal faults, developing parallel to SHmax, may have affected the Pliocene cover (Fig. 5e).

The base of the "Sundgau gravel" (Fig. 5) thus undoubtedly indicates a young (post 2.9 Ma) tectonic episode that postdates "classical" Jura folding (10.5 to 3.4 Ma; Kälin 1997). In the following section, we will focus on two major anticlines situated at the border between the northern Ajoie and the southern Rhinegraben (Figs. 2, 5).

## Anticlines of Réchésy and Florimont

Geological data

Two folds delimit the boundary between the Folded Jura and south-western Rhinegraben in the northern Ajoie area: the Florimont and Réchésy anticlines (Fig. 2), that were studied by previous authors (Hummel 1914; Théobald 1934; Erzinger 1943; Liniger 1964, 1967). Hummel (1914) and Liniger (1964, 1967) postulated a polyphase history of these structures, beginning with an extensional flexure related to the opening of the Rhinegraben in Eo-Oligocene times, followed by Mio-Pliocene folding. Liniger (1967) argued for three phases of Mio-Pliocene folding: (1) after the deposition of the "Hipparion sands" of Serravallian age (corresponding to the Lower Ajoie Member of the Bois de Raube Formation), (2) after the deposition of the "Vogesenschotter" (Upper Ajoie Member of the Bois de Raube Formation, dated as Upper Serravallian to Lower Tortonian) and (3) after the deposition of the "Sundgau gravel" (ages after Kälin 1997, see also Fig. 3). He also proposed compressive reactivation of faults, which root in the basement. Their activity was suggested to be combined with further northward propagation of décollement in the Triassic evaporitic layers, i.e. from the former Jura front, situated south of Porrentruy, towards the E-W-striking Oligocene flexures which delimit the Rhinegraben area to the south (Liniger 1967, Fig. 1).

The strongly curved fold axes of these two peri-anticlines plunge slightly to either sides—the Allaine valley in the west and the Coeuvatte valley in the east (Fig. 2)—and hence, display an en-échelon alignment (Berner 2001). The WSW-ENE trending Florimont anticline, located to the west, has a relatively steep dipping northern and a gently dipping southern limb (see cross-section in Fig. 6). The anticlines are separated from each other by a NNW-striking strike-slip fault that accommodated the simultaneous formation of both anticlines. The Réchésy anticline to the east is subdivided into two different segments: a western and WSW–ENE-trending one and an eastern, roughly E–W-trending one. The western segment depicts a nearly symmetrical hinge with moderately dipping limbs, whereas the eastern segment

Fig. 7 Reflection seismic profile across the Florimont and Réchésy structures (data courtesy of Shell International EP). **a** Un-migrated and stacked time section. **b** Interpreted section: *T* Lower Rupelian marls onlapping onto flexure; *A* Top Malm; *D* Top Dogger; *L* Top Liassic; *M* Top Muschelkalk formation; *BM* unconformity at the base of the Mesozoic; *cross-hatched* faulted zone associated with the late Paleozoic trough border faults. Base of the Pliocene Sundgau gravel, derived from the contours given in Fig. 5, as well as the topography are superimposed onto the topmost part of the figure. The vertical scale in meters is chosen such as to coincide with that of the reflection seismic line. According to the two-way-travel-times of seismic waves (derived from the borehole Buix, see Fig. 2 for location), 1 s TWT equals ca. 1,500 m depth), hence vertical exaggeration is by a factor of 1.26. For location see Figs. 2 and 5
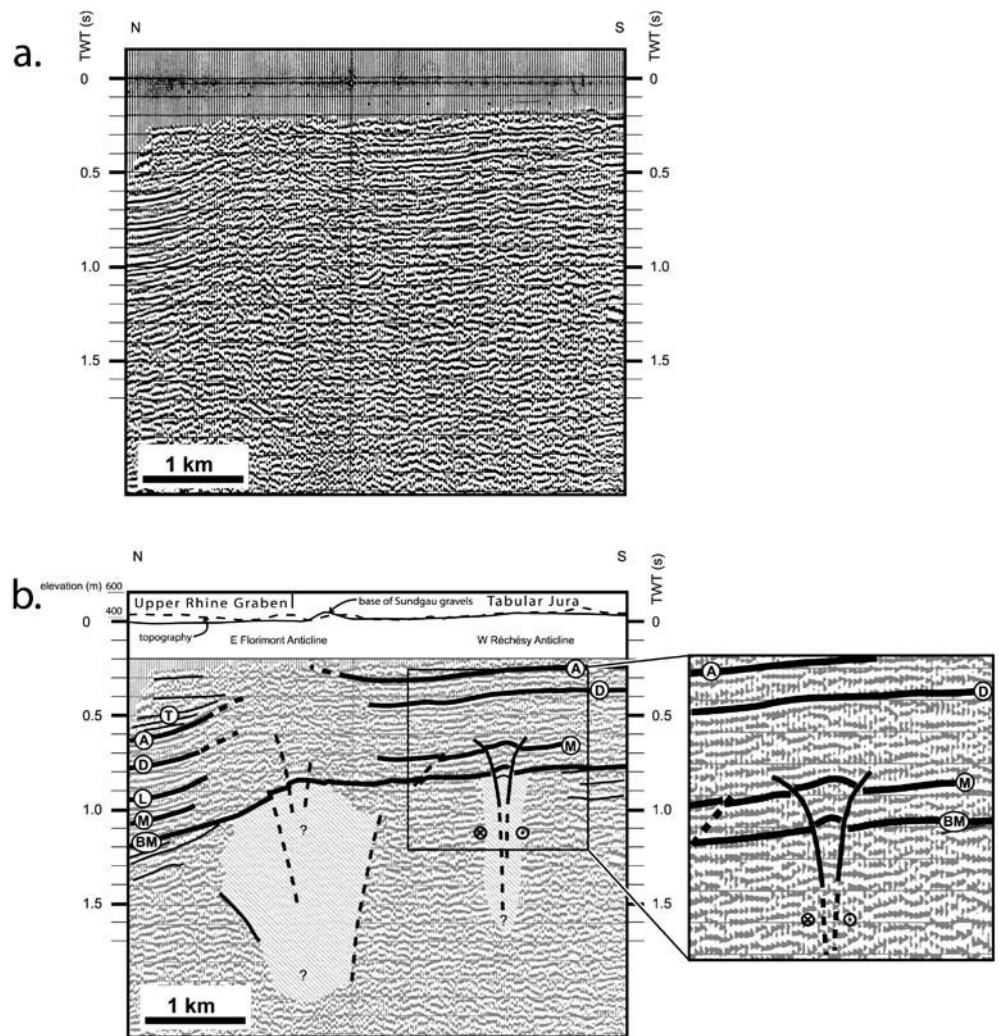

shows an asymmetry with a steeper northern limb (Fig. 2), as it is the case for the Florimont anticline (Fig. 6).

There, the steep dip of strata in the northern part (Fig. 6) is predominantly the result of extensional flexuring. This can be inferred from the onlap geometry of Early Oligocene synrift sediments, discernible on seismic profiles (Fig. 7, see below). The gently dipping southern limb, on the other hand, can be clearly attributed to a later episode of shortening: a closer look at the base of the "Sundgau gravel" (which unconformably overlie both synrift and Mesozoic sediments) reveals that their maximum elevation is located precisely above the hinge of the Mesozoic sediments. This spatial coincidence strongly suggests that the southern limb was formed after the deposition of the "Sundgau gravel" (Fig. 6). However, an embryonic fold may have already existed prior to the deposition of the gravel—this is evidenced by the slightly higher dip angle in the Mesozoic substratum with respect to the gravel.

Seismic data

Reflection seismic records provide detailed insight into the internal structure of the anticlines. Figure 7 shows a N–S-trending industry reflection seismic profile, situated at the border between the Rhinegraben's southernmost end and the adjacent Tabular Jura (see Figs. 2 and 5 for location). It crosses the en-échelon-aligned Florimont and Réchésy anticlines across their eastern and western ends, respectively. Diagnostic seismic reflectors were identified in a nearby borehole (located in Fig. 2). Additionally, the base of the Sundgau gravels (as inferred from Fig. 5) has been projected into the topmost part of Fig. 7. Note, however, that the resolution of the seismic profile (on the order of a few tens of metres) does not permit an identification of the gravel's base.

The section displays an asymmetric anticline with two angular unconformities. During a first stage of deformation, i.e. during opening of the Rhinegraben, an extensional flexure deformed the Mesozoic sediments (BM to A). Onlap of Tertiary strata (T) onto this flexure are interpreted as the sedimentary response to extension and

216
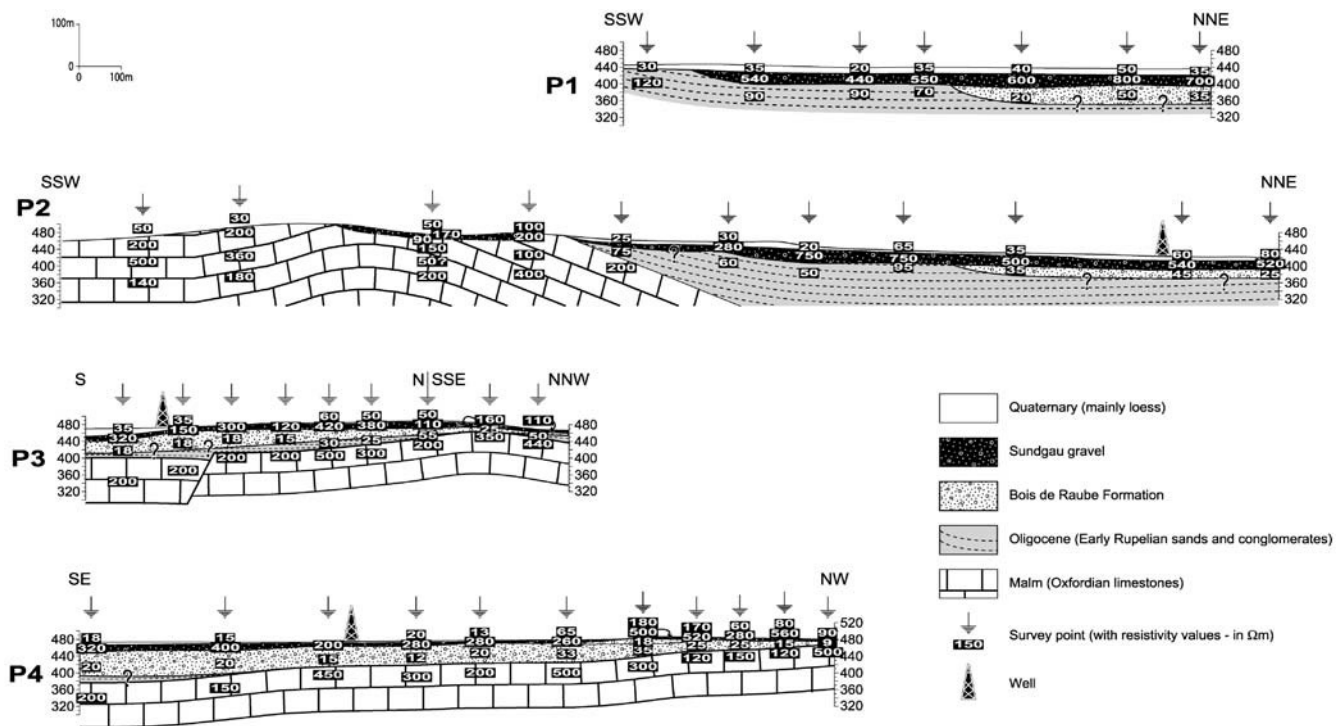
Fig. 8 Interpreted geoelectric survey lines (measurements provided by the Institut für geowissenschaftliche Gemeinschaftsaufgaben at Hanover, courtesy of Mr. P. Elsass, BRGM Alsace). Interpretation of the logs is based on the base map of the Sundgau gravel, results of the reflection seismic interpretation, the geological map and complemented by additional field data. For position of sections (P1–P4) see Fig. 5

subsidence. This extension started in Late Priabonian to Early Rupelian times, as evidenced by the sedimentation of coarse conglomerates, which are shed from the developing rift flanks (Duringer 1988). It lasted until the Early Aquitanian.

Flexuring was facilitated by the presence of Mid- to Upper Triassic evaporites at the base of the Mesozoic (with up to 80 m thick intercalations of pure halite within the Middle Muschelkalk; Jordan and Nüesch 1989) and most probably occurred above discrete basement faults. Such basement faults could coincide with and reactivate older faults, which belong to the Permo-Carboniferous trough system (see insert in the right bottom of Fig. 1). Mesozoic sediments overlie Permian strata with a marked angular unconformity, as is visible in the left part of the seismic section (beneath the reflector labelled "BM").

The base of the Pliocene "Sundgau gravel" marks another unconformity (Fig. 7). The gravel's base and the Mesozoic reflectors from north to south are congruent across a large part of the section: a northern culmination of the base of the "Sundgau gravel" is located precisely above the hinge of the Florimont anticline (compare Fig. 6). Further south, the base of the "Sundgau gravel" enters a small depression before gently rising again towards the southern end of the cross section (Fig. 7). This second, less pronounced culmination coincides with the western end of the Réchésy anticline. The wavelength and amplitude of the gravel's base and Mesozoic reflec-

tors are identical across this part of the section, strongly suggesting a linked origin.

By tracing these gentle culminations down into deeper strata, a pronounced up-warping within Triassic to Liassic strata can be recognised (Fig. 7, right inset). We interpret the up-warping of the Sundgau gravel and underlying strata to be related to the formation of a positive flower structure. The up-warped Mesozoic reflectors are clearly seen to emanate from rather diffuse fault zones situated within the Permo-Carboniferous "basement" (note the extensively disturbed reflectors in Fig. 7). The location of two such fault zones, precisely beneath the crests of both anticlines, hints towards a reactivation of pre-existing faults delineating the Paleozoic graben system (Fig. 1). In the Mesozoic to Cenozoic cover this reactivation caused further shortening of the formerly extensional flexures. This folding has produced the southern and gentle limbs of the two anticlines, and steepened the northern limbs, which coincide with the pre-existing flexure. Since, this folding has also affected the Pliocene sediments, it hence postdates them at least partly.

Geoelectric data

Geoelectric resistivity surveys allow detailed insights into shallow subsurface structures of parts of the eastern Réchésy anticline. The measured resistivity values along four profiles (Fig. 8), trending SW–NE and SE–NW,

respectively (for location see Fig. 5), were interpreted by using additional information from borehole, field and reflection seismic data. Profiles P2 and P3 (Fig. 8) include the crest of the Réchésy anticline while profiles P1 and P4 are situated in the northern and southern limb of this anticline, respectively.

Three major unconformities could be identified. A first one, the angular unconformity between the Jurassic bedrock (Resistivity values [ρ]=120–500 Ωm) and the Oligocene deposits ([ρ]=25–120 Ωm) has already been described and is visible on the geological cross-section of the Florimont anticline (Fig. 6) as well as on the seismic profile (Fig. 7). The two younger unconformities, at the bases of the Miocene deposits (Bois de Raube Formation) and the "Sundgau gravel" respectively, are characterised by a rather gentle discordance north of the anticlines (Fig. 8, P1 and P2). The angular unconformity increases towards the crest and the southern limb of the anticline (Fig. 8, P3 and P4).

The base of the second unconformity (Miocene) is made up by fluviatile gravel and sands shed from the Vosges Mountains (Bois de Raube Formation) and characterised by [ρ]=15–50 Ωm. This Miocene formation often overlies Oligocene sediments, but locally rests on Jurassic bedrocks (Fig. 8, P3 and P4). North of the Réchésy anticline, i.e. within the southern Rhinegraben, the Miocene strata beneath the base "Sundgau gravel" erosional unconformity are sub-horizontally bedded (Fig. 8, P1 and P2). At the eastern end of the gently plunging anticline, Miocene deposits are preserved over the entire structure and they extend southwards from the crest (Fig. 8, P3 and P4). Note that the Miocene sediment outcrops are confined in an area between the western Ferrette anticline to the east, the Réchésy anticline to the NW and the Vendlincourt anticline to the SW (Fig. 2) in the northern Ajoie. This area probably corresponds to one of the main southward flowing Miocene river channel systems (Liniger 1967; Kälin 1993). Since these Miocene series are warped up near the anticline, syn- and/or post-depositional differential uplift has to be inferred (see discussion below).

The third unconformity is marked by the base of the Pliocene "Sundgau gravel" ([ρ]=110–800 Ωm), as the E–W-trending paleo-Aare formed an at least locally flat surface (see above). This is confirmed by the observation that its deposits discordantly overlie Jurassic, Oligocene or Miocene strata, as clearly shown by the geoelectric resistivity surveys (Fig. 8). The geoelectric logs also provide independent evidence that the "Sundgau gravel" was differentially uplifted after its deposition (Fig. 8, P2, P3 and P4; compare with data provided in the base map of Fig. 5). A paleo-channel, situated in the fold crest, depicts a difference in altitude of about 30 m with respect to the base of the "Sundgau gravel" north of the anticline (Fig. 8, P2). Note that the "Sundgau gravel" found on the northern limb of the Réchésy anticline are incised into the Oligocene deposits, whereas their southernmost extent is truncated due to erosion (Fig. 8, P1 and P2). Hence, crest and southern limb of the Réchésy anticline have been

eroded since the deposition of the Sundgau gravel, while erosional unconformities are preserved further north and within the southernmost Rhinegraben area.

Tectonically induced young uplift inferred from the drainage pattern

Erosion and deposition on the one hand, and growth of active structures on the other, modify a relief, evolving from ongoing tectonic activity. Drainage systems adapt to changes in surface slope and thus potentially record information about the evolution of faults and folds (e.g. Seeber and Gornitz 1983; Schumm 1986; Keller and Pinter 2002). These concepts were applied to the relief and drainage systems associated with the Réchésy, the Florimont and the Vendlincourt anticlines (see Fig. 9 and their location in Fig. 1).

The Réchésy anticline represents the structure with the largest structural and topographic amplitude in the study area. The drainage divide (Fig. 9b) clearly follows the fold crest and the local drainage system precisely mirrors structure and symmetry of the anticline. Streams formed during or after fold formation and flow perpendicular to the drainage divide and the structural contours, as derived from the folded former plain (Fig. 5). A hint of a former radial organisation of the local drainage pattern around the plunging nose of the anticline is still visible at its western termination. There, the radial patterns are disturbed by a longitudinal river in the south, which flowed parallel to the evolving structure, and by the transverse Coeuvatte River in the west (Fig. 9). This river flows perpendicular to the fold and gathers the catchment areas of the radial streams. Further east, the Réchésy anticline is cut by the valley of the antecedent Vendline River, which is fairly deeply entrenched in a gorge. Two prominent wind gaps appear 500 m and 2,500 m west of the Vendline valley; such gaps are too wide and too deep to have result from the conjunction of regressive erosion of rills north and south of the Réchésy anticline. They most simply mark the former course of a stream that crossed what is now the water divide (Profile A-A' in Fig. 9a and c). These broad and presently dry open valleys were formerly occupied by the Vendline River, their highest parts now being situated about 40 m and 100 m above the present-day Vendline valley floor. A further wind gap occurs at the western end of the anticline (Profile A-A' in Fig. 9c). This wind gap clearly represents an old course of a river, which formerly crossed the culmination of the present-day anticline axis in a gorge at this point and is now 60 m above the present-day Coeuvatte valley floor. As a consequence of folding, the gorge has been abandoned and the river was deflected around the plunging western nose of the anticline (Fig. 9). About 250 m further north and on the northern limb of the anticline, a dry valley (Fig. 9a, marked by an open circle) shows at least three levels of in-boxed erosional terraces. This tributary valley represents a hanging valley, which was captured and truncated by the present-day Coeuvatte

218
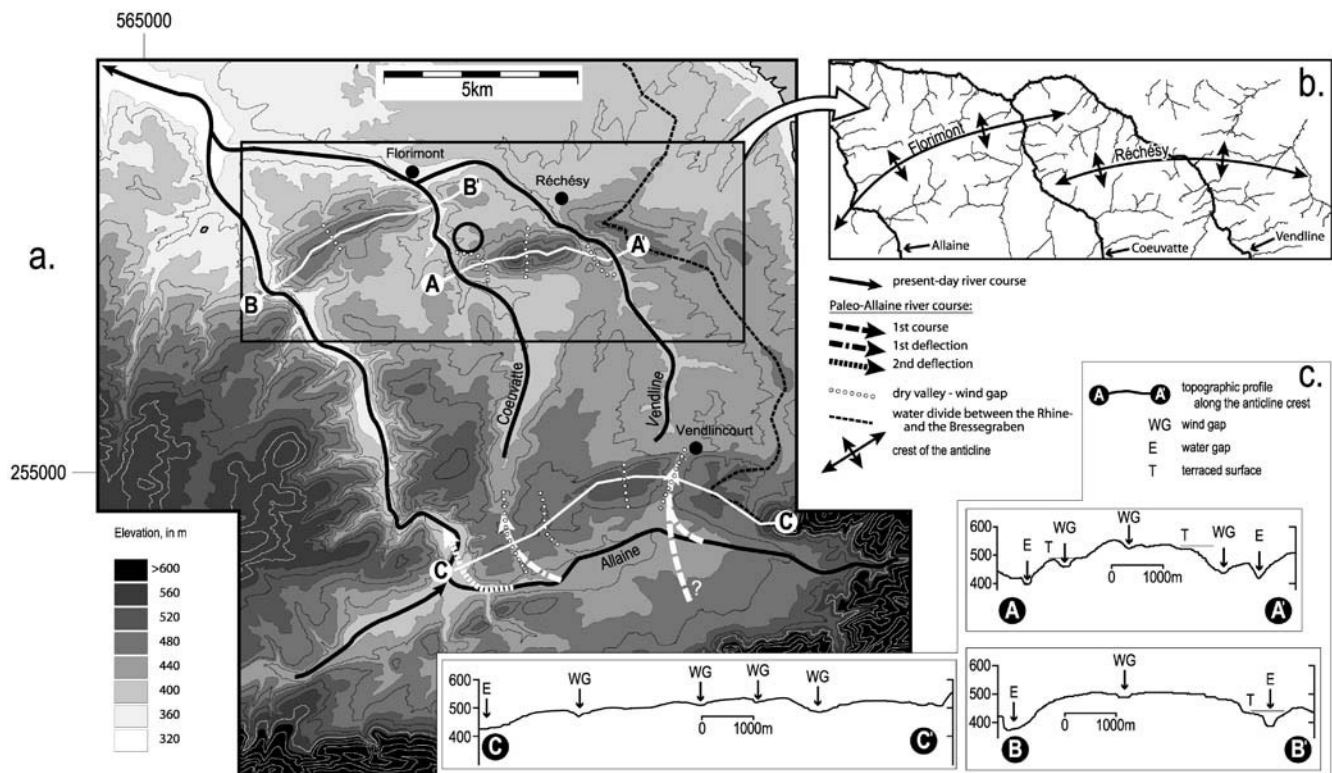
Fig. 9 a Topographic features in the northern Ajoie. *Dashed white lines* show traces of the profiles *A* and *B* indicated in **c**). Inserted *rectangle* indicates position of the drainage map. **b** Drainage map and sketched fold crests of the Florimont and the Réchésy anticlines

River. This again indicates abandonment of old valleys due to young uplift.

Although the relief of the arcuate Florimont anticline (Fig. 9) appears roughly symmetric, the associated drainage system is asymmetric. The northern limb is characterised by an annular valley system, individual dry valleys being separated by saddles (Fig. 9a and b). However, the upper course of these transverse valleys is oriented parallel to the axis of the anticline. These upper valley segments possibly represent remnants of an ENE–WSW-trending paleo-river (paleo-Vendline), which was forced to the north due to uplift of the anticlines crest. At the western and eastern plunging ends of the Florimont anticline hints of a radial drainage system are again recognizable (Fig. 9b). To the west this system was later captured by the young, consequent course of the Allaine River. The Allaine was deflected at this place due to uplift of the anticline. To the east, the antecedent Coeuvatte River, flowing in a gorge, cuts across the growing structure. At this point entrenching due to uplift is documented by an erosional terrace surface (Profile B-B' in Fig. 9). A small wind gap situated 2,000 m northeast of the present-day Allaine valley indicates that a minor paleo-stream crossed the present-day water divide.

Synthesis

Topographic profiles along the crest of the anticlines (Fig. 9c), reveal a decrease in wind gaps elevations in the direction of fold plunge. This implies lateral propagation of the anticlines, as demonstrated by Jackson et al. (1996) and Burbank et al. (1996). This, combined with the present-day drainage pattern, allows for the synthesis of the tectonic and morphological evolution of the area.

Prior to the growth of the Réchésy and Florimont anticlines, most of the drainage of the Ajoie south of them was directed northward across the area occupied by the present-day Vendlincourt anticline (Fig. 9), which is another post-"Sundgau gravel" anticline of the same generation, previously studied by Meyer et al. (1994). This anticline is also characterised by the occurrence of wind gaps (Profile C-C' in Fig. 9). This system probably represented a tributary catchment to the Middle Pliocene "Sundgau" paleo-Aare river (Fig. 4b). The eastern wind gap on the Vendlincourt anticline (Profile C-C' in Fig. 9) demonstrates that a first river course flowed to the north through the present-day Vendline valley. This course was afterwards diverted by the growing Vendlincourt anticline. Therefore, the paleo-Allaine river began to cross the area of the present-day Réchésy anticline west of the gorge formed by the present-day Vendline, as documented by the wind gaps at the culmination of the Réchésy anticline, facing the present-day Coeuvatte upstream valley, and that one further west ("paleo-Allaine river

1st course" in Fig. 9). Consequently, the Vendlincourt anticline developed slightly before the Réchésy anticline. As the Réchésy anticline developed, minor S-N flowing tributary streams have been disrupted and diverted in the propagation direction of the growing anticline and incorporated into the main drainage branch of the paleo-Allaine. As a result, the drainage basin of the paleo-Allaine increased, until stream power was sufficient to maintain its position at the western nose of the Réchésy anticline, where propagation did not yet occur. As documented by the wind gap near the western termination of the Réchésy anticline and due to its growth, the diversion of the paleo-Allaine river (=present Coeuvatte River) led to an enlargement of the catchment area, which produced the incision of the water gap at the western termination of the Réchésy anticline first, and then the present-day water gap (Fig. 9).

As a next step, the Coeuvatte valley was cut off from the paleo-Allaine river by the westward propagation of the Vendlincourt fold. Growth of the Vendlincourt structure caused further westward diversion of the Allaine River ("paleo-Allaine river 2nd deflection" in Fig. 9), as suggested by Meyer et al. (1994).

The Allaine probably crossed the Florimont fold as an antecedent river. The enlargement of its catchment area due to the growth of the Vendlincourt anticline led to an increase in stream power, which resulted in the incision of a deep gorge (western water gap in Profile B-B' in Fig. 9). In contrast, the single small wind gap at the culmination of the Florimont anticline was formerly occupied by a minor stream, which had insufficient power to maintain its course across the rising anticline.

The controlling mechanism for the evolution of the drainage network can be mostly referred to the local tectonic movements in northern Ajoie. In fact, the regional and local base level, i.e. the Bressegraben and the downstream Doubs valley (Fig. 4) were subjected to uplift during Quaternary (Rat 1978; Sissingh 1998). No significant base level lowering, generating enhanced backward erosion and a control on the drainage system, occurred. Furthermore, the adjacent area to the north of the study area, which belongs to the same catchment area as the northern Ajoie, reveals a very mature relief with less erosional forms (Giamboni et al. 2004). Only the eastern part of the southern Rhinegraben, included in the Rhine River catchment area, was strongly affected by regional base lowering in the southern and northern Upper Rhinegraben (Giamboni et al. 2003).

Concluding, the origin of terraced dry valleys, wide wind gaps and entrenched water gaps observed at the Réchésy and Florimont anticlines as well as the evolution of the paleo-Allaine river are to be referred to the young uplift of the anticlines in the northern Ajoie.

Summary and discussion

The tectonic history of the area at the boundary between the southern Rhinegraben and Tabular Jura, from Late Eocene to recent times, comprises four tectonic episodes. Each of them is characterised by a particular kinematic scenario. Their timing is constrained by structural and stratigraphic evidence.

The first episode (Fig. 10a) corresponds to the contemporaneous opening of the southern Rhinegraben and the Bressegraben (Illies 1977), and took place under regionally WNW–ESE-oriented extension from Priabonian to Early Aquitanian times (Illies 1977). Thereby, the sinistral Rhine-Bresse Transform Zone, which linked the two grabens, formed along pre-existing crustal discontinuities inherited from Variscan orogeny (Laubscher 1970). These pre-existing structures in the basement were reactivated with sinistrally transtensive wrench movements. Accommodation of these movements within the Mesozoic sedimentary cover occurred by formation of numerous ENE- to NNE-striking normal faults and E–W-striking flexures (Fig. 1). Related subsidence is documented by the onlap of Tertiary strata onto the flexures, marking a prominent unconformity. (Figs. 6, 7, 8, 10a).

A second unconformity, between Paleogene Rhinegraben fill and base of Middle Miocene sediments, documents a drastic change in the geodynamic setting. Due to the arrival of the northward migrating Alpine forebulge, presumably in Early Neogene times (Laubscher 1987, 1992), the entire southern Rhinegraben and adjacent areas became part of the immediate Alpine foreland. This is reflected in a change of the regional stress pattern from a vertical s1 and a WNW–ESE-trending s3 (extension) to a horizontal NNW–SSE-trending s1 (compression) (Larroque et al. 1987; Larroque and Laurent 1988). This change was accompanied by large-scale uplift and southward tilting of the southern Vosges—Black Forest dome together with the southern Rhinegraben, subjecting them to erosion. It found its sedimentary response in the deposition of the Middle Miocene fluviatile Bois de Raube (Kälin 1997 and Fig. 10b) and Juranagelfluh Formations (e.g. Buxtorf and Koch 1920; Laubscher 1961; Diebold et al. 1992; Kälin 1997). Locally, these Middle Miocene deposits reveal canyon-like entrenching. Existence and extent of a first (Early Miocene) transpressional reactivation of Eo-/Oligocene structures along the southern Rhinegraben margins remain speculative (Fig. 10b and Laubscher 2001).

A third tectonic episode postdates the deposition of the Bois de Raube and Juranagelfluh Formations (minimum age 10.5 Ma, Kälin 1997). On a more regional scale, the southernmost part of the Rhinegraben, which comprises the Delémont and Laufen basins (Fig. 1), now became involved in the "classical" thin-skinned folding and thrusting of the Jura Mountains. The exact location of the northern edge of the thin-skinned wedge is well constrained only southeast of Basel, i.e. at the boundary between the Folded and the Tabular Jura, and in the southernmost Ajoie, south of Porrentruy (Fig. 1). Style (thin- vs. thick-skinned) and age of folding in an intermediate area (Ferrette and the Blauen anticlines, see Fig. 1) remain a matter of debate (see below).

220

Fig. 10 Sketches of the evolution of the northern Ajoie flexural folds developed at the boundary between the Tabular Jura and the southern Rhinegraben. *Black arrows* illustrate major tectonic events. **a** Subsidence during Priabonian to Early Aquitanian in connection with Rhinegraben formation. **b** Regional uplift during Late Aquitanian to Early Burdigalian times, followed by the deposition of Middle Miocene sediments. **c** Gentle folding during Late Miocene to Early Pliocene, simultaneous with the main phase of thin-skinned deformation in the southerly adjacent Jura mountains. **d** Local planation followed by the deposition of the Sundgau gravel. **e** Post 2.9 Ma folding, related to inversion/reactivation of Paleozoic basement faults. Figure is not to scale
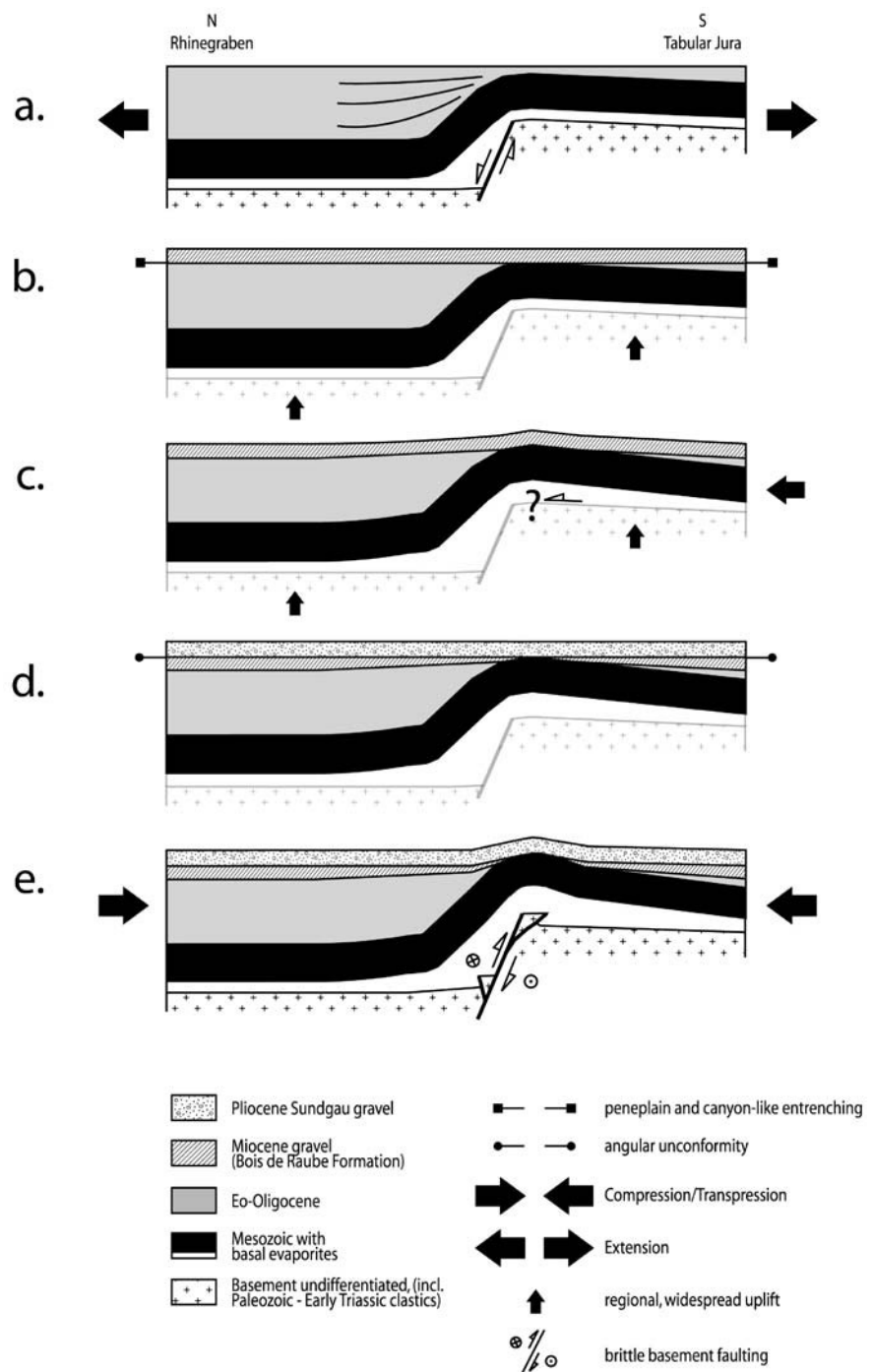
The fourth and youngest episode is associated with the unconformable deposition of the "Sundgau gravel" (Fig. 10d) and its subsequent folding (Figs. 5, 7, 10e). The thick-skinned origin of this deformation is indicated by zones of intensively faulted Permo-Carboniferous strata, above which the pronounced up-warping of Mesozoic strata points to the existence of positive flower structures (Fig. 7). Due to this reactivation, former flexures of purely extensional origin became shortened and now form gentle anticlines, traceable at the surface by contouring the folded base of the Pliocene gravel. At least

part of the shortening in the Ferrette anticline, hitherto considered to have a purely thin-skinned origin (e.g. Fischer 1965), occurred during this fourth episode of thick-skinned deformation (Fig. 5).

Paleostress trajectories, derived from fault plane data along the folded northern margin of the Jura, in the vicinity of the en-échelon aligned anticlines, and accordingly attributed to the post-Pliocene episode of folding of the sedimentary skin, reveal N–S- to NW–SE-trending s1-directions (Ustaszewski et al. 2001). This agrees with maximum horizontal stress directions, inferred from in-

situ stress measurements, performed in the Jura Mountains (Becker 2000) and southern Rhinegraben (Häring 2001). However, focal plane mechanisms of recent earthquakes reveal NW–SE-trending directions of maximum horizontal stress and dominantly strike-slip (but not reverse) faulting in the seismogenic basement (e.g. Plenefisch and Bonjer 1997; Deichmann et al. 2000). The reasons for this discrepancy are yet unknown. Strain partitioning in the transpressively reactivated Rhine-Bresse Transform Zone, allowing for the accommodation of strike-slip faulting and thrusting at different locations in basement and cover, is one possibility.

Geomorphological analysis allowed for a reconstruction of stream diversions and changes in the drainage pattern of the Ajoie and the south-westernmost part of the Rhinegraben. The drainage system in the area of the Réchésy, Florimont and Vendlincourt folds has recorded information on the growth of these folds and interactions with the evolving hydrosystem. These changes occurred in response to active uplift and postdate the deposition of the "Sundgau gravel" (post 2.9 Ma). Hence, the present-day drainage system formed during Late Pliocene to Pleistocene times. Ongoing tectonic activity is expected, as shown by complementary studies in the Sundgau area north of the study area (Nivière and Winter 2000; Giamboni et al. 2003). Disruption and displacement of the Allaine river catchment confirm the young age (post-Sundgau gravel) of the Vendlincourt anticline previously inferred by Meyer et al. (1994). Furthermore, structures such as wind gaps formed early are useful to reconstruct the evolution of the catchment areas and the changes in stream power of paleo-river systems.

The basic observations derived from geophysical, structural and seismotectonic analysis clearly indicate that within the prevailing stress field in the Western European plate (overall NW-SE-oriented maximum horizontal stresses) dextral transpressive reactivation of basement faults in the Paleogene Rhine-Bresse transform zone might very well explain both the en-échelon alignment of some observed anticlines (Fig. 5) and the basement-rooted earthquake foci with predominant strike-slip mechanisms.

Conclusions

The deformation of the Pliocene Sundgau gravel indicates neotectonic activity in the southern Rhinegraben. Furthermore, the present-day drainage system stores informations on the evolving folding, suggesting an ongoing tectonic activity. Reflection seismic data reveal that en-échelon anticlines at the surface are related to thick-skinned inversion of ENE- to NNE-striking basement faults within the Rhine-Bresse transform zone, contradicting the often invoked thin-skinned tectonism in the southern Rhinegraben. The paleostress trajectories attributed to the post-Pliocene episode are consistent with the present day stress field, which depicts a N–S- to NW–SE- orientation of the maximum horizontal stress.

Moreover, focal plane mechanisms of recent earthquakes dominantly reveal NW–SE-oriented directions of maximum horizontal stress and strike-slip faulting in the seismogenic basement. These settings allow the ENE-striking Paleozoic basement faults to be reactivated in a dextral transpressive way. NNE-oriented faults are reactivated as sinistral strike-slip faults. However, stress decoupling favoured by the presence of a décollement layer between the basement and the cover, leads to accommodation of predominantly strike-slip faulting in the basement as well as thrusting and folding in the cover.

References

Allenbach R (2001) Synsedimentary tectonics in an epicontinental sea: a new interpretation of the Oxfordian basins of northern Switzerland. Eclogae Geol Helv 94(3):265–287

Allenbach R (2002) The ups and downs of "Tectonic Quiescence"—recognizing differential subsidence in the epicontinental sea of the Oxfordian in the Swiss Jura Mountains. Sediment Geol 150:323–342

Allenbach R (2003) Spatial patterns of Mesozoic facies relationships and the age of the upper Rhinegraben Lineament. Int J Earth Sci (in revision)

Allia V (1996) Sedimentologie und Ablagerungsgeschichte des Opalinustons in der Nordschweiz. Dissertation am Geologisch-Paläontologischen Institut der Universität Basel, Basel, 185 pp

Becker A (2000) The Jura Mountains—an active foreland fold-and-thrust belt? Tectonophysics 321:381–406

Berger J P (2000) Chronostratigraphic chart for the South and North Jura Molasse, the South Rhine Graben, the North Rhine Graben and the Mainzer Becken. http://comp1.geol.unibas.ch/groups/3_3/3_3Main.htm

Bergerat F, Chorowicz J (1981) Etude des images Landsat de la zone transformante Rhin-Sa(France). Geol Rundsch 70(1):354–367

Bergerat F, Mugnier J-L, Guellec S, Truffert C (1990) Extensional tectonics and subsidence of the Bresse basin: an interpretation from Ecors data. In: Roure F, Heitzmann P, Polino R (eds) Deep structures of the Alps. vol 1, vol spec Soc Geol Ital, Mémoire de la Société géologique de la Suisse, Zh, pp 145–156

Berner P (2001) Kartierung Sundgau/Ajoie 2000. Diplomarbeit am Geologisch-Paläontologischen Institut der Universität Basel, Basel, 19 pp

Bitterli-Brunner B, Fischer H, Herzog P (1984) Geologischer Atlas der Schweiz 1:25000 - Blatt 80: Arlesheim—mit Erläuterungen. Geologische Kommission der Schweiz. Naturf. Ges., 1/25000

Bolliger T, Engesser B, Weidmann M (1993). Première découverte de mammifères pliocènes dans le Jura Neuchâtelois. Eclogae Geol Helv 86:1031–1068

Bonvalot J (1974) Les cailloutis de la Forêt de Chaux (Jura): leurs rapports avec les matériaux détritiques de Sundgau et du Nord de la Bresse, Université de Dijon, Dijon, 89 pp

Brianza M, Hauber L, Hottinger L, Maurer H (1983) Die geologischen Resultate der Thermalwasserbohrung von Leymen

222

(Haut-Rhin, Frankreich) sch von Basel, unter besonderer Berichtigung der Schwerminerale. Eclogae Geol Helv 76(1): 253–279

Burbank D, Meigs A, Brosovic N (1996) Interactions of growing folds and coeval depositional systems. Basin Res 8:199–223

Burkhalter R M (1996) Die Passwang-Alloformation (unteres Aalénien bis unteres Bajocien) im zentralen und nichen Schweizer Jura. Eclogae Geol Helv 89:875–934

Buxtorf A (1901) Geologie der Umgebung von Gelterkinden. Beitr geol Karte Schweiz 11

Buxtorf A, Koch R (1920) Zur Frage der Pliocaenbildungen im nordschweizerischen Juragebirge. Verh Natf Ges Basel 31:113–132

Contini D, Kuntz G, Angély B, Laffly J L, Kerrien Y, Landry J, Théobald N (1973) Carte Géologique et Notice Explicative—Feuille 3522 Montbéliard. BRGM, Orleans, 1/50000

Debrand-Passard S, Courbouleix S (1984) Synthèse géologique du sud-est de la France. Mém BRGM 125–126:1-615

Deichmann N, Ballarin Dolfin D, Kastrup U (2000) Seismizität der Nord- und Zentralschweiz. Nagra Tech. Ber. NTB 00–05, Nagra, Wettingen, 93pp

Diebold P (1990) Die tektonische Entwicklung der Nordschweiz. Nagra Informiert 2/90:47–55

Diebold P, Naef H (1990) Der Nordschweizer Permokarbontrog. Nagra Informiert 2/90:29–36

Diebold P, Noack T (1997) Late Palaeozoic troughs and Tertiary structures in the eastern Folded Jura. In: Pfiffner OA, Lehner E, Heitzmann P, Mueller S, Steck A (eds). Deep structure of the Swiss Alps: results of the NRP 20. Birkhäuser, Basel, pp 59–63

Diebold P, Naef H, Ammann M (1992) Zur Tektonik der zentralen Nordschweiz—Interpretation aufgrund regionaler Seismik, Oberflächengeologie und Tiefbohrungen. Nagra Tech. Ber. NTB 90–04, Nagra, Wettingen

Doebl F (1970) Die tertiären und quartären Sedimente des schen Rheingraben. In: Illies JH, Mueller S (eds). Graben problems. Schweizerbart, Stuttgart, pp 56–66

Doebl F, Teichmr R (1979) Zur Geologie und heutigen Geothermik im mittleren Oberrhein-Graben. Fortschr Geol Rheinl West-falen 27:1–27

Duringer P (1988) Les conglomérats des bordures du rift céno-zoïque rhénan. Dynamique sédimentaire et contrôle limatique. PhD Thesis, Université. Pasteur, Strasbourg, 278 pp

Erzinger E (1943) Die Oberflächenformen der Ajoie (Berner Jura). Mitteilungen der geogr.-ethnologischen Gesellschaft in Basel 6:1–138

Fabbri O, Gaviglio P, Marquer D (2001) Palaeotectonic and neotectonic analyses in the Rhine-Bresse Transfer Zone: insights and perspectives from preliminary studies in the Besançon and Massif de la Serre areas. In: Dèzes P (ed) 2nd EUCOR-URGENT Workshop, October 7–11th 2001. Mont Saint-Odile Strasbourg (France), 36 pp

Fejfar O, Heinrich W-D, Lindsay EH (1998) Updating the Neogene rodent biochronology in Europe. Mededelingen Nederlands Instituut voor Toegepaste Geowetenschappen TNO 60:533–554

Fischer H (1965) Geologie des Gebietes zwischen Blauen und Pfirter Jura. Beitr geol Karte Schweiz NF 122:107

Fischer H (1969) Geologischer Überblick über den südlichen Oberrheingraben und seine weitere Umgebung. Regio Basiliensis 10(1):57–84

Giamboni M, Schneider B, Wetzel A (2004) Geomorphic response of alluvial rivers to active tectonics: example from the southern Rhinegraben. Z f Geomorphologie (submitted)

Giamboni M, Wetzel A, Schumacher M (2003) Plio-Pleistocene folding in the southern Rhinegraben recorded by the evolution of the drainage network. Eclogae Geol Helv (accepted)

Gonzalez R, Wetzel A (1996) Stratigraphy and paleogeography of the Hauptrogenstein and Klingnau Formations (middle Bajo-cian to late Bathonian), northern Switzerland. Eclogae Geol Helv 89:695–720

Häring M (2001) Horizontale Hauptspannung im Grundbgebirge. http://www.geothermal.ch

Hummel KL (1914) Die Tektonik des Elsgaues (Berner Tafeljura). Berichte der Naturforschenden Gesellschaft zu Freiburg i.Br. 20:1–82

Illies JH (1977) Ancient and recent rifting in the Rhinegraben. Geol En Mijinbouw 56(4):329–350

Illies JH, Greiner G (1979) Holocene movements and state of stress in the Rhinegraben rift system. Tectonophysics 52:349–359

Jackson J, Norris R, Youngson J (1996) The structural evolution of active fault and fold systems in central Otago, New Zealand: evidence revealed by drainage patterns. J Struct Geol 18(2/3):217–234

Jordan P, Nüesch R (1989) Deformation structures in the Muschel-kalk anhydrites of the Schafisheim Well (Jura overthrust, northern Switzerland). Eclogae Geol Helv 82(2):429–454

Kälin D (1993) Stratigraphie und Säugetierfaunen der Oberen Sassermolasse der Nordwestschweiz. ETHZ, Zh, 238 pp

Kälin D (1997) Litho- und Biostratigraphie der mittel- bis obermiozänen Bois de Raube-Formation (Nordwestschweiz). Eclogae Geol Helv 90:97–114

Keller EA, Pinter N (2002) Active tectonics: earthquakes, uplift and landscape. Prentice Hall, Upper Saddle River, 362 pp

Koch R (1923) Geologische Beschreibung des Beckens von Laufen im Berner Jura. Beitr geol Karte Schweiz NF 48(2. Abt.):61

Krohe A (1996) Variscan tectonics of central Europe: Postaccre-tionary intraplate deformation of weak continental lithosphere. Tectonics 15:1364–1388

Larroque JM, Laurent P (1988) Evolution of the stress field pattern in the south of the Rhine Graben from the Eocene to the present. Tectonophysics 148:41–58

Larroque JM, Etchecopar A, Philip H (1987) Evidence for the permutation of stresses s1 and s2 in the Alpine foreland: the example of the Rhine Graben. Tectonophysics 144:315–322

Laubscher H (1961) Die Fernschubhypothese der Jurafaltung. Eclogae Geol Helv 54(1):221–282

Laubscher H (1970) Grundsätzliches zur Tektonik des Rhein-grabens. In: Illies JH, Mr S (eds) Graben problems. Interna-tional Upper Mantle Projekt. Schweizerbart, Stuttgart, pp 79–87

Laubscher H (1982) Die Stecke des Rheingrabens—ein kinematis-ches und dynamisches Problem. Eclogae Geol Helv 75(1):101–116

Laubscher H (1986) The eastern Jura: relations between thin-skinned and basement tectonics, local and regional. Geol Rundsch 75(3):535–553

Laubscher H (1987) Die tektonische Entwicklung der Nordschweiz. Eclogae Geol Helv 80(2):287–303

Laubscher H (1992) Jura kinematics and the Molasse Basin. Eclogae Geol Helv 85(3):653–675

Laubscher H (2001) Plate interactions at the southern end of the Rhine Graben. Tectonophysics 343:1–19

Laubscher H, Noack T (1997) The deep structure of the Basel Jura. In: Pfiffner OA, Lehner E, Heitzmann P, Mueller S, Steck A (eds) Deep structure of the Swiss Alps: results of the NRP 20. Birkhäuser, Basel, pp 54–58

Liniger H (1964) Beziehungen zwischen Pliozän und Jurafaltung in der Ajoie. Eclogae Geol Helv 57(1):75–90

Liniger H (1966) Das plio-altpleistozäne Flussnetz der Nord-schweiz. Regio Basiliensis 7(2):158–177

Liniger H (1967) Pliozän und Tektonik des Juragebirges. Eclogae Geol Helv 60(2):407–490

Liniger H (1970) Geologischer Atlas der Schweiz 1:25000 - Blatt 55: Bonfol—mit Erläuterungen. Geologische Kommission der Schweiz Naturf Ges, 1/25000

Matter A (1987) Faziesanalyse und Ablagerungsmillieus des Permokarbons im Nordschweizer Trog. Eclogae Geol Helv 80:345–367

Ménillet F, Coulon M, Fourquin C, Paicheler J-C, Lougnon J-M, Lettermann M (1989) Carte Géologique et Notice Explicative – Feuille 3620 Thann. BRGM, Orleans, 1/50000

Meyer B, Lacassin R, Brulhet J, Mouroux B (1994) The Basel 1356 earthquake: which fault produced it? Terra Nova 6:54–63

Miall A (1996) The geology of fluvial deposits: sedimentary facies, basin analysis and petroleum geology. Springer, Berlin Heidelberg New York, 582 pp

Müller W H, Blümling P, Becker A, Clauss B (1987) Die Entkoppelung des tektonischen Spannungsfeldes an der Jura-Überschiebung. Eclogae Geol Helv 80(2):473–489

Müller WH, Naef H, Graf HR (ed) (2001) Geologische Entwicklung der Nordschweiz, Neotektonik und Langzeitszenarien, Zer Weinland. NAGRA Technischer Bericht, 99–08. NAGRA, Wettingen, 226 pp

Nivière B, Winter T (2000) Pleistocene northwards fold propagation of the Jura within the southern Upper Rhine Graben: seismotectonic implications. Glob Planet Change 27:263–288

Petit C, Campy M, Chaline J, Bonvalot J (1996) Major palaeohydrographic changes in Alpine foreland during the Pliocene-Pleistocene. Boreas 25:131–143

Pfiffner OA, Erard PF, Stäuble M (1997) Two cross sections through the Swiss Molasse Basin. In: Pfiffner OA, Lehner E, Heitzmann P, Mueller S, Steck A (eds) Deep structure of the Swiss Alps: results of the NRP 20. Birkhäuser, Basel, pp 59–63

Pflug R (1982) Bau und Entwicklung des Oberrheingrabens. Wissenschaftliche Buchgesellschaft Darmstadt—Erträge der Forschung 184:1–145

Philippe Y (1995) Rampes latérales et zones de transfert dans les chaînes plissées: géometrie, conditions de formation et pièges structuraux associés. PhD Thesis, Savoie, 272 pp

Plenefisch T, Bonjer K-P (1997) The stress field in the Rhine Graben area inferred from earthquake focal mechanism and estimation of frictional parameters. Tectonophysics 275:71–97

Rat P (1978) Les phases tectoniques au Tertiaire dans le Nord du Fossé bressan et ses marges bourguignonnes en regard des systèmes d'erosin et de sédimentation. C R Soc géol France:26–28

Ruhland M, Blanat J G (1973) Carte Géologique et Notice Explicative—Feuille 3722 Ferrette - 1/50000. BRGM, Orléans

Schumacher ME (2002) Upper Rhine Graben: role of pre-existing structures during rift evolution. Tectonics 21(1):10.1029/2001TC900022 (6-1-6-17)

Schumm A (1985) Patterns of alluvial rivers. Annu Rev Earth Planet Sci 13:5–27

Schumm SA (1986) Alluvial river response to active tectonics. In: Council NR (ed) Active tectonics. National Academy Press, Washington, DC, pp 80–94

Seeber L, Gornitz V (1983) River profiles along the Himalayan arc as indicators of active tectonics. Tectonophysics 92:335–367

Sissingh W (1998) Comparative Tertiary stratigraphy of the Rhine Graben, Bresse Graben and Molasse Basin: correlation of Alpine foreland events. Tectonophysics 300:249–284

Sittler C (1972) Le Sundgau, aspect géologique et structural. Bull Sci géol 25:93–118

Théobald N (1934) Les alluvions du Pliocène supérieur de la région du Sundgau. Bull Soc Ind Mulhouse 101:1–36

Théobald N, Devantoy J (1963) Carte Géologique de la France et Notice Explicative—Feuille 3621 Belfort. BRGM, Orleans, 1/50000

Théobald N, Dubois G, Goguel J (1958) Carte Géologique de la France et Notice Explicative—Feuille 3721 Altkirch-Huningue. BRGM, Orleans, 1/50000

Théobald N, Schweitzer M, Hudeley H (1976) Carte Géologique de la France et Notice Explicative—Feuille 3820 Mulhouse. Belfort. BRGM, Orleans, 1/50000

Thury M, Gautschi A, Mazurek M, Mr W H, Naef H, Pearson F J, Vomvoris S, Wilson W (1994) Geology and hydrogeology of the crystalline basement of Northern Switzerland. Nagra Tech. Ber. NTB 93–01, Nagra, Wettingen, 452 pp

Ustaszewski K, Schmid SM, Giamboni M (2001) The frontal folds of the Jura mountains revisited: subsequent folding of Oligocene extensional structures during a thick-skinned phase of Jura folding? J Conf Abstr 6(1):630

Wetzel A, Allenbach R, Allia V (2002) Reactivated basement structures affecting the sedimentary facies in a tectonically "quiescent" epicontinental basin: an example from NW Switzerland. Sediment Geol 157:153–172

Ziegler PA (1990a) Collision related intra-plate compression deformations in Western and Central Europe. J Geodyn 11:357–388

Ziegler PA (1990b) Geological atlas of Western and Central Europe. Shell Internationale Petroleum Maatschappij BV, The Hague, 238 pp

Ziegler PA (1992) European Cenozoic rift system. Tectonophysics 208:91–111

Ziegler PA, Cloetingh S, Van Wees J-D (1995) Dynamics of intra-plate compressional deformation: the Alpine foreland and other examples. Tectonophysics 252:7–59

Chapter 5 -

Fault reactivation in brittle-viscous wrench systems – dynamically scaled analogue models and application to the Rhine-Bresse Transfer Zone

Kamil Ustaszewski[+], Markus E. Schumacher[+], Stefan M. Schmid[+] and Dick Nieuwland[++]

[+]) Dept. of Geosciences, Bernoullistrasse 32, University Basel, CH-4056 Basel, Switzerland

[++]) Dept. of Tectonics and Structural Geology, Faculty of Earth and Life Sciences, Vrije Universiteit, De Boelelaan 1085, 1081 HV Amsterdam, The Netherlands

Abstract

Analogue experiments on oblique rifting and subsequent transpressional reactivation were performed with two-layer slabs of sand and silicone. In this brittle-viscous system, transtensional and transpressional wrench faulting was induced by movements of a basal rigid plate. The dynamically scaled analogue models are confronted with the structural evolution of the Rhine-Bresse Transfer Zone (RBTZ) that linked Palaeogene rifting in the Upper Rhine and Bresse Grabens and that appears to have been transpressively reactivated in Neogene to recent times. Fault patterns produced in the sand layer above the basal silicone layer are compared with structural elements in the sedimentary cover, separated from the basement by an evaporitic décollement layer.

In order to investigate strain-rate dependence of fault reactivation and graben inversion, transpressional shortening was performed under different displacement rates. Experimental results suggest that the reactivation of pre-existing structures in a brittle cover above a viscous décollement is strongly dependent on the strain rate within the viscous layer. Under low to intermediate displacement rates (2.6 cmh^{-1}), deformation concentrates within the basal viscous layer and former normal faults within the cover are not reactivated. The reactivation at higher displacement rates (5 cmh^{-1}) results in a complete inversion of graben structures within the cover. Ongoing shortening produces lobed thrust fronts, which crosscut pre-existing normal faults.

Late Pliocene to recent en-échelon aligned folds and isolated thrust faults in the cover of the RBTZ are attributed to thick-skinned reactivation of basement faults. A comparison of natural and experimentally obtained structures suggests that fault reactivation occurred under low displacement rates (<1 mm/a). This results in a low mechanical coupling between

basement and cover in areas with significantly thick décollement layers, providing an explanation for decoupled stresses between basement and cover, such as observed in the northern Jura Mountains.

Keywords

Analogue modelling, strain rate, rifting, fault reactivation, inversion, Rhine-Bresse Transfer Zone

5.1 Introduction

5.1.1 Objectives and previous modelling work

Selective reactivation of pre-existing crustal fault segments is a phenomenon frequently observed at various scales, because it can occur at local stresses lower than those needed for the creation of new faults (cf. Fig. 17 in Richard and Krantz, 1991). In general, faults represent surfaces of reduced or negligible cohesive strength. Their reactivation is basically controlled by the coefficient of friction and the pore fluid pressure. Hence, reactivation of pre-existing faults occurs if the resolved shear stress along a fault plane is large enough to exceed frictional resistance (Byerlee, 1978). This requires the principal stresses to be in a favourable orientation with respect to the trend of the pre-existing fault.

A number of experiments on fault reactivation have been performed in previous studies. Most of this work focused on basement-driven reactivation of faults, usually simulated in analogue experiments by introducing a basal discontinuity in the model, which triggers and localises deformation in the overlying cover (Richard and Krantz, 1991; Nalpas *et al*., 1995; Brun and Nalpas, 1996; Dubois *et al*., 2002). Because of the higher resolved shear stress, transpressional reactivation of normal faults within the cover occurs more easily than pure compressional reactivation. Hence, reactivation is favoured if the direction of the greatest principal stress σ1 is oblique to the fault trend. Reactivated basement faults, which lead to reactivation of structures in the cover, exhibit a substantial wrench component (Richard and Krantz, 1991). Brun and Nalpas (1996) found that reactivation of graben-bounding normal faults requires an angle of less than 45° between the compression direction and the fault trend, and that inversion becomes even more significant at angles lower than 30°. Dubois *et al*. (2002) have performed experiments on normal fault reactivation in brittle-viscous systems, adding sand layers during deformation. Their results suggest that the kinematics of reactivated normal faults also depend on the thickness of the sedimentary overburden above the basement fault.

The strain-rate dependence of the strength of viscous horizons (e.g. evaporites), often found between basement and cover, is an additional important parameter. It influences the coupling between basement and cover. Hence, strain rate, which controls the transmission of stresses between brittle and ductile/viscous layers, also becomes very important. In this case,

reactivation also depends on the rheology of the viscous materials involved. Hitherto little attention has been paid to this effect and experiments were usually performed at constant strain rates (e.g. Schreurs and Colletta, 1998).

In this study, we will also address the strain rate dependence during transpressional reactivation of normal faults in brittle-viscous systems, keeping the geometry constant throughout all experiments. The results of the model will be applied to a natural example, the Rhine-Bresse Transfer Zone (RBTZ) of the European Cenozoic Rift System. There, Middle Triassic evaporites act as a regional décollement horizon between the pre-rift sedimentary cover and the basement. This transfer zone accommodated predominantly transtensive motions during Palaeogene times (Lacombe *et al*., 1993; Schumacher, 2002). The area also bears evidence for late Neogene to recent shortening and uplift, which is most presumably linked to basement-induced transpressional fault reactivation in its sedimentary cover, as will be discussed below. Deformation rates for this phase of reactivation are rather ill-defined in the field, but can be estimated on the base of our dynamically scaled sand-silicone models.

5.1.2 Regional geology and evidence for thick-skinned reactivation

The Rhine-Bresse Transfer Zone (RBTZ) represents a major W-E trending intracontinental transfer zone within the Cenozoic rift system of Europe (Fig. 1a). It connects late Eocene to Oligocene extension in the Upper Rhine graben (URG) with contemporaneous extension in the Bresse graben. This rifting implies coeval sinistral transtensional movements along the RBTZ (Laubscher, 1970; Bergerat and Chorowicz, 1981; Illies, 1981; Lacombe *et al*., 1993). Pre-existing Late Variscan and Permo-Carboniferous WSW-ENE trending fault systems are responsible for the localisation of transfer zones and for the structural segmentation of the European Cenozoic rift system. Most important in this context is a set of fault-controlled troughs of Permo-Carboniferous age, generally trending parallel to this Variscan structural grain. Important additional pre-existing structures are Palaeozoic NNE-SSW- ("Rhenish") and NW-SE-oriented ("Hercynian") faults. Palaeogene transtensional movements, controlled by pre-existing structures in the basement, were accommodated by the formation of numerous ENE- to NNE-striking normal faults in the Mesozoic sedimentary cover, and, additionally – owing to the presence of evaporites at the base of the Mesozoic succession – by flexures. Basement faults within the RBTZ crop out only in the Massif de la Serre (labelled "MS" in Fig. 1a). This small basement horst is bounded by ENE- and NE-trending normal faults in the north and south, respectively, which were active in the Late Palaeozoic and reactivated during Palaeogene transtension (Chauve *et al*., 1983; Coromina and Fabbri, 2003). Subcrop maps showing the Permo-Carboniferous trough system (Diebold and Naef, 1990; Laubscher and Noack, 1997) and Variscan lineaments (Debrand-Passard and Courbouleix, 1984), as well as our work based on industry seismic reflection data, point towards the existence of numerous, NE- to ENE-striking (N45°E to N80°E) faults in

the subsurface of the RBTZ and the southernmost URG. Geomorphologic, geological and geophysical data give evidence for Late Pliocene to recent uplift and shortening in the RBTZ and the southernmost Upper Rhine Graben, summarised below.
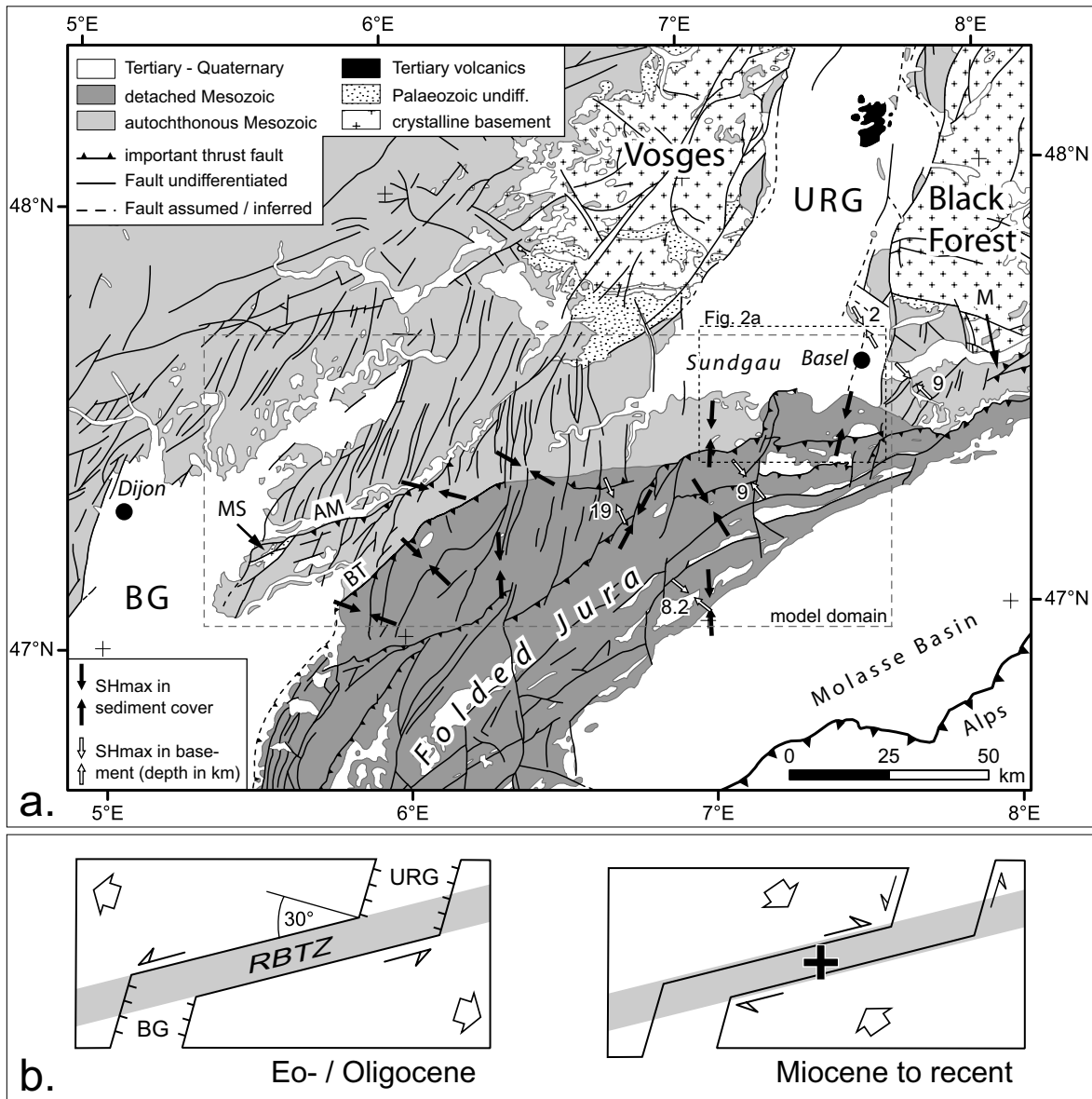
Fig. 1: a: Geological overview of the western European Rhine-Bresse transfer zone (RBTZ), connecting the Bresse Graben (BG) and Upper Rhine Graben (URG). Maximum horizontal stress orientations in cover (black double arrows) and basement (white double arrows), derived from in-situ stress measurements and earthquake focal mechanisms (Becker, 2000; Reinecker et al., 2003; Häring, 2001) are shown. Note decoupled stresses between basement and cover particularly in the eastern Folded Jura. Large dashed rectangle depicts the modelled domain. AM = Avant-Mont thrust, BT = Besançon thrust, MS = Massif de la Serre, M = Mandach and Mettau thrusts. Small dashed rectangle indicates position of Fig. 2a.

b: Sketches of the kinematic framework of the RBTZ from Palaeogene to recent times. "+" indicates uplift (modified after Lacombe et al., 1993).

5.1.2.1 Geomorphologic data

Differential vertical movements between the area of the transfer zone and the Upper Rhine Graben since the Late Pliocene (Post 2.9 Ma; Liniger, 1963; Petit *et al*., 1996; Giamboni *et al*., 2004) can be inferred from the abandonment of the riverbed of the Palaeo-Aare, which drained westward across the Sundgau into the Bresse depression in Middle Pliocene times (4.2 to 2.9 Ma; Petit *et al*. 1996), and the associated capture of the Rhine into the Rhine Graben. These drainage network changes were accompanied by shifts in the location of Quaternary depocenters, leading to an almost complete lack of corresponding deposits in the RBTZ, as revealed from isopach maps (Doebl, 1970). The only Quaternary deposits are found along the Doubs and Ognon rivers, which form relatively narrow valleys, entrenching themselves into Mesozoic sediments (note outlines of river meanders in the RBTZ marked by their Late Pliocene to Quaternary infill, Fig. 1a). Additionally, the offset of Pliocene or younger piedmont deposits along the Besançon thrust (labelled "BT" in Fig. 1a) to the south indicates an uplift of the hangingwall of about 100 m with respect to the footwall in the Doubs valley (Dreyfuss and Glangeaud, 1950; Fabbri *et al*., 2001).

The gently folded base of the Late Pliocene fluvial Sundgau gravels in the southernmost Upper Rhine Graben reveals ENE- to NE-striking syn- and anticlines, testifying to Late Pliocene to recent shortening of the sedimentary cover (Giamboni *et al*., 2004; Fig. 2b). Systematically northward tilted Pleistocene river terraces of Rhine tributaries in the Sundgau (Nivière and Winter, 2000) and immediately north of the Avant Mont thrust (labelled "AM" in Fig. 1a) along the Ognon River (Goguel and Dreyfuss, 1967; Dreyfuss and Kuntz, 1970; Campy, 1984) give additional support to the hypothesis that uplift and shortening within the RBTZ has remained active during the Quaternary.

5.1.2.2 Recent stress field

While WNW-ESE-oriented extension prevailed in the RBTZ in the Eo- to Oligocene, it was subjected to NW-SE- to WNW-ESE-oriented compressive stresses since the early Miocene (Lacombe *et al*., 1993 and Fig. 1b). These reoriented stresses, exerted from the nascent Alps in the south, led to the cessation of rifting in the southern URG. During the Late Miocene to Lower Pliocene, the southernmost parts of the RBTZ were incorporated into thin-skinned Jura folding and thrusting. The present day stress field in parts of the Folded Jura Mountains and their foreland, however, appears incompatible with presently ongoing Jura décollement tectonics, because currently observed maximum horizontal stresses (inferred from in-situ stress measurements) deviate up to 90° from the σ1-directions during the main stage of Jura folding (Becker, 2000; and references therein). Additionally, the reoriented recent stress directions extend far into the non-detached foreland. This led Becker (2000) to exclude ongoing décollement tectonics in the sense of Laubscher (1961). The maximum horizontal stresses in the cover of the RBTZ are NW-SE- to WNW-ESE-oriented (black double arrows

in Fig. 1a), making pre-existing ENE-oriented faults prone to dextral reactivation. The maximum horizontal stresses in the seismogenic basement of the southern URG and adjacent areas reveal a consistent NW-SE-orientation (Plenefisch and Bonjer, 1997; Deichmann *et al*., 2000). However, in the detached cover of the northern Jura Mountains, maximum horizontal stresses are more N-S oriented (Müller *et al*., 1987; Becker, 2000), indicating that stresses between cover and basement are still decoupled there (compare black and white double arrows in Fig. 1a).

The ENE-striking, north-verging Avant-Mont thrust ("AM" in Fig. 1a), is an isolated thrust fault in the autochthonous Mesozoic, traceable for almost 50 km along strike. It nucleated most presumably above a pre-existing fault formed during Eo-/Oligocene transtension and has been hitherto regarded as the outermost thrust of the "thin-skinned" Jura fold and thrust belt (Philippe, 1995). On the other hand, it is yet unclear how the Avant-Mont thrust is geometrically and kinematically linked to the detached Mesozoic of the thin-skinned Jura fold belt. In the west it appears to terminate against an Oligocene normal fault, delimiting the Massif de la Serre horst ("MS" in Fig. 1a) to the south. Towards the east, shortening along it progressively diminishes until becoming insignificant. In-situ-stress measurements indicate WNW-directed maximum horizontal stresses (Fig. 1a), making the Avant-Mont thrust prone for accommodating a combined reverse- and dextral motion in a "thick-skinned" manner. Other isolated thrust faults in the autochthonous Mesozoic such as the Avant-Mont thrust are found east of Basel (e.g. Mandach and Mettau thrusts, "M" in Fig. 1a; Wildi, 1975; Laubscher, 1986; Laubscher, 1987). Although their development was generally attributed to the nucleation of décollement-related thrusts and folds above pre-existing faults and flexures in the basement (Wildi, 1975; Laubscher, 1977; Laubscher, 1986; Laubscher, 1987; Müller *et al*., 2002) their geometrical link with the detached Mesozoic of the Folded Jura Mountains is as questionable as in the case of the Avant-Mont thrust.

5.1.2.3 Subsurface data

Figure 2a depicts faults offsetting the Base Mesozoic surface in the southernmost part of the Upper Rhine Graben, which were active during Eo-/Oligocene extension. They were independently mapped by different authors (Gürler *et al*., 1987; Ustaszewski *et al*., submitted) on the base of reflection seismic profiles. Figure 2a shows that the approximately N20° trending faults reveal a conspicuous and systematic dextral drag where they approach the ENE-trending faults delineating the RBTZ. These faults affect a stratigraphic level situated below the Triassic décollement horizon. Thus, this drag cannot be explained by compression and/or wrenching related to thin-skinned Jura thrusting/folding, which only affected the detached sedimentary cover but not the Base Mesozoic surface. At the surface, two en-échelon anticlines are situated exactly above ENE-trending basement faults, which have gently folded the base of the Pliocene Sundgau gravels (Giamboni *et al*., 2004; Fig. 2b).
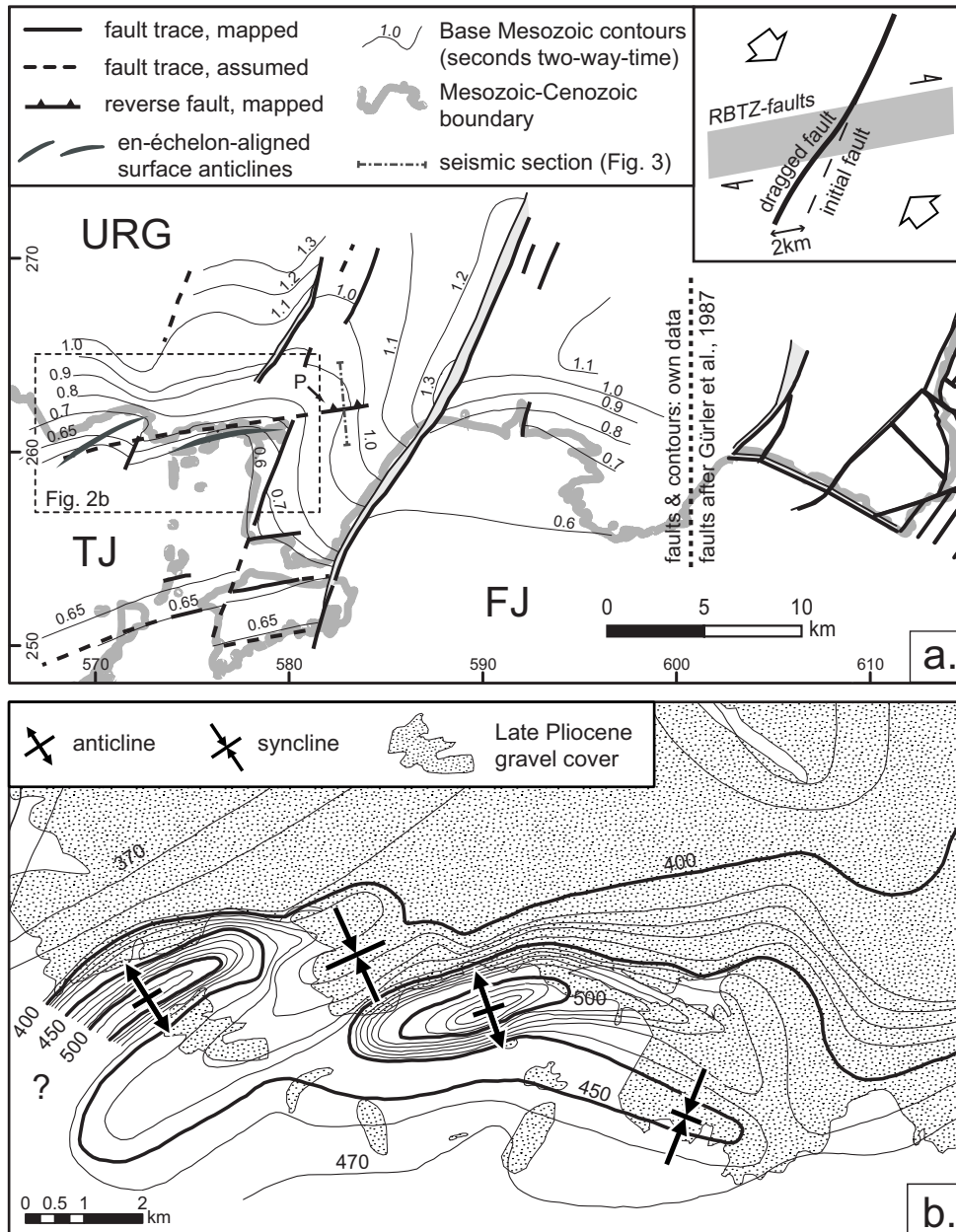
Fig. 2: a: Close-up on a part of the southernmost Upper Rhine Graben (URG) and adjacent Jura Mountains, showing faults dissecting the Base Mesozoic (western part) and Top-Buntsandstein surfaces (eastern part of figure). Note the systematic dextral drag of N20°-trending faults along ENE-trending faults, which is interpreted as the result of dextral reactivation of ENE-trending faults in the Neogene (insert at top right). Numbers at edges refer to Swiss National grid. FJ = Folded Jura, TJ = Tabular Jura, P = Pfetterhouse reverse fault.

b: Contours of the base of Late Pliocene Sundgau gravels (in m above sea level; isohypse distance 10 m) in the area of en-échelon aligned surface anticlines, testifying to Post-Late Pliocene to recent shortening (after Giamboni *et al.*, 2004).
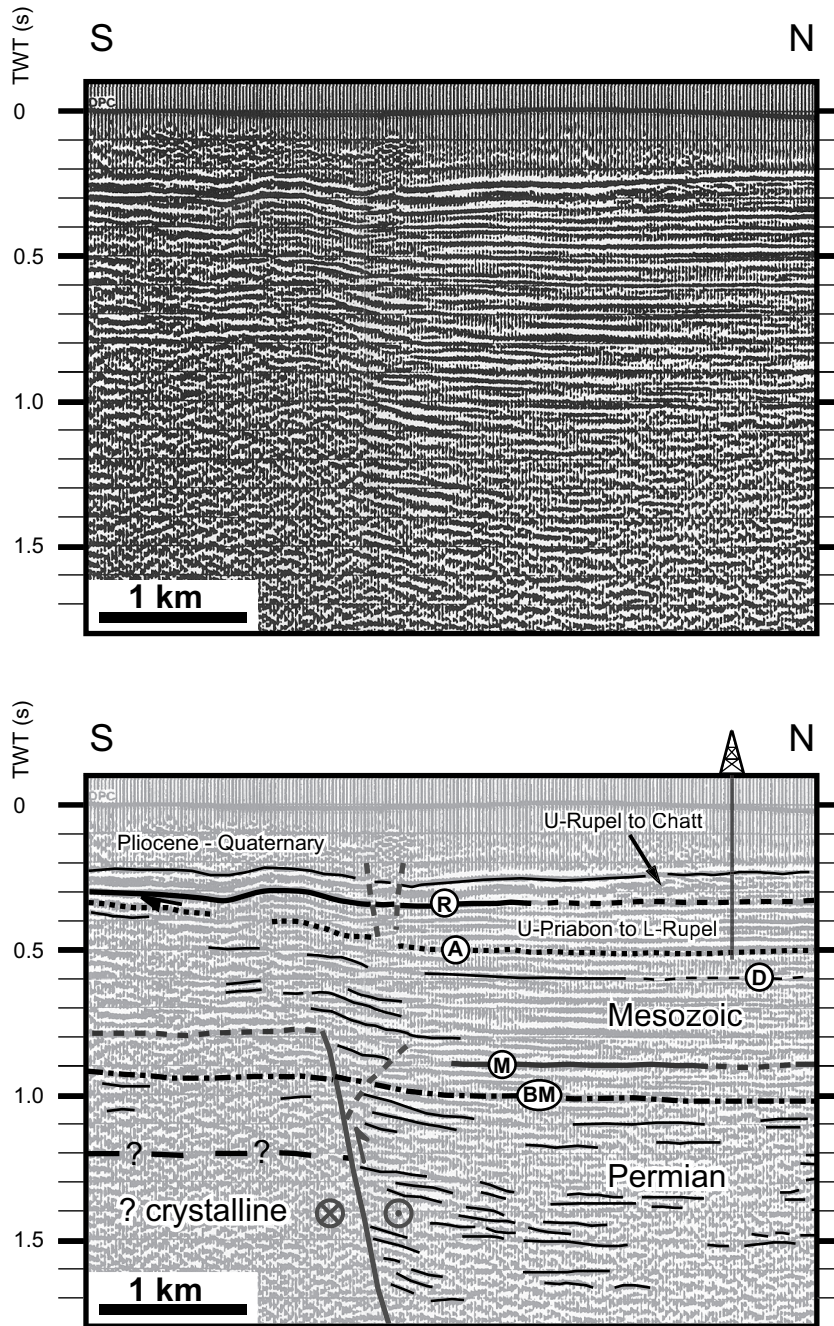
Fig. 3: N-S-trending reflection seismic line crossing a reactivated ENE-trending basement fault in the southernmost Upper Rhine Graben. For the location see Fig. 2. a: un-migrated, stacked time section, b: interpreted section. BM = base Mesozoic, M = top Muschelkalk, D = top Dogger, A = top Malm, R = Upper Rupelian. During Eo- to Oligocene rifting, an extensional flexure has developed in the Mesozoic sediments above a north-dipping normal fault, delimiting a Permo-Carboniferous trough (note the differently reflective basement beneath the Mesozoic across the fault). Synrift sediments show a southward-tapering wedge and are of Upper Priabonian to Late Chattian age. Compressive/transpressive reactivation of the normal fault led to the inversion of the flexure, evidenced in the gently folded Upper Rupelian reflector (marked "R"). Seismic data courtesy of Shell International EP.

Eastward, a reverse fault trending ENE in the along-strike continuation of the en-échelon-aligned anticlines was mapped in the subsurface of the Oligocene fill within an adjacent graben (labelled "P" in Fig. 2a and Fig. 3). Fig. 3 shows a reflection seismic line traversing this reactivated ENE-trending fault. An extensional flexure has developed in the Mesozoic sediments above a steeply north-dipping normal fault during Eo- to Oligocene rifting. This normal fault delimits a Permo-Carboniferous trough, as depicted by differently reflective basement beneath the Mesozoic sediments across the fault. Synrift sediments, tapering southward, are of Upper Priabonian to Late Chattian age. Compressive or rather transpressive reactivation of the normal fault led to the inversion of the flexure. This is evidenced in the gently folded Upper Rupelian reflector (marked "R"). According to the seismic information available (Fig. 3), fault reactivation could have occurred as early as in the Late Chattian. Seen in a larger context, however, reactivation rather occurred after the establishment of NW-SE-oriented greatest principal stress in Aquitanian times (Laubscher, 1992; and Fig. 1b, right). The evidence provided in Figures 2 and 3 shows that dextral reactivation of ENE-oriented basement faults in the RBTZ has inverted formerly extensional flexures in the cover, leading to dextrally dragged N20° trending faults (top right insert in Fig. 2a).

The geomorphologic, geological and geophysical observations described in this section testify to Neogene (particularly Upper Pliocene to recent) thick-skinned tectonic activity in the RBTZ. We intended to compare natural structures with experimentally obtained ones by means of dynamically scaled analogue modelling. In order to provide qualitative constraints on the strain rates during the reactivation of ENE-oriented basement faults in the RBTZ, our experiments were performed with varying displacement rates. Prior to designing an experimental setup, however, estimates on amount and direction of displacement within the RBTZ, as well as natural strain rates were required. Furthermore, the rheology of the model materials chosen needed to be properly downscaled to match that of the pre-rift sediments in the RBTZ.

5.2 Geological boundary conditions and strain-rates

5.2.1 Estimates of displacement and strain rates in the RBTZ

The orientation of σ3 in the southern URG and the RBTZ during the main rifting pulse was WNW-ESE (Lacombe *et al.*, 1993). The strike azimuth of the Permo-Carboniferous trough system (the likeliest candidate for the reactivation of the basement fault zone controlling transtension within the RBTZ) is between N70°E and N80°E, as deduced from various subcrop maps (Debrand-Passard and Courbouleix, 1984; Diebold and Naef, 1990; Müller *et al.*, 2002). The angle between this basement fault zone and σ3 is thus on the order of 30° (Fig. 1b, left). Assuming that all extension due to rifting in the southern Upper Rhine Graben was transferred into the RBTZ, an overall displacement of 5-6 km may be deduced

(Brun *et al.*, 1992). This extension was accommodated within a time-span of about 7 Ma, as the main subsidence pulse spanned from 35 to 28 Ma (Schumacher, 2002). This results in a displacement rate (U) of about 1 mm a^{-1}, and, given an initial rift width of 30-35 km (Allemand and Brun, 1991), in a strain rate $\dot{\varepsilon}$ of the order of 10^{-15} s^{-1}.

Estimating the Neogene displacement rates is more difficult: Figure 2a reveals that the N20° trending faults are systematically dextrally dragged where they approach the ENE-trending faults delineating the RBTZ. According to Fig. 2, the drag amounts to some 2 to 2.5 km and occurred along dextrally reactivated, ENE-oriented basement faults since Neogene times. Laubscher (2003) argued that compressive reactivation of Palaeogene extensional flexures initiated already in the Late Aquitanian to Early Burdigalian (around 20 Ma). In this case, these movements would correspond to displacement rates on the order of 0.1 mm/a or even less, if continuous up to present. If, on the other hand, we assume that the inferred amount of wrench motion was accommodated only since the Late Pliocene (post-dating both Jura-folding and the deposition of the Pliocene Sundgau gravels, i.e. post-2.9 Ma), an average displacement rate on the order of 1 mm/a is deduced. An independent estimate, achieved by palinspastically restoring the gently folded base of the Sundgau gravels, yields a minimum horizontal displacement rate on the order of 0.05 mm/a over 2.9 Ma. Thus, Neogene displacement rates in the RBTZ range between <0.1 and 1 mm/a, if continuous fault activity in the considered time slots is assumed.

5.2.2 Rheology of the pre-rift sediments

Disregarding Tertiary syn-rift sediments, the overall thickness of the Mesozoic sediments in the southern URG approximates 1000 to 1100 m, as revealed by boreholes (Schmidt *et al.*, 1924; Häring, 2001; Fig. 4, bottom). This pile of sediments predominantly consists of limestones, which responded to rift-related extension mainly by brittle failure. Intercalated Aalenian shales are considered as brittle layers in our modelling since they reveal no transition from cataclastic to plastic behaviour with increasing differential stresses (Nüesch, 1991). Therefore they are unlikely to have had any significant effect for strain partitioning during rifting. However, viscous behaviour is expected for the Triassic Muschelkalk and Gipskeuper series, where rock salt, anhydrite and/or gypsum predominate. While the Gipskeuper contains frequent shale intercalations, very pure and up to 80 m thick rock salt is present in the basal Triassic Muschelkalk series. For convenience, we assumed an overall thickness of viscous rock salt of 100 m, which yields a thickness ratio of brittle to viscous sediments on the order of 10:1 in the overall stratigraphic column.

The basement consists either of crystalline rocks or of Permian clastic deposits (sandstone, quartzite and conglomerate). Both revealed brittle behaviour in their top part during Palaeogene rifting as can be inferred from the cataclastic behaviour of these rocks, where they are exposed along the URG-border faults.
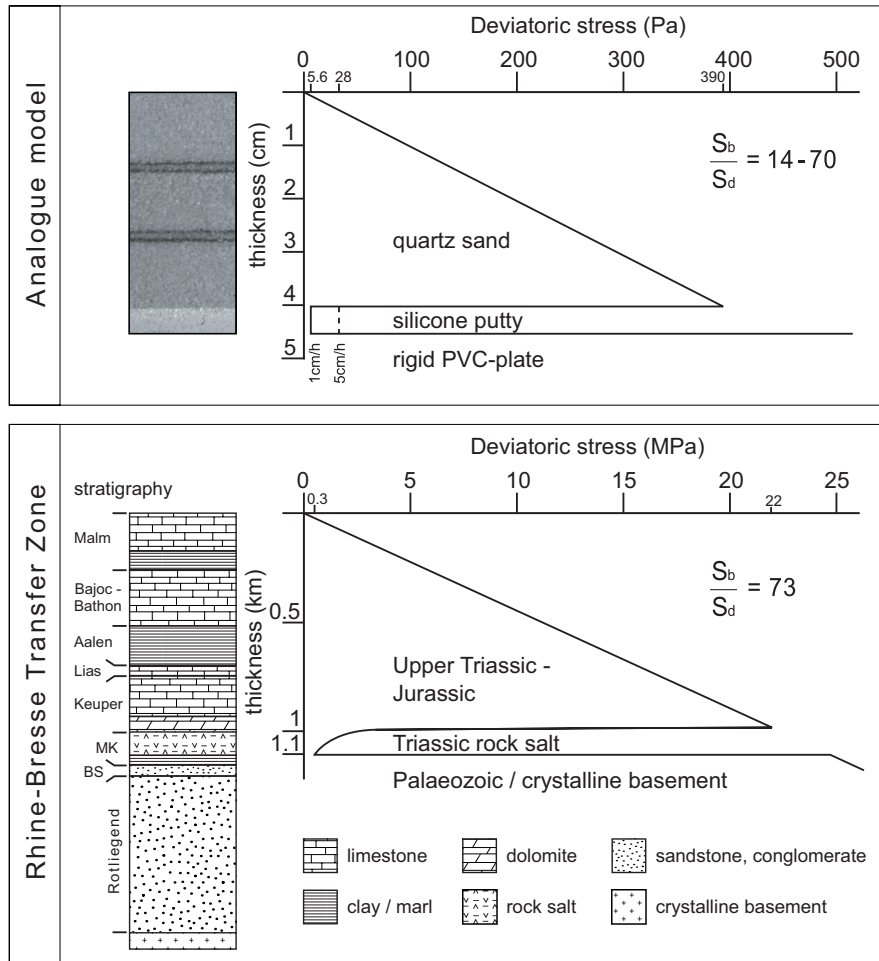
Fig. 4: Strength profiles for the dynamically scaled experiments (top) and the RBTZ (bottom) using a simplified stratigraphy for the Mesozoic pre-rift series based on various borehole data. Abbreviations: BS = Buntsandstein, MK = Muschelkalk.
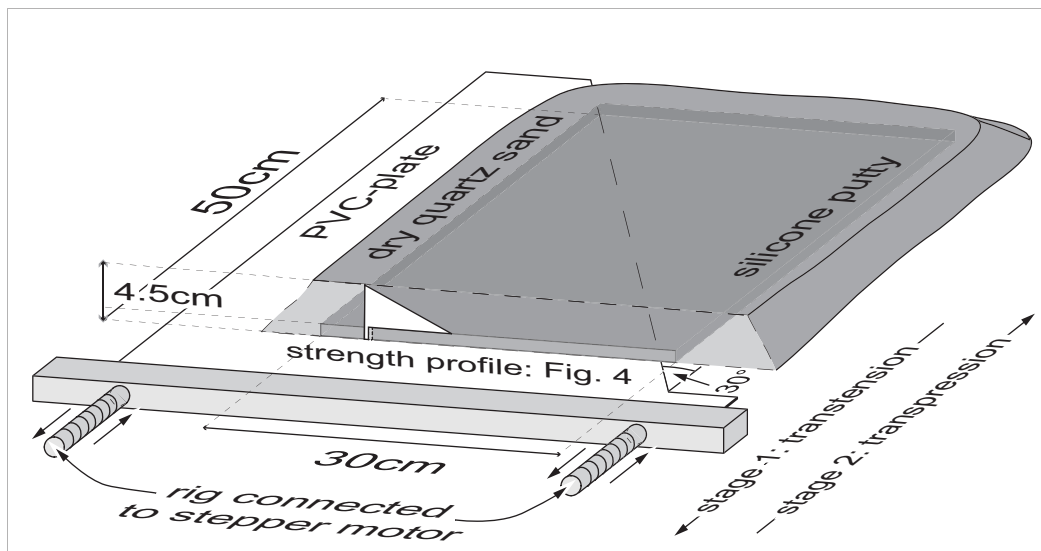
5.3 Experimental setup

Sand-silicone models were built in order to investigate the effects of basement fault reactivation on the deformation of a brittle sedimentary cover above a basal viscous décollement layer. Two successive deformation stages were applied: an initial phase of oblique rifting with sinistral transtensional motion and a subsequent phase of dextral transpressional reactivation (Fig. 5). The analogue models were dynamically scaled for the sedimentary pile overlying a Palaeozoic basement in the area of the southern Upper Rhine Graben and the RBTZ. They match the natural "prototype" in terms of yield stresses acting on brittle and viscous materials during Eocene-Oligocene rifting (see Fig. 4 for the strength profiles obtained and Appendix for details regarding dynamical scaling).

The analogue models were underlain by a 1 mm thin, rigid PVC plate, which was cut at an angle of 30° to the extension direction (Fig. 5). The oblique edge of the plate represents a pre-existing discontinuity, which induces deformation in the covering sand. A basal layer of silicone putty, 50 x 30 cm large and 5 mm thick, was placed above this discontinuity. The silicone putty including its edges was entirely covered by 4 cm of dry quartz sand, in order to prevent gravitational sideward flow of silicone (Fig. 5). Coloured marker layers of sand were sprinkled in defined steps in order to visualise vertical displacements across faults. A

rectangular grid of coloured sand lines with a spacing of 5 and 7.5 cm, respectively, was sprinkled on the smoothed surface of the model in order to visualise lateral displacements induced during the experiment.

Computer-controlled stepper motors imposed the deformation on the rig. Displacement rates during the experiment run ranged from 1 to 5 cm/h. Top view photographs were taken at several steps during the different experimental runs, allowing for tracing fault evolution during each deformation increment. After completion of the experiment, the model was covered by an additional layer of sand in order to seal its relief, and subsequently sprinkled with water, until the pore space was saturated. This provided the necessary cohesion for cutting the model into slices, perpendicular to the trend of the pre-existing discontinuity in the PVC plate. Photographs were taken from all sections.

Fig. 5: Schematic block diagram of the experimental setup. A rectangular block of silicone putty (50*30*0.5cm) is entirely covered by 4 cm of dry quartz sand. Deformation in the two-layer model is induced by a 1 mm thick, rigid basal PVC plate, which is driven by an electronically controlled stepper motor.

experiment	v1	v2	Sb	Sd	Sb/Sd	displ1	displ2	new fts 1	react. fts 2	new fts 2	figures
OR1	5.0	5.0	490	28	18	18	50	R, P	both R & P	new thrusts	
OR2	5.0	5.0	392	28	14	29	60	R, P	both R & P	new thrusts	
OR3	1.0	1.0	392	5.6	70	20	61	R, P	none	none	
OR4	*2.6*	*-*	*392*	*15*	*26*	*20*	*-*	*R, P*	*-*	*-*	*7, 8*
OR5	*2.6*	*2.6*	*392*	*15*	*26*	*20*	*65*	*R, P*	*mainly P*	*few thrusts*	*9, 10*
OR6	2.6	2.6	294	-	-	10	35	only R	only R	thrusts	
OR7	*1.0*	*5.0*	*392*	*5.6*	*70*	*20*	*60*	*R, P*	*both R & P*	*new R & thrusts*	*6, 11, 12*
OR8	1.0	2.6	392	5.6	70	20	60	R, P	mainly P	none	

Table 1: Parameters of performed experiments and resulting fault patterns. Experiments referred to in text and figures are shown in bold italics. v1 = displacement rate during stage 1 (cmh^{-1}), v2 = displacement rate during stage 2 (cmh^{-1}), Sb = strength of brittle layers (Pa), Sd = strength of viscous layer (Pa), Sb/Sd = strength ratio, displ1 = displacement during transtensive stage (mm), displ2 = displacement during transpressive stage (mm), new fts 1 = neo-formed faults at stage 1, react. fts 2 = faults reactivated at stage 2, new fts 2 = neo-formed faults at stage 2, R = R-shear, P = P-shear.

5.4 Experimental results

Two-phase experiments were performed under varying displacement rates (see Table 1 for technical parameters). Displacement rates during the first deformation phase (transtension) were performed at 1 and 2.6 cm/h. The subsequent phase of transpressional reactivation was performed at displacement rates of 1, 2.6 and 5 cm/h, in order to vary coupling across the viscous layer by a factor of 5 (see Appendix). One experiment (OR4, Fig. 7 & 8) was terminated after completion of the first transtensional stage in order to compare purely transtensional structures to those caused by subsequent transpressive reactivation. In the following two sections (4.1 and 4.2), we describe the sequential development of structures seen in top view during experimental runs and in cross sections for three experiments (OR4, OR5, and OR7).

5.4.1 Stage 1 (transtension)

The first surface faults appear in the brittle cover after 3-5 mm displacement (Fig. 6a). Forming right above the basement fault with a spacing of typically 2 to 3 cm (measured perpendicular to the fault trend), they display a right-stepping en-échelon alignment and sinistral, oblique slip sense of motion as deduced from the displacement of the grid lines at the model surface. The polarity of the normal fault component switches precisely above the basal pre-cut discontinuity (Fig. 6a). These en-échelon faults are oriented at angles between 15° and 20° to the basement fault and may be interpreted as synthetic Riedel (R) shears (Fig. 6a). Such angles are quite typical of wrench faults with transtensional kinematics (cf. Mandl, 1988, p. 77).

Progressive deformation widens the fault zone by along-strike propagation of the en-échelon faults, usually away from the basement discontinuity (Fig. 6). During this widening, individual faults begin to overlap each other (Fig. 6b and c). Their ends often become fringed and slightly curved, facilitating fault coalescence as deformation advances. Due to this fringing, the angle between basal discontinuity and the outermost tips of en-échelon fault segments may increase to 30-35°. Fault formation always progresses from outside to inside the rift. This is depicted in three cross-sections cut through an experiment that was terminated after the transtensive stage (OR4, Fig. 8).

Between 5 and 10 mm displacement, a second fault set appears at the surface, trending either sub-parallel to the basement discontinuity or at an angle as small as 5° (but in the opposite direction compared to earlier formed R-shears). Displacements are primarily sinistral, the vertical throw being significantly smaller than in case of the first fault set. These faults are interpreted as P-shears (Fig. 6b). The linkage of individual faults of these two sets leads to the formation of small, lozenge-shaped pull-apart basins (Fig. 6c). Fault dips range between 65° to 80° for both sets of faults, the viscous basal layer being visibly thinned below the graben structure (Fig. 8).
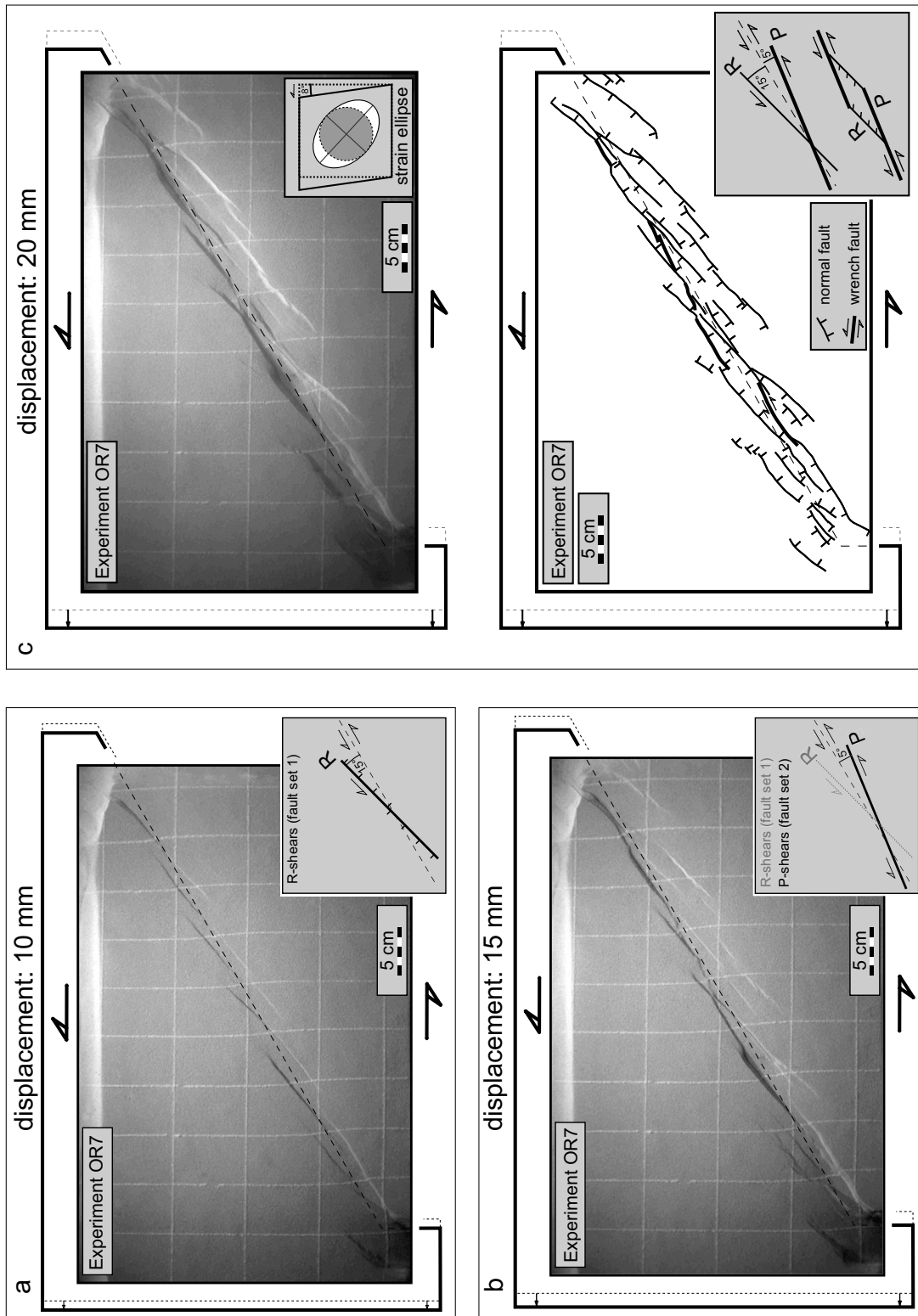
Fig. 6: Stepwise development of surface faults during oblique rifting at a displacement rate of 1 cm/h (transtensional phase of experiment OR7). Illumination from top part of figure. (a) Surface faults forming first (after 10 mm displacement) are en-échelon aligned, synthetic R-shears. Note the switch in fault polarity right above the trace of the basement fault. (b) After 15 mm displacement, a set of P-shears appears. Coalescence of the two fault sets (after 20 mm transtension) allows for the formation of lozenge-shaped pull-apart basins (schematically shown by insert at lower right)
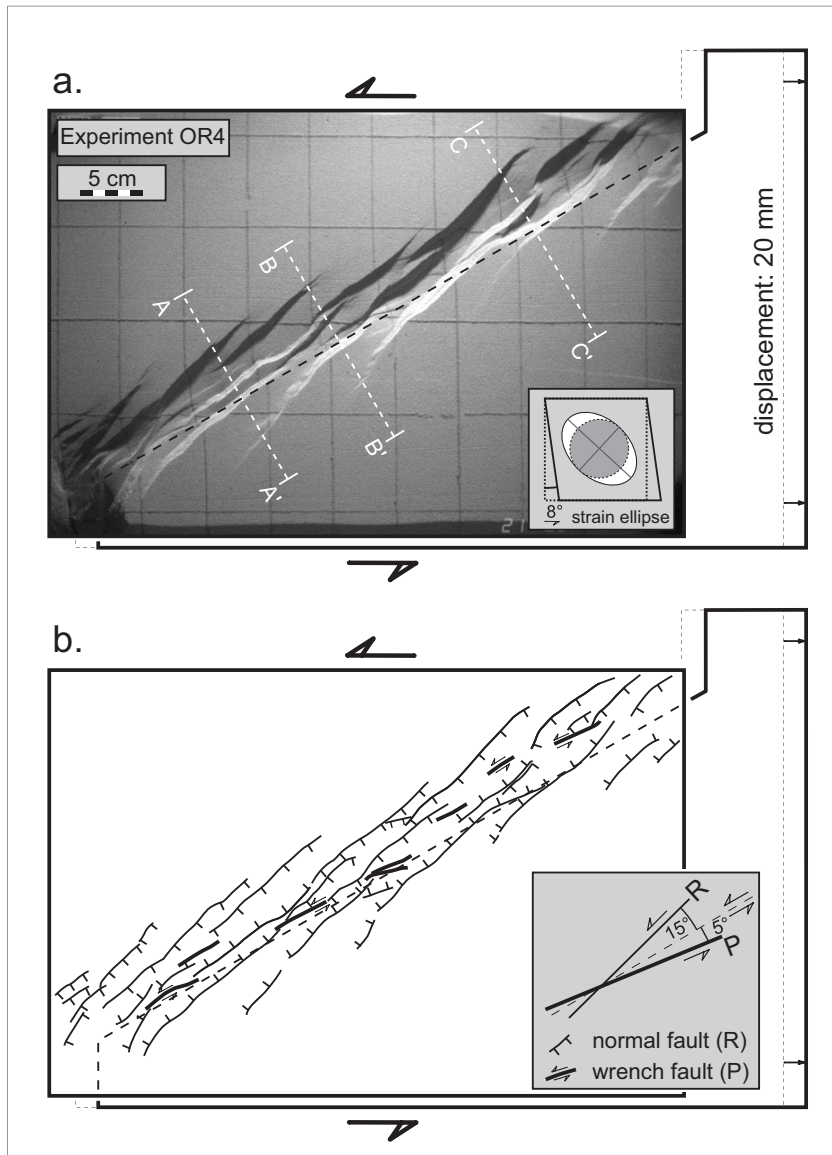
Fig. 7: Oblique rift model (transtensional wrench faulting, experiment OR4). Illumination from top part of figure. (a) Fault pattern and representative strain ellipse after 20 mm transtensional displacement. Locations of cross-sections (Fig. 8) are indicated. (b) Line drawing of the fault pattern. Note the switch in normal fault polarity with respect to the location of P-shears.
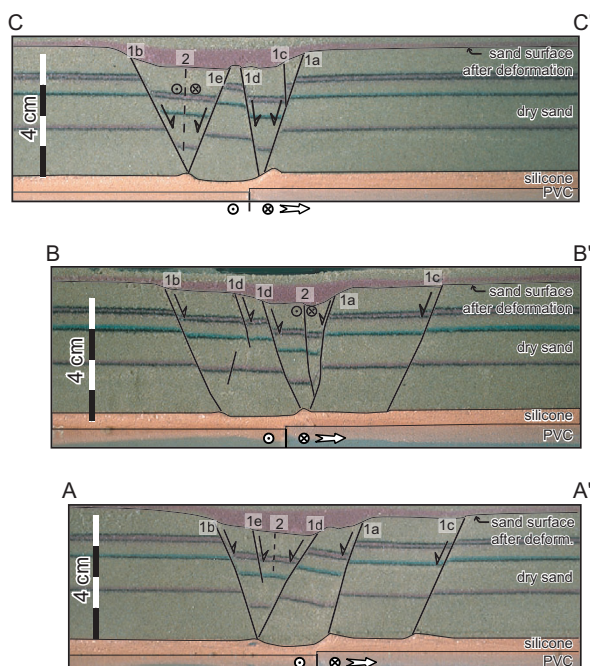
Fig. 8: Cross-sections across the oblique rift structure (experiment OR4) after 20 mm transtension. For location of the sections see Fig. 7. Note the characteristic thinning or "necking" of the viscous base below the graben. Genetic chronology of faults is indicated by numbers 1 and 2. Lower case letters indicate relative chronology in which the individual faults appear in the section plane by along-strike propagation. First faults (1a, 1b) are synthetic R-type shears and form the external boundary faults of the graben. Along-strike propagation of these en-échelon aligned faults (labelled "1c") causes widening of the rift. Younger R-type faults (1d, 1e) form in the interior part of the rift. Faults of generation 2 are P-type shears and form in the centre of the rift.

The total displacement was restricted to 20 mm in most experiments. At this stage, the oblique rifts did not develop into a continuous graben structure, which would have complicated the tracing of movements during subsequent reactivation. The final fault pattern after completion of the transtensional stage displays an array of en-échelon aligned oblique-slip normal faults with several graben and horst structures (Fig. 6c, 7 and 9a) and - occasionally – well defined basins that formed by the linkage of R- and P-shears (Fig. 6c and 9a).

5.4.2 Stage 2 (transpression)

The reactivation of numerous pre-existing faults produced during the first deformation stage was only observed at high displacement rates (v = 5 cm/h). Transpression at lower displacement rates (v = 1 to 2.6 cm/h) led to strain localisation in the vicinity of the pre-cut PVC-plate, without fault inversion propagating towards the surface of the brittle cover.

5.4.2.1 Reactivation at low displacement rates (v = 1 to 2.6 cm/h)

Deformation in the sand layer concentrates along reactivated P-shears ("rP" in Fig. 9b). R-shears are not reactivated, presumably due to higher angles between fault strike and shortening direction, resulting in lower resolved shear stresses. Therefore, graben structures are not inverted, even after 65 mm of shortening (Fig. 9b). Movement along reactivated P-shears is readily seen in the displacement of the vertical marker lines (compare Fig. 9a and b). During an advanced stage of transpressional shortening (between 40 and 50 mm), small surface thrust faults appear. These thrusts are transferred along pre-existing R-type faults (Fig. 9b). Subordinate narrowing of the rift is achieved by combined reverse and dextral strike-slip faulting along reactivated P-type faults (compare Figs. 9a and b).

Cross sections reveal that the viscous material has accumulated in the vicinity of the velocity discontinuity. The characteristic necks, which formed in the silicone putty as a result of transtension (compare Fig. 8 and 10), are "filled up" during this stage. The thickening of the viscous material is slightly more pronounced on the side opposite to the indenting plate. The P-type faults in the graben centre are reactivated in dextral strike-slip mode. They show a significantly curved trace in cross section. The convergence point of both reactivated and neo-formed faults at the viscous décollement horizon is always significantly offset with respect to the location of the edge of the basal plate (Fig. 10).

Shortening during reactivation under lower displacement rates is therefore compensated predominantly by thickening of the viscous base in the vicinity of the pre-existing basal discontinuity. Only a subordinate amount of this shortening is transferred into fault inversion within the brittle cover. There, deformation is strongly concentrated along reactivated P-shears in the rift centre, leading to the development of vertical shear-zones (cross-sections in Fig. 10).
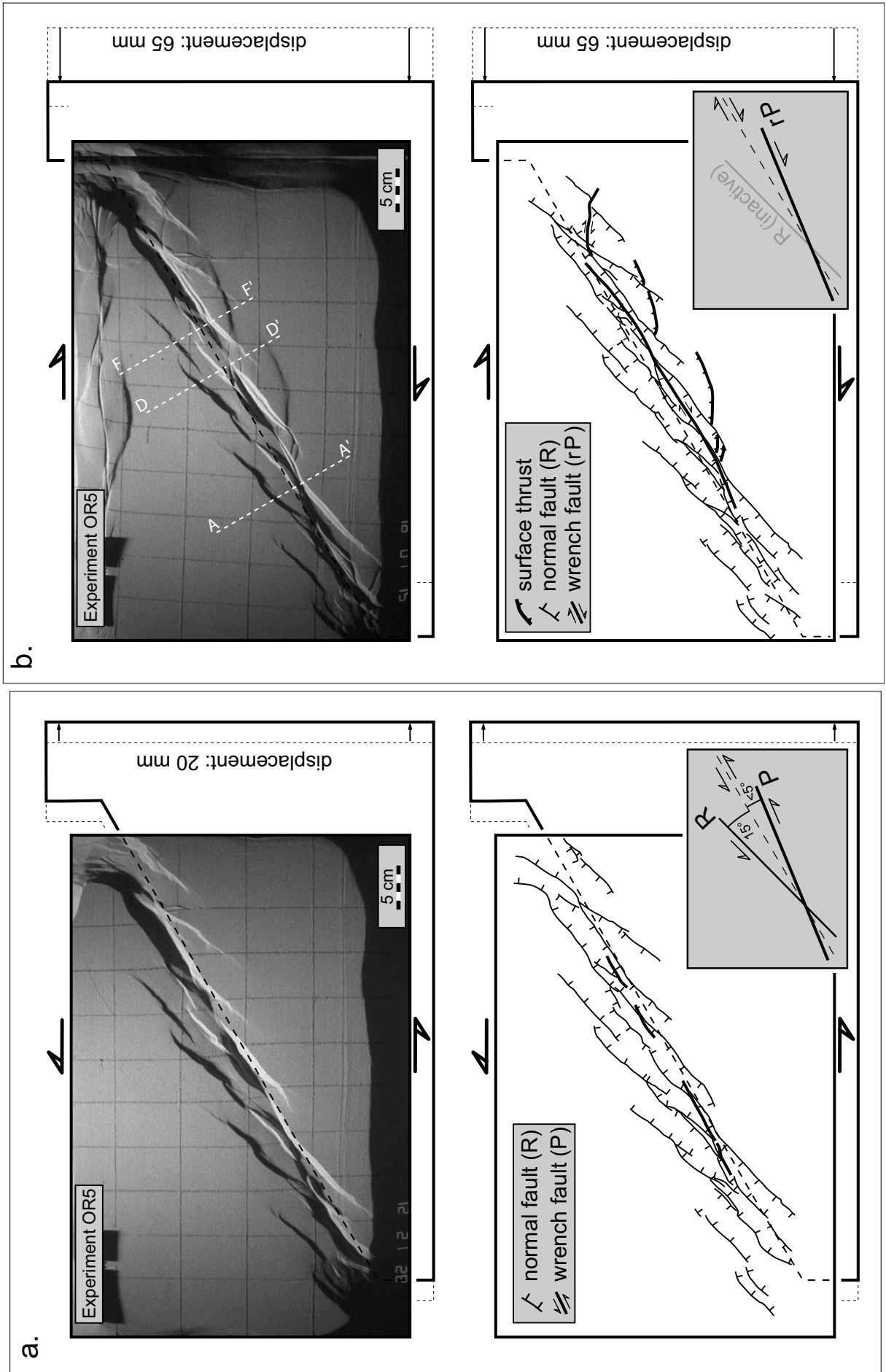
Fig. 9 (previous page): (a) Fault patterns of an oblique rift model (transtensional wrench faulting, experiment OR5) after 20 mm of transtension. Illumination from top part of figure. Local depocenters are formed by linkage of R- and P-shears as well as by the corrugation of fault ends.
(b) Fault pattern of the same experiment after subsequent transpressional reactivation at a low displacement rate of 2.6 cm/h and 65 mm displacement. No inversion of the graben occurred. Illumination is from above. Strike-slip fault in top-part of the picture represents boundary effect due to lateral confinement of the silicone putty, but did not affect structures evolving in central rift. Locations of cross-sections (Fig. 10) indicated. rP = reactivated P-type fault.
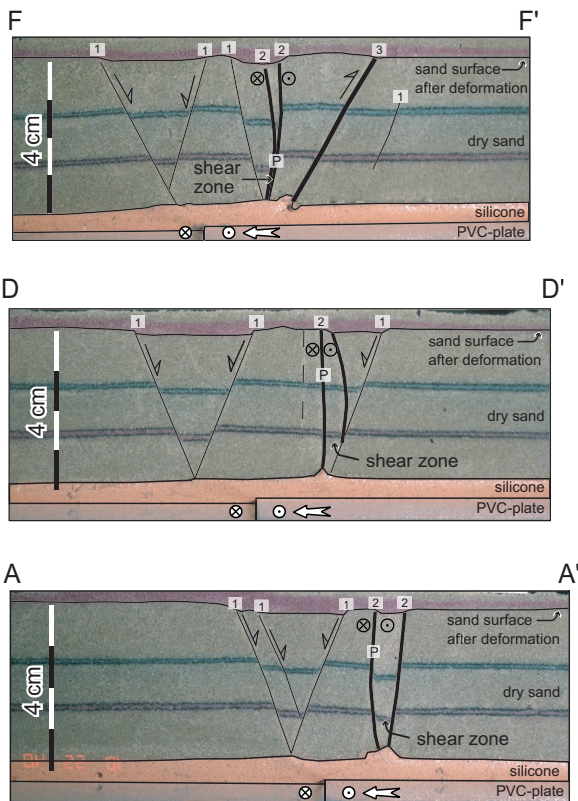
Fig. 10: Cross-sections through a transpressively reactivated oblique rift model (low displacement rate, experiment OR5). For locations see Fig. 9b. Numbers 1 to 3 indicate the nature of faults during transpressional reactivation. 1: not reactivated (R-type) faults, 2: reactivated (P-type) faults, 3: reverse faults formed during transpressional reactivation. Reactivated and neo-formed faults are drawn with thicker stroke. Note the slightly thickened silicone in the vicinity of the edge of the basal plate.

5.4.2.2 Reactivation at high displacement rates (v = 5 cm/h)

Reactivation of inherited faults within the brittle cover is observed from the very beginning of the transpressive deformation stage. Normal faults immediately become reactivated as dextral strike-slip faults with a reverse component (Fig. 11a). In the initial stage of reactivation, they accommodate most of the shortening, leading to the almost entire inversion of graben structures. After 35 mm displacement, almost all faults (of both R- and P-type) have been reactivated (Fig. 11a). The first surface thrust faults appear at the margin of the wrench corridor. They branch off from inherited R-type faults at the periphery of the rift and propagate away from the rift in a strongly curved, lobate-shaped manner (see "surface thrust/reverse fault" in Fig. 11a).

After 60 mm displacement (end of experiment, Fig. 11b), the former oblique rift has been uplifted along thrust faults that have propagated away from the basement fault to either side. Thrust fronts have widely coalesced and paralleled the basal discontinuity. The strain ellipse indicates shortening of the original rift width by some 25%, significantly more than
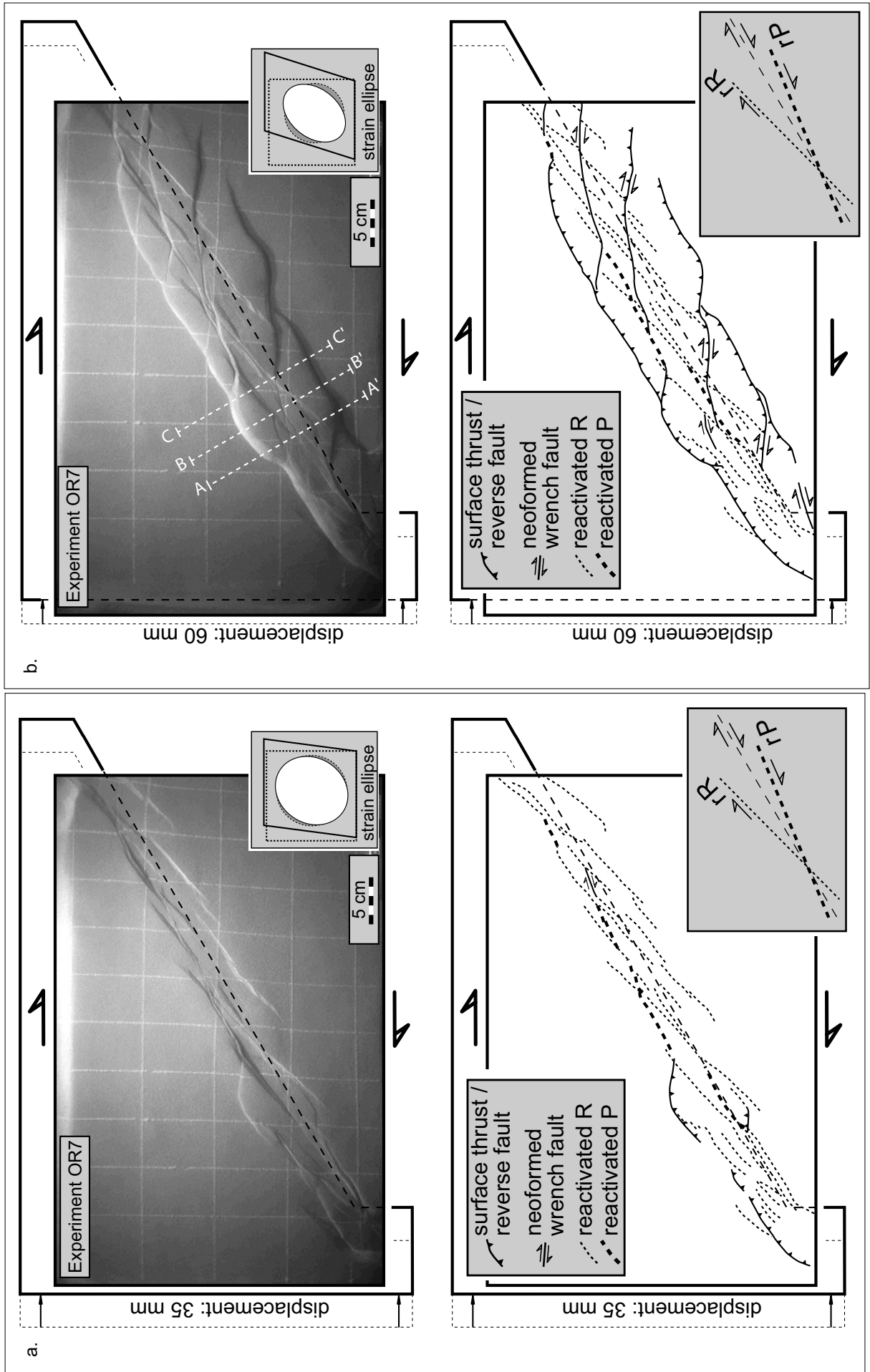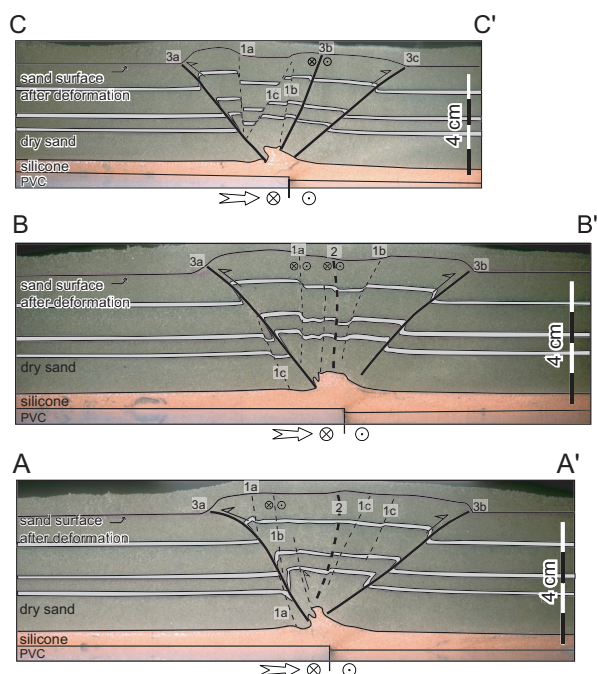
Fig. 12: Cross sections through a transpressively deformed oblique rift model (high displacement rate, experiment OR7). For locations see Fig. 11b. Numbers 1 to 3 indicate the nature of faults during transpressional reactivation. 1: reactivated R-type faults, 2: reactivated P-type faults, 3: neo-formed reverse faults. Lower case letters indicate relative sequence in which the individual faults appear in the section plane by along-strike propagation. Strokes and dashes correspond to Fig. 11.

during reactivation at low displacement rates. Newly formed dextral, synthetic Riedel-type strike-slip faults (at angles of 20-25° with respect to the basal discontinuity) branch off from inherited R-type faults and tend to link with reactivated P-shears in the interior part of the oblique graben. This gives the resulting coalesced structure a slightly sigmoidal shape (Fig. 11b).

In cross-section (Fig. 12), the neo-formed reverse faults reveal a dip angle of only 40-45°, i.e. considerably less than the dip of inherited normal faults. Most of the shortening is taken up by the neo-formed reverse faults as soon as they appear at the surface of the model. Reactivated faults reveal much less activity from this point onward. In cross sections, neo-formed reverse faults emanate from the pre-existing basement discontinuity. As they propagate towards the surface, they intersect and offset inherited normal faults. The offset segments are thus transported in the hanging wall of reverse faults, i.e. graben structures are not actively inverted but passively uplifted (sections A-A' to C-C' in Fig. 12). Note that in the high displacement rate experiment both reactivated and neo-formed faults converge precisely above the basal discontinuity. There, the basal silicone putty is visibly thickened and even becomes involved in thrusting. This is in great contrast to the low-displacement rate experiment (compare Figures 10 and 12).

5.5 Discussion

5.5.1 Limitations of the models

Since the length scale ratio of our models is on the order of $L^* \approx 4 \times 10^{-5}$ (see Appendix) the models do not encompass the entire area of the RBTZ but only represent the kinematic setting found within an area of 7.5 by 12.5 km, encompassing one or a few individual faults within this transfer zone. This limits direct comparison between experiments and natural structures. However, using a larger model area and properly scaling the thickness of the sediments at the same time, proved to be impractical.

Furthermore, the amounts of displacement applied during both stages of the experiment are highly exaggerated when compared to the RBTZ. Especially the displacements applied during stage 2 greatly exceed those observed within the RBTZ. However, large displacements were necessary in order to ease the distinction between inherited and neo-formed structures in the experiments. This again limits a direct comparison of the experiments with the RBTZ.

In order to allow for a better observation of fault patterns during all stages of the experiments, no sand was filled into the subsiding areas. Such an additional load by syn-rift sedimentation would certainly have modified the principal stresses during the transpressive stage of the experiments. As shown by Dubois *et al*. (2002), the sedimentary fill of the graben controls the position of the intermediate and least principal stress and – consequently - the kinematics of reactivated normal faults. Additional load increases the vertical principal stress, hence reactivated faults tend to have a more pronounced strike-slip component. Conversely, they will display a greater reverse component in the absence of additional overburden. However, since the amount of rift-related sedimentation is small within in the RBTZ, this particular restriction does not significantly limit the application of the models.

5.5.2 Rheological and kinematic implications

Before discussing possible applications of our models to the case of the RBTZ, we discuss some important implications of general geological interest. Analogue modelling clearly showed that transpressional reactivation of pre-existing faults resulting from oblique rifting in a brittle cover overlying a viscous décollement layer is strongly dependent on the applied displacement rate.

In the low displacement rate experiments (1 to 2.6 cm/h) the viscous layer accommodates a large amount of shortening by ductile, i.e. not localised, deformation. Reactivation of faults in the brittle cover is insignificant except for dextrally reactivated P-shears in the rift centre. The graben itself remains non-inverted. Only few surface thrusts, which are transferred along inherited R-type faults, form during a later stage of the deformation (experiment OR5, Fig. 9b). Cross-sections (Fig. 10) reveal that the basal silicone accumulates in the vicinity of the basal discontinuity.

Conversely, reactivation of pre-existing faults is favoured under higher displacement rates (5 cm/h). The viscous basal layer immediately transmits the shortening to the brittle cover. Almost all pre-existing faults are reactivated as dextral faults with a substantial reverse component. Graben structures, as well as pull-apart basins, are completely inverted. During an advanced stage of deformation, shortening is taken up by neo-formed thrust faults, which emanate from the basal discontinuity and propagate outward from the oblique rift. These initially strongly curved thrust faults coalesce into thrust fronts parallel to the trend of the basement fault. The thrust faults typically crosscut pre-existing normal faults with lower dip-angles (sections A-A', B-B' in Fig. 12, experiment OR7), widening the deformed belt.

5.5.3 Applications of the modelling results to a possible transpressive reactivation of the RBTZ

In this section, our experimental results are confronted with structures in the RBTZ. We restrict this comparison to the autochthonous Mesozoic, where shortening related to Late Miocene to Pliocene thin-skinned Jura folding can be largely excluded.

As described in section 1.2, a purely thin-skinned origin of the "Avant-Mont thrust" ("AM" in Fig. 1) in the autochthonous Mesozoic is unlikely. The Avant-Mont thrust resembles the thrust fronts, which formed during the reactivation stage in our high displacement rate experiments, trending parallel to the basal discontinuity. However, in the high displacement rate experiments such thrust fronts develop only after shortening amounts that highly exceed those expected during the postulated dextral inversion of the RBTZ (Fig.11a, b). On the other hand, the low displacement rate experiments (OR5, Fig. 9b and 10) demonstrated that cover faults trending (sub)-parallel to the basal discontinuity are reactivated as dextral strike-slip faults over a considerable length, whereas adjacent normal faults at higher angles to the main discontinuity are not reactivated. This comes closer to the case of the Avant-Mont thrust, which forms an isolated thrust surrounded by un-inverted normal faults. In summary, a thick-skinned component during the formation of the Avant-Mont thrust at low displacement rates is very likely.

The best-documented thick-skinned reactivation of ENE-oriented faults within the RBTZ is found W of Basel (Fig. 2 and 3), the evidence being extensively discussed in section 1.2 and in Giamboni *et al*. (2004). Dextral transpressive reactivation of ENE-oriented Late Palaeozoic graben faults led to the compressive/transpressive reactivation of Palaeogene en-échelon flexures in the cover, while nearby situated N20°-trending normal faults remained largely un-inverted (Fig. 2 and 3). This local transpressive reactivation of RBTZ-faults without inversion of the graben structures resembles the situation simulated in an experiment carried out at slow displacement rates (Fig. 9b). However, the natural complexities cannot be achieved in the models (no NNE-striking basement faults in addition to the ENE-striking RBTZ fault were implemented into the model), hence more detailed comparisons of geometrical details are impossible.

Lobate shaped thrust segments are frequently found in the domain of the Folded Jura Mountains, especially along its northern front W of Basel (Figs.1 and 2). It would be appealing to infer analogies to those formed during our experiments (Fig. 11a), at least from a geometrical viewpoint. However, it has been demonstrated that such thrust fronts form in the detached sedimentary cover during Mio-/Pliocene Jura folding along Eo-/Oligocene normal faults, which nucleate (thin-skinned) lateral ramps due to oblique convergence (Tschanz and Sommaruga, 1993; Philippe, 1995). Also, the experimentally produced lobate thrusts appear at shortening amounts greater than transtensional displacements, which is certainly not the case in the RBTZ.

Furthermore, the low displacement rate experiments demonstrate that, due to low coupling across the décollement layer, certain cover faults remain unaffected by motion of the basal plate. Low coupling between basement and cover may, in turn, lead to differently oriented stresses. This phenomenon is observed in the northernmost Folded Jura Mountains, where basement and cover reveal differently oriented maximum horizontal stresses (Fig. 1a, Müller *et al*., 1987). We believe that low displacement rates in the basement of the RBTZ (section 1.2) and late increments of thin-skinned Jura folding (Müller *et al*., 2002), could explain the observed stress decoupling.

6. Conclusions

Our modelling work leads to the following conclusions:

(1) Higher displacement rates improve coupling between basement and cover, separated by a viscous layer. This leads to "basement-triggered", combined strike-slip / reverse reactivation of inherited R- and P-type faults in a brittle cover overlying a viscous décollement layer. Reactivation at low displacement rates, on the other hand, tends to reactivate P-shears only.

(2) Following full inversion of pre-existing extensional structures, new lobate-shaped thrust faults develop at both high and low displacement rates. However, thrust formation is again much more pronounced at higher displacement rates.

(3) Thrusting and uplift at low displacement rates is mostly restricted to neo-formed surface thrusts, whereas it is observed along all inverted faults at high displacement rates.

Applications of the modelling results to the RBTZ are possible, despite the limitations in the experimental setup (primarily in terms of geometrical complexity). Based on geological evidence, some Late Pliocene to recent structures can be attributed to the reactivation of ENE-trending basement faults. One such example are the reactivated Palaeogene flexures above ENE-trending faults, leading to dextrally dragged N20°-trending faults at the southern end of the Upper Rhine Graben (Fig. 2 and 3). Geological estimates of the current displacement rates (though vague) reveal values on the order of <1mm/a. Partial stress decoupling between the basement and its sedimentary cover is presently observed in

the northern Alpine foreland of Northern Switzerland (Müller *et al*., 1987) and in parts of the RBTZ (Fig. 1a). Hence, the experiments performed at low displacement rates (1-2.6 cm/h), characterised by weak coupling between cover and "basement", come nearest to the situation in the RBTZ. According to the modelling this weak coupling allows for the preservation of former non-inverted normal faults. Additionally, it allows for a superposition of basement-induced dextral/reverse motions and thin-skinned, Jura type tectonics (caused by stresses exerted in the Alps and transmitted into their foreland along a basal Triassic décollement) in Late Pliocene to recent times. Combining field evidence and experimental results, it is concluded that post-Late Pliocene thrusting and uplift in the cover of the RBTZ could have resulted from strike-slip faulting along ENE-trending basement faults at low displacement rates, presumably camouflaged by late increments of thin-skinned folding in the northern Folded Jura Mountains.

Appendix: dynamical scaling of analogue models

Any analogue model is representative of a natural system only if it is properly dynamically scaled (Hubbert, 1937). This requires similar stress ratios acting in both model and nature, as well as appropriately downscaled rheological properties of the modelling materials. The geometries resulting from faulting in a brittle cover above ductile or viscous parts of the crust are strongly dependent on the mechanical coupling between the brittle and ductile/viscous material. This coupling can be estimated by calculating the ratio of strength between brittle and viscous/ductile parts of the crust (regardless whether lithospheric or uppermost crustal scale processes are considered) and represented graphically following the concept of Brace and Kohlstedt (1980).

For a dynamically scaled experiment, the strength ratio of the analogue model should equal that of its natural prototype within one order of magnitude:

$$\left(\frac{S_b}{S_d}\right) \text{model} \approx \left(\frac{S_b}{S_d}\right) \text{nature}$$

Suffixes b and d signify properties of brittle and ductile/viscous material, respectively.

A1. Brittle strength

The yield strength of a brittle material equals the deviatoric stress

$$S_b = \sigma 1 - \sigma 3$$

and depends upon the thickness of overburden h_b [m], its density ρ [gcm^{-3}], the internal friction angle ϕ [°], the cohesion τ_0 [MPa] and the mass acceleration due to gravity, g [ms^{-2}]. The letters in angular parentheses indicate the physical dimension.

In extensional regimes, the maximum principal stress ($\sigma 1$) is vertical and equals the lithostatic load:

$$\sigma 1 = \rho \cdot g \cdot h_b$$

From the Mohr-Coulomb fracture criterion follows

$$\sigma 1 = a + b \cdot \sigma 3$$

where

$$a = 2\tau_0 \sqrt{b}$$

and

$$b = \frac{(1 + \sin\phi)}{(1 - \sin\phi)}$$

An appropriate value for cohesion (τ_0) of crust under extension is 5 MPa (Byerlee, 1978). The internal friction angle (ϕ) for most rock types is around 30° and thus $b = 3$. Consequently,

$$a = 1.73 \cdot 10^7 \text{ Pa}$$

Using values of 2.5 gcm^{-3} for the average density of the Mesozoic limestone-shale sequence of the southern Rhine Graben (see above) with a thickness h_b of 1000 m on the average, one obtains values for the maximum and minimum principal stresses of

$$\sigma 1 = 2.45 \cdot 10^7 \text{ Pa}$$

$$\sigma 3 = 2.41 \cdot 10^6 \text{ Pa}$$

and for the yield strength at the base of the sedimentary succession considered

$$S_b(\text{nature}) = \sigma 1 - \sigma 3 = 2.2 \cdot 10^7 \text{ Pa}$$

Dry quartz sand reveals a Mohr-Coulomb type behaviour of failure $\tau = \tau_0 + \sigma_n \tan\phi$, an internal friction angle ϕ around 30° (Krantz, 1991) and was therefore a representative material for modelling the brittle Mesozoic sediments.

Due to negligible cohesion of sand ($\tau_0 = 0$), the brittle strength in the scaled analogue model simplifies to

$$S_b = \frac{2}{3} \cdot \rho \cdot g \cdot h_b$$

Using a length scale ratio $L \approx 4 \times 10^{-5}$, the thickness of brittle layers in the model is downscaled to $h_b = 4$ cm.

The density of dry, sprinkled sand is 1.5 gcm^{-3}. The brittle strength thus becomes

$$S_b (\text{model}) = \sigma 1 - \sigma 3 = 392 \text{ Pa}$$

A2. Viscous strength

The strength of viscous material - or its resistance to (shear) deformation - depends on its viscosity μ [Pa s] and the strain rate $\dot{\varepsilon}$ [s^{-1}].

$$S_d = \sigma_d = \mu \cdot \dot{\varepsilon} = \mu \cdot \left(\frac{U}{h_d} \right)$$

where

       U displacement rate [ms^{-1}]

and

       h_d thickness of ductile/viscous material [m].

For rock salt with an almost Newtonian type viscosity $\mu_n \approx 10^{18}$ Pa s (Nalpas and Brun, 1993), $h_d = 100$ m and a displacement rate of $U_n = 3 \cdot 10^{-11}$ ms^{-1} (= 1 mma^{-1}) applied, one obtains

$$S_d (\text{nature}) = \mu_n \cdot \left(\frac{U_n}{h_d} \right) = 3 \cdot 10^5 \text{ Pa}$$

This value is in good agreement with the strength values for rock salt, ranging from $0.1 - 1$ MPa, as reported by Carter and Hansen (1983).

In the experiment, we used silicone putty ("Rhodorsil Gum", manufactured by Rhone Poulenc, Paris) with a Newtonian viscosity $\mu_m \approx 10^4$ Pa s, a constant thickness h_d of 5 mm. Applying displacement rates U_m in the range from 1 to 5 cmh^{-1} (= $2.8 \cdot 10^{-6}$ to $1.4 \cdot 10^{-5}$ ms^{-1}), we obtain values of viscous strength S_d (model) between 5.6 and 28 Pa.

The brittle-viscous strength ratios for the models therefore range from

$$\left(\frac{S_b}{S_d} \right) \text{model} = 14 - 70$$

whereas the natural counterpart reveals a strength ratio

$$\left(\frac{S_b}{S_d} \right) \text{nature} = \frac{2.2 \cdot 10^7 \text{ Pa}}{3 \cdot 10^5 \text{ Pa}} = 73$$

The obtained coupling ratios are graphically represented in strength profiles (Fig. 4). Limiting factors in obtaining more precise strength estimates are the uncertainties on salt rheology and its original thickness during rifting. The estimation of strength ratios is only valid if the salt behaves as a Newtonian solid and under dry conditions (zero pore pressure). Note also that the calculation is made for the first, transtensional stage of the experiments only, i.e. considering tensile strengths.

References:

Allemand, P. and Brun, J.-P., 1991. Width of continental rifts and rheological layering of the lithosphere. Tectonophysics, 188: 63-69.

Becker, A., 2000. The Jura Mountains - an active foreland fold-and-thrust belt? Tectonophysics, 321: 381-406.

Bergerat, F. and Chorowicz, J., 1981. Etude des images Landsat de la zone tranformante Rhin-Saône (France). Geologische Rundschau, 70(1): 354-367.

Brace, W.F. and Kohlstedt, D.L., 1980. Limits on Lithospheric Stress Imposed by Laboratory Experiments. Journal of Geophysical Research, 85(B11): 6248-6252.

Brun, J.P., Gutscher, M.A. and teams, D.-E., 1992. Deep crustal structure of the Rhine Graben from DEKORP-ECORS seismic reflection data: a summary. Tectonophysics, 208: 139-147.

Brun, J.P. and Nalpas, T., 1996. Graben inversion in nature and experiment. Tectonics, 15(2): 677-687.

Byerlee, J.D., 1978. Friction of Rocks. In: J.D. Byerlee and M. Wyss (Editors), Pure and Applied Geophysics. Contribution to Current Research in Geophysics, pp. 615-626.

Campy, M., 1984. Signification dynamique et climatique des formations et terrasses fluviatiles dans un environnement de moyenne montagne. Bulletin de l'Association française pour l'Etude du Quaternaire, 1: 87-92.

Carter, N. and Hansen, F., 1983. Creep of rocksalt. Tectonophysics, 92: 275-333.

Chauve, P., Campy, M., Pernin, C. and Morre-Biot, N., 1983. Carte Géologique detailée de la France, feuille Pesmes, XXXIII-23. Service de la Carte Geologique de la France.

Coromina, G. and Fabbri, O., 2003. Late Paleozoic NE-SW ductile-brittle extension in the La Serre horst, eastern France. Comptes Rendu, submitted.

Debrand-Passard, S. and Courbouleix, S. (Editors), 1984. Synthèse Géologique du Sud-Est de la France, volume 2: Atlas, 126. BRGM, G3 pp.

Deichmann, N., Ballarin Dolfin, D. and Kastrup, U., 2000. Seismizität der Nord- und Zentralschweiz. NAGRA Technischer Bericht, 00-05. NAGRA, Wettingen, 94 pp.

Diebold, P. and Naef, H., 1990. Der Nordschweizer Permokarbontrog. Nagra informiert, 2: 29-36.

Doebl, F., 1970. Die tertiären und quartären Sedimente des südlichen Rheingrabens. In: J.H. Illies and S. Mueller (Editors), Graben Poblems. Proceedings of an International Rift Symposium held in Karlsruhe October, 10-12, 1968. E. Schweizerbart'sche, Stuttgart, pp. 56-66.

Dreyfuss, M. and Glangeaud, L., 1950. La valée de Doubs et l'évolution morphotectonique de la région bisontine. Annales scientifiques de l'Université de Besançon, 5: 2.

Dreyfuss, M. and Kuntz, G., 1970. Carte Géologique detailée de la France, feuille Gy, XXXIII-22. Ministère de l'industrie et de la recherche, Service Géologique National, Paris.

Dubois, A., Odonne, F., Massonnat, G., Lebourg, T. and Fabre, R., 2002. Analogue modelling of fault reactivation: tectonic inversion and oblique remobilisation of grabens. Journal of Structural Geology, 24: 1741-1752.

Fabbri, O., Gaviglio, P. and Marquer, D., 2001. Paleotectonic and neotectonic analyses in the Rhine-Bresse Transfer Zone: Insights and perspectives from preliminary studies in the Besançon and Massif de la Serre areas. In: P. Dèzes (Editor), 2nd EUCOR-URGENT Workshop, 7th-11th October, 2001, Abstract Volume, Mont Saint-Odile (France), pp. 36.

Giamboni, M., Ustaszewski, K., Schmid, S.M., Schumacher, M.E. and Wetzel, A., 2004. Plio-Pleistocene Transpressional Reactivation of Paleozoic and Paleogene Structures in the Rhine-Bresse Transform Zone (Northern Switzerland and Eastern France). Geologische Rundschau, online first, DOI: 10.1007/s00531-003-0375-2.

Goguel, J. and Dreyfuss, M., 1967. Carte Géologique detailée de la France, feuille Besançon, XXXIII-23. Service de la Carte Géologique de la France, Paris.

Gürler, B., Hauber, L. and Schwander, M., 1987. Die Geologie der Umgebung von Basel mit Hinweisen über die Nutzungsmöglichkeiten der Erdwärme, Schweizerische Geologische Kommission, Bern.

Häring, M., 2001. Horizontale Hauptspannung im Grundgebirge. http://www.geothermal.ch/.

Hubbert, M.K., 1937. Theory of scale models as applied to the study of geologic structures. Bull. Geol. Soc. America, 48: 1459-1520.

Illies, J.H., 1981. Mechanism of Graben formation. Tectonophysics, 73(1-3): 249-266.

Krantz, R., 1991. Measurements of friction coefficients and cohesion for faulting and fault reactivation in laboratory models using sand and sand mixtures. Tectonophysics, 188: 203-207.

Lacombe, O., Angelier, J., Byrne, D. and Dupin, J., 1993. Eocene-Oligocene tectonics and kinematics of the Rhine-Saone continental transform zone (Eastern France). Tectonics, 12(4): 874-888.

Laubscher, H., 1961. Die Fernschubhypothese der Jurafaltung. Eclogae Geologicae Helvetiae, 54(1): 222-282.

Laubscher, H., 1970. Grundsätzliches zur Tektonik des Rheingrabens. In: J.H. Illies and S. Mueller (Editors), Graben Problems. Proceedings of an International Rift Symposium held in Karlsruhe 1968, International Upper Mantle Project. E. Schweitzerbart'sche, Stuttgart, pp. 79-86.

Laubscher, H., 1977. Fold development in the Jura. Tectonophysics, 37: 337-362.

Laubscher, H., 1986. The eastern Jura: Relations between thin-skinned and basement tectonics, local and regional. Geologische Rundschau, 75(3): 535-553.

Laubscher, H., 1987. Die tektonische Entwicklung der Nordschweiz. Eclogae Geologicae Helvetiae, 80: 287-303.

Laubscher, H., 1992. Jura kinematics and the Molasse Basin. Eclogae Geologicae Helvetiae, 85(3): 653-675.

Laubscher, H., 2003. The Miocene Dislocations in the northern foreland of the Alps: Oblique subduction and its consequences (Basel area, Switzerland-Germany). Jahresbericht und Mitteilungen des oberrheinischen geologischen Vereins, 85: 423-439.

Laubscher, H. and Noack, T., 1997. The deep structure of the Basel Jura. In: O.A. Pfiffner, P. Lehner, P. Heitzmann, S. Mueller and A. Steck (Editors), Deep structure of the Swiss Alps. Results of NRP 20. Birkhäuser, pp. 54-58.

Liniger, H., 1963. Geologische Beobachtungen in der Ajoie (Berner Jura). Regio Basilensis, 4: 39-47.

Mandl, G., 1988. Mechanics of tectonic faulting. Models and Basic Concepts. Developments in Structural Geology, 1. Elsevier, Amsterdam, 407 pp.

Müller, W.H., Blümling, P., Becker, A. and Clauss, B., 1987. Die Entkoppelung des tektonischen Spannungsfeldes an der Jura-Überschiebung. Eclogae Geologicae Helvetiae, 80(2): 473-489.

Müller, W.H., Naef, H. and Graf, H.R. (Editors), 2002. Geologische Entwicklung der Nordschweiz, Neotektonik und Langzeitszenarien, Zürcher Weinland. NAGRA Technischer Bericht, 99-08. NAGRA, Wettingen, 226 pp.

Nalpas, T. and Brun, J.-P., 1993. Salt flow and diapirism related to extension at crustal scale. Tectonophysics, 228: 349-362.

Nalpas, T., Le Douaran, S., Brun, J.P., Unternehr, P. and Richert, J.P., 1995. Inversion of the Broad Fourteens Basin (offshore Netherlands), a small-scale model investigation. Sedimentary Geology, 95: 237-250.

Nivière, B. and Winter, T., 2000. Pleistocene northwards fold propagation of the Jura within the southern Upper Rhine Graben: seismotectonic implications. Global and Planetary Change, 27: 263–288.

Nüesch, R., 1991. Das mechanische Verhalten von Opalinuston. PhD Thesis, ETH Zürich, Zürich, 244 pp.

Petit, C., Campy, M., Chaline, J. and Bonvalot, J., 1996. Major palaeohydrographic changes in Alpine foreland during the Pliocene-Pleistocene. Boreas, 25: 131-143.

Philippe, Y., 1995. Rampes Laterales et Zones de Transfert dans les Chaines Plissées: Géometrie, Conditions de Formation et Pièges structuraux associés. PhD Thesis, Université de Savoie & Institute Francais du Pétrole, Paris, 272 pp.

Plenefisch, T. and Bonjer, K., 1997. The stress field in the Rhine Graben area inferred from earthquake focal mechanisms and estimation of frictional parameters. Tectonophysics, 275: 71-97.

Reinecker, J., Heidbach, O. and Mueller, B., 2003. The 2003 release of the World Stress Map (available online at www.world-stress-map.org).

Richard, P. and Krantz, R., 1991. Experiments on fault reactivation in strike-slip mode. Tectonophysics, 188: 117-131.

Schmidt, C., Braun, L., Paltzer, G., Mühlberg, M., Christ, P., Jacob, F. 1924. Bohrungen von Buix bei Pruntrut und Allschwil bei Basel. Beiträge zur Geologie der Schweiz. pp. 74.

Schreurs, G. and Colletta, B., 1998. Analogue modelling of faulting in zones of continental transpression and transtension. In: R.E. Holdsworth, R.A. Strachan and J.F. Dewey (Editors), Continental Transpressional and Transtensional Tectonics. Geological Society Special Publication. Geological Society, London, pp. 59-79.

Schumacher, M.E., 2002. Upper Rhine Graben: Role of preexisting structures during rift evolution. Tectonics, 21(1): 1006, doi:10.1029/2001TC900022.

Tschanz, X. and Sommaruga, A., 1993. Deformation associated with folding above frontal and oblique ramps around the rhomb shaped Val-de-Ruz basin (Jura Mountains). Annales Tectonicae, 7(1): 53-70.

Ustaszewski, K., Schumacher, M.E. and Schmid, S.M., submitted. Contemporaneous faulting and extensional flexuring during Palaeogene rifting - a case study from the southern Upper Rhine Graben. Geologische Rundschau.

Wildi, W., 1975. Die Mettauer Überschiebung im Aargauischen Tafeljura (Nordschweiz). Eclogae Geologicae Helvetiae, 68(3): 483-489.

Chapter 6 - Post-Late Pliocene to recent thick-skinned tectonics at the southern end of the Upper Rhine Graben

Abstract

This chapter provides additional evidence for basement-rooted deformation in the southernmost Upper Rhine Graben postdating the deposition of the Mid- to Late Pliocene fluvial "Sundgau gravels". Systematically arranged, NE- to ENE-trending folds, traceable at the base of these gravels, are thought to have formed under NW-SE shortening, in agreement with maximum horizontal stress orientations determined from seismotectonics (Kastrup et al., 2004). Outcrop-scale normal faults and map-scale anticlines in the Sundgau gravels found along the NNE-trending Illfurth fault within the Upper Rhine Graben are interpreted as releasing and restraining bends along this fault, respectively, which developed due to sinistral strike-slip faulting.

A contour map of the Base-Tertiary surface and of the faults dissecting it, constructed using numerous reflection seismic and well data, reveals also the compressive or transpressive reactivation of ENE-oriented basement faults. The spatial coincidence between folds at the Base-Tertiary level and at the base of the Sundgau gravels suggests a post-Late Pliocene age of this deformation. The restoration of the folded gravel's base indicates horizontal displacement rates in the order of c. 0.05 mm/a, if their (biostratigraphically determined) minimum age of 2.9 Ma is considered as the starting time of deformation. River deflections around the crests of en-échelon surface anticlines suggest that the deformation has continued into the Quaternary.

These observations imply a change from thin-skinned to presumably ongoing thick-skinned tectonics after the Late Pliocene. This transition occurred without any (detectable) reorientation of the stress field in the sedimentary cover since the onset of thin-skinned Jura folding, when "palaeostresses" from fault-slip data and recent in-situ stresses are compared.

6.1 Introduction

6.1.1 Research objectives

The present day architecture of the north-western Alpine foreland has largely resulted from an interplay between extensional and collisional tectonics that took place since the early Cenozoic. The resulting interference is particularly complex, where the southern Upper Rhine Graben (URG), formed during Eo- to Oligocene extension, abuts the fold and thrust belt of the northern Folded Jura Mountains, which formed as a consequence of Alpine

subduction and collision in the Late Miocene to Early Pliocene. At present, the southern end of the URG is characterised by increased seismicity, as seen in the clustering of seismic events in both the historical and the instrumental earthquake catalogues of Switzerland (Swiss Seismological Service, 2003). The city of Basel, for instance, has been repeatedly harmed by earthquakes in medieval times. The most severe earthquake occurred in 1356 AD with an estimated epicentral intensity between IX and X (Mayer-Rosa and Cadiot, 1979) and resulted in the almost complete destruction of the city. Despite dedicated research (Meyer et al., 1994; Nivière and Winter, 2000; Meghraoui et al., 2001; Lambert et al., 2005), the seismic source of the 1356 AD earthquake (strike slip, thrust or normal fault?) has not yet been unambiguously identified. There is also no general agreement yet, whether the currently ongoing deformation in the north-western Alpine foreland is affecting predominantly the sedimentary cover ("thin-skinned" tectonics) or basement and cover to same amounts ("thick-skinned"). Solving this question is a key issue for seismic hazard assessment studies, which require the detailed knowledge of present-day fault kinematics. This study contributes to this debate by combining new results from the following datasets: (1) geomorphologic observations, (2) kinematic data from fault-slip analysis and (3) evidence from reflection seismic lines and newly compiled subsurface maps. The results presented here favour the interpretation that basement-rooted (i.e. thick-skinned) tectonics are dominant since the Late Pliocene, whereas Jura-type décollement tectonics may have ceased at about that time. The stress field evolution in the sedimentary cover is discussed by comparing "palaeostresses" (derived from the fault-slip data presented in chapter 3) and recent stresses. Eventually, it is discussed whether the observed structures could be related to an incipient (and potentially seismogenic) inversion of the Permo-Carboniferous trough system in the subsurface.

6.1.2 Geological setting

The study area (Fig. 1) is located at the junction of the southernmost URG and the northern Jura fold and thrust belt. Both the geography and the geological frame are sufficiently explained in the previous chapters of this thesis. Some familiarity with these is assumed, as a repetition is avoided here.

The orientation of maximum horizontal stresses (SHmax) in the north-western Alpine foreland, inferred from the inversion of seismotectonic dislocations, is consistently NW-oriented (Plenefisch and Bonjer, 1997; Deichmann et al., 2000; Reinecker et al., 2003; Kastrup et al., 2004). The preferred focal mechanism is strike-slip faulting down to c. 15 km and predominantly normal faulting from 15 km down to the MOHO. In all these cases, the extension axes show a very stable NE-SW-orientation. On the other hand, SHmax in the sedimentary cover, deduced primarily from in-situ stress measurements, is rather NW- to NNE-oriented (Baumann, 1981; Müller et al., 1987; Becker, 1999; Becker, 2000; Reinecker et al., 2003) and decoupled from the basement (comprising crystalline basement and Permo-Carboniferous troughs) along rheologically weak Middle and Upper Triassic evaporite layers,
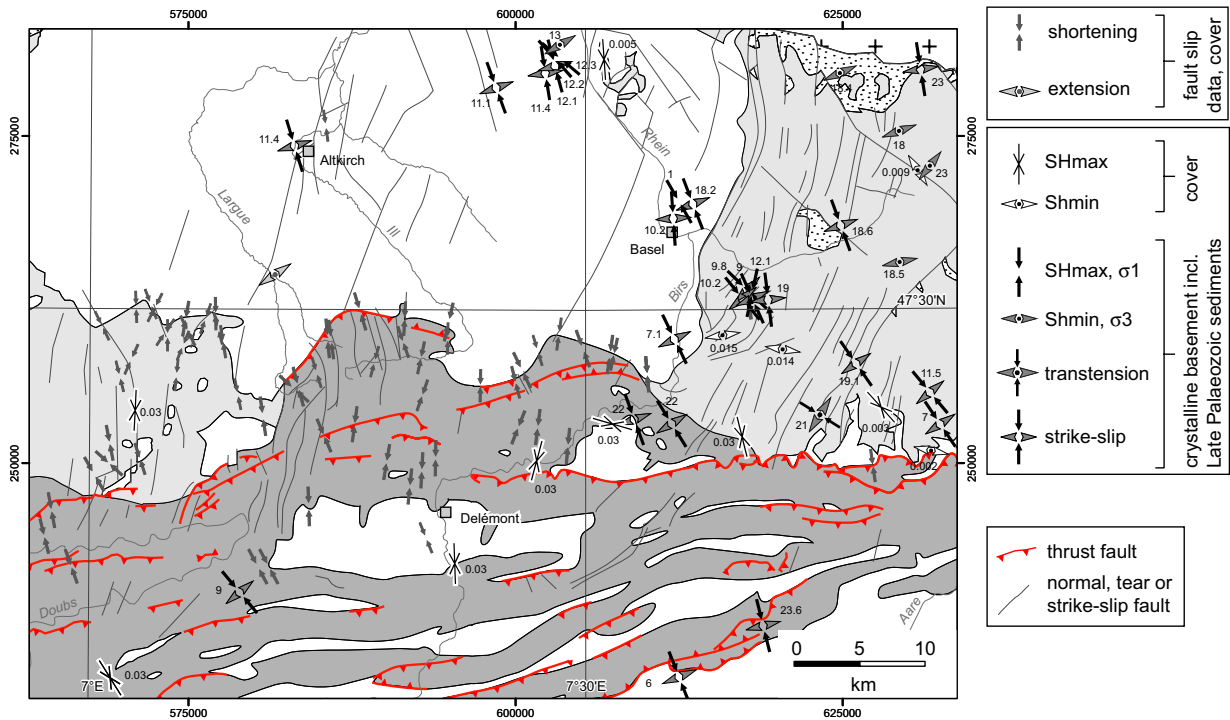
Fig. 1: tectonic overview map of the SE corner of the Upper Rhine Graben around Basel. Patterns for tectonic units and fault types are identical to Fig. 1 in chapter 3. Anticline crests are not shown for reasons of legibility. Superimposed are the shortening directions derived from the fault-slip ("palaeostress") analysis presented in chapter 3 (converging grey arrows). Also shown are the recent stresses, taken from the 2003 release of the World Stress Map project (Reinecker et al., 2003). The depth of each event is indicated in km. The near-surface data in the sedimentary cover stem from borehole in-situ stress measurements, whereas events deeper than 1 km stem from the inversion of seismotectonic data. The SH$_{max}$-orientations from near-surface events tend to parallel to the "palaeostress"-directions determined from the fault-slip data, particularly in the detached Mesozoic and in the autochthonous Mesozoic in the Ajoie. SH$_{max}$-orientations from seismotectonics, on the other hand, are predominantly NW-SE-oriented.

particularly well-documented in the northern Folded Jura (Müller et al., 1987). It is therefore still under dispute whether the currently observed deformation represents the actively ongoing propagation of the thin-skinned Jura fold- and thrust belt (Nivière and Winter, 2000; Müller et al., 2002) or whether it is related to an entirely new thick-skinned phase (Meyer et al., 1994; Lopes Cardozo and Granet, 2003; Giamboni et al., 2004a; Ustaszewski et al., 2005). The north-western Alpine foreland is characterised by convergence rates in the order of less than 1 mm/a (Müller et al., 2002), typical of an intraplate setting, but geodetic measurements are still at the limit of significance (Tesauro et al., 2005).

6.2 Field evidence for post-Late Pliocene tectonics

Fluvial gravels of Middle to Late Pliocene age, cropping out in the southernmost URG and the adjacent Jura Mountains, play a key role in deciphering the tectonics post-dating the main phase of Jura folding. These so-called Sundgau gravels unconformably overlie both the Palaeogene synrift sediments in the URG and the autochthonous Mesozoic in the Tabular Jura of the Ajoie. The Sundgau gravels were deposited by a shallow braided river draining westward across the region of southern Alsace ("Sundgau") towards the Bresse
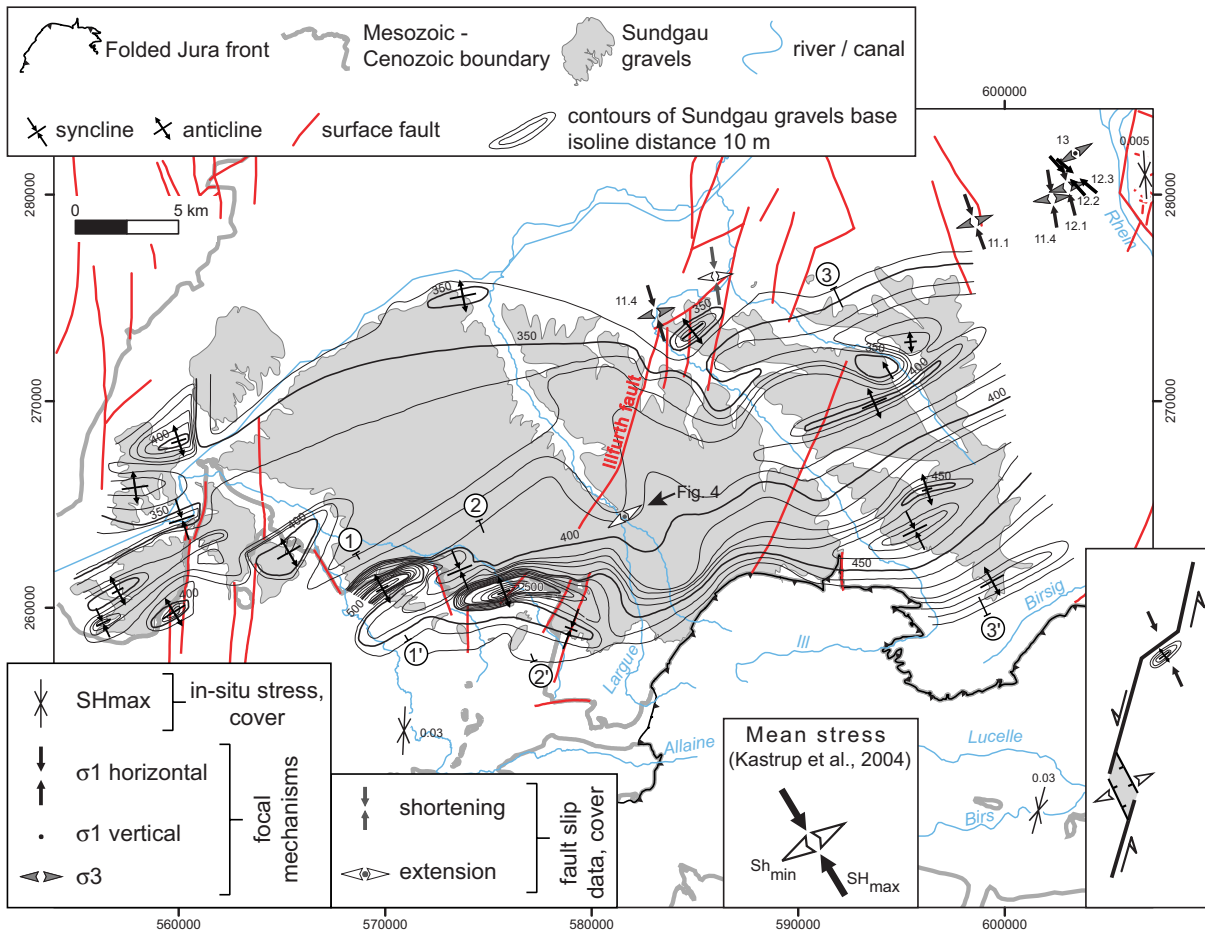
Fig. 2: contour map of the base of the Late Pliocene Sundgau gravels in metres above sea level (after Giamboni et al., 2004a). Data on the recent stress field comprise in-situ stress measurements and earthquake focal mechanisms, extracted from the World Stress Map project 2003 release (Reinecker et al., 2003). The numbers next to the stress symbols indicate the depth of the events in km. The traces of the cross sections 1 to 3 (Fig. 3) are indicated. The clustered events in the NE corner correspond to the Sierentz 1980 earthquake swarm. Bottom right inset: kinematic sketch of the Illfurth fault and its southern continuation, explaining occurrence of restraining and releasing bends.

Graben and eventually into the Mediterranean Sea. The stratigraphic age of the Sundgau gravels ranges from 4.2 to 2.9 Ma (Petit et al., 1996). At this time the drainage divide between the North and the Mediterranean Seas was located at the Kaiserstuhl volcano, approximately 60 km N of the area investigated. The abandonment of the riverbed occurred post-2.9 Ma when the drainage divide shifted southward into the Sundgau. The southward migration of the water divide occurred either due to a slow-down or the end of upwarping of the Vosges-Black Forest arch (Dèzes et al., 2004), or due to accelerated subsidence in the northern URG, concomitant with lowering of the local base level and subsequent regressive erosion (Doebl, 1970; Schumacher, 2002; Giamboni et al., 2004b).

The thickness of the gravels varies between 5 and 20 m (Théobald et al., 1958; Liniger, 1970a; Liniger, 1970b; Ruhland et al., 1973). They consist of predominantly clast-supported, crudely bedded gravel beds with a shifting network of shallow channels. Intercalations of sand lenses are found only occasionally. These sedimentological criteria suggest that deposition occurred on a nearly planar and horizontal surface, which can be used

as a reference plane for deciphering vertical tectonic movements that postdate the deposition of the gravels. Contouring the base of the Sundgau gravels revealed an array of syn- and anticlines with average amplitudes of 30-50 m and maximum amplitudes of up to 150 m in the southwest, testifying to post-Late Pliocene horizontal shortening and vertical uplift in the area of the southernmost URG (Giamboni et al., 2004a). The fold amplitudes exceed the average gravel thickness by up to an order of magnitude, making it thus highly unlikely that the folds represent merely the infilling of a pre-existing topography. The contours of the base of the Sundgau gravels and the orientations of recent stresses are shown in Fig. 2. The recent stresses were derived from the World Stress Map project (Reinecker et al., 2003) and are inferred from earthquake focal mechanisms and in-situ stress measurements. The depth of the events in kilometres is plotted next to each symbol. Two datasets derived from palaeostress analysis (datasets 23 and 28 presented in chapter 3) are also plotted. The mean stress regime reveals strike-slip characteristics and a maximum horizontal stress (SHmax) around 330° (Kastrup et al., 2004). Evidently, the Sundgau gravel folds trend perpendicular to SHmax.

6.2.1 Estimating displacement rates

In order to quantify the amount of horizontal shortening recorded by the Sundgau gravels, three cross sections through their gently folded base have been compiled and restored (Fig. 3). Profiles 1 and 2 cross the two en-échelon aligned anticlines. Cross-section 3 runs east of the Ill Valley and traverses several similarly trending syn- and anticlines. The cross sections are perpendicular to the isohypses and approximately parallel to the recent SHmax. The shortening of the base Sundgau gravels varies between 1 (cross section 3) and 2.8% (cross section 1) across the 3 transects. Assuming that the shortening commenced at around 2.9 Ma before present (the minimum age of the Sundgau gravels) yields horizontal displacement rates in the order of 0.05 mm/a for all three cross sections considered.

The vertical uplift rates can best be estimated along the en-échelon anticlines, where the amplitude of the Late Pliocene gravel base is in the order of 150 m. Assuming that growth of the anticline began after the deposition of the gravels (minimum age 2.9 Ma; Petit et al., 1996) gives also an average uplift rate in the order of 0.05 mm/a. This estimate is in agreement with uplift rates deduced from uplifted Pleistocene alluvial terraces along the Rhine tributaries Largue, Ill and Thalbach in the Sundgau (Giamboni et al., 2004b).

6.2.2 Left-lateral strike-slip faulting along NNE-oriented faults

An isolated anticline in the base of the Sundgau gravels with an amplitude of approximately 20 m is located at a kink of the Illfurth fault (Fig. 2). In the current stress field, the Illfurth fault is favourably oriented to accommodate sinistral strike-slip motion. The isolated anticline thus formed at a restraining band of the Illfurth fault (far right inset in Fig. 2). Further to the S, in the Largue valley, conjugate normal faults affect the Sundgau gravel

Profile 1: Florimont anticline

$$v_h \approx \frac{\Delta l}{t} \approx 0.05 \text{ mm/a}$$

$l_1 = 4.81 \text{ km}$

$l_0 = 4.95 \text{ km}$ $\Delta l = 140 \text{ m}$

Profile 2: Réchésy anticline

$$v_h \approx \frac{\Delta l}{t} \approx 0.05 \text{ mm/a}$$

$l_1 = 6.9 \text{ km}$

$l_0 = 7.05 \text{ km}$ $\Delta l = 150 \text{ m}$

Profile 3: Ill valley

$l_1 = 17 \text{ km}$

$l_0 = 17.15 \text{ km}$ $\Delta l = 150 \text{ m}$

$$v_h \approx \frac{\Delta l}{t} \approx 0.05 \text{ mm/a}$$
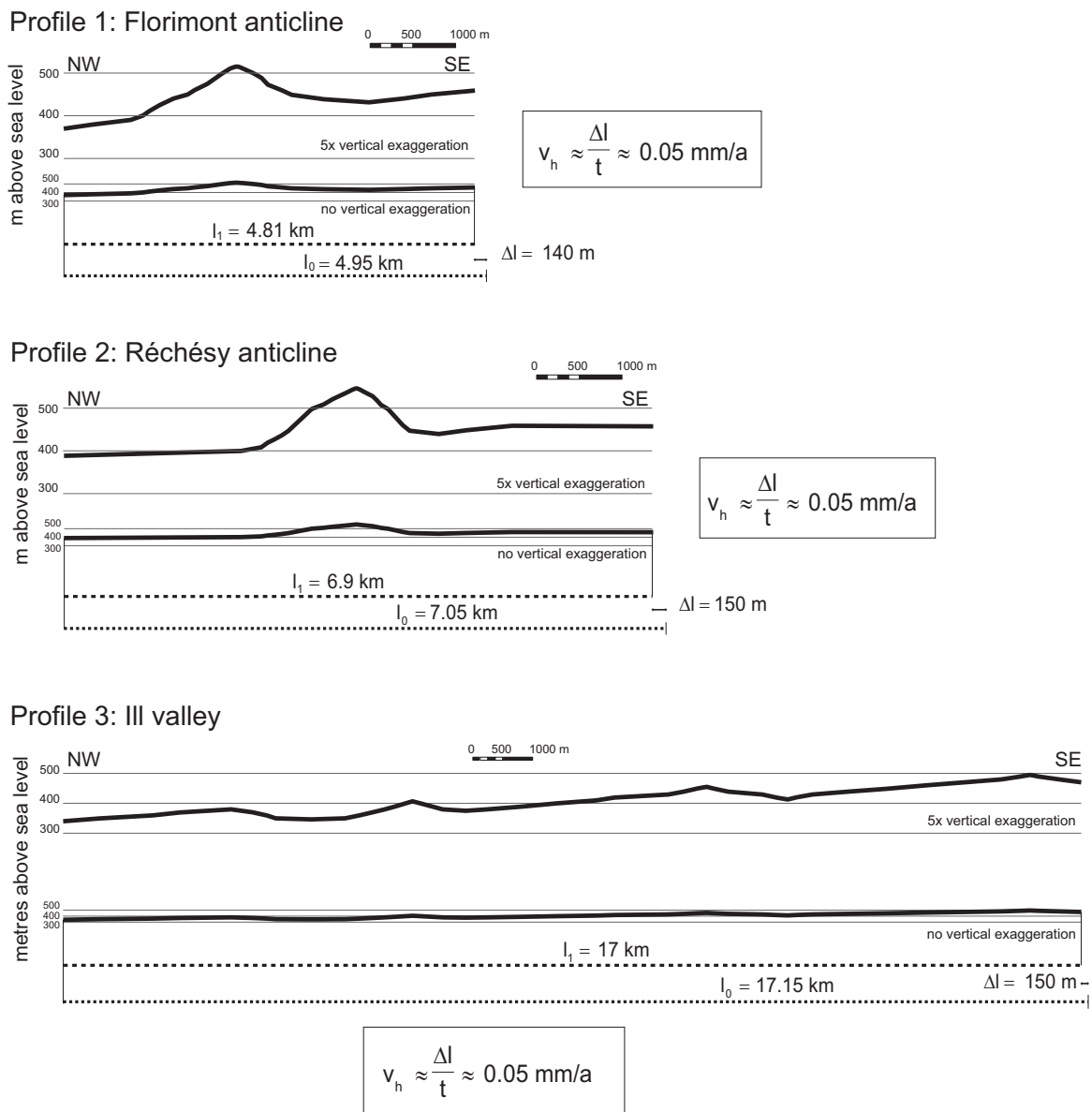
Fig. 3: Three cross sections through the folded base of the Sundgau gravels, obtained shortening amounts and derived horizontal displacement rates assuming that shortening started after the deposition of the gravels (minimum age 2.9 Ma). See Fig. 2 for location of the sections.

cover (Fig. 4). As depicted in Fig. 2, this outcrop is located near the southernmost tip of the Illfurth fault. Southward into the Tabular Jura, a similarly oriented fault is found, but offset to the E with respect to the Illfurth Fault. The normal faults affecting the Late Pliocene gravel cover are traceable by intercalated sand lenses in the grain-supported gravels (Fig. 4a and b). The extension direction is approximately NE-SW (Fig. 4c). The formation of the conjugate normal faults is interpreted to have occurred at a releasing bend between the overstepping NNE-trending faults (bottom right inset in Fig. 2). The observation of both restraining and releasing bends along the Illfurth Fault shows that it accommodated left-lateral strike-slip motion after the deposition of the Sundgau gravels.
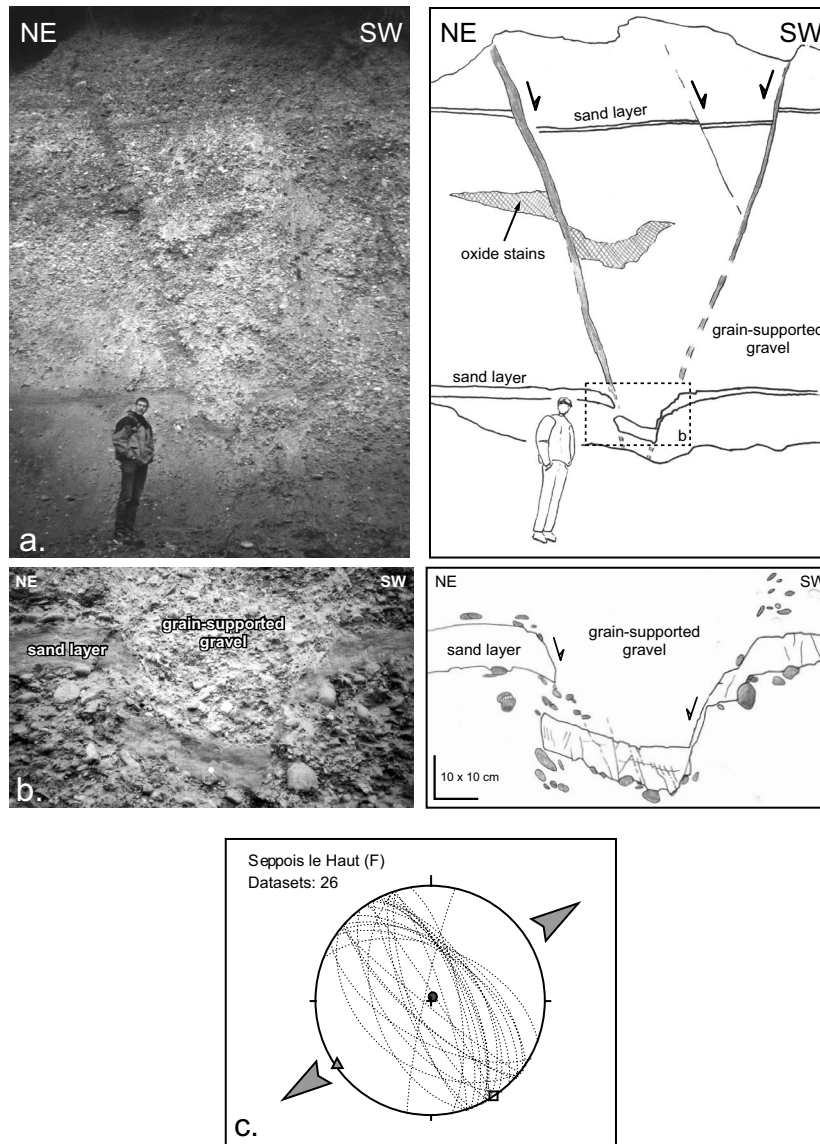
Fig. 4: (a) conjugate normal faults affecting the Late Pliocene Sundgau gravels. Intercalated sand lenses in the grain-supported gravels and oxide stains serve as markers. See Fig. 2 for location. (b) sand layer affected by cm- to dm-scale conjugate normal faults. Outside of the faulted sand layer the shear zone is traceable by rotated and broken pebbles. (c) stereographic representation of the faults and of the shortening and extension axes derived by the "Bisector method" (cf. chapter 2). Lower hemisphere, equal area projection.

6.2.3 Is the deformation ongoing at present?

The Post-Late Pliocene shortening is most strongly manifested around the two en-échelon aligned, doubly plunging peri-anticlines at the URG – Tabular Jura boundary. In Fig. 5, all geological and geomorphologic data from this area have been compiled. Shortening directions derived from palaeostress analysis (see chapter 3) are roughly N-S oriented (Fig. 5a). The two anticlines form very conspicuous topographical features and stand out clearly on a shaded relief map (Fig. 5b and c). The topography of the anticlines has essentially resulted from folding of the Mesozoic sediments. This is seen in the close correlation between the trend of the hill slopes and the dip directions and angles measured in Upper Jurassic and Palaeogene sediments around the two anticlines (Fig. 5c). The contours of the base of the Sundgau gravels (Fig. 5d) also correlate very closely with the topography, showing that the topography was created after the deposition of the Sundgau gravels. Moreover, the Allaine and Couevatte rivers are deflected away from the centre of the Florimont anticline as they cross its hinge. This suggests that the growth of the anticline and the propagation of the crest to either ends might have continued up to the present.
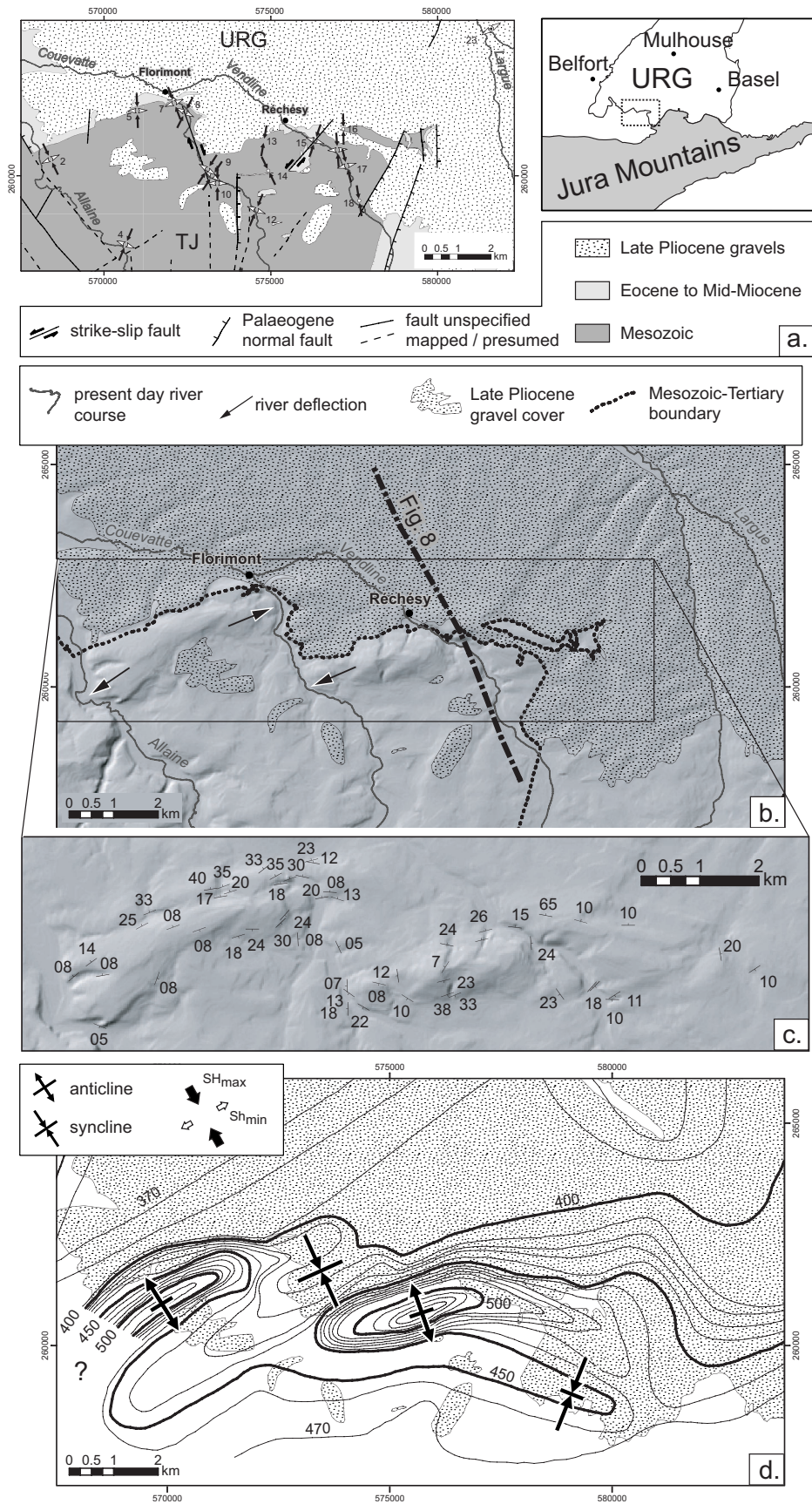
Fig. 5: (a) simplified geological map and palaeostress orientations from fault-slip data in the vicinity of the en-échelon aligned anticlines. Arrows and numbering correspond to fault-slip data presented in chapter 3. (b) Shaded relief map showing the juvenile morphology of the two anticlines. Note the deflection of the Allaine and Coeuvatte rivers around the fold hinges. Digital terrain map reproduced by permission of swisstopo (BA045907). (c) Dip directions and angles of bedding planes measured in Mesozoic and Palaeogene sediments. (d) Contoured base of the Sundgau gravels. Top left inset: recent stress field (Kastrup et al., 2004).

6.3 Subsurface evidence for compressively reactivated basement faults

6.3.1 Map of the base of the Tertiary surface

In order to investigate whether basement faults in the URG were reactivated under compression after Palaeogene extension, a contour map of the base of the Tertiary surface (from now on base-Tertiary for short) and of the faults dissecting it was compiled. 45 industry type reflection seismic lines located in the southernmost URG and the southerly adjacent Tabular and Folded Jura (bottom centre inset in Fig. 6) were available for interpretation. Ten exploration wells (Schmidt et al., 1924; BRGM, unpublished) are aligned along or close to the seismic lines and enabled the correlation of seismic reflectors with the lithologies encountered in exploration wells. Four of the wells that penetrated through the Tertiary succession permitted a calculation of seismic interval velocities (Fig. 6). The base of the Tertiary succession is marked by an unconformity, which gives rise to a discrete reflector due to high acoustic impedance contrasts between the uppermost Mesozoic (mostly limestones) and lowermost Tertiary layers (often siderolithic clays). Occasionally, an angular unconformity is developed. After identification of the base-Tertiary on the seismic lines, its depth (in seconds two-way-travel time, s TWT) was plotted on a map and contoured manually. In a next step, the contours were depth-converted using seismic velocities obtained from several exploration wells (Fig. 6). In the northwestern part, the base-Tertiary contour map was linked to a structural model of the Dannemarie Basin (Bourgeois et al., 2004). The base-Tertiary contours are shown as isolines in metres above sea level with a distance of usually 100 m (Fig. 7). Towards the Jura front, where the base-Tertiary surface can be directly observed in outcrop, the contours are drawn in intervals smaller than 100 m. In the southernmost part, the base-Tertiary contours are essentially based on the available geological maps (Fischer, 1965; Liniger, 1970b; Ruhland et al., 1973; Bailly et al., 1985). The contours are restricted to the main part of the URG and do not extend onto the Tertiary outcrops within the Jura.

The depth of the base-Tertiary ranges from 1600 m below sea level in the Dannemarie Basin to 500 m above sea level at the southwestern edge of the Ferrette Jura. The salient feature of the base-Tertiary map is the existence of three eastward tilted half-grabens, each bounded by a NNE-trending normal fault in the east. The half-grabens developed gentle hanging-wall synclines, presumably due to drag along the bounding normal faults. Towards the Jura front, the base-Tertiary sways into an ENE-WSW- to E-W-trend along a zone of extensional flexures underlain by Permo-Carboniferous faults (bottom right inset in Fig. 7). This structural configuration is the result of Palaeogene rifting.

The normal fault bounding the Ferrette half-graben is overthrusted by Mesozoic sediments along the W rim of the Ferrette Jura during the phase of thin-skinned Jura folding. This was also evidenced by boreholes (Schneegans and Théobald, 1948). On the other hand, immediately N of the northern tip of the Ferrette Jura, the Ferrette fault itself was reactivated, as evidenced by two top-to-the-E reverse faults that splay off from the normal fault and
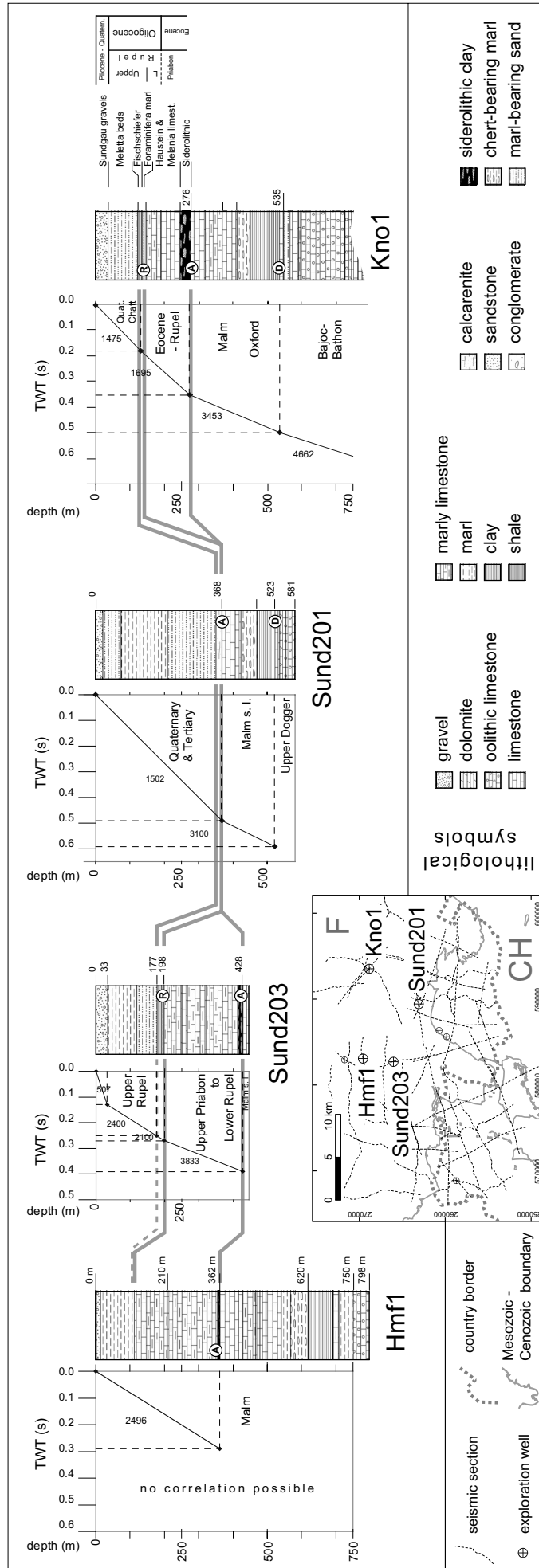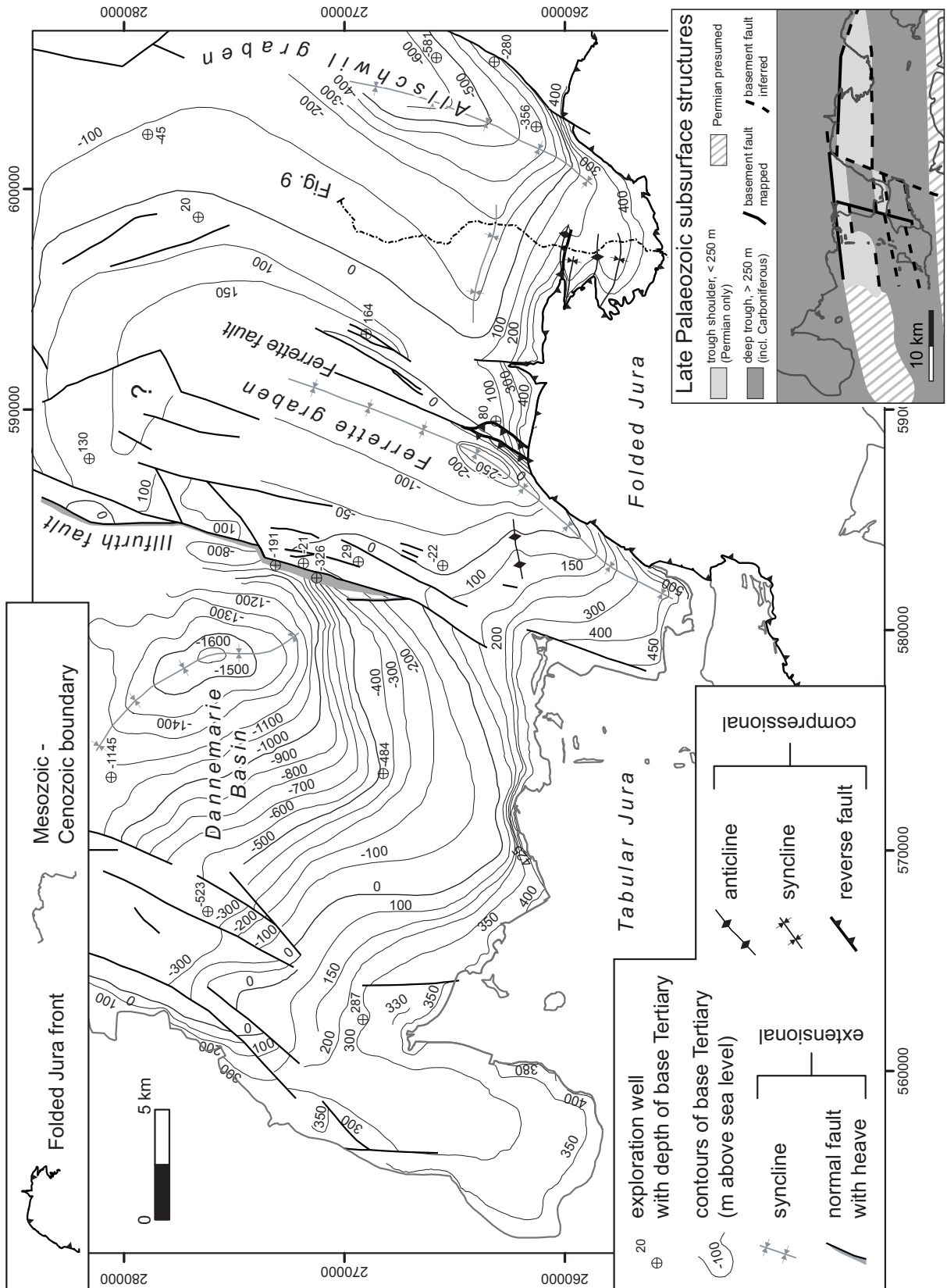
Fig. 6: Four correlated well logs showing the Palaeogene stratigraphy and the derived seismic interval velocities (in ms^{-1}) that were used for depth-conversion of the base-Tertiary map (Fig. 7).

Fig. 7: contour map of the base Tertiary surface and of the faults dissecting it. The contour lines are in metres above sea level. The lower right inset shows the known Late Palaeozoic tructures in the subsurface.

offset the base-Tertiary. According to the seismic information available, this reactivation could have occurred already in the early Neogene, because the splay faults cut through Uppermost Rupelian and Chattian sediments. An early Neogene age of this fault reactivation is also inferred from the fact that the Late Pliocene gravels that cover this part of the URG show no difference in elevation across those splays (compare Fig. 2 and 7). The Ferrette Jura front appears to seal the compressive fault splays of the Ferrette fault. However, a detailed map of the Ferrette Jura reveals a "back-thrust" in the along-strike prolongation of on of the splays. The compressive reactivation of the Ferrette fault might have been concomitant with thrusting of the Ferrette Jura or post-dating it. However, this fact cannot be verified with the current knowledge: such a back-thrust in the Ferrette Jura might be also purely thin-skinned since it was shown that its western rim was under sinistral transpression (see chapter 3).

An important observation is the fact that the reactivation of the Ferrette fault occurred exactly where NNE- and ENE-trending basement faults interfere, suggesting that its reactivation presumably occurred in a restraining bend position. This is evidenced in an ENE-trending anticline, which was identified W of the compressive splays of the Ferrette fault. This ENE-trending anticline formed more or less in the along-strike prolongation of the two en-échelon anticlines at the Jura-URG border still further to the E. It is therefore presumed that this anticline has formed above the same ENE-trending basement-fault. According to the seismic information, an early Neogene age for the reactivation of the ENE-trending basement fault underlying this anticline can be inferred. Again, a purely post-Late Pliocene age is less likely, because the Sundgau gravel base reveals no upwarping above this anticline (compare Fig. 2 and 7). More presumably, this reactivation could have been coeval with activity along the Rheintal Flexure in the Aquitanian or Burdigalian (Laubscher, 2001).

At the eastern termination of the Ferrette Jura, the E-W-trending anticlines plunge beneath the Tertiary infill of a small embayment of the URG that encroaches onto the Jura. At the southern limb of the northernmost of these gentle anticlines, a top-to-the-S reverse fault was mapped. It is noteworthy that this vergence is opposed to the transport direction of the detached sediments during the thin-skinned phase of Jura folding.

6.3.2 Fault reactivation evidenced in reflection seismic lines

Fig. 8 shows a reflection seismic line traversing the eastern one of the two en-échelon-aligned anticlines. This anticline formed along a compressively (or transpressively) reactivated extensional flexure of Palaeogene age (see chapter 2). The Palaeogene age of the flexure is seen in the S-ward tapering and onlap of the Palaeogene synrift sediments. Topography and the height of the base of the Sundgau gravels are superimposed into Fig 8b. As can be seen, the dip of the Mesozoic reflectors corresponds well with the dip of the Sundgau gravel's base. A good correlation exists also between the topographic crest and the position of a basement fault zone (or high), suggesting a compressive or transpressive reactivation of this basement fault.

132
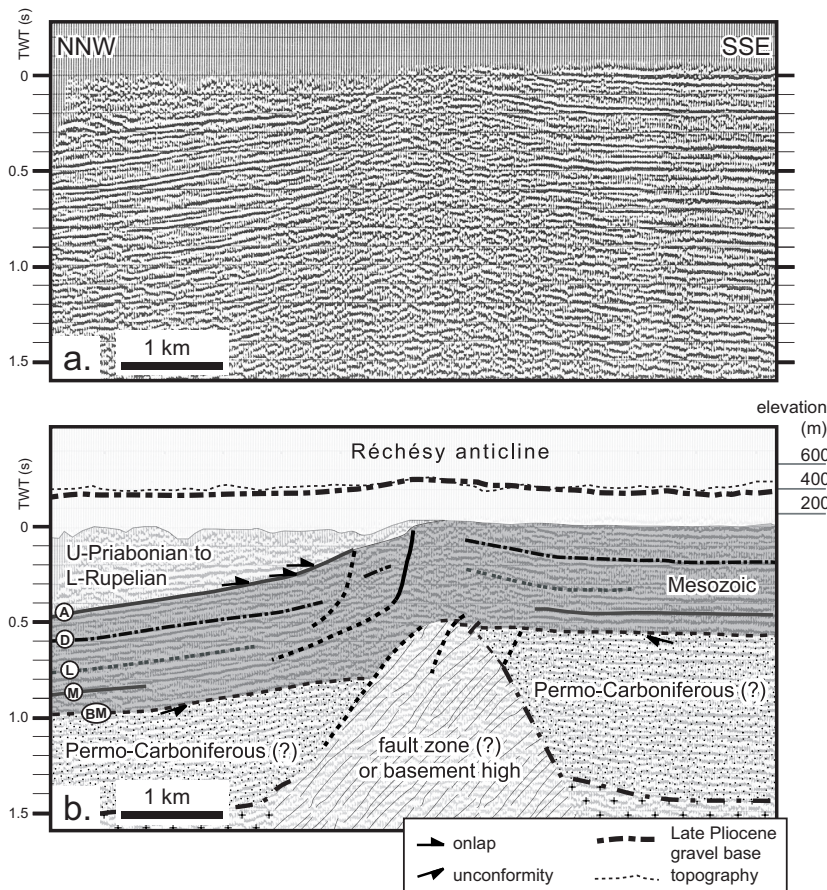
Fig. 8: reflection seismic line across the "Réchésy" anticline. See Figure 4 for location of the section. a. original, stacked section, b. interpreted section. BM=base Mesozoic, M=top Muschelkalk, L=top Lias, D=top Dogger, A=top Malm, hatched=fault zone associated with late Palaeozoic faults. Base of the Late Pliocene gravels (cf. Figure 2) and topography are superimposed. The vertical scale is vertically exaggerated by a factor of 1.2 to coincide with the depth in s TWT (calculated using seismic velocities from boreholes nearby). Note the close correlation between the dip of Mesozoic reflectors and the gravel's base. Moreover, fold crests in both gravels and Mesozoic sediments coincide and are located precisely above the basement fault zone. This suggests a thick-skinned origin of the Post-Late Pliocene folds.

Fig. 9 shows a reflection seismic line trending approximately N-S along the Allschwil half-graben. The southern end of the line runs into a Tertiary embayment east of the eastern termination of the Ferrette Jura. The Mesozoic succession reveals a very constant thickness and gently rises in elevation from N to S. A steeply N-dipping basement fault offsets the base of the Mesozoic by about 0.1 s TWT, corresponding to c. 170 m. Owing to weak layers in the Middle and Upper Triassic, the Mesozoic succession developed an extensional flexure above this basement fault. The extensional flexure was covered by an onlapping Upper Priabonian to Lower Rupelian succession (between reflectors "A" and "R"). This succession reveals a wedge-shape, tapering out towards the S. The less reflective parts above the "R" reflector are attributed to Uppermost Rupelian to Chattian synrift sediments, which are in turn covered by Late Pliocene gravels. The extensional flexure was compressively reactivated, as seen in a top-to-the-S reverse fault that offsets the prominent Upper Rupelian reflector. The throw amounts to 0.05 s TWT, which corresponds to c. 40 - 50 m, given the seismic interval velocities in the Upper Oligocene syn-rift succession (Fig. 6). Based on the seismic information, fault reactivation could have occurred already in the early Neogene. More probably, however, it occurred after the Late Pliocene. This is inferred from the facts that (a) the spatial position of the anticline in the hanging-wall of the top-to-the-S reverse fault corresponds to the position of an anticline mapped in the base of the Sundgau gravels (compare Figs. 2 and 7) and (b) the amplitudes of these anticlines are both in the order of 30 - 50 m. Another important aspect of this reverse fault is the observed top-to-the-S geometry itself. It excludes the possibility that
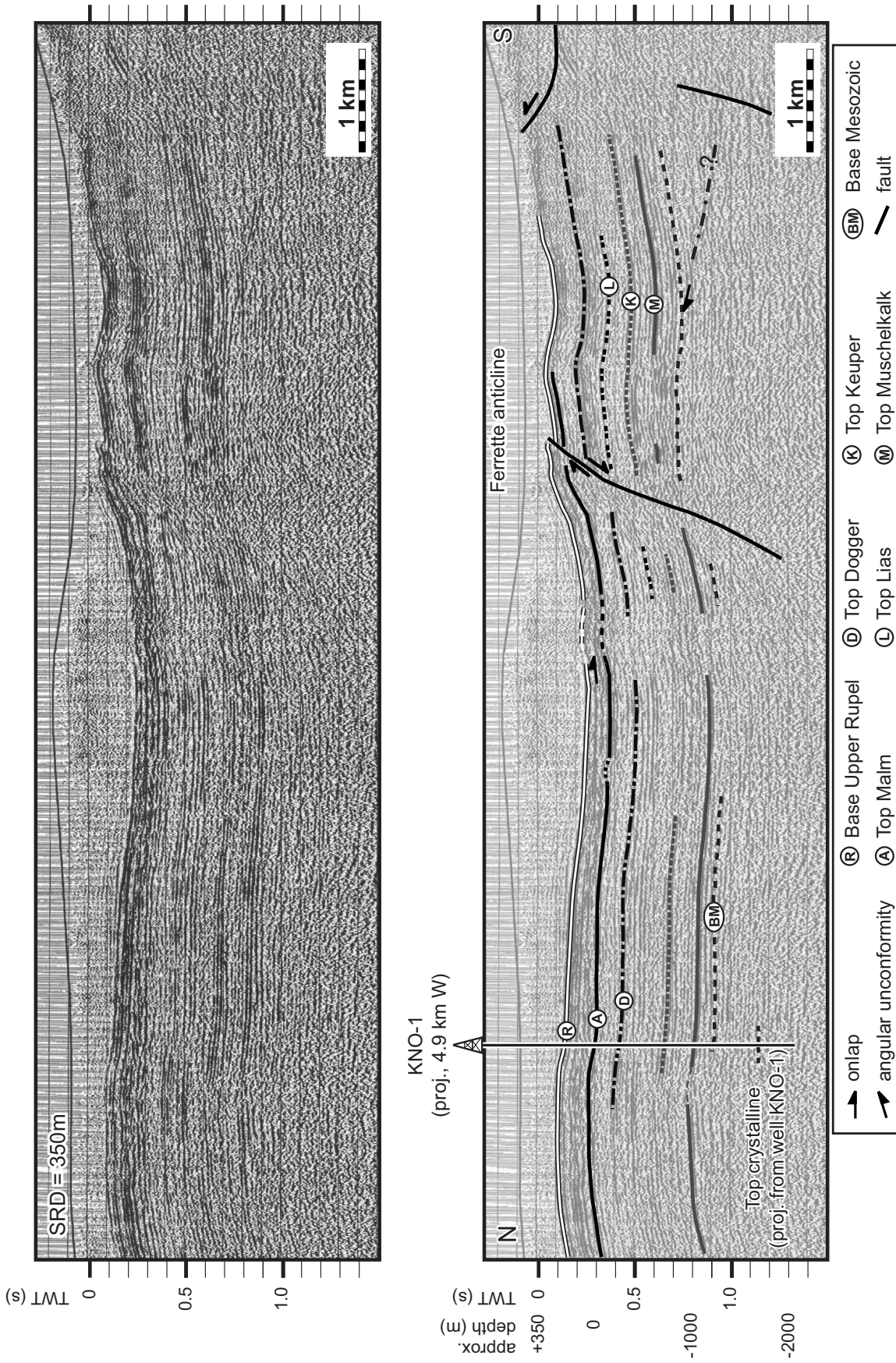
Fig. 9: N-S-trending industry-type reflection seismic line traversing a compressively reactivated extensional flexure of Palaeogene age. For location see Fig. 7.
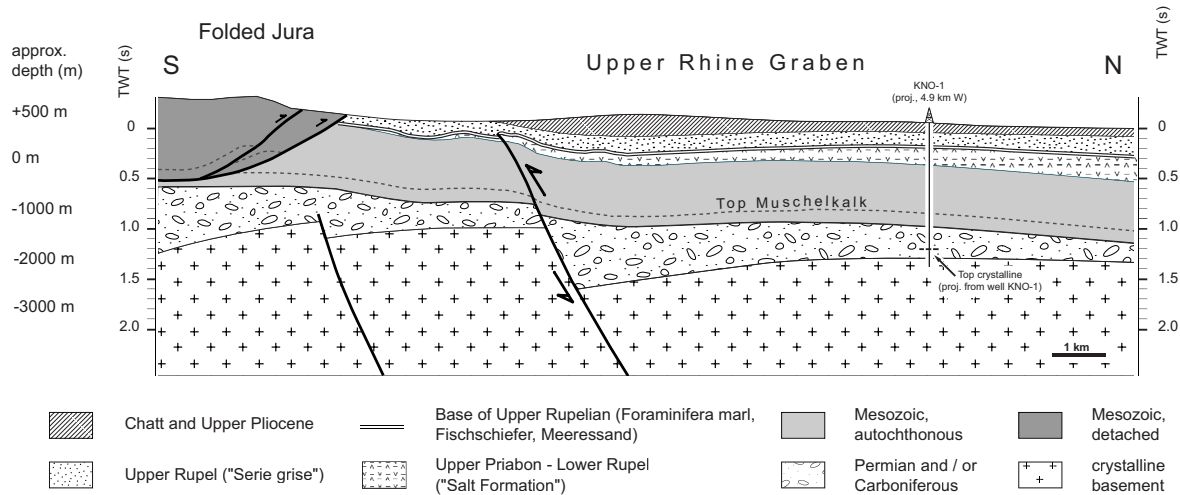
Fig. 10: schematic cross section based on the reflection seismic line of Fig. 9, illustrating how the compressive reactivation of an E-W-trending Palaeogene extensional flexure could be related to the incipient inversion of an underlying Permo-Carboniferous trough.

the compressive reactivation of the flexure is related to the ongoing N-ward propagation of a décollement in the Triassic weak layers.

In summary, it can be stated that both NNE- and ENE-trending basement-rooted faults in the southern URG have been reactivated under compression in the Neogene. Part of the reactivation occurred already in the early Neogene, pre-dating (or partly concomitant?) with thin-skinned Jura folding. The pre-Late Pliocene age of this reactivation is evidenced by the observation that the Late Pliocene Sundgau gravels do not reveal up-warping above compressively reactivated faults in the subsurface. On the other hand, ENE- to E-trending basement faults have been active again after the Late Pliocene. This is evidenced in the spatial coincidence between basement faults and folds mapped in both the base-Tertiary and base-Sundgau gravel maps. Their post-Late Pliocene age is furthermore constrained by the comparable amplitudes of these folds in both the base-Tertiary and the base-Sundgau gravel.

6.4 Discussion

6.4.1 Comparing palaeostresses and recent stresses

The recent stress field in the sedimentary (Mesozoic to Tertiary) cover, constrained by in-situ stress measurements, reveals N-S- to NNW-SSE-oriented maximum horizontal stresses (SHmax, Fig. 1 and 2). These orientations largely coincide with the shortening directions obtained from palaeostress analysis (chapter 3 and Fig. 1), particularly in the Folded Jura. This implies that no significant stress field change had occurred in this area since the onset of thin-skinned Jura folding (Becker, 2000). On the other hand, a NW-SE-oriented SHmax prevails in the basement of both URG and the Jura Mountains (Plenefisch and Bonjer, 1997; Kastrup et al., 2004). This anticlockwise rotation of SHmax from cover to basement is

systematically found throughout northern Switzerland and suggest a mechanical decoupling between sedimentary cover and its basement along Mid- to Late Triassic weak layers (Müller et al., 1987). In combination with geodetic measurements, which show the region of the northern Folded Jura Mountains to be uplifted with respect to their autochthonous northern foreland, ongoing thin-skinned propagation of the Jura Mountains was conjectured (Müller et al., 2002). On the other hand, this interpretation is contradicted by the considerably low SHmax magnitudes of generally less than 5 MPa in the cover of the northern Folded Jura Mountains, compared to considerably higher values of up to 9 MPa in the western and south-western Jura (Becker, 1999; Becker, 2000). This observation suggests that the recent stresses in the northern Folded Jura are merely residual stresses from the main stage of thin-skinned folding/thrusting. Thus, if ongoing thin-skinned propagation in this part of the Jura is inactive at present (as suggested by Becker, 2000), but replaced by basement-induced deformation, the observed stress decoupling between cover and basement could hint at relatively low displacement rates in the basement. Low displacement rates along basement faults favour decoupling between basement and cover across a viscous weak layer (Ustaszewski et al., 2005).

6.4.2 Kinematic framework for neotectonics in the southern URG

The best-documented evidence for post-Late Pliocene tectonics is the deformation recorded by the Late Pliocene Sundgau gravels. Their base reveals an array of NE-SW- to ENE-WSW-oriented syn- and anticlines with amplitudes up to 150 m. Restoring the gently folded base gives shortening amounts in the order of 1 to 3%. Assuming that shortening commenced at 2.9 Ma, this yields horizontal displacement rates in the order of 0.05 mm/a. This corresponds to a strain rate ($\dot{\varepsilon}$) in the order of $2 \cdot 10^{-16}$ s^{-1}. This value is in agreement with recently reported values based on interpolated GPS data of $\dot{\varepsilon}$ in the order of $3 \cdot 10^{-16}$ s^{-1} (Tesauro et al., 2005). The spatial coincidence between folds mapped in the base of the Sundgau gravels and reactivated basement faults, recognised in reflection seismic lines, points towards a thick-skinned origin of the shortening. Furthermore, the observation of anticlines located at restraining bends and normal faults located at releasing bends of NNE-trending URG faults strongly supports the hypothesis that the Sundgau folds formed in a wrench corridor between sinistrally active NNE-trending faults, where ENE-trending faults acted as restraining bends. Left-lateral strike-slip faulting along NNE-trending faults is in good agreement with seismotectonic evidence (Plenefisch and Bonjer, 1997; Deichmann et al., 2000). On the other hand, the reactivation of ENE-trending faults is hitherto supported mostly by geological evidence alone (Meyer et al., 1994; Giamboni et al., 2004a; Ustaszewski et al., 2005). Seismotectonic evidence supporting the reactivation of such ENE-trending faults is scarce. The February 02nd 2004 earthquake in the RBTZ near Rigney, France (Mw=4.5, focal depth 12 km) yielded a focal mechanism indicating reverse faulting (Swiss Seismological Service, 2004). Although it is not admissible to directly assign one of the nodal planes to the

actual fault plane that slipped during the earthquake, preference is given to the ENE-oriented and SE-dipping nodal plane. This is deduced from the fact that ENE-trending basement faults are abundant in the RBTZ. Thus, the focal mechanism of the Rigney earthquake could be regarded as seismotectonic evidence for the compressive inversion of Permo-Carboniferous troughs in the northern Alpine foreland (Ziegler, 1990; Philippe, 1994; Pfiffner et al., 1997).

In summary, the available geological evidence shows that both NNE- and ENE-trending basement faults have been reactivated since the Late Pliocene. NNE-trending faults are reactivated in left-lateral strike-slip mode, concomitant with the reactivation of ENE-trending faults as reverse faults (with a possible dextral strike-slip component). The reactivation of ENE-trending faults is responsible for the highest Sundgau folds observed and is presumably related to the incipient inversion of Permo-Carboniferous trough border faults (Fig. 10). Such an inversion might be caused by increased collisional coupling between the Alpine orogen and its northern foreland (Ziegler et al., 2004).

6.5 Conclusions

Since the Late Pliocene, the southern URG has experienced the thick-skinned reactivation of differently oriented faults. This is evidenced by the spatial coincidence between NE- to ENE-trending syn- and anticlines in the base of Late Pliocene fluvial gravels and mapped basement faults. The most prominent anticlines with amplitudes up to 150 m formed right above ENE-trending faults bordering an extensive Permo-Carboniferous trough system, hinting at their incipient inversion.

A restoration of the gently folded base of the gravels yields horizontal displacement rates in the order of 0.05 mm/a, assuming that deformation commenced after the biostratigraphically determined minimum age of the gravels (i.e. post-2.9 Ma). Deflected rivers in the hinges of the most prominent post-Late Pliocene anticlines suggest that the deformation might be still ongoing at present.

Interestingly, the switch from formerly thin- to presently ongoing thick-skinned tectonics occurred without any detectable reorientation of the stresses in the sedimentary cover, when comparing palaeostresses derived from outcrop-scale fault slip data and recent in-situ stresses. Thus, the transition from thin-skinned tectonics, which led to folding of the Jura fold and thrust belt, to basement-rooted deformation might be related to increased collisional coupling between the Alpine orogen and its northern foreland under a largely unchanged convergence direction between the Adriatic and the European plates.

References

Bailly, C., Chauve, P. and Martin, J., 1985. Carte Géologique de la France à 1/50 000, Delle, feuille XXXVI-22. Ministère de'l industrie et de la recherche, Bureau de recherches géologiques et minières, Service Géologique National, Orléans.

Baumann, H., 1981. Regional Stress Field and Rifting in Western Europe. Tectonophysics, 73: 105-111.

Becker, A., 1999. In Situ Stress data from the Jura mountains - new results and interpretation. Terra Nova, 11: 9-15.

Becker, A., 2000. The Jura Mountains - an active foreland fold-and-thrust belt? Tectonophysics, 321: 381-406.

Bourgeois, O., Le Carlier de Veslud, C., Ford, M. and Diraison, M., 2004. 3D modelling of the Dannemarie Basin, Nancy.

BRGM, unpublished. Banque du sous-sol.

Deichmann, N., Ballarin Dolfin, D. and Kastrup, U., 2000. Seismizität der Nord- und Zentralschweiz. NAGRA Technischer Bericht, 00-05. NAGRA, Wettingen, 94 pp.

Dèzes, P., Schmid, S.M. and Ziegler, P.A., 2004. Evolution of the European Cenozoic Rift System: interaction of the Alpine and Pyrenean orogens with their foreland lithosphere. Tectonophysics, 389(1-2): 1-33.

Doebl, F., 1970. Die tertiären und quartären Sedimente des südlichen Rheingrabens. In: J.H. Illies and S. Mueller (Editors), Graben Poblems. Proceedings of an International Rift Symposium held in Karlsruhe October, 10-12, 1968. E. Schweizerbart'sche, Stuttgart, pp. 56-66.

Fischer, H., 1965. Geologischer Atlas der Schweiz 1:25 000, Atlasblatt 49, Rodersdorf, mit Erläuterungen. Schweizerische Geologische Kommission, Bern.

Giamboni, M., Ustaszewski, K., Schmid, S.M., Schumacher, M.E. and Wetzel, A., 2004a. Plio-Pleistocene Transpressional Reactivation of Paleozoic and Paleogene Structures in the Rhine-Bresse transform Zone (northern Switzerland and eastern France). International Journal of Earth Sciences, 93(2): 207–223, DOI: 10.1007/s00531-003-0375-2.

Giamboni, M., Wetzel, A., Nivière, B. and Schumacher, M.E., 2004b. Plio-Pleistocene folding in the southern Rhinegraben recorded by the evolution of the drainage network (Sundgau area; Northwestern Switzerland and France). Eclogae Geologicae Helvetiae, 97(1): 17-31, DOI: 10.1007/s00015-004-1112-4.

Kastrup, U. et al., 2004. Stress field variations in the Swiss Alps and the northern Alpine foreland derived from inversion of fault plane solutions. J. Geophys. Res., 109(B01402): doi:10.1029/2003JB002550.

Lambert, J., Winter, T., Dewez, T. and Sabourault, P., 2005. New hypotheses on the maximum damage area of the 1356 Basel earthquake (Switzerland). Quaternary Science Reviews, 24: 381-299.

Laubscher, H., 2001. Plate interactions at the southern end of the Rhine graben. Tectonophysics, 343: 1-19.

Liniger, H., 1970a. Bemerkungen zur Tektonik am Südende des Rheingrabens. In: J.H. Illies and S. Mueller (Editors), Graben Problems. Proceedings of an International Rift Symposium held in Karlsruhe 1968, International Upper Mantle Project. Scientific Report. E. Schweitzerbart'sche, Stuttgart, pp. 103-106.

Liniger, H., 1970b. Geologischer Atlas der Schweiz 1:25 000, Atlasblatt 55: Bonfol, mit Erläuterungen. Kümmerly & Frey, Bern.

Lopes Cardozo, G.G.O. and Granet, M., 2003. New insight in the tectonics of the southern Rhine Graben-Jura region using local earthquake seismology. Tectonics, 22(6): 1078, doi:10.1029/ 2002TC001442.

Mayer-Rosa, D. and Cadiot, B., 1979. Review of the 1356 Basel earthquake: basic data. Tectonophysics, 53: 325-333.

Meghraoui, M. et al., 2001. Active normal faulting in the Upper Rhine Graben and paleoseismic identification of the 1356 Basel earthquake. Science, 293: 2070-2073.

Meyer, B., Lacassin, R., Brulhet, J. and Mouroux, B., 1994. The Basel 1356 earthquake: which fault produced it? Terra Nova, 6: 54-63.

Müller, W.H., Blümling, P., Becker, A. and Clauss, B., 1987. Die Entkoppelung des tektonischen Spannungsfeldes an der Jura-Überschiebung. Eclogae Geologicae Helvetiae, 80(2): 473-489.

Müller, W.H., Naef, H. and Graf, H.R. (Editors), 2002. Geologische Entwicklung der Nordschweiz, Neotektonik und Langzeitszenarien, Zürcher Weinland. NAGRA Technischer Bericht, 99-08. NAGRA, Wettingen, 226 pp.

Nivière, B. and Winter, T., 2000. Pleistocene northwards fold propagation of the Jura within the southern Upper Rhine Graben: seismotectonic implications. Global and Planetary Change, 27: 263–288.

Petit, C., Campy, M., Chaline, J. and Bonvalot, J., 1996. Major palaeohydrographic changes in Alpine foreland during the Pliocene-Pleistocene. Boreas, 25: 131-143.

Pfiffner, O.A., Erard, P. and Stäuble, M., 1997. Two cross sections through the Swiss Molasse Basin (lines E4-E6, W1, W7-W10). In: O.A. Pfiffner, P. Lehner, P. Heitzmann, S. Mueller and A. Steck (Editors), Deep structure of the Swiss Alps. Results of NRP 20. Birkhäuser, pp. 64-72.

Philippe, Y., 1994. Transfer Zone in the Southern Jura Thrust Belt (Eastern France): Geometry, Development and Comparison with Analogue Modeling Experiments. In: A. Mascle (Editor), Hydrocarbon and Petroleum Geology of France. Special Publication of the European Association of Petroleum Geologists. A. Springer, pp. 327-346.

Plenefisch, T. and Bonjer, K., 1997. The stress field in the Rhine Graben area inferred from earthquake focal mechanisms and estimation of frictional parameters. Tectonophysics, 275: 71-97.

Reinecker, J., Heidbach, O. and Mueller, B., 2003. The 2003 release of the World Stress Map (available online at www.world-stress-map.org).

Ruhland, M., Blanalt, J.G. and Bômont, M., 1973. Carte Géologique detaillée de la France à 1/50 000, Ferrette, feuille XXXVII-22. Ministère du développement industriel et scientifique, Bureau de recherches géologiques et minières, Service Géologique National, Orléans.

Schmidt, C. et al., 1924. Bohrungen von Buix bei Pruntrut und Allschwil bei Basel. Beiträge zur Geologie der Schweiz. Geotechnische Serie, X. Lieferung: 74.

Schneegans, D. and Théobald, N., 1948. Observations nouvelles sur le Chevauchement frontal du Jura Alsacien. Bull. Soc. Geol France, 18: 89-95.

Schumacher, M.E., 2002. Upper Rhine Graben: Role of preexisting structures during rift evolution. Tectonics, 21(1): 1006, doi:10.1029/2001TC900022.

Swiss Seismological Service, ETH Zürich, 2003. ECOS - Earthquake Catalog of Switzerland, Swiss Seismological Service, http://seismo.ethz.ch/.

Swiss Seismological Service, ETH Zürich, 2004. Regional Moment Tensor Catalog, http://www.seismo.ethz.ch/ moment_tensor/2004/homepage.html.

Tesauro, M., Hollenstein, C., Egli, R., Geiger, A. and Kahle, H.-G., 2005. Continuous GPS and broad-scale deformation across the Rhine Graben and the Alps. International Journal of Earth Sciences, 94(4): 525-537, doi: 10.1007/s00531-004-0453-0.

Théobald, N., Dubois, G. and Goguel, J., 1958. Carte Géologique de la France à 1/50 000, feuille Altkirch-Huningue + notice explicative, XXXVII-21, Service de la Carte Géologique de la France, Paris.

Ustaszewski, K., Schumacher, M.E., Schmid, S.M. and Nieuwland, D., 2005. Fault reactivation in brittle-viscous wrench systems - dynamically scaled analogue models and application to the Rhine-Bresse Transfer Zone. Quaternary Science Reviews, 24(3-4): 363-380, doi:10.1016/j.quascirev.2004.03.015.

Ziegler, P.A., 1990. Collision related intra-plate compression deformations in Western and Central Europe. Journal of Geodynamics, 11(4): 357-388.

Ziegler, P.A., Schumacher, M.E., Dèzes, P., van Wees, J.-D. and Cloetingh, S., 2004. Post-Variscan evolution of the lithosphere in the Rhine Graben area: constraints from subsidence modelling. In: M. Wilson (Editor), Permo-Carboniferous magmatism and rifting in Europe. Geological Society of London Special Publications. Geological Society, pp. 289-317.

Chapter 7 - summary

This thesis highlights the control of pre-existing faults on the geological history of NW Switzerland and neighbouring France and Germany. Throughout the Cenozoic, the tectonic evolution of this area, situated at the intersection between the European Cenozoic rift system and the northwestern Alpine foreland, was governed by faults inherited from the Late Palaeozoic. From the Early Palaeogene up to the Late Neogene, these faults were repeatedly reactivated in changing stress fields and with differing kinematics. These faults also strongly control neotectonic activity in the area. Certain basement faults even played a role when they remained inert themselves - for instance during the thin-skinned phase of Jura folding and thrusting, where thrust faults and transfer zones in the sedimentary cover nucleated along pre-existing basement steps. In the following, some key results of this study are summarised.

7.1 Constraints on the timing of the transition from rift-perpendicular extension to sinistral strike-slip faulting in the URG

The evolution of the southern URG took place under changing tectonic regimes. Rifting initiated in the Upper Eocene under WNW-ESE- to W-E-oriented extension, i.e. roughly perpendicular to the rift axis, as shown in chapter 2. This extension direction prevailed until the end of the Palaeogene. Extension in both the URG and the westerly adjacent Bresse Graben was simultaneous and was connected by sinistral transtension in the RBTZ, which nucleated along ENE-trending, Late Palaeozoic basement faults. In the sedimentary cover of the southern end of the URG, the simultaneity of rift-perpendicular extension in the URG and sinistral transtension in the RBTZ is documented by simultaneous growth faulting along NNE-trending half-grabens and extensional flexuring above ENE-trending faults.

Rift-related subsidence in the southern URG has ceased by early Neogene times and was related to a major stress field change from approximately E-W-oriented extension to NW-SE-oriented compression. Apart from uplift and erosion of both the southern graben segment and its rift flanks, this stress field change subjected the URG as a whole to sinistral shear. In the study area, the transition from rift-perpendicular extension to sinistral shear is evidenced in the transpressive reactivation of NNE-trending faults concomitant with the reactivation of ENE-oriented faults after the Late Chattian. This confirms the fact that the URG had at least a two-stage evolution, with an initial phase of rift-perpendicular extension until the Late Chattian and a later phase of sinistral oblique rifting since the early Neogene.

7.2 Control of basement faults on décollement tectonics

Chapter 3 shows that the northernmost, frontal folds of the Jura fold and thrust belt are characterised by dramatic along-strike asymmetries, including an along-strike decrease in shortening from W to E. Considering this and the shortening directions derived from fault-slip analysis, the strike-slip component along a NNE-oriented sinistral oblique ramp, bounding the asymmetric anticlines to the W, was deduced despite the lack of suitable markers. It is believed that the chosen approach could be applied to similar settings along oblique or lateral ramps in other fold and thrust belts, where suitable markers are absent.

7.3 Displacement-rate dependence of fault reactivation in brittle-viscous oblique rift-wrench systems

Dynamically scaled analogue models of oblique rift systems have shown that the transpressive reactivation of faults in the brittle cover, separated from a basal plate by a viscous décollement horizon, depends not only on kinematic aspects (i.e. requiring appropriate angles between shortening direction and fault trend), but also on the mechanical coupling between brittle cover and viscous base. This coupling, in turn, depends on the displacement rate applied to the basal plate. "Slow" reactivation tends to reactivate only few faults in the cover and deformation tends to be more distributed. "Fast" reactivation, on the other hand, tends to reactivate a great number of faults and leads to the inversion of entire oblique rifts. Applied to the RBTZ, the experimental results suggest that thick-skinned reactivation of certain faults was rather a "low displacement rate" process. Moreover, current low displacement rates along basement faults may explain the observed stress decoupling in parts of the northern Jura. The so inferred low displacement rates are in agreement with the generally low displacement rates currently observed in the area.

7.4 Neotectonic scenario ... and remaining open questions

This thesis has demonstrated that tectonic activity at the URG-Jura junction has not ceased after Mio-Pliocene Jura folding. Instead, it has continued up to recent. Ongoing NW-SE-oriented compression produced an array of NE-SE- to ENE-WSW-trending folds in the southernmost URG, traceable at the base of the Late Pliocene fluvial Sundgau gravels. Contrary to the foregoing Jura phase, this latest phase involves basement shortening, as well. The horizontal displacement rates are at least on the order of 0.05 mm/a. The deformation recorded by the Sundgau gravels can be attributed to (a) wrenching of the sedimentary cover above NNE-trending, URG-parallel, sinistral strike-slip faults and (b) reverse (or dextral transpressive?) faulting along ENE-trending faults. The activity along ENE-trending faults is possibly related to the incipient inversion of Permo-Carboniferous troughs. It is reasoned
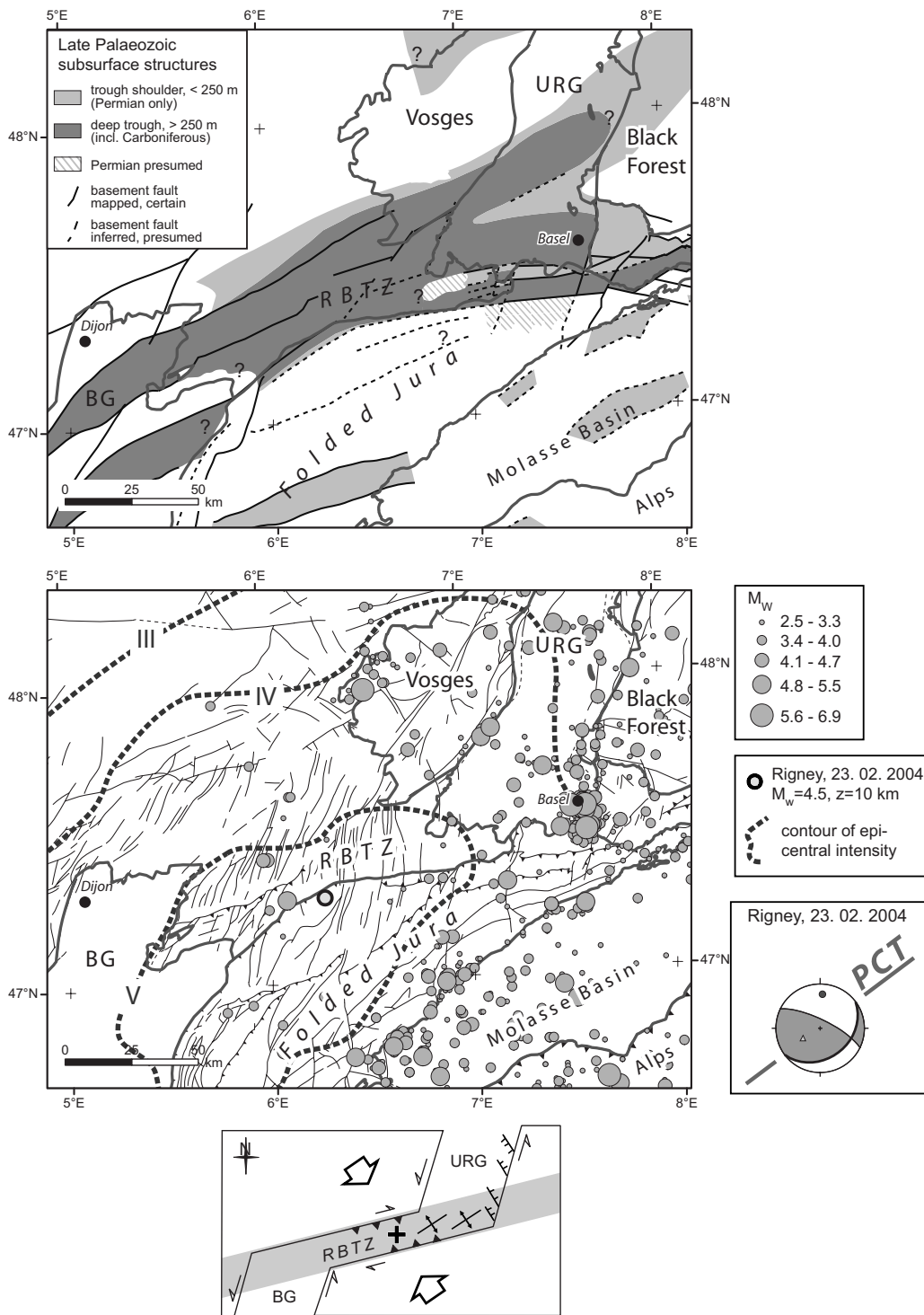
Fig. 1: Top: Late Palaeozoic subsurface structures in the wider study area, superimposed on the surface outlines of the major tectonic elements. BG = Bresse Graben, RBTZ = Rhine-Bresse transfer zone, URG = Upper Rhine Graben. Middle: Surface faults and epicentres of historically and instrumentally recorded earthquakes, including the Feb. 23rd 2004 earthquake at Rigney, E Besançon. Contours of epicentral intensities are ellipsoidal with the long axis paralleling ENE-trending subsurface faults. The SE-dipping nodal plane also parallels dominant subsurface faults and is therefore thought to represent the fault plane. This suggests that the inversion of PCT border faults (assuming a listric geometry at greater depths) is viable in the currently NW-SE-oriented stress field. Bottom: kinematic sketch illustrating the current kinematics. Both URG and BG are active as sinistral rifts. The RBTZ is largely under compression. Even though resolved shear stresses may be small, minor dextral wrench component can be inferred to act along ENE-trending basement faults. Local normal faulting occurs along (N)NW-trending faults at the eastern border of the URG. Seismicity distribution from ECOS (2004) for a timespan from 1265 AD until 2004. Focal mechanism from Swiss Seismological Service (2004). Contours of epicentral intensity from RéNaSS (2004).
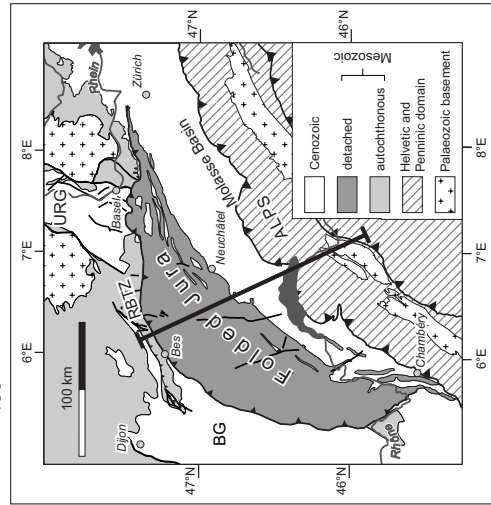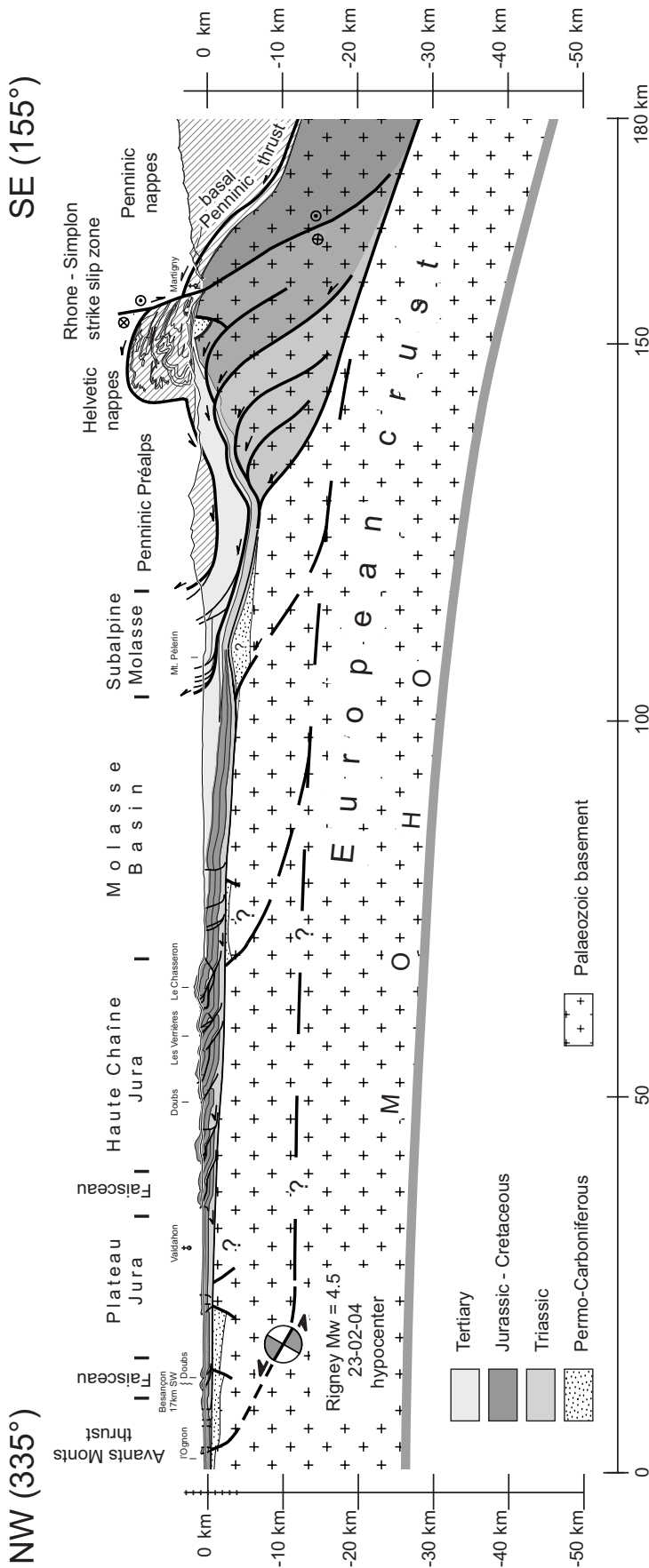
Fig. 2: top: a crustal-scale cross-section across the NW Alps, the Molasse Basin and the Jura fold and thrust belt (modified after a cross-section by Burkhard & Sommaruga, 1998). Bottom right: tectonic overview of the NW Alpine foreland with location of the section trace. The extent and depth of Permo-Carboniferous troughs underneath the NW Molasse Basin and the Jura are taken from Fig. 1. The hypocenter of the Rigney earthquake plots exactly on the cross-section, so it was superimposed onto it at the corresponding depth. In this interpretation, the earthquake is thought to have occurred along a listric-shaped normal fault, which borders a Permo-Carboniferous graben and which is linked to the Avant-Monts-thrust at surface. The observed reverse faulting mechanism is believed to indicate the incipient inversion of the Late Palaeozoic troughs. Such an interpretation follows that of Mosar (1999), who proposed ongoing "tectonic underplating" by accretion of European crust underneath the southern Jura fold and thrust belt to account for increased seismicity and elevated uplift-rates underneath the Jura-Molasse transition.

that the ongoing inversion of such ENE-trending faults is also potentially seismogenic, as demonstrated by the Mw 4.5 event on February 2nd 2004 at Rigney, near Besançon, France (Fig. 1 and 2). However, it remains a topic for future research to reconcile whether a similar seismic source can be conjectured for the prominent earthquake of Basel in 1356 AD.

In this thesis, the following possibilities are invoked to explain the observed incipient inversion of Permo-Carboniferous troughs in a geodynamic context: (a) active tectonic underplating of European crust in the Alpine foreland (Mosar, 1999), possibly triggered by (b) post-5 Ma uplift of the Molasse Basin and concomitant erosion of its infill (Cederbom et al. 2004), causing the deactivation of intracrystalline glide in the basal décollement and thus possibly favouring a transition from thin- to thick-skinned tectonics, (c) increased collisional coupling between the Alpine orogen and its northern Alpine foreland (Dèzes et al., 2004).

In the future, however, the combination of more accurate geodetic measurements, extended periods of instrumentally recorded seismicity and yet more geological observations should allow verifying the above outlined ideas.

References

Burkhard, M. and Sommaruga, A., 1998. Evolution of the western Swiss Molasse basin: structural relations with the Alps and the Jura belt. In: A. Mascle, C. Puidgefàbregas, H.P. Luterbacher and M. Fernàndez (Editors), Cenozoic Foreland Basins of Western Europe. Geological Society, London, pp. 279-298.

Cederbom, C.E., Sinclair, H.D., Schlunegger, F. and Rahn, M., 2004. Climate-induced rebound and exhumation of the European Alps. Geology, 32(8): 709-712, doi: 10.1130/G20491.1.

Dèzes, P., Schmid, S.M. and Ziegler, P.A., 2004. Evolution of the European Cenozoic Rift System: interaction of the Alpine and Pyrenean orogens with their foreland lithosphere. Tectonophysics, 389(1-2): 1-33.

Mosar, J., 1999. Present-day and future tectonic underplating in the western Swiss Alps: reconciliation of basement/wrench-faulting and décollement folding of the Jura and Molasse basin in the Alpine foreland. Earth and Planetary Science Letters, 173: 143-155.

RéNaSS, 2004. Réseau National de Surveillance Sismique, http://renass.u-strasbg.fr/, (accessed on 2004-04-04).

Swiss Seismological Service, E.T.H.Z., 2003. ECOS - Earthquake Catalog of Switzerland, Swiss Seismological Service, http://seismo.ethz.ch/.

Swiss Seismological Service, E.T.H.Z., 2004. Regional Moment Tensor Catalog, http://www.seismo.ethz.ch/moment_tensor/2004/homepage.html, (accessed on 10. 04. 2004).

Appendix 1: subsurface data

The data presented in this section were required for calibrating particular reflectors on reflection seismic lines, constructing the subsurface fault patterns and contour maps of the Base Mesozoic and Base Tertiary surfaces, as well as the geological cross sections.
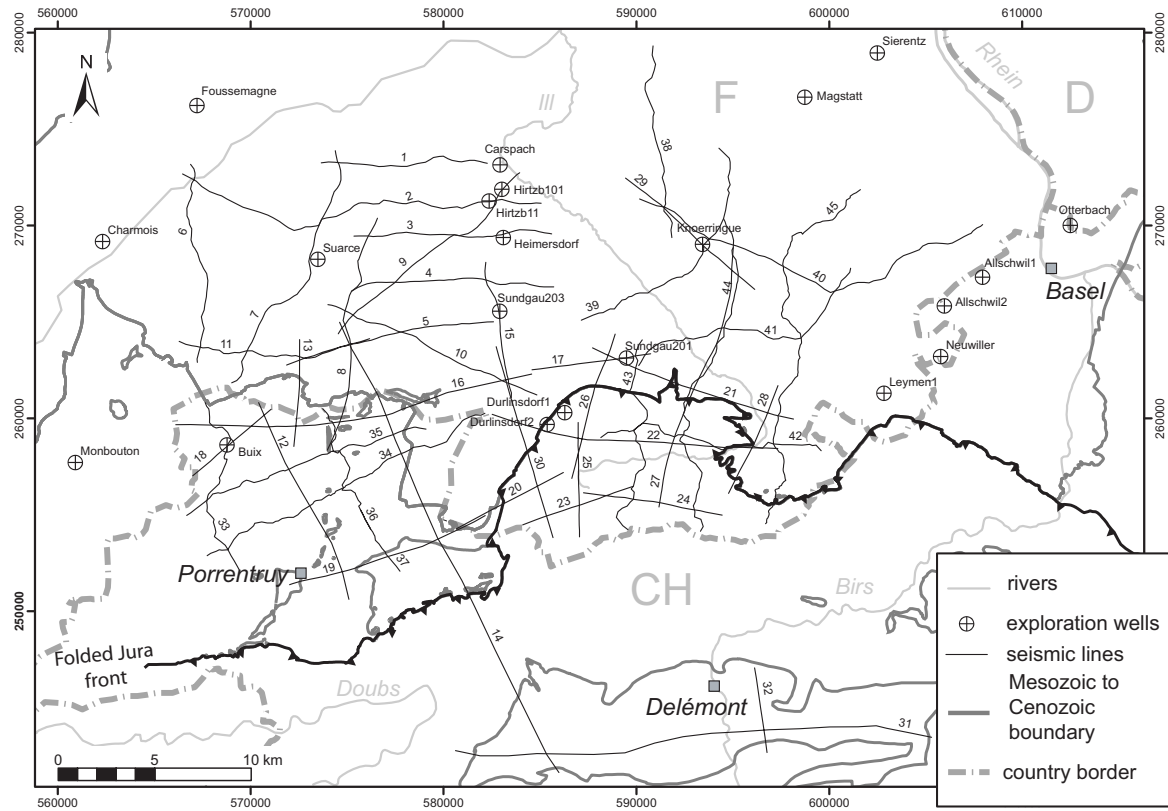

Fig. A1-1: location map showing traces of reflection seismic lines and exploration wells used in this study. The lines were acquired during French and Swiss campaigns between the mid-1970-ies to 1980-ies. Numbers on map margin refer to Swiss National coordinates.

No.	Seismic line	No.	Seismic line	No.	Seismic line
1	79HU2	16	73BE7	31	74BE10
2	78HU4	17	HUV2a	32	74BE11
3	79HU3	18	73BE6	33	80JU2
4	79HU4	19	73BE9	34	80JU3
5	78HU5	20	HUV5	35	80JU4
6	78HU1	21	HUV2b	36	80JU1
7	78HU2	22	HUV3	37	80JU1EXT
8	80HU1	23	HUV4a	38	85ALT16
9	79HU1	24	HUV4b	39	85ALT13
10	79HU5	25	HUV9a	40	85ALT15
11	HUV1	26	HUV9b	41	85ALT14
12	73BE8	27	HUV13	42	E87A20
13	HUV12	28	HUV6b	43	E87A17
14	73BE5 HUV11	29	HUV14	44	E87A18
15	79HU6	30	HUV10	45	E87A19

Table A1-1: list of reflection seismic lines used in this study. The numbers in the left column correspond to those used in Fig. A1-1, the right-hand columns give the originally assigned names.
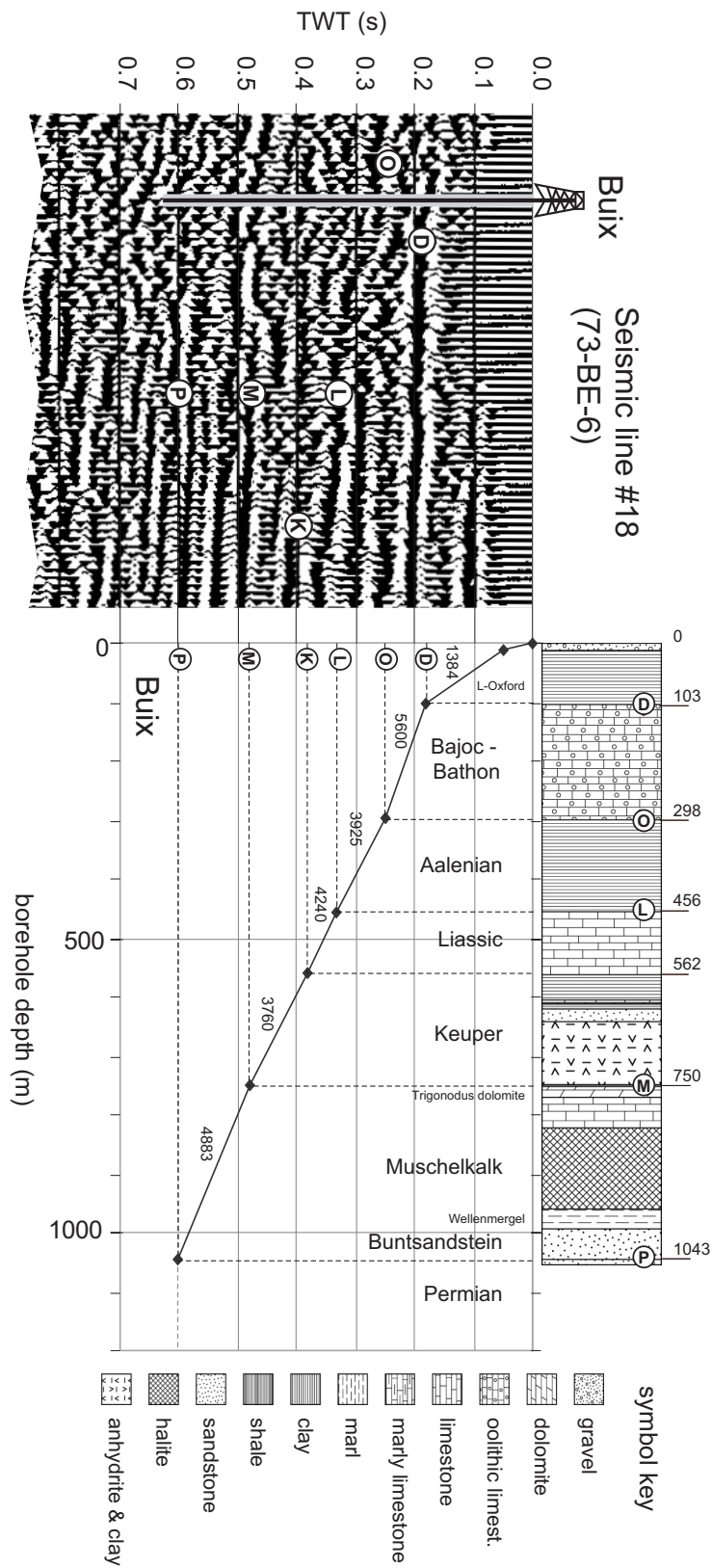
Fig. A1-2: correlation of seismic reflectors with lithologies in exploration well Buix. Derived seismic interval velocities are in metres per second (ms^{-1}). Lithology log is from Schmidt et al. (1924).
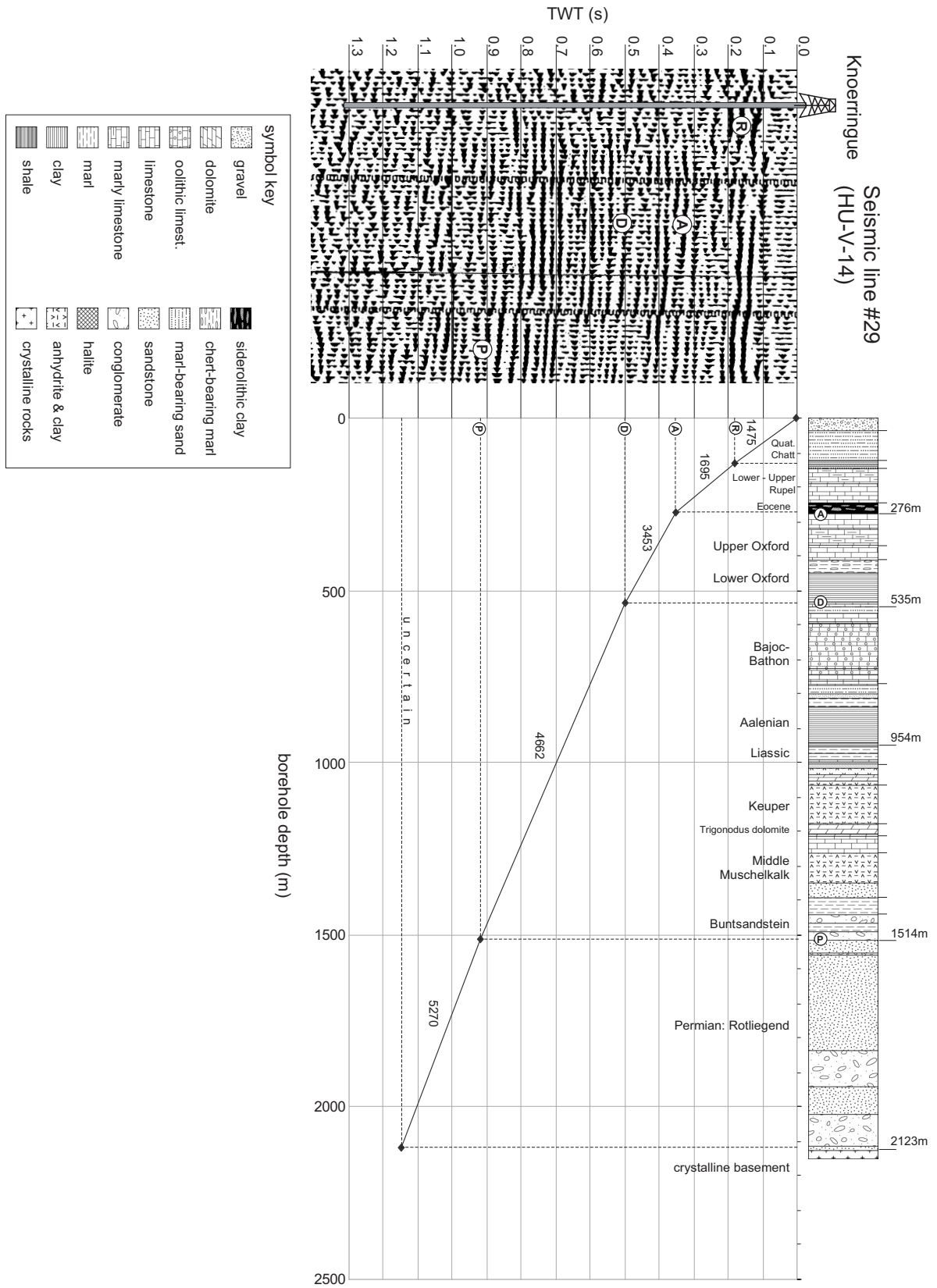
Fig. A1-3: correlation of seismic reflectors with lithologies in exploration well Knoerringue. Derived seismic interval velocities are in metres per second (ms⁻¹).
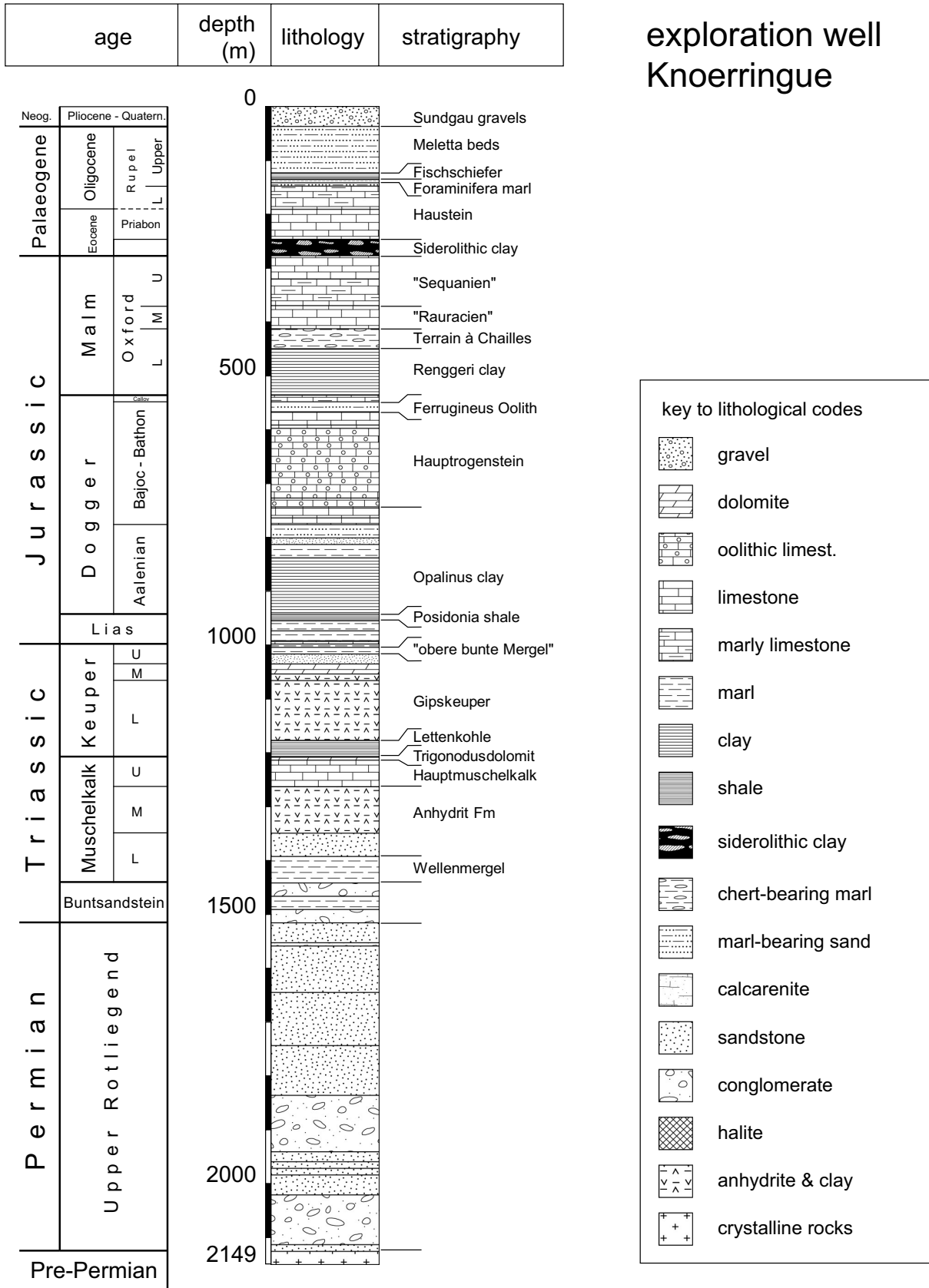
Fig. A1-4: well log for borehole Knoerringue (BRGM banque du sous-sol, unpublished)

depth (m)	lithology	stratigraphy
0		Rhine gravels
		Meletta beds / Septarienton
		Fischschiefer
		Foraminifera marl
		Meeressand
		bunte Mergel / untere Salzfolge
500		Siderolithic
		"Sequanien"
		"Rauracien Korallenkalk" / Vorbourg Kalk
		Terrain à Chailles / Liesberg Schichten
		Renggeri clay
		Hauptrogenstein
1000		"unterer Dogger"
		Opalinus clay
		Lias s. l.
		obere bunte Mergel
		Gansinger Dolomit
		Schilfsandstein
		Gipskeuper
		Lettenkohle
		Trigonodusdolomit
1500		Trochiten- & Nodosuskalk
		Anhydritgruppe
		Wellenmergel
		Buntsandstein
2000		
		Ober-Rotliegend
2500		
2755		granite

exploration well Otterbach

key to lithological codes

	gravel
	dolomite
	oolithic limest.
	limestone
	marly limestone
	marl
	clay
	shale
	chert-bearing marl
	marl-bearing sand
	calcarenite
	sandstone
	conglomerate
	halite
	anhydrite & clay
	crystalline rocks

Fig. A1-5: well log for borehole Otterbach (from Häring 2003)
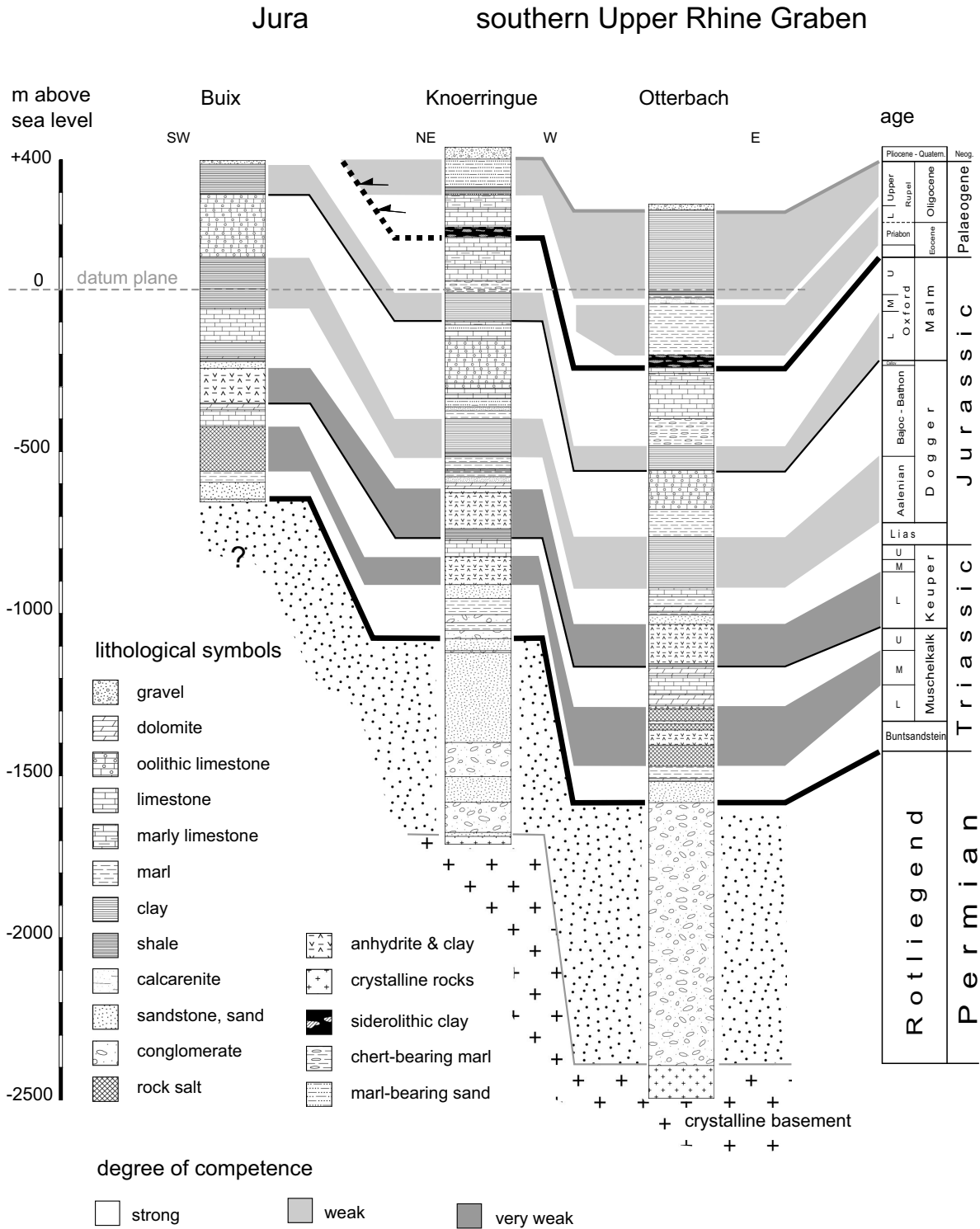
Fig. A1-6: correlated well logs for boreholes Buix, Knoerringue and Otterbach. The relative competency of the encountered lithologies is indicated and reveals the presence of weak layers, particularly in the Middle and Upper Triassic series.

well log Durlinsdorf 1 (D1)

well log Durlinsdorf 2 (D2)
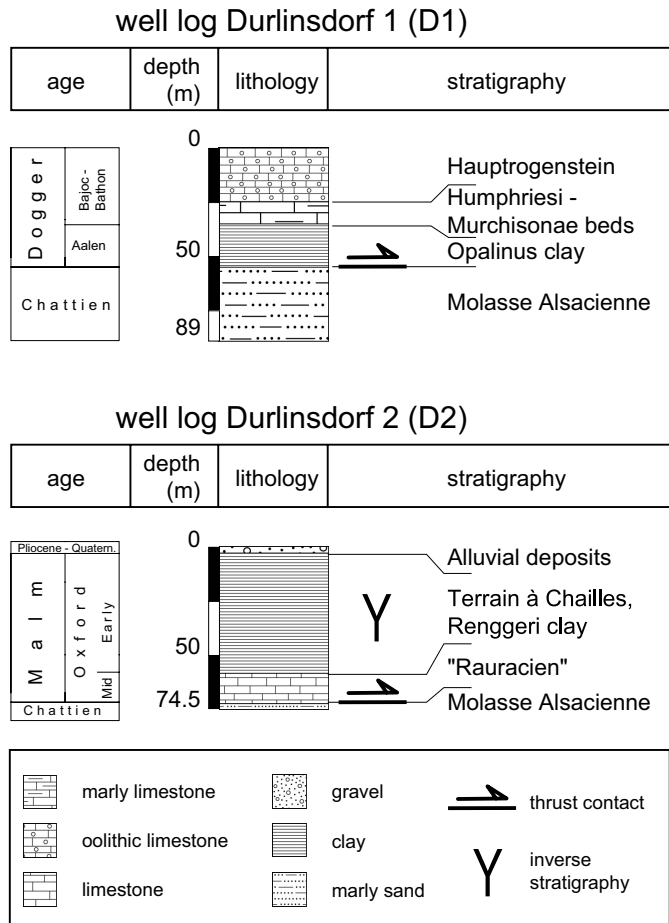
Fig. A1-7: well logs for boreholes at the front of the Ferrette Jura, illustrating the overthrusting of Tertiary sediments by Mesozoic (after Schneegans and Théobald 1948).

References

Häring M (2003) Das Neueste zum Projekt Deep Heat Mining in Basel, http://www.geothermal.ch/Einstieg_d.html. http://www.geothermal.ch/Einstieg_d.html (accessed on 01-09-2003)

Schmidt C, Braun L, Paltzer G, Mühlberg M, Christ P, Jacob F (1924) Bohrungen von Buix bei Pruntrut und Allschwil bei Basel. Beiträge zur Geologie der Schweiz. Geotechnische Serie, X. Lieferung:74

Schneegans D, Théobald N (1948) Observations nouvelles sur le Chevauchement frontal du Jura Alsacien. Bull. Soc. Geol France 18:89-95
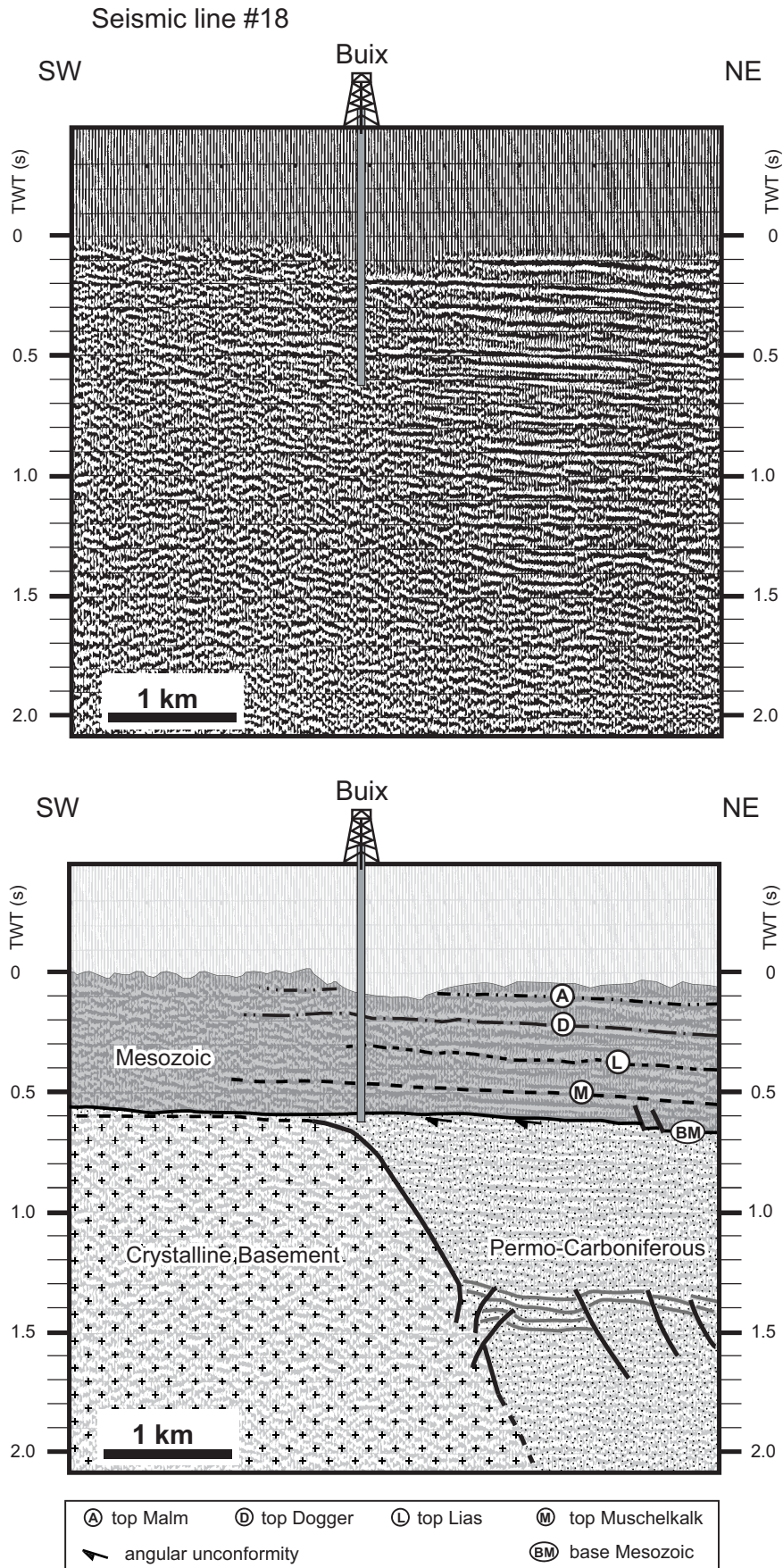
Fig. A1-8: reflection seismic line #18. top: original, stacked section, bottom: interpreted section, illustrating the contrasting seismic facies of crystalline basement and Permian/Permo-Carboniferous sediments.

A1-8

Appendix 2: Joint measurements in the Sundgau gravels

Chapters 4 and 6 provide ample evidence of Post-Late Pliocene shortening in the area of the southernmost Upper Rhine Graben based on the observation that the base of the Late Pliocene Sundgau gravels is gently folded. During these investigations the question arose whether this evidence could be verified by independent observations, preferably at the outcrop scale. Outcrops of Sundgau gravels reveal that a great number of pebbles are jointed. For reasons provided further below, it was assumed that the majority of these joints originated as (extensional) fractures by brittle failure (opening parallel to the maximum compressive stress) and not due to weathering (e.g. dissolution of "inherited", randomly oriented mineralised veins in pebbles after their deposition).

The next question was whether a discrimination between tectonic joints (i.e. joints related to fracturing during gentle map-scale folding of the gravels under (N)NW-oriented SHmax) and non-tectonic joints (i.e. fracturing due to vertical compaction of the gravel beds under their own load) was possible. Joints of tectonic origin are expected to be subvertical and show preferential azimuths parallel to SHmax. Joints related to compaction, on the other hand, would be subvertically oriented as well, but with rather randomly distributed azimuths.

Joint were measured at 8 outcrops, mostly in abandoned gravel pits. The Sundgau gravels are grain-supported and mostly matrix-poor. Their sedimentological characteristics are described in detail in chapter 4. The fractures/joints are frequently developed at point-point contacts between individual pebbles and can occasionally be traced across several pebbles. Sporadically, they show cm-scale displacements (see chapter 6 and Fig. A2-1). Any striations or plumose structures on joint surfaces are absent. The investigated outcrops yielded usually a great number of joints except where the gravels are cemented (locality #7). This suggests that a certain part of the joints can be attributed to weathering (dissolution of old mineralised veins in pebbles). Weathering is also responsible for the in-situ disintegration of granitic and calcareous pebbles. This high intensity of weathering can be attributed to the lack of overburden except for a subordinate Loess cover. This permits unhindered seepage of meteoric water into the gravel beds. In contrast, weathering is delayed when cementation had occurred because of decreased permeability for meteoric water.

Figure A2-2 shows the locations of the joint measurements plotted onto the map of the base of the Sundgau gravels contours (numbers 1 to 8). Figure A2-3 shows the frequency distributions of joint azimuths and dip angles at the 8 sampling locations. The inset at the lower right displays all joints implemented into one diagram. Nearly all datasets shown in Fig. A2-3 reveal relatively well-defined azimuth maxima. The N120°-140° and N160°-180°-oriented maxima in datasets #2 and #6 could possibly have formed as shear fractures in the recent stress field. The significance of the N30° to N100°-trending maxima in datasets #1, #3, #4 and #8 is unclear. Presumably these joint azimuths are overrepresented (compared

to the earlier mentioned trends) due to cut effects (i.e. joints paralleling the exposure walls went unnoticed during data collection). Joints of doubtlessly tectonic origin were only found at locality #5, where their formation is associated with the formation of c. NW-SE-trending, dekametric normal faults (see Figure 3 in chapter 4). The evidence is discussed more exhaustively in chapter 6.

Combined into one plot, the scatter of joint azimuths is large, but the two sets of possible shear fractures (N120°-130° and N160°-180°) can still be identified. The perhaps most robust feature of this summary plot is that around one third of all joints reveal dip angles between 80° and 90°. Dip angles of less than 50° are nearly absent. This suggests that weathering-joints constitute only a subordinate part of the entire dataset and that the causes for the joint formation are either compaction or tectonic imprint.

In conclusion, it is stated that part of the measured joints are of tectonic origin, but joints related to both compaction and weathering blur the tectonic signal up to an extent of statistical insignificance. It is believed that more numerous measurements and still more careful observations could help clarifying this matter.

Fig. A2-1: fracture with cm-displacement in a quartzite pebble within the grain-supported Sundgau gravels, locality #1 (Faverois). Bottom left inset: lower hemisphere, equal area plot of the fracture.
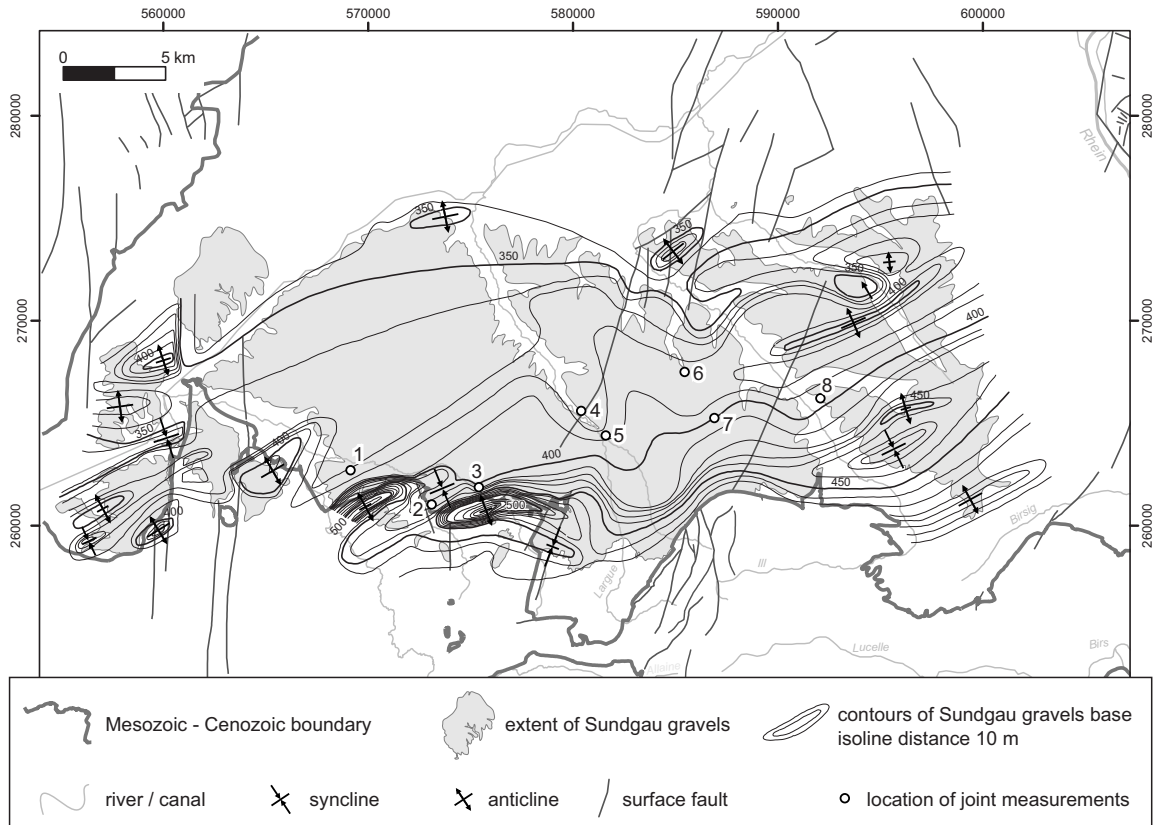
Fig. A2-2: contour map of the base of the Late Pliocene Sundgau gravels with the joint sampling locations.
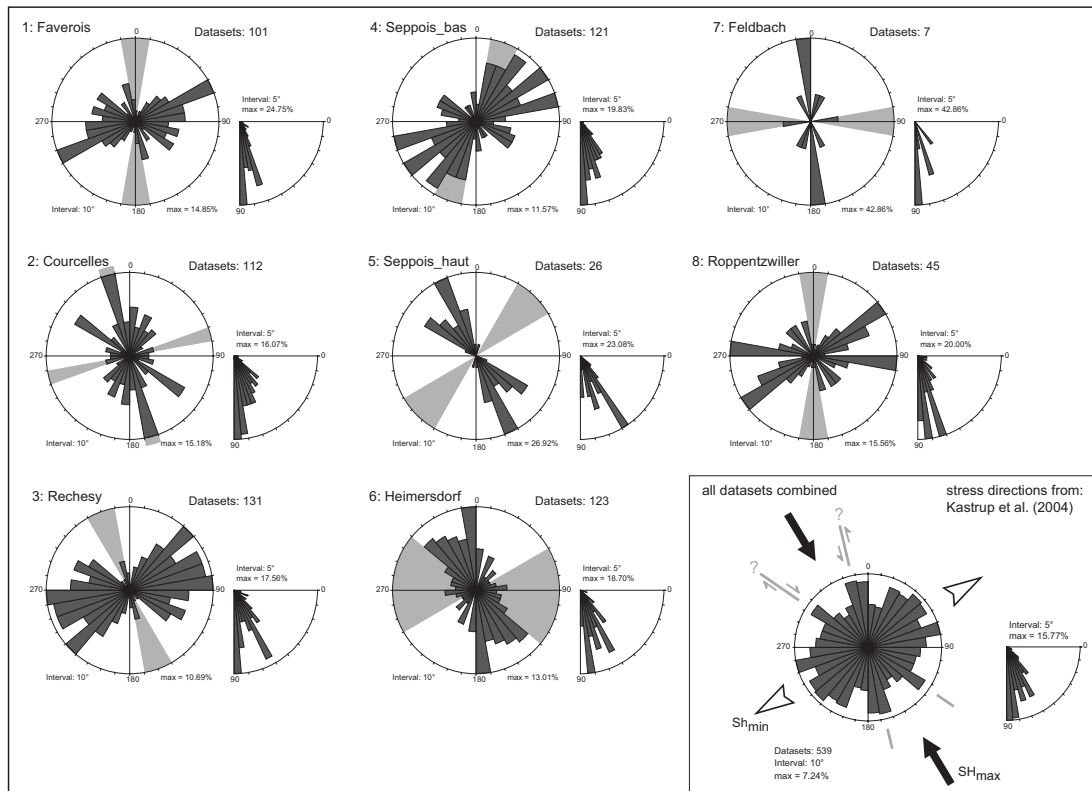
Fig. A2-3: frequency distribution diagrams of joint azimuths and dip angles (dark grey) at 8 sampling locations. Interval width is 10° for azimuths and 5° for dip angles. Orientations of the exposure walls are in light grey. Bottom right inset: all datasets combined. The converging and diverging arrows show the azimuths of horizontal stresses derived from seismotectonic dislocations (Kastrup et al., 2004).

Acknowledgements

Curriculum Vitae of Kamil Marek Ustaszewski

Date of birth   February 12th, 1974
Place of birth   Warsaw / Poland
Nationality   Austrian

Education

May 2000 – June 2004   doctoral student in Basel with Prof. Stefan Schmid and
                                       Prof. Peter Ziegler
                                       PhD title: "Reactivation of pre-existing crustal
                                       discontinuities: the southern Upper Rhine Graben and
                                       the northern Jura Mountains – a natural laboratory"

Oct. 1993 – Jan. 2000   Student of Geology at the Leopold-Franzens University
                                       of Innsbruck, Austria
                                       Title of the diploma thesis: "Stratigraphische und
                                       strukturgeologische Untersuchungen am Ostrand der
                                       Engadiner Dolomiten, (Ortler Gruppe, Südtirol)",
                                       supervised by Prof. Rainer Brandner

Oct. 1992 –July 1993   Studying Chemistry at the Leopold-Franzens
                                       University of Innsbruck

June 1992   Matura in Innsbruck, Austria

Practical training

Oct. 2001   organisation of the 1st ENTEC field trip and training
                                       course

Since May 2000   teaching assistant in several field courses and lectures
                                       in structural geology at the University of Basel

1997 – 1999   geological mapping in Südtirol, Italy for "Projekt
                                       Basiskarte Südtirol" and "Carta geologica Italiana"

Sept. - Oct. 1999   tunneling geologist with Ingenieurbüro Lässer-
                                       Feizlmayr in Tirol, Austria

Aug. 1999   participation in a geographical project of the Austrian
                                       Alpine club (Oesterreicher Alpenverein) in the "Hohe
                                       Tauern" National park, Austria

1998	teaching assistant in ore prospecting geology and subsurface mapping, University of Innsbruck
1997	teaching assistant in crystal optics, University of Innsbruck with Univ.-Doz. Dr. Christine Miller
1996-98	laboratory assistant in mineral separation, University of Innsbruck with Univ.-Doz. Dr. Christoph Spötl
1995-96	field surveying assistant for Vermessungsbüro Avanzini, a private land surveying company, Innsbruck